CRANFIELD UNIVERSITY

MOHD SOFIAN BASRAH

INTEGRATION OF ANTI-LOCK BRAKING SYSTEM AND REGENERATIVE BRAKING FOR HYBRID/ELECTRIC VEHICLES

SCHOOL OF AEROSPACE, TRANSPORT AND MANUFACTURING
Advanced Vehicle Engineering Centre

PhD
Academic Year: 2016–2017

Supervisor: Dr Efstathios Velenis & Dr Dongpu Cao
November 2017

CRANFIELD UNIVERSITY

SCHOOL OF AEROSPACE, TRANSPORT AND MANUFACTURING
Advanced Vehicle Engineering Centre

PhD

Academic Year: 2016–2017

MOHD SOFIAN BASRAH

Integration of Anti-lock Braking System and Regenerative Braking for Hybrid/Electric Vehicles

Supervisor: Dr Efstathios Velenis & Dr Dongpu Cao
November 2017

This thesis is submitted in partial fulfilment of the requirements for the degree of PhD.

Abstract

Vehicle electrification aims at improving energy efficiency and reducing pollutant emissions which creates an opportunity to use the electric machines (EM) as Regenerative Braking System (RBS) to support the friction brake system. Anti-lock Braking System (ABS) is part of the active safety systems that help drivers to stop safely during panic braking while ensuring the vehicle's stability and steerability. Nevertheless, the RBS is deactivated at a safe (low) deceleration threshold in favour of ABS. This safety margin results in significantly less energy recuperation than what would be possible if both RBS and ABS were able to operate simultaneously. Vehicle energy efficiency can be improved by integrating RBS and friction brakes to enable more frequent energy recuperation activations, especially during high deceleration demands. The main aim of this doctoral research is to design and implement new wheel slip control with torque blending strategies for various vehicle topologies using four, two and one EM. The integration between the two braking actuators will improve the braking performance and energy efficiency of the vehicle. It also enables ABS by pure EM in certain situations where the regenerative brake torque is sufficient. A novel method for integrating the wheel slip control and torque blending is developed using Nonlinear Model Predictive Control (NMPC). The method is well known for the optimal performance and enforcement of critical control and state constraints. A linear MPC strategy is also developed for comparison purpose. A pragmatic brake torque blending algorithm using Daisy-Chain with sliding mode slip control is also developed based on a pre-defined energy recuperation priority. Simulation using high fidelity model using co-simulation in Matlab/Simulink and CarMaker is used to validate the developed strategies. Different test patterns are used to evaluate the controllers' performance which includes longitudinal and lateral motions of the vehicle. Comparison analysis is done for the proposed strategies for each case. The capability for real-time implementation of the MPC controllers is assessed in simulation testing using dSPACE hardware.

Keywords

MPC; nonlinear predictive control; brake blending; slip control; regenerative braking

Contents

List of Figures

List of Tables

Nomenclature

Quantity	Description
δ	Steering angle
ε	Convergence factor
μ	Tyre-road friction coefficient
ψ	Vehicle yaw angle
$\dot{\psi}$	Vehicle yaw rate
ϕ	Boundary layer
ω	Wheel angular speed
a_x	Vehicle longitudinal acceleration
a_y	Vehicle lateral acceleration
F_x	Longitudinal tyre force
F_z	Normal tyre force
g	Gravitational acceleration constant
l_F	Longitudinal distance of centre of mass from the front track
l_R	Longitudinal distance of centre of mass from the rear track
m	Vehicle mass
s_x	Longitudinal tyre slip
w_L	Lateral distance of centre of mass from the left wheel
w_R	Lateral distance of centre of mass from the right wheel

B	Pacejka's Magic Formula stiffness factor
C	Pacejka's Magic Formula shape factor
D	Pacejka's Magic Formula peak value
J_w	Wheel moment of inertia about axis of rotation
N	Horizon
N_p	Prediction horizon
N_u	Control horizon
R_w	Wheel radius
T	Torque
T_e	EM torque
T_h	EHB torque
t_s	Sampling time
T_{sim}	Simulation time
V_x	Vehicle velocity

List of Abbreviations

2WD	Two Wheel Drive
4WD	Four Wheel Drive
ABS	Anti-lock Braking System
AWD	All Wheel Drive
BBW	Brake-by-Wire
BEV	Battery Electric Vehicle
BMS	Battery Management System
CAN	Controller Area Network
CM	Centre of Mass
DC	Daisy-Chain
DOF	Degree of Freedom
EBD	Electronic Brake Force Distribution
EHB	Electro-Hydraulic Brake
EM	Electric Machine
EOM	Equation of Motion
ESC	Electronic Stability Control
ESP	Electronic Stability Program
EV	Electric Vehicle
FWD	Front Wheel Drive

GPS	Global Positioning System
FB	Friction Brake System
HEV	Hybrid Electric Vehicle
HIL	Hardware-in-the-loop
ICE	Internal Combustion Engine
IVCS	Integrated Vehicle Control Structure
MF	Magic Formula
MIL	Model-in-the-loop
MPC	Model Predictive Control
NLP	NonLinear Program
NMPC	Nonlinear Model Predictive Control
OCP	Optimal Control Problem
PHEV	Plug-in Hybrid Electric Vehicle
QP	Quadratic Program
RBS	Regenerative Braking System
RTI	Real Time Iteration
RWD	Rear Wheel Drive
SOC	State of Charge
SUV	Sport Utility Vehicle
SMC	Sliding Mode Control
TCS	Traction Control System

Acknowledgements

My sincerest gratitude to my supervisors Drs. Velenis and Cao for all the guidance and efforts through this research work. I would also like to thank Drs. Siampis and Longo for all the invaluable inputs and introducing me to the MPC world.

I would like to dedicate my greatest appreciation to my wife, Shima and my children, Syaurah and Sumayah. Thank you for being my strength tirelessly and keep having faith in me. Last but not least, thank you to my family in Malaysia for sending their prayers and support.

A special gratitude to the Autolads, especially Deepak, Ed and Kostas.

In loving memory of my beloved father, Basrah.

List of Publications

The following publications have been produced as a result of the work conducted in this thesis:

Journal articles

- M. S. Basrah, E. Siampis, E. Velenis, D. Cao, and S. Longo. Wheel slip control with torque blending using linear and nonlinear model predictive control. Vehicle System Dynamics, vol. 55, no. 11, pages 1665-1685, 2017.

- M. S. Basrah, E. Siampis, E. Velenis, D. Cao, and S. Longo. Wheel slip control with torque blending using real-time nonlinear model predictive control for AWD electrified vehicles. (in publication process).

Conference papers

- M. S. Basrah, E. Siampis, E. Velenis, D. Cao, and S. Longo. Integration of torque blending and slip control using real-time nonlinear model predictive control. in Advanced Vehicle Control (AVEC' 16), Proceedings of the 13th International Symposium on, pages 585592, 2016.

- M. S. Basrah, E. Velenis, and D. Cao. Four wheel torque blending for slip control in a hybrid electric vehicle with a single electric machine. in Sustainable Energy

Engineering and Application (ICSEEA), 2015 International Conference on, IEEE, 2015.

Chapter 1

Introduction

Vehicle electrification is part of a major initiative by automotive manufacturers towards a solution to emissions and global warming issues [25]. The diminishment of the fossil fuel resources is another major contribution to the rapid growth of hybrid electric vehicle technology [26]. Vehicle electrification entails the incorporation of electric machines (EM) and energy storage in the vehicle's powertrain. The existence of the new braking source of torque (referred as the braking actuator in this work) creates the opportunity not only to increase energy efficiency but to enhance the performance of the safety aspect of the vehicle [28]. Anti-lock braking system (ABS) is an important feature of active vehicle safety to ensure vehicle stability and steerability when the drivers attempt to stop the vehicle during emergency braking. The ABS controls the braking force accordingly when the system identifies incipient wheel lock [48]. The driver will be unable to steer the vehicle as it continues to slide if the front wheels are locked, while the vehicle is prone to spin out and losing control if the rear wheels lock. In addition, brake stopping distance is significantly longer if the wheels are locked during braking in most road surfaces [60]. Regenerative braking can be deployed to support friction braking system (FB) during braking events to recuperate energy for future use and also during emergency situations,

such as to avoid wheel locking. Currently, only conservative strategies have been applied for the deployment of EM during braking, which is disabled if any risk of emergency situation emerges [11, 28, 114].

The regenerative braking system (RBS) in a hybrid electric vehicle (HEV) is an important component to increase the vehicles' energy efficiency and reduce CO_2 emissions [26]. Regenerative braking is delivered by the electric machine in generator mode and can also be referred as electric braking in this work. Active safety is a crucial feature in road vehicles to avoid or minimize accidents in emergency situations. The Anti-lock braking system (ABS) is an example feature of active safety to ensure vehicle stability and steerability when drivers attempt to stop the vehicle during emergency braking. Vast works of literature focus on ABS control concept to achieve better efficiency and braking performance. The ABS braking force is controlled accordingly when the system identifies incipient wheel lock [10,103]. The driver will be unable to steer the vehicle as it continues to slide if the front wheels are locked. The vehicle is prone to spin out and losing control if the rear wheels lock. In addition, brake stopping distance is significantly longer if the wheels are locked during braking in most road surfaces [60].

Research and technology on low carbon transportation have been developing within the last few decades. Hybrid Electric Vehicles (HEV) are an alternative to the internal combustion engine based vehicles which offer lower or zero carbon emission and better energy efficiency with the use of regenerative braking.

In the present mass production electrified vehicles, the regenerative and friction brake actuators operate independently from each other. RBS is usually applied during low vehicle deceleration while friction braking is generally used when the deceleration demand is relatively high. Emergency braking may lead to high wheel slip and there is a danger of locking the wheel. Current HEVs will cut-off the regenerative braking and apply conventional friction brakes to ensure that the braking torque command can be delivered. More

importantly, when the wheel slip is above a certain threshold, the ABS will be activated to prevent the wheels from locking. Priority is always given to the friction brakes under emergency braking and the normal approach is to simply disable the RBS [11,28,114]. In recent years, there are research works can be found in the literature propose the cooperation between fricion braking and regenerative braking during 'normal braking' (without any risk of wheel locking) operation [38, 74, 119]. The main focus is on maximising energy recuperation and the strategy is to revert to pure friction braking under the emergency braking conditions.

On a low road adhesion surface, there is a high possibility of wheel locking even at lower deceleration demands. In this case, the RBS will be turned off at a safe margin and FB is utilized as the ABS is likely to be activated. For a high deceleration demand on a high adhesion road surface, the RBS is deactivated considering the limitation of the brake torque range of the electric motor. In other words, the Electric Machine (EM) is safely disabled during the emergency braking (ABS is activated) due to the fact that occupants' safety precedes the energy recuperation [68, 82]. These lead to conservative application strategy of RBS deployment and will give adverse effects on the energy recuperation.

Understanding the capability of the electric machine as a braking actuator is an important factor which motivates this research. Electric machines have limited torque range for braking but have very quick and precise response, and the applied torque can be measured easily [78]. On the other hand, FB is capable of delivering high retarding torque but limited by the high delay in response. With the combination of the two actuators, ABS performance can be improved and the energy regeneration has a wider activation window to increase efficiency.

This work concentrates on enabling the integration of the slip control and torque blending between the braking actuators, namely the friction brakes and regenerative braking systems. The main motivation is to allow for a wider window of regenerative braking

activation during high decelerations or emergency braking. Additionally, the distinct advantage of using an electric motor such that accurate and fast control can be applied in improving the slip control operation. Electric machines have limited torque range for braking but have very quick and precise response, and the applied torque can be measured easily [78]. On the other hand, FB is capable of delivering high retarding torque but is limited by the high delay of response [29, 78]. With the combination of the two actuators, ABS performance can be improved and the energy regeneration can have a wider activation window to increase efficiency.

A drive cycle of 5km driving on Nürburgring Nordschleife in IPG CarMaker is used to illustrate the impact of implementing different regenerative braking cut-off threshold. The vehicle model details are shown in 2.2. The vehicle speed and acceleration profiles are shown in Figure 1.1. If the threshold can be increased from 0.1g ($1m/s^2$) deceleration and higher, there is a possibility to increase the overall energy recuperation of real-world driving and braking as illustrated in Figure 1.2. The implementation of regenerative braking torque integration enables the vehicle control engineer to expand the energy recuperation window.

A lot of research has been carried out on slip control and wheel deceleration control for passenger cars but mostly designed for the conventional friction braking. In [28], the authors conclude that EM offers torque control improvement with regenerative braking and Traction Control System (TCS) capability, but not used for the improvement of ABS performance. On the other hand, there are only a few results addressing the design of ABS utilizing only electric motor or the blending of the two actuators. Therefore, the area of interest is on integrating electric motor and friction braking for ABS application using various HEV topologies. Novel strategies to combine friction and regenerative braking during low wheel slip braking have been reported in [38, 119]. However, the strategies only consider normal braking conditions when there is a low risk of wheel

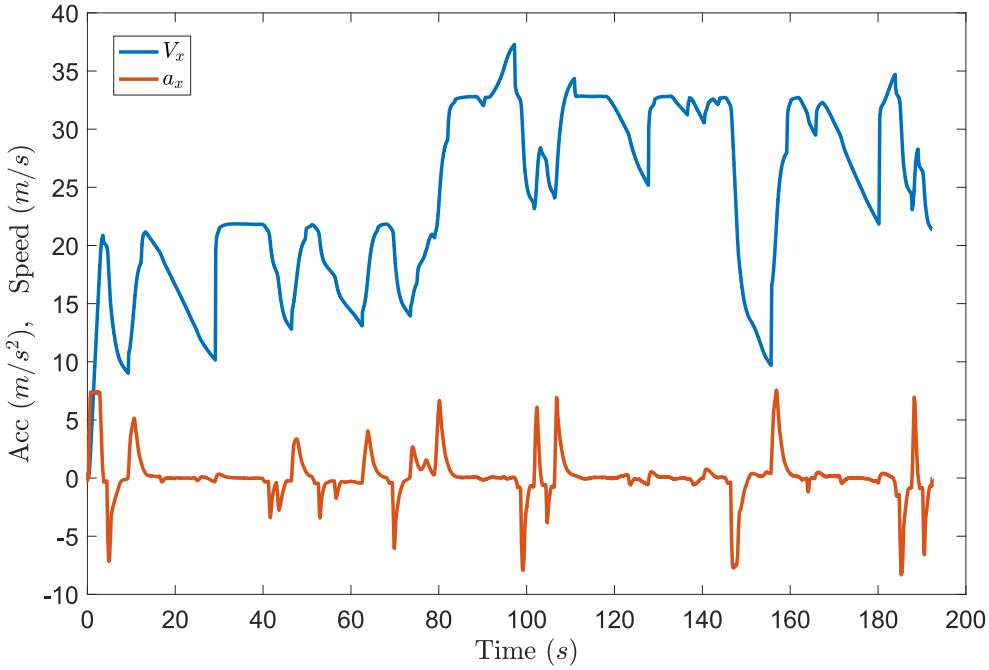

Figure 1.1: Vehicle speed and acceleration profile for Drive cycle on Nürburgring Nordschleife.

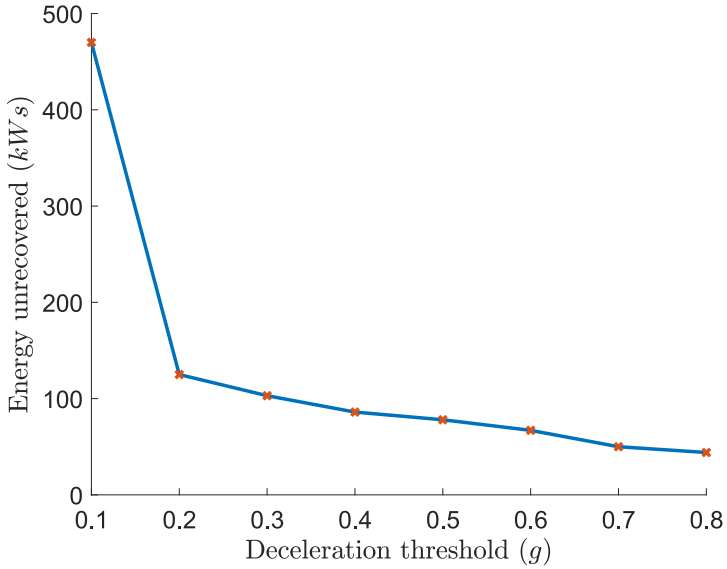

Figure 1.2: Energy unrecovered for different deceleration threshold.

locking. On the other hand, torque blending for slip control is a fairly new research area and several articles report torque allocation algorithms using rule-based methods [27, 79]. A brake torque allocation strategy using a static control allocation or daisy chain method is proposed in [9]. A clear advantage of this approach is the low computational effort for online implementation.

The research will support *Evoque_e* project; a joint academia and industry project in developing three different topologies of prototype HEVs sponsored by Innovate UK and led by Jaguar Land Rover [116].

Most articles on ABS system design validate their proposed design using straight line braking on various road surfaces. Authors claim that the proposed slip controller is capable of improving the braking performance and maintaining the stability of the vehicle. In this work, we consider the benefit of using combined braking with steering input to validate the proposed design. It is also worth to consider selecting optimum slip ratio target for different manoeuvres for the brake actuators to satisfy to compromise between vehicle steerability and braking performance.

Maximum braking force can be achieved by regulating the wheel slip at certain values in the stable region (before reaching peak value) as shown in Figure 1.3. The lateral grip of the vehicle can be maintained at certain slip ratio and deteriorate when the slip increases. Therefore, there is a range of slip ratio which is optimized for both longitudinal and lateral forces during braking in order to stop quickly while preserving the steering response.

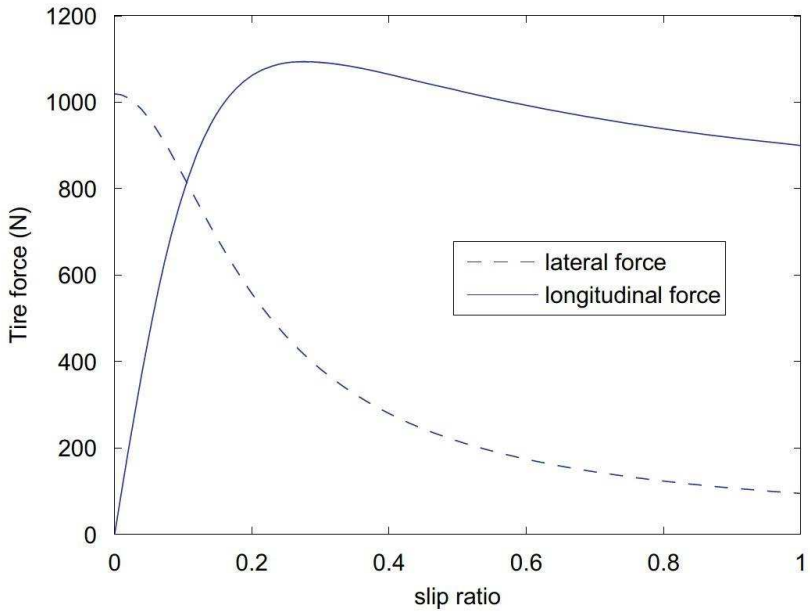

Figure 1.3: Longitudinal and lateral tyre forces in a range of slip (adopted from [118]).

1.1 Literature Review

A literature survey is presented in this section to study and report existing researches and technologies of ABS for hybrid and electric vehicles.

1.1.1 Brake Actuators for Electrified Vehicle

HEVs depend on regenerative braking system to recuperate electrical energy to improve the vehicles' energy efficiency and reduce CO_2 emissions. A friction braking system is also available to allow the vehicles come to standstill in a safe manner. This section describes the braking actuators available in the electrified vehicles.

Figure 1.4 shows both torque range and response time of different braking actuators in electrified vehicles. With different interesting vehicle configurations, integration between two actuators will enable us to design a hybrid ABS.

Friction Braking

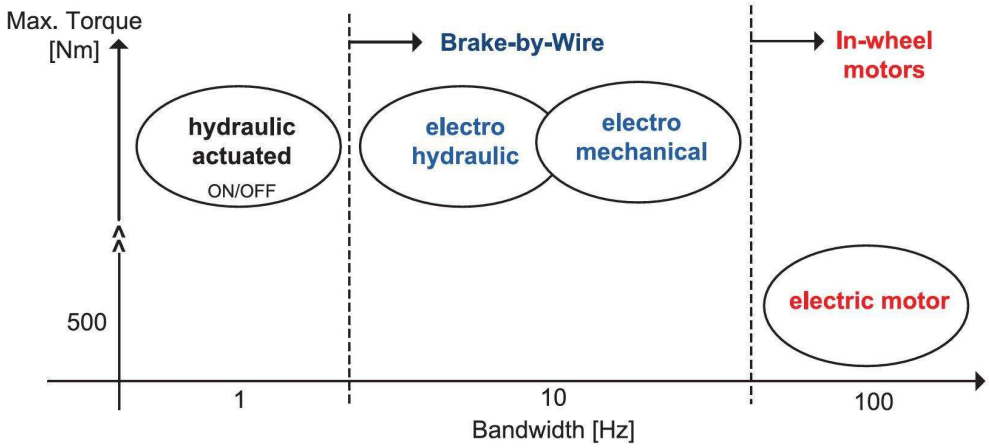

Figure 1.4: Qualitative features of brake actuators in HEV (adopted from [29]).

Most passenger vehicles are fitted with friction brake system by the Original Equipment Manufacturers (OEM) as the use of service brakes. This is the type of conventional actuator which is commonly used for the development of ABS.

The advantage of FB is the low cost and the ability to deliver high retarding torque during braking. Based on Figure 1.5, the driver brake input from the brake pedal is amplified mechanically by the brake booster (1) and the master brake cylinder (2) will transmit the brake fluids to each brake calipers (4 and 5) to apply the brake torque. The proportional control valve (3) regulates the brake force to the rear axle [48].

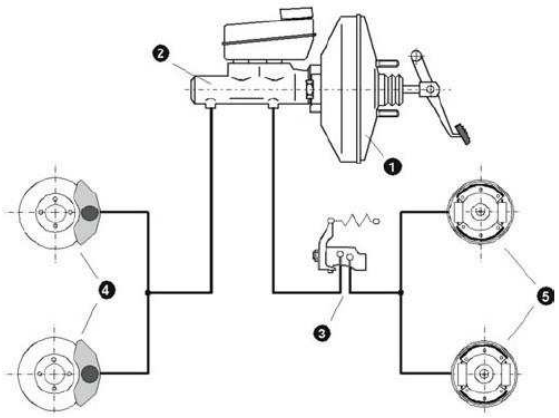

Figure 1.5: Components of hydraulic brake system (adopted from [48]).

Typically, OEMs use multi-circuit brake system which allows braking force to be transmitted through two or more circuits. Therefore, it will be possible to supply the brake force required even in the event of circuit failures [98].

Figure 1.6 and equations (1.1) - 1.2) describe the friction brake model as pressure control of increase, hold, or decrease which represents a conventional system of a passenger car [27, 72, 88, 123]. In these articles, the mathematical expressions of the friction brake system are based on empirical observation and neglect the complicated physics. Current ABS control algorithms are limited to use the three discrete cases of pressure application rather than continuously controlling pressure which affect the braking efficiency.

$$Q = \begin{cases} k_1\sqrt{P_m - P_w}\,, & \text{pressure increase} \\ 0\,, & \text{pressure hold} \\ k_2\sqrt{P_w - P_r}\,, & \text{pressure decrease} \end{cases} \tag{1.1}$$

$$P_w = k_3 \int Q dt \tag{1.2}$$

where P_w is the wheel cylinder pressure, P_m is the master hydraulic pressure, P_r is the reservoir hydraulic pressure, Q is the hydraulic flow in brake caliper, k_1 and k_2 are coefficients determined by orifice size and brake fluid's viscosity, and k_3 is the coefficient decided by brake parts' characteristic.

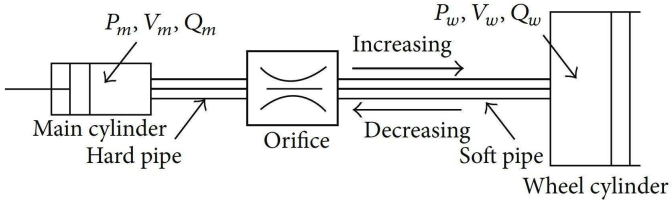

Figure 1.6: Hydraulic pressure theory of the brake system in [123].

Brake-by-Wire

Electro-hydraulic Brake system (EHB) is a type of Brake-by-wire system (BBW) which uses hydraulic in the system. EHB decouples the brake pedal from the brake actuation. Based on Figure 1.7, the amplification of brake force is provided by the electric pump rather than a brake booster [98, 108]. The system calculates the driver's deceleration demand based on the input from a pedal stroke sensor and generates brake pressure command to the brake calipers accordingly. Moreover, EHB has the advantage of having a high-pressure hydraulic reservoir to deliver the brake pressure to individual wheels. In contrast to the simpler control strategy of conventional hydraulic systems which use pressure increase, decrease or hold constant, the BBW delivers the brake pressure continuously as commanded by the controller. This increases the controllability and provides flexibility to the ABS algorithm design for better braking performance. Modern electronic braking control can be integrated directly with EHB without the needs of additional hardware [48].

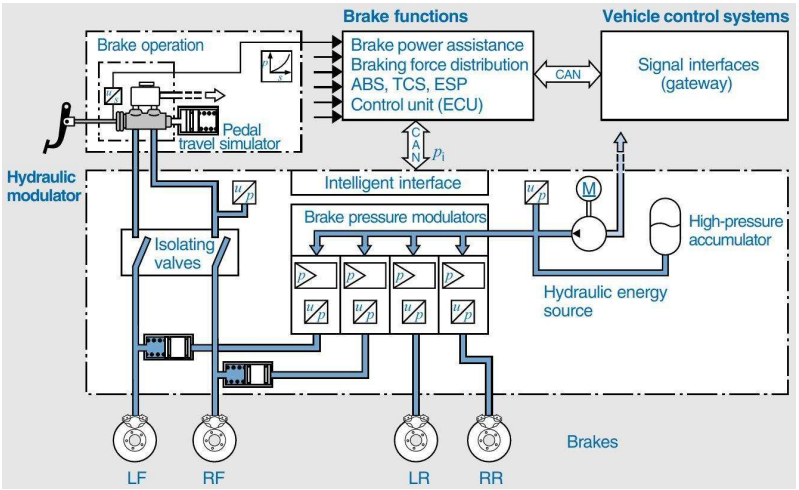

Figure 1.7: EHB schematics adopted from [98]).

Another type of BBW is the Electro-mechanical Brake system (EMB), usually called dry BBW. As illustrated in Figure 1.8, the system contains no brake fluid but operates using individual electro-mechanical brake modules in each corner. Similar to the EHB,

the brake pedal is decoupled from the brake system. Brake clamping force is applied by

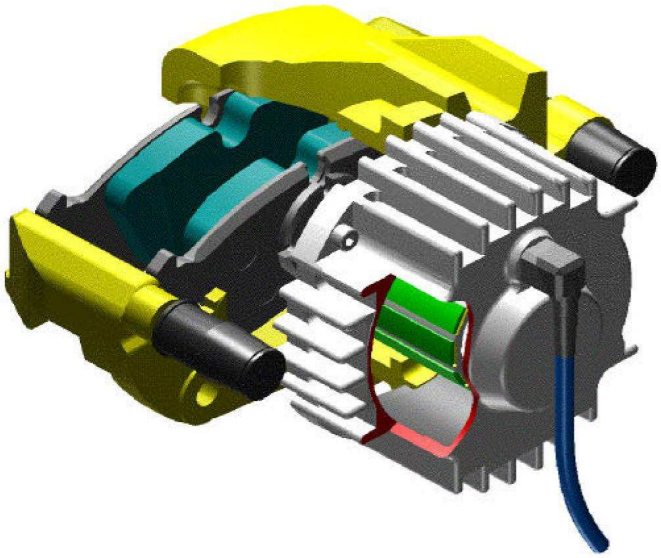

Figure 1.8: Electromechanical brake system by ITT Automotive (adopted from [106]).

the friction couples (brake pads and discs) but being delivered by an electric motor module instead of the hydraulic force [48]. It gives the advantage of fast braking dynamics, no operating noise and minimized pedal feedback during ABS activation. Measurement of the brake torque applied to the wheel can be done using the motor current [53]. This will avoid any estimation requirements on the brake force that will lead to complex control modelling when using hydraulic system. Table 1.1 presents the comparison between EHB, EMB and conventional friction brake system of a vehicle. It shows clear evidence that BBW can offer better response, accuracy, and driver's comfort in ABS implementation.

Regenerative Braking

Electrified vehicles are fitted with Electric Machines (EM) which act as motors or generators. During braking, the EM will enable the regenerative braking mode to capture kinetic energy as electric energy to be stored for future use [32]. Various type of EMs can

	FB	EHB	EMB
Technology	Friction	Electro-hydraulic	Electro-mechanical
Force modulation	Discrete (On/Off)	Continuous	Continuous
Ergonomics	Pedal vibration	No vibration	No vibration
Environmental issues	Toxic oils	Toxic oils	No oil

Table 1.1: Comparison of brake system actuators (adopted from [103]).

be fitted in different ways to enhance the vehicle performance as well as vehicle dynamics. In-Wheel Motors (IWM), for example, allow individual wheels control and are capable of improving the vehicle stability in any situation. In the case of EMs fitted on either front or rear axle and connected to the wheels through shafts and gears, there will be no individual wheels control but with a proper control algorithm, an advantage of the higher efficiency of energy regeneration and braking performance can be gained. Presently, OEMs do not employ RBS during ABS events but rely solely on FB.

There are clear advantages of applying EMs as a braking actuator which includes fast response and ease of control [97]. Electric motors' torque response is in milliseconds and 10-100 times faster than friction brake system. Additionally, motor torque measurement can be done easily based on the motor current. Hence, road surface condition estimation can be implemented using a driving/braking force observer [49]. There are limitations of RBS that need to be considered in electrified vehicles' design. EMs operating temperature, speed and battery State of Charge (SOC) play important roles in determining the available braking torque of RBS. The retarding torque application is then limited in certain situations. In other words, friction brake systems usually coexist with RBS in order to supplement the required brake torque [32].

There are results in the literature on blending friction brakes and regenerative brakes which focus on energy maximisation but not for ABS implementation [38,47,119]. Hence, the motivation of this research is to allow RBS to be integrated with EHB in ABS opera-

tion.

1.1.2 Slip Control for Electrified Vehicle

ABS has been fitted into mass production vehicles with the objective to reduce accident risks caused by wheel locking [10]. The driver will be unable to steer the vehicle as the vehicle continue sliding if the front wheels are locked. The vehicles are prone to spin out and losing control if the rear wheels lock [60]. Brake stopping distance is significantly longer if the wheels are locked during braking. ABS can prevent these three major disadvantages of wheel locking during panic braking or braking on very slippery road surfaces. An additional benefit of ABS is avoiding tyre flat spots problem due to locked wheels by hard braking.

According to Bosch, there are requirements that ABS must satisfy as part of an active safety system [10]:

1. To be able to maintain steering response and vehicle stability on all road conditions.

2. Capable of adapting quickly to road surface traction changes (μ-change).

3. Must maintain steering response and stability while achieving shortest possible stopping distance during cornering.

4. Capable of minimizing the inevitable yaw rate to allow an average driver to countersteer while braking on different friction levels of the vehicle's two sides (μ-split).

This section will discuss the different ways in which ABS can be deployed using different methods and actuators.

Anti-lock Braking System

There are numerous approaches in developing ABS algorithm reported in the literature. Different approaches are presented but with the same objectives, to improve the braking performance, maintain vehicle stability and steering response. Few examples of different methods in delivering ABS strategy include Logic Threshold Control (LTC), Sliding Mode Control (SMC), Fuzzy Logic Control (FLC), wheels deceleration control, and some combinations of different controllers.

Chiang et al. implement conventional rule-based LTC method for a friction braking system [27]. Based on two slip ratio threshold (lower and upper limit), the brake pressure is either increased, maintained or decreased as described in section 1.1.1. Slip dynamic equation is transformed into a form of a Linear Parameter Varying (LPV) system in article [72]. A static-state feedback control algorithm is employed to track the target slip ratio. Similar to presented approach in [27], discrete brake pressure control is used. In [84], author presents a state-of-the-art five-phase ABS logic algorithm to control both wheel deceleration and wheel slip. The error or offset can be described as:

$$x_1 = \lambda - \lambda^* \tag{1.3}$$

$$x_2 = \dot{\omega} r - a^* \tag{1.4}$$

where λ^* is the slip ratio threshold and a^* is the wheel deceleration threshold. The article uses a rule-based method for controlling the wheel slip and wheel deceleration without the need for the formulation of the nonlinear relationship between the tyre-road friction characteristics and vehicle speed estimation. The brake torque is varied (decreased, increased or maintained constant) along five phases to avoid the wheel dynamics to be in the unstable region and stay in the stable region. The controller is designed for conventional FB with discrete actuator control (pressure increase, decrease or hold). However,

this type of control method is not robust to adapt to any road surface changes.

Satzger et al. use a linearised wheel slip dynamic equation to design a gain scheduling proportional-integral (PI) controller for ABS [101]. A pole-placement method is used for controller tuning which claimed to be robust against the uncertainties introduced by tyre-road contact friction and vertical load. Savaresi and Tanelli describe different methods in braking controls according to the braking actuators dynamics [103]. For continuous actuators dynamics (i.e brake-by-wire), the methodology used include wheel slip control and wheel deceleration control. The works in [104] proposed a mixed wheel slip-deceleration control. This method is based on linearised braking dynamics models and claimed to be effective and flexible which consider the advantages of both deceleration control and slip control.

For nonlinear wheel slip control, a Lyapunov-based control law is normally designed. One key advantage of nonlinear method approach as compared to linearized model method is the ability to recognize present operating condition based on the tyre-road friction curve (μ-s_x curve), hence performance and safety are improved by adapting even when operating beyond the μ-s_x curve's peak point. Figure 1.9 shows the nonlinear relationship between road friction coefficient, μ and longitudinal slip, s_x.

Guo and Wang [43], Yin and Jin [123], Anwar [3], Bera et al. [13], Hsiao and Lin [52], Jing et al. [58], Baek et al. [5], and Huh et al. [53] proposed using SMC to design anti-lock braking control due to its robustness against external disturbances and parameter variations of the system.

The slip control is designed to eliminate the slip error:

$$s_{error} = s_{actual} - s_{target} \tag{1.5}$$

Article [43] includes a fuzzy logic in control design to determine an optimising param-

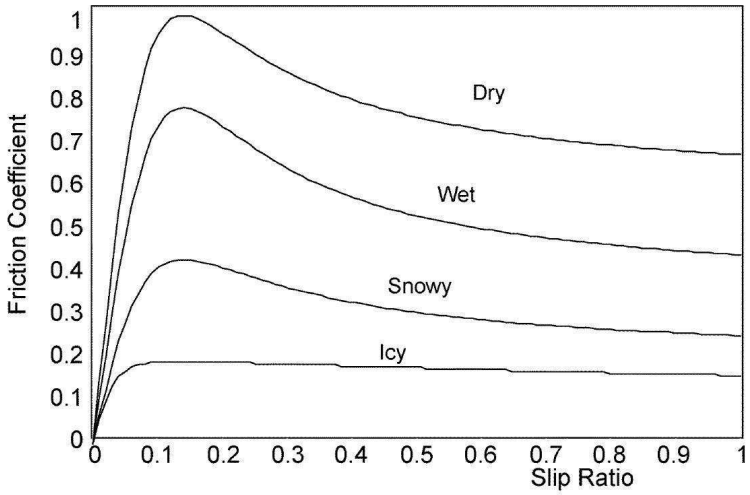

Figure 1.9: μ-s_x curve for different conditions (adopted from [70]).

eter to be fed into the SMC. The sliding surface is defined as the slip error or difference between the desired slip and the actual slip as shown in equation 1.5. Generally, the target slip is assumed to be constant and does not vary over time. An exponential law approach instead of saturation is implemented to reduce chattering. The controller's base formulations are represented as:

$$\dot{s} = -\varepsilon sgn(s) - ks \tag{1.6}$$

where s is the sliding surface, ε and k are positive constants used as tuning parameters.

Based on Figure 1.10, the FLC will optimize the tuning parameter, ε to be fed into the slip controller. It is desirable to have increased the value of the ε for more robust control effect, but with an adverse effect of high chattering. The authors assumed that some parameters are known such as normal load on the wheel, f_z, vehicle speed, V_x, and wheel angular speed, ω. Based on various road surfaces, the friction coefficient between tyre and road surface, μ were obtained experimentally.

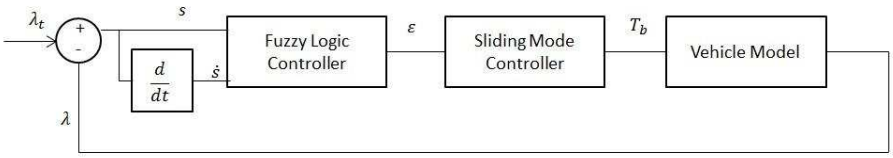

Figure 1.10: Block diagrams for FLC-SMC in [43].

Article [53] presents the idea of sliding mode controller for ABS with continuous switching law (saturation) with a boundary layer, ϕ instead of discontinuous (signum). The control input is presented in equation 1.7. Several parameters are estimated such as the braking force, f_x and the friction between brake disc-pad contact, μ_b [41, 124].

$$P = P_{eq} - k\ sat(\frac{s}{\phi}) \tag{1.7}$$

where P is the control input brake pressure, P_{eq} is the equivalent control brake pressure, k is the control gain, s is the sliding surface, and ϕ is the boundary layer.

The authors in [3] present the use of hybrid braking system comprising of electro-hydraulic brake and eddy-current brake (ECB) for sliding mode ABS control. As the friction coefficient of road-tyre, μ is needed in slip control formulation, the author uses an approximated linear curve of friction coefficient-slip with a slope, α. A saturation type of control law similar to [53] is used to reduce chattering effect associated with SMC as a contrast to sign function used in [13, 43].

In article [29], de Castro et al. propose an adaptive slip controller (based on Lyapunov control law) combined with gain scheduling method as illustrated in Figure 1.11. The main aim is to maintain the actual slip value, s_{actual} near to the given target, s_{target}. An adaptive and robust method is used to handle the parametric uncertainties of the tyre-road adhesion. Linear parameterization of the $\mu - s_x$ curves from Burckhardt model [18, 65] is

used.

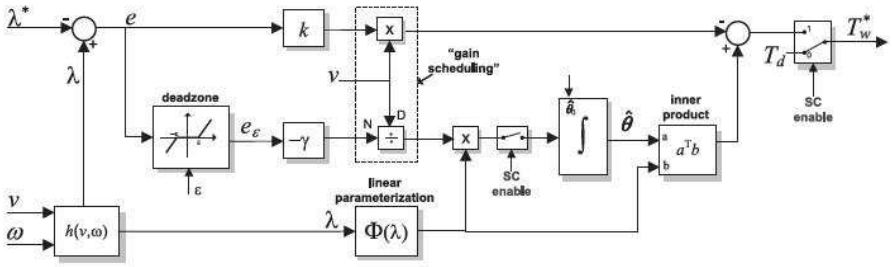

Figure 1.11: Adaptive slip controller (adopted from [29]).

The authors make the assumption that vehicle speed, V_x is known from vehicle speed observers such as the ones implemented by [42,65,113,129]. Wheel speed, ω is also considered known but it can be easily measured using a wheel speed sensor which normally is available in conventional ABS systems. The other two parameters used are maximum friction coefficient of tyre-road contact μ_{max} and vertical load force, f_z acquired from highest adhesion possible in tyre-road contact and the relation of front-rear load transfer during braking respectively [39]. The main task is to determine the wheel torque, T_{wheel} so the error can be eliminated in a fast manner. The article discusses the challenge of generating optimum slip target to maximise the tyre-road adhesion due to the nonlinearity of μ-s_x curve. In this case, a constant slip target (a point before peak) is used with all type of road surfaces in terms of tyre-road adhesion. Force and torque disturbances are neglected since they are relatively small compared to the brake torque value. Based on the control law equation, the slip error dynamics will behave infinitely fast as vehicle speed approaches zero. Hence, deactivation of the slip controller is designed for a positive vehicle speed before the car comes to complete standstill. Vehicle speed influences the slip controller according to the control law equation. At higher speed, the adaptation rate of the controller is smaller.

Ivanov et. al. propose in [55] an ABS controller which uses feedforward (predictive)

and feedback (reactive) brake torque control to follow longitudinal slip target as illustrated in Figure 1.12. The predictive torque is calculated based on driver's pedal input while the reactive torque control is done by using proportional-integral (PI) control method. The total brake torque is given by:

$$T_{brake} = T_{demand} + T_{react} \tag{1.8}$$

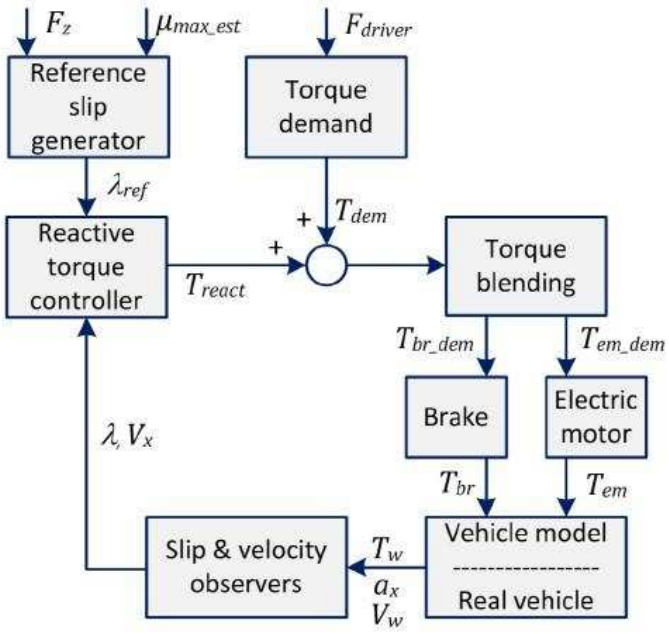

Figure 1.12: Overview of ABS controller in [55].

Torque demand, T_{demand} comes from the driver brake pedal input which considers the road condition (μ_{max}) and estimated normal wheel force, f_z. A design of target slip generator is based on a lookup table but later adapted for the use of the sign of μ-s_x curve as described in Figure 1.13.

Article [55] states that a slip reference value is selected based on friction force between tyre and road surface which include normal wheel force and road friction coefficient. This

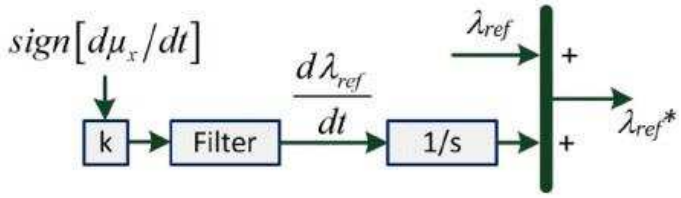

Figure 1.13: Slip target generator algorithm in [41].

is done using a lookup table. This requires estimation of road μ and normal wheel force, f_z which is not discussed in the article. Another important input being estimated is the longitudinal slip, s_x which also being estimated along with vehicle speed by observers. These observers are not presented in the article. The final output of the slip reference generator is the slip target, s_{ref} after adaptation procedure considering the sign of μ-s_x curve slope. The intention is to determine underbraking (positive slope) and overbraking (negative slope) condition and let the ABS controller react accordingly.

Currently, electrified vehicles only utilize RBS during low deceleration braking. Whenever high deceleration demand is requested by the driver, the friction braking system will be activated while the RBS is deactivated. Articles [68] and [128] addresses the issue of a recurring ON-OFF cycle of regenerative braking during ABS event. This could cause vehicle instability if the brake torque transition is not properly controlled as well as affecting driver's comfort. Oleksowicz et al. identify a big challenge to implement ABS without individual wheel braking capability of the electric motor which could cause excessive slip on one wheel. This affects vehicle stability during braking and will defeat the main purpose of the active safety feature of the vehicle [82]. Support by the friction brakes is required to improve the brake performance while maximising energy recuperation during an ABS event. The initial motivation of this doctoral research is to eliminate these problems by integrating the two actuators for ABS implementation.

Electric ABS (e-ABS)

The idea of implementing ABS using regenerative braking is relatively rare and only limited literature exists [54]. OEMs apply ABS using friction brakes and one obvious limitation of RBS is that the brake torque delivery is relatively low compared to friction brakes. This is limited by the motor size fitted in any HEVs. Designing ABS using the electric machine is also limited when battery SOC is high or when operating in field weakening region [29]. Another drawback of RBS is limited to the vehicle architecture. Without four individual electric machines on each wheel, there is a challenge in delivering good electric ABS performance.

De Castro et al. design an SMC with conditional integrators in controlling the wheel slip of EVs to improve the steady-state error introduced when using continuous SMC law (using saturation) [24]. The conditional integrator is only added to the boundary layer, ϕ while preserving the robustness and performance of the SMC outside the boundary layer. Another advantage is the ability to increase the boundary layer's width and attenuate chattering effect. Nevertheless, validation is carried out on a vehicle equipped with EMs only on front wheels.

Tur et al. discuss the possibility of implementing ABS solely by regenerative braking [115]. An ABS using an electric machine which is modelled as permanent magnet brushed DC machine is compared to the conventional ABS by friction braking. A modified permanent magnet brushed DC machine equations are used to represent an AC machine. The author does not discuss the control algorithm of the ABS in detail. A PI controller is used for the ABS algorithm for both friction braking and electric ABS. A 300Nm electric motor included in the model is connected through gears to match the high braking torque of friction brakes. Simulation results show better performance as the slip reached 20% (longitudinal slip target) at 0.5 seconds faster compared to conventional friction ABS

with a similar control algorithm. The authors only consider single-corner vehicle model and did not validate the proposed design with either double-corner or four-wheel vehicle model.

Article [52] considers an electrified vehicle with IWM and without friction brake system. Again, the author only considers one-wheel vehicle model. The modelling starts with motor dynamics for the IWM. Then, the wheel dynamic equation and longitudinal motion equation is used to derive equations written in state-space form. A nonlinear sliding observer is developed in order to estimate friction force, f_x and vehicle speed, V_x based on two measured parameters; wheel speed, ω and motor current, I_m. Slip control based on SMC is designed considering the slip error. The article does not address any chattering issue in the control design.

Hori uses a prototype EV (modified Nissan March) with individual IWM and without friction brake system installed on the car [49]. The proposed design is to implement an anti-skid control based on the four IWMs as the braking actuator. Two methods are proposed; wheel acceleration control with feedback (called model-following control, MFC) and slip ratio control.

Based on Figure 1.14, the proposed controller works with the assumption of with vehicle body seen as one inertia system:

$$M_{actual} \approx M_w + M_v(1 - s_x) \tag{1.9}$$

$$M_{model} \approx M_w + M_v, \quad (when\ s_x = 0) \tag{1.10}$$

where M_{actual} is the total mass, M_w is the wheel mass, M_v is the vehicle mass, s_x is the slip ratio, and M_{model} is the reference model total mass. The controller will reduce the sudden drop of inertia during high wheel slip. The second method (slip ratio control)

is using proportional-integral (PI) control method illustrated in Figure 1.15. The transfer function is derived from the wheel dynamics equation and the longitudinal vehicle motion equation. Simulation results from both control methods are presented in the article but no comparison is pointed out.

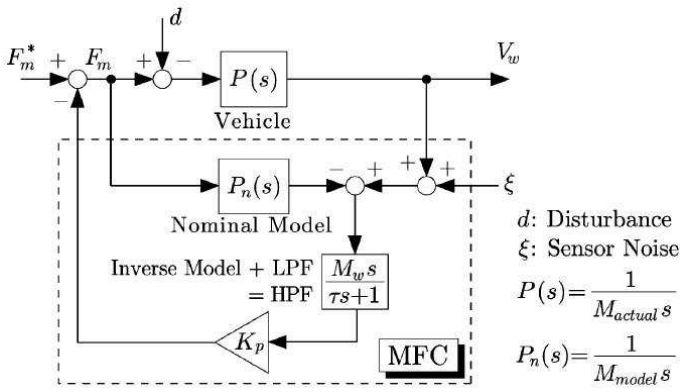

Figure 1.14: Block diagram of MFC in [49].

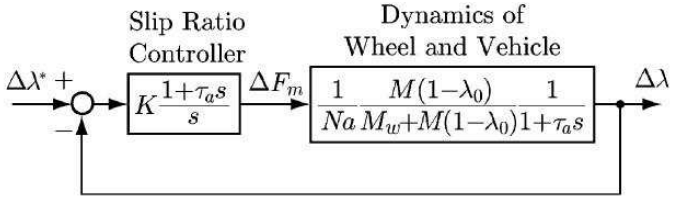

Figure 1.15: Block diagram of PI controller in [49].

Jalali et al. propose a slip control for an EV with four IWMs [56]. The idea is to replace FB in ABS implementation using only electric machines. An FLC method is chosen due to its robustness and flexibility to deal with complex non-linear dynamics system [62]. FLC can tolerate uncertainties and external disturbances introduced by the wheel and vehicle dynamics. The inputs to the controller are slip ratio error, $e(\lambda)$ and rate of change of the slip error, $\dot{e}(\lambda)$ while the output is motor torque, T_{corr}. Figure 1.16 illustrates how the IWMs are implemented for controlling the wheel slip during ABS activation by eliminating the friction brake system. Figures 1.17 and Figure 1.18 show

how the rule table and the range of the surface of the FLC are designed and tuned based on the inputs and output parameters.

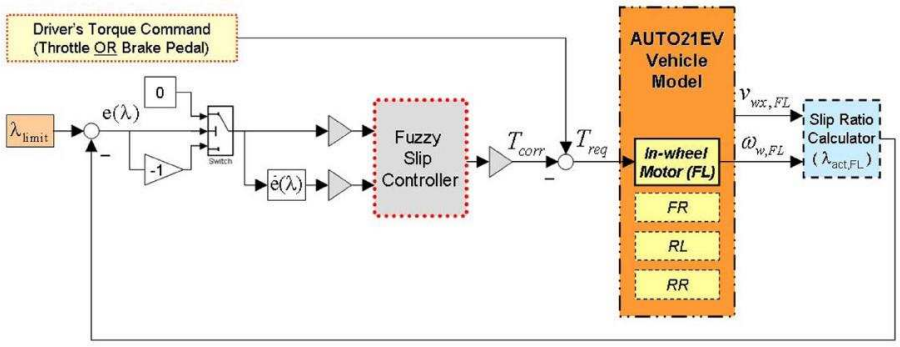

Figure 1.16: Block diagram of proposed FLC ABS in [56].

Control Rule Base		e(λ)			
		ZE	PS	PM	PL
ė(λ)	NL	ZE	ZE	ZE	ZE
	NM	ZE	ZE	ZE	NS
	NS	ZE	ZE	NS	NM
	ZE	ZE	NS	NM	NL
	PS	NM	NL	NVL	NVL
	PM	NL	NVL	NVL	NVL
	PL	NVL	NVL	NVL	NVL

Figure 1.17: FLC rule base table in [56].

Hybrid ABS

ABS application is normally developed and delivered using conventional FB. In recent technological advancements, ABS is also developed using BBW which deliver continuous braking pressure inputs rather than discretely controlled pressure (pressure increase, decrease or hold) [3, 53, 103, 108]. This research aims at delivering a hybrid ABS which can be applied using more than one braking actuator. Advantages of having regenerative

Acronym	Linguistic variable
PVL	Positive very large
PL	Positive large
PM	Positive medium
PS	Positive small
ZE	Zero
NS	Negative small
NM	Negative medium
NL	Negative large
NVL	Negative very large

Table 1.2: Acronym of linguistic variables.

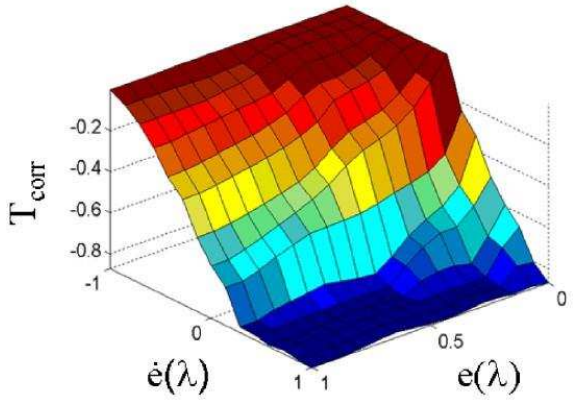

Figure 1.18: FLC control surface in [56].

braking are identified; including better vehicle energy efficiency and improvement of active safety system such as ABS with the use of fast torque response. ABS improvement can be either in terms of shorter braking distance or better steering response.

A proposed design in this doctoral research is to allow only the regenerative braking during ABS stops in certain conditions. For example, on a very slippery surface and with sufficient motor torque available, ABS can be implemented by the RBS to stop the vehicle safely without the need of friction braking. Additional benefits can also be introduced, such as failsafe backup mode feature. As an over-actuated system, both regenerative braking and brake-by-wire can be used as a backup system to each other rather than the

just one-way backup (friction brakes are normally used as backup braking devices for the regenerative braking [29,55]). The fundamental equation for the hybrid ABS design used is:

$$T_{demand} = T_f + T_e \tag{1.11}$$

where T_f is the friction brake torque, T_e is the regenerative brake torque, and T_{demand} is the brake torque demand by the ABS controller.

A novel approach of brake torque distribution method when braking is proposed in [79]. A coordination strategy between regenerative braking by the two electric machines and mechanical friction brakes is presented. The regenerative braking is affected by the state of charge of the battery. A trade-off in utilising friction brakes is high brake torque achieved during high speed or emergency braking but the response is slower compared to electric machine's regenerative braking.

The cooperative control strategy between two braking actuators is based on the slip ratio range both for front and rear axles. The coordination between two brake actuators is constructed around four strategies:

1. Slip ratio 0 - 0.1; both friction and electric braking are applied as braking is in the stable region of $\mu - slip$ curve.

2. Slip ratio 0.1 - 0.2; the electric braking is applied normally whereas the friction braking is held constant. This is near the peak region of the $\mu - slip$ curve.

3. Slip ratio exceeds 0.2; braking torque is set to zero to avoid wheel locking.

4. Full battery SOC; only friction brakes are applied.

For left and right torque distribution, a differential gear is used to deliver the demanded wheel torque. To avoid yaw moment created due to torque imbalance between left and

right in a split-μ manoeuvre, maximum slip between left and right is selected for each axle. In brake torque distribution perspective, regenerative braking is limited to inverters and battery limit. Load transfer between front and rear is considered for braking forces calculation when slip is between 0-0.2. Comparison between different actuators applied during ABS activation is reported. The article states that brake blending capability provides shortest stopping distance as compared to electric machine ABS and friction ABS.

Article [43] proposes to apply only RBS during ABS activation if the torque demand is less than half of the motor torque available. Both FB and RBS share similar slip controller's algorithm which is the SMC. However, the EM is only available on the front axle. The main objectives are to regenerate energy and maintain vehicle stability and steerability during ABS braking events. The results show that more energy can be recovered on low friction coefficient surface due to the longer braking time and distance. Furthermore, more energy is lost as heat converted from kinetic energy from friction braking on a high friction coefficient road. This is caused by higher deceleration demands which will saturate the electric machine's torque. Friction brakes will compensate to satisfy the driver's deceleration command. Both electric and friction braking torques are applied based on the rule-based ABS torque distribution strategy.

Rosenberger et al. propose two strategies in combining two different braking devices in ABS application [99]

1. Constant energy regeneration: This strategy allows the conventional ABS to modulate friction brake torque while regenerative braking torque is held constant.

2. Dynamic split: This strategy considers brake torque modulation by electric machine while friction brakes are maintained at a constant value.

In the second method, several advantages are identified including noise and pedal vibration reduction due to limited hydraulic brake's valve switching. Another advantage

is the faster response and better control quality by the use of EM's high bandwidth.

An ABS algorithm from a series-production car was used without any modification since the research is focused more on the brake torque blending. The signals from the ABS control are bypassed to allow the brake actuators to satisfy the brake torque demand during ABS events. A state machine is used to implement the control logic torque allocation. The concept is to allocate a constant torque to one actuator and dynamic torque modulation to the other. There is no detail discussion for the torque allocation logic but the article states that the constant value torque will be calculated based on both of the actuators' torque limit and EM's torque availability. Each time the applied torque exceeds the torque limits or the difference between applied EM torque and available EM torque exceeds a certain threshold, a new calculation is executed. It is found that with strategy 2, better results can be achieved with 2.63m shorter braking distance compared to the passive system. Initial velocity used is 100km/h and road model used is dry asphalt.

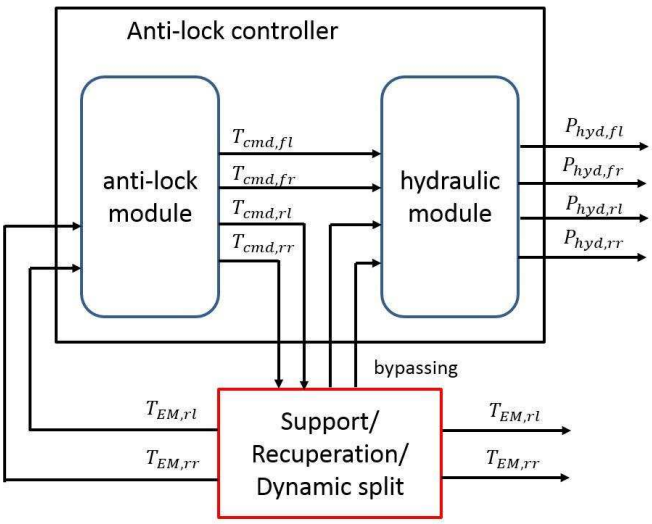

Figure 1.19: Proposed combined ABS actuators in [99].

Ivanov et al. approach in ABS torque blending proposed these strategies [55]:

1. Full EM mode: All torque command is allocated to the electric motors if T_{demand} is

lower than maximum T_e available.

2. Full friction braking mode: Friction brakes will satisfy the T_{demand} during high SOC. Alternate acceleration and braking mode for torque modulation performed by EM using frequency filtering method.

3. Intermediate case: Priority is given to regenerative braking but both actuators are activated in ABS brake modulation.

A coordination algorithm to accommodate both regenerative braking and friction brakes during the ABS cycle is presented in [128]. A combination of feedforward and feedback loop is used to coordinate the two actuators. Fuzzy logic is introduced in the lower level controller to apply the change of friction brake force based on slip error and rate of slip error.

As illustrated in Figure 1.20, the distribution between friction braking and electric motor braking is calculated by comparing the demanded brake force by the driver with the available regenerative brake force based on the speed, the battery SOC, and the present Continuous Variable Transmission (CVT) ratio. Although energy recuperation capability during ABS is proven, the article focuses more on CVT ratio variation problem [13].

In [3], the author presents the idea of blending between EHB and EMB for antilock braking control. The brake blending algorithm is proposed for the case of two braking actuators available on the front axle. In this unique hybrid braking configuration, the article presents the use of combined Eddy Current Brake (ECB) and EHB. ECB is a contactless brake system which uses retarding force generated between eddy current and magnetic flux [71]. Priority is given to ECB during torque demand from the driver while EHB will supplement ECB in case the available torque is insufficient to meet the input command. Nevertheless, the hybrid brake system is used in Internal Combustion Engine (ICE) vehicle instead of HEV. Therefore, the sole purpose of generating energy from the ECB is to

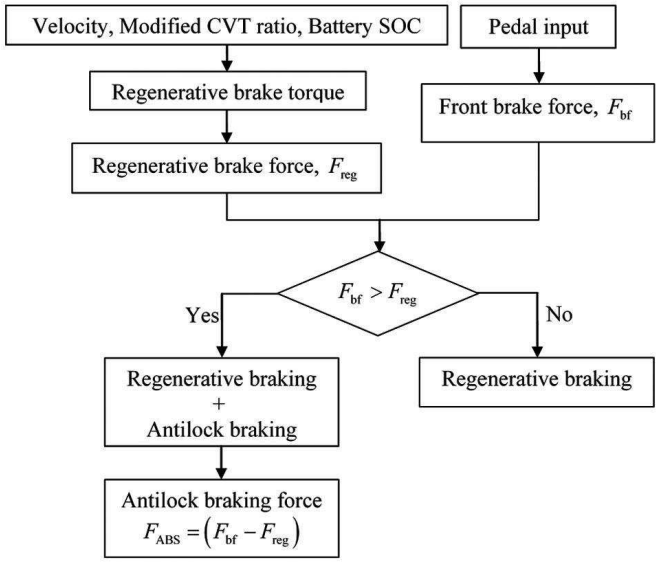

Figure 1.20: Flowchart of brake actuators blending in ABS adopted in [13].

power the system itself rather than for the use of the vehicle propulsion. The author discusses the drawback of using ECB in which the system needs two different power sources including generator and battery. In other words, besides the necessity of an external power source to improve the initial system performance, the brake control algorithm needs to ensure that the net energy recuperated is positive accounting for the ECB consumption of electric power during braking. There is also a possibility of ECB being energized by a battery during low brake torque demand on low road adhesion surface where the generator is not activated. Another limitation is that the ECB torque varies with the wheel speed. EHB or FB has to support during a low-speed condition when ECB torque is very low. Advantages of the ECB include quick response time, smaller in size, no friction materials (brake pads and discs) wear, and no performance deterioration at high temperature [71]. The hybrid brake actuator controller will allocate the ABS torque command to the two actuators for front wheels only. Rear wheel braking has no brake blending and article assumes the torque delivery will be sufficient at all time. The article does not discuss in detail the torque allocation algorithm except stating that the excess torque demand will

be delivered by EHB brakes. There is no validation regarding energy recuperation and lateral stability demonstrated.

A slip control for a hybrid brake system comprises of FB and RBS is presented in [58]. The authors do not discuss the ABS algorithm implemented in detail. There is no strategy of brake torque blending in ABS operation despite there is a control allocation algorithm. The control allocation is only blending the braking actuators during a normal situation where ABS is not active. However, there is a multiplicative weight coefficient according to the slip ratio limit to ensure smooth brake torque transition between regenerative braking and friction brakes during ABS activation.

In [82], two problems are identified concerning the interaction of friction brakes and regenerative braking for ABS implementation. First is the hardware limitation such as energy storage and motor size. Integration of the two actuators could also lead to poor performance during critical braking situation. The article focuses on the comparison of different strategies in the interaction of friction brakes and electric motor's braking when ABS is active. ABS strategies analysed in this article include no brake blending, ramp down of the EM braking (torque modulation by friction brakes), and with brake blending (torque modulation by friction brakes).

The difference between first and second strategy is that the regenerative braking torque is being terminated immediately for the first case during ABS event. On the other hand, the second strategy allows gradual termination of the motor torque before friction brakes take over for ABS torque modulation. For the first strategy, there is a possibility of momentarily lacking brake torque between the transitions of the two actuators. The final strategy proposes motor torque be ramped down during ABS event to a certain value, rather than being terminated. Friction brake is still responsible for ABS torque modulation.

By ramping down motor torque to a certain value for ABS on a high-μ road, results

suggest that higher percentage of energy recuperation is possible but at the expense of slightly longer braking distance. On a low-μ road, ramping down to zero or immediate termination of regenerative braking would increase energy regeneration with a slight penalty on braking distance. However, ramping down the motor torque to a residual value gives adverse effects to both stopping distance and energy recuperation.

Integration of mechanical braking and regenerative braking (EMs connected to the rear axle) for ABS of a series hybrid electric bus is discussed in [114]. The article states that low or zero rotational wheel speed is undesirable to be able to generate power. The method applied is an adaptive rule-based controller but ABS torque modulation is implemented only for electric motor braking. Therefore, there is no ABS application on the front axle for this topology consideration.

The general control algorithm proposed detects the road condition based on slip ratio calculation (slip threshold used is 20% and adapts by decreasing, increasing or holding the brake torque value. The electric machine can be switched to positive acceleration mode if the wheel is locked while there is no regenerative brake torque applied. Comparison between regenerative braking with and without ABS clearly shows that wheel slip can be maintained at a near target value. Additionally, energy recovery during ABS event is vastly improved.

Articles [87] and [88] discuss a control strategy in combining regenerative brake system with friction braking during an ABS event in a parallel hybrid electric vehicle. FLC is used to design the slip controller which then the brake torque output will be distributed to two different braking devices [87]. Different approaches are used for each actuator's ABS algorithm in [88]. Friction braking system uses logic threshold (conventional ABS algorithm based on wheel slip and wheel deceleration control). There are two slip ratio thresholds and the second threshold level will trigger the ABS algorithm for regenerative braking. FLC is designed for electric motor's ABS strategy with slip ratio error and bat-

tery SOC as inputs. The controller's output is the motor torque adjustment, ΔT. Equations 1.12 and 1.13 show the coordination between FB:

$$T_{req} = T_{friction} + T_{motor\_max}\beta \tag{1.12}$$

$$\beta = \frac{T_{motor} + \Delta T}{T_{motor\_max}} \tag{1.13}$$

where β is the electric motor load signal, T_{motor} is the regenerative brake torque, T_{motor_max} is the instantaneous maximum motor torque based on speed, ΔT is the motor torque adjustment by the controller, $T_{friction}$ is the friction brake torque and T_{req} is the input brake torque requested by the driver.

The brake torque allocation strategy used by Yin and Jin in [123] is the same as in [88]. However, the friction brake ABS is using a sliding mode controller with saturation function in order to reduce chattering effect:

$$T_{ABS} = F_x R - T_f - T_m + (1-\lambda)\frac{J}{R}\dot{v} + ksat(\frac{s}{\phi}) \tag{1.14}$$

where F_x is the longitudinal force, R is the wheel radius, T_f is the rolling resistance's torque, T_m is the motor torque, λ is the wheel slip, $\dot{v}$ is the vehicle acceleration, k is the tuning parameter, s is the sliding surface, and ϕ is the boundary layer.

Regenerative brake ABS is designed using a fuzzy logic method with inputs of slip ratio error, battery SOC, and motor speed. The output is the electric motor load signal, β. Results indicate that the longitudinal slip ratio is controlled near the target value and energy recuperation increases battery SOC during ABS activation.

Chiang et al. introduce an integrated ABS strategy on a series braking system [27]. Both RBS and FB have individual slip control strategy and the system can implement ABS using either with RBS only (low deceleration demand) or combined with FB (high

deceleration demand). With an IWM installed in each wheel, individual wheel brake control is allowed for this type of implementation. However, it will be challenging for any axle-mounted EM configuration to deliver good ABS performance without complement from individual friction brakes. The brake torque distribution between the actuators is based on a set of simple rules:

1. if $T_{dem} \leq T_{m\_avail}$, then $T_m = T_{dem}$, $T_{hyd} = 0$

2. if $T_{dem} > T_{m\_avail}$, then $T_m = T_{m\_avail}$, $T_{hyd} = T_{dem}$-T_m

where T_{dem} is the brake torque demand, T_{m_avail} is the available motor torque, T_m is the motor torque applied and T_{hyd} is the friction brake's torque.

The available motor torque, T_{m_avail} is determined by a motor characteristic curve which depends on the maximum power of the motor, the vehicle speed, and the battery SOC. The equation for the available motor torque is as follows:

$$T_{m\_avail} = T_{m\_max} W_{SOC} \tag{1.15}$$

where T_{m_max} is the maximum motor torque and W_{SOC} is the weighting factor for battery SOC. The maximum motor torque depends on the rated motor torque, the motor speed (corresponds to vehicle speed) and the motor rated power. Priority is given to RBS in ABS application and supplemented by FB when necessary to ensure the slip target is satisfied.

Authors proposed an ABS algorithm for the RBS and the calculation for the motor target torque, T_{m_target} based on a slip reference value is done by using the following

equations:

$$T_m = \begin{cases} T_m\,, & 0 \leq \lambda < \lambda_t \\ T_{m\_target}\,, & \lambda_t \leq \lambda \leq 1 \end{cases} \tag{1.16}$$

$$T_{m\_target} = J_w \omega_t + r F_d - T_h \tag{1.17}$$

$$F_d = \frac{T_h + T_m - J_\omega \dot{\omega}}{r} \tag{1.18}$$

$$\dot{\omega}_t = \frac{a(\lambda_t + 1)}{r} \tag{1.19}$$

where T_m is the motor torque applied, λ_t is the slip target, F_d is the estimated friction force between tyre and road, $\dot{\omega}_t$ is the target wheel angular acceleration, a is the vehicle acceleration, T_h is the friction brake torque, r is the wheel radius, J_ω is the wheel inertia and ω is the wheel angular acceleration. The target wheel angular acceleration, $\dot{\omega}_t$ is based on Yin et al. [122], which state that if the wheel acceleration and vehicle acceleration are well controlled, then the wheel slip is well controlled.

A strategy in coordinating RBS and FB for ABS implementation is proposed in article [72]. However, authors only indicate that the priority is given to the friction braking during ABS activation where the EM only acts as auxiliary braking.

Another coordination control strategy between friction braking and electric machine braking during ABS event is implemented using logic threshold control method [111]. Regenerative braking torque will be gradually replaced by the friction brakes at high brake torque demand. In other words, the electric motor will perform ABS braking at low road adhesion but as the brake demand by driver increases, the FB will take over and supply the high torque request. Authors presented the idea of deploying only EM braking (individual wheel braking) during ABS activation but limited for low deceleration demand

and on a low friction coefficient road surface. The article introduces the use of composite ABS control method for the coordination of FB and RBS. Based on the simulation results, wheels are never locked during ABS activation but regenerative braking torque is reduced to zero being replaced by friction braking, hence energy recuperation is not maximised. The result also shows that motor braking torque is available in the early stage of ABS activation but then ramped off once friction brakes are activated.

1.1.3 Optimisation for ABS Torque Blending

In a complex electrified vehicle and over-actuated system, there are numerous combinations of the control strategy in delivering brake torque allocation. If the slip control system and torque allocation strategy are considered as decoupled, the slip controller output is the desired brake torque while the brake torque allocator will specify how the torque should be apportioned optimally between friction brakes and electric motor's braking. This is subject to the consideration of the constraints of the actuators' rate and range limits.

Kanarachos et al. propose a hybrid brake system comprises of RBS, EHB, and EMB. The EHB is used on the rear axle while EMB is only implemented for the front axle [61]. There is a single EM connected on the front axle of the EV. The proposed controller is designed based on state-dependent Riccati equation (SDRE) which is a sub-optimal method for nonlinear systems.

The article proposes a control allocation strategy focusing on maximising regenerative braking by solving a quadratic cost function based on Riccati equation. The algebraic equation is solved online but computational load problem is reduced by deriving an optimum number of iterations. Both soft constraints (included in state dynamics) and hard constraints (penalty matrix function introduced) are taken into consideration in the control allocation design.

The system dynamics block will derive the nonlinear equations of the system to a linear-like state space form. Then, a goal handling block is used to set the constraints of the system which are the motor torque limits and the longitudinal slip of the wheels. A penalty function is included in the original cost function to be minimized. Feedback block is designed based on a linear quadratic regulator (LQR) theory by minimizing the quadratic cost function. The setpoint calculation block will calculate the reference values for the lower level control (for each brake actuators). In the article, the state variables are the forward velocity, lateral velocity, roll angle, yaw angle, yaw rate and the four angular wheels motion. The algebraic Riccati equation is solved online for real-time implementation. Finally, authors made a comparison with a constrained LQR method to demonstrate the advantage of using nonlinear method approach. We note that [61] presents control of vehicle deceleration and does not strictly fall under the classical slip control framework where a wheel slip reference is tracked.

Authors in the article [99] propose the use of dynamic control allocation based on [46]. Unfortunately, the real-time application of ABS with 5ms sampling time cannot cope with the computing time of the optimisation control allocation method. Hence, a state machine (based on control logic) is used to reduce computing time of the optimization algorithm.

Brake torque distribution strategy can be implemented based on Control Allocation (CA) concept [14, 46, 91, 92]. Online or real-time optimisation can be computational demanding but with simplification in terms of numerical algorithm calculation could enable real-time implementation. In article [29], the braking torque allocator between friction brakes and electric machine is proposed using dynamic CA concept. As illustrated in Figure 1.21, the article proposes a two-layered hybrid ABS concept which decouples the slip control algorithm and braking torque allocator. The torque allocator block implements the dynamic CA method. The distribution is based on the actuators' different bandwidths. Additionally, constraints based on actuators' range and rate limits are considered. Work-

ing in discrete time, the optimisation problem can be mathematically formulated as follows:

$$\begin{aligned} &\underset{T_f,T_e}{\text{minimize}} \quad \alpha_f T_f^2 + \alpha_e(T_e)T_e^2 + (\beta_f(T_f - T_f[k-1])^2 + \beta_e(T_e - T_e[k-1])^2) \\ &\text{subject to} \quad T_f + T_e = T_w,\ T_i^{min} \leq T_i \leq T_i^{max},\ i \in \{e,f\}. \end{aligned} \tag{1.20}$$

$$\alpha_e(T_e) = \begin{cases} \alpha_e^- , & T_e < 0 \\ \alpha_e^+ , & T_e \geq 0 \end{cases} \tag{1.21}$$

where α_f and α_e are the penalty weights for both actuators, β_f and β_e are the weights for dynamic penalty. The constraints are the actuators' range and limit. Equation 1.21 indicates the two modes of EM considered, including acceleration, α_e^- and regeneration, α_e^+.

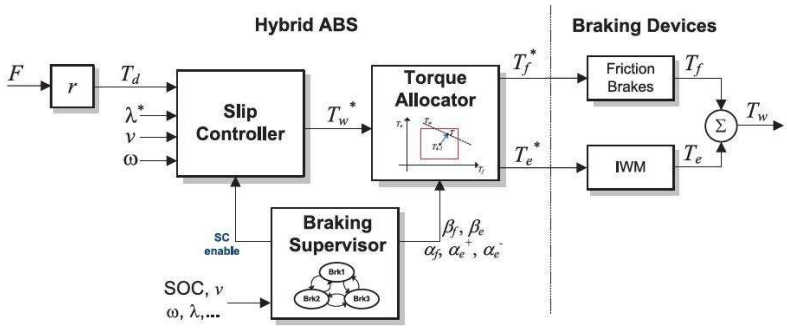

Figure 1.21: Overview of hybrid ABS proposed in [29].

Friction brake has high torque limit but only positive torque (with the assumption of positive torque is braking torque). The rate is limited to the physical constraint of the brake pressure and force by the hydraulic system. On the other hand, electric machine's torque limit varies based on SOC and wheel speed with both positive and negative (acceleration torque). The rate limit is usually high depending on the current rate of the batteries being charged. Having redundancy of braking actuators allows the torque allocator to

choose a combination of braking torques to achieve the objectives of the brake blending. Regenerative braking is usually given the priority not only to recuperate energy but due to its larger bandwidth compared to FB. In this case, the torque allocator has to consider brake torque demand frequency in formulating optimisation problem. The cost function comprises of two parts; penalisation of each braking devices and their bandwidth weight assignment. Another challenge in torque allocation strategy is the selection of weights for the brake actuators which have to consider their characteristics, EV operational mode and designer's intentions. Torque-sharing ratio (desired) between actuators can be defined based on frequency. Finally, the numerical solver is used to calculate the pair of torque allocator weights for each actuator to follow the desired torque-sharing ratio defined. The article uses linear filtering approximation (simplified case) and then move to numerical solver method [45] for real-time implementation. Results indicate that individual wheel slip is controlled near to reference value by both braking actuators.

Satzger et al. propose a brake blending strategy for hybrid ABS in EVs using Model Predictive Control (MPC) for torque allocation [101]. Similar to [29], and as shown in Figure 1.21, the article decouples the slip controller and torque allocator. The objective is to find the actuator setpoints in minimizing the cost function subject to actuators' dynamics and constraints. The formulation approach is based on [120] and [44]. The article claims that MPC allocation method is able to incorporate the actuators' delays and high-order models in the formulation. Authors use MPC combined with CA to handle the actuator range and rate limitations (inequality constraints) and the actuator dynamics (equality constraints). Main advantage claimed is the systematic approach in dealing with the actuator dynamics, thus the torque blending process able to handle more complex and accurate actuator models. Articles compare the MPC allocation method with the dynamic CA implemented in [29] and a static CA method called Daisy Chain (DC). However, the computational time is claimed to be longer than dynamic CA approach.

Article [29] proposes a torque allocation strategy using optimization methods which consider the two brake actuators dynamics. The disadvantage lies with decoupling of the slip controller and the torque blending algorithm, which requires the calculation of the required total braking torque and the actuators braking torque independently. The proposed approach achieves robustness in wheel slip tracking in the presence of tyre-road adhesion variations by incorporating an adaptive slip control algorithm. A linear MPC method is proposed for the torque allocation to work along with a linear slip controller in [101]. This approach still requires an independent slip control algorithm to determine commanded ABS torque before the allocation procedure can take place. A combined slip control and torque allocation algorithm using linear MPC is presented in [102]. The authors demonstrate the enhanced performance of the controller compared to cascaded control approaches, as in [29] and [101]. The MPC controller of [102] uses a low order internal model of slip dynamics, which is linearised with respect to the desired equilibrium condition, assuming slowly varying speed when compared to wheel slip variations. An interesting discussion on stability and robustness of the linear MPC scheme for slip control is presented in [102], considering, however, the unconstrained problem.

In this research, we plan to develop linear and nonlinear MPC strategies for handling both slip control and brake torque integration taking into account the actuators constraint. The plan is to compare both optimal and static control allocation proposed methods with the capability for real-time implementation. Moreover, the challenge will be the integration of the MPC strategy with the electrified AWD vehicle topologies of the project using four EMs, two EMs and one EM.

1.1.4 Hybrid Electric Vehicle Architectures

The vehicle topology plays an important role in designing a controller that will work efficiently and robust to various situations. There are three different HEV configurations planned for the research within the *Evoque_e* project. This section discusses the HEV architectures that are considered in delivering the aim of the research.

Plug-in Hybrid Electric Vehicle

A Plug-in Hybrid Electric Vehicle (PHEV) has two different power sources (Internal Combustion Engine (ICE) and electric motors with energy storage) which can propel the vehicle independently. It is also known as Range-Extended Electric Vehicle (REEV) which the ICE is used once the energy is exhausted by the EM [77].

A PHEV with single EM connected through gears and propeller shafts attached to all wheels is considered in this research. Equal motor torque distribution is delivered to each wheel. If we look at ABS controller design, there is a challenge in integrating the regenerative braking and friction braking due to the limitation of the topology. Firstly, there is no individual wheel braking capability. In addition, the lack of independent axle braking will also be challenging for the brake torque blending during ABS activation to compensate the load transfer effect. Hence, supplementary brake torque by EHB is necessary to overcome the limitation of the vehicle configuration.

Yin and Jin introduce a vehicle architecture with EM on front axle only [123]. Similarly, Guo and Wang use a single electric machine on the front axle with conventional friction braking for each wheel [43]. Based on the availability of motor braking torque, a strategy to distribute the brake torque demand, T_d to two different actuators were defined only for the front wheels. The article considers the possibility to apply regenerative braking during ABS events only on the front axle. These articles propose a coopera-

tion strategy between FB and RBS during ABS application. The topology considered by Zhang et al. is that of a hybrid vehicle with one electric machine connected to rear axle through differential and gearbox [128].

All PHEV topology discussed above have introduced coordination strategy for regenerative braking and friction brakes blending in ABS implementation but share no similarity with the 4WD PHEV configuration in *Evoque_e* project.

Battery Electric Vehicle

A Battery Electric Vehicle (BEV) is propelled by the electric motor without any ICE support [69]. Li et al., Kanarachos et al., and Jing et al. discuss a BEV topology with single EM driving front wheels in the article [72], [61], and [58].

Bera et al. on the other hand apply the developed strategy on a BEV architecture with single EM on the rear wheels through a CVT in [28]. Rosenberger et al. introduce the prospect of supplementing the friction braking during ABS event with an electric machine as an additional actuator [99]. A single motor with side shafts connected through each of the rear wheels is used. The article mentions the capability of expanding the topology to both axles but does not discuss in further details. The stiffness of the powertrain is reduced with the presence of the side shafts and highly sensitive to torsional vibrations. Guo and Wang implement their proposed method using a BEV with two EMs on the front wheels [43]. This allows the electrified vehicle to have independent wheel torque control by the electric motors only for the front wheels.

The electric vehicle's topology used in article [79] consists of one electric motor on each of the front and rear axles, connected through shafts with gears. Front and rear axles can be controlled independently for both acceleration and braking. The article suggests that this configuration has advantages in stability during acceleration and braking events.

Load transfer and wheels locking due to deceleration could lead to instability of the vehicle especially during cornering or on low adhesion road surface. Comparisons are made between two axles-wheel driven EV, rear-wheel driven EV, and front-wheel driven EV in terms of stability and braking performance. Most importantly, the article considers the ability to brake safely on low road surface friction coefficient (road μ=0.1). As expected, the two axles-wheel driven EV achieves shorter braking distance compared to the rear-wheel driven EV. This is due to the ability to compensate load transfer between front and rear axle for better braking performance. The authors propose a propulsion torque distribution method to avoid instability problems of cornering during acceleration on the low-μ surface but it is not relevant to this research topic.

A BEV architecture with an independent axle motor-driven vehicle is considered for this research. One key advantage of this topology compared to the PHEV is that braking torque on each axle can be exploited to compensate load transfer but there is no individual wheels control similar to IWM's topology. However, the friction brakes (EHB) are used to compensate this drawback. This type of configuration (independent axle-motor and with EHB) also never been covered in the literature.

AWD BEV with four EMs

Another interesting modern electrified vehicle architecture included in this research project is the all-wheel drive (AWD) BEV implemented by either In-Wheel Motors (IWM) or On-Board Motors (OBM) (OBM is also known as Near-Wheel Motor (NWM). To demonstrate individual wheel control strategy, four IWMs provide the opportunity in delivering direct wheel torque application without the needs of differentials and gears. With the increase of unsprung mass for each corner modules, there are adverse effects towards the vehicle's handling and ride quality [28, 78]. However, the implementation of IWMs

can avoid the issue of torsional vibration of the drivetrains. Hence, control quality is better as the net torque applied by the controller has higher accuracy.

Murata [78], De Castro et al. [29], Chiang et al. [27], and Song et al. [111] present the idea of method using four IWMs for ABS in coordination with FB. Murata validates the improvement of ABS performance with the use of IWMs with the support of friction brake as compared to conventional friction ABS on a road of μ=0.1. Higher actuation frequency of the electric motors enhances the performance of ABS which helps to reduce stopping distance on low-μ condition. This type of vehicle topology avoids propulsive and braking torque transmitted through mechanical differential thus giving independent wheel control. Another observation is how the acceleration mode of IWM could reduce quick slip response during ABS event [29].

Hsiao and Lin [52], Jalali et al. [56], and Hori [49] report the application of ABS using IWMs. However, these articles do not consider any brake torque blending capability between different actuators.

Ivanov et al. present the design and testing of ABS for EV equipped with four NWMs in article [55]. The topology considered is an electrified Sports Utility Vehicle (SUV) with two different braking devices; individual controlled electric machines and EHB system. Another similar work in testing state-of-the-art ABS control using IWM is done by Akaho et al. [1]. Ivanov et al. however focus on NWM connected through half-shaft and gearbox instead of IWM. The challenge is to consider the torsional dynamics of the drive train during ABS event.

An AWD electric vehicle driven by four EMs is considered in this research. With high torque capacity for each EM used for such light vehicle weight, there is a possibility to introduce an e-ABS (and even e-TCS) and minimize the use of friction brakes during ABS activation.

1.1.5 Test Manoeuvres

Test procedures are very important in evaluating certain criteria during vehicle design and development. Most articles found in the literature validate their work using simulation testing. Only a few works validated the developed method using real vehicle hardware. It is critical to choose appropriate test manoeuvres to assess the performance of the proposed control design and strategy.

In terms of ABS testing, a straight line braking is the standard practice to validate the controller performance similar to what has been tested in [114], [78], [29], [123], [27], [72], [87], [88], [43], [3], [13], [52], [58], [55], [128], [82], [115], [56], [79], [99], [111], and [61]. Generally, the road surface types used include different road friction coefficient (varies from μ=0.1-1.0) to represent actual road conditions such as dry asphalt, wet asphalt, packed snow and polished ice.

Article [29] and [27] validate the proposed control design using simulations environments on a μ-jump road (road surface transition either from low-μ to high-μ or vice versa). This braking test manoeuvre is used to evaluate the adaptability of the slip control to road surface change and robustness check.

Most literature covered states the advantage of the proposed controller in controlling wheel slip during hard braking and maintaining the vehicle lateral stability but do not present results of such manoeuvres. Only [49] considers braking in turn manoeuvre in evaluating the ABS performance in combinations of longitudinal and lateral movements. It is worth to note that for the non-ABS case, the vehicle will lose its stability due to the wheel locking. On the other hand, a vehicle equipped with ABS will maintain the steering response and can be stopped safely.

A μ-split braking manoeuvre simulation is performed in [27], [82], [56], and [79] to evaluate the ABS performance. The vehicle is decelerating on a road with different

friction coefficient on the left and the right side. Braking on different road adhesion on both sides will create torque imbalance (yaw moment towards the high-μ side of the road) and without ABS, the vehicle will lose the stability and may spin out.

Only [3] includes a braking while changing lane test manoeuvre. This is another relevant assessment of the ABS performance in maintaining the vehicle steerability and stability. With ABS, wheel locking can be avoided and the vehicle can steer to change the lane safely to prevent a collision.

In this research, we consider both longitudinal and lateral motions of the vehicle in evaluating the proposed control design.

1.1.6 Literature Review: Summary

As has been highlighted in the previous sections, several key articles are presented in table form to highlight the gaps identified. Table 1.3 shows the summary of the literature survey covered in this report in certain key areas which include the vehicle architecture, ABS algorithms, brake torque allocation strategy, and validation methods including test manoeuvres.

Reference	Topology	ABS and actuator(s)	Torque allocation	Validation
Guo [43]	BEV: FWD, 2 EMs	FB and EM: SMC with FLC	Simple rule-based	Simulation (no detail): Straight line (various μ)
De Castro [29]	BEV: 4WD, 4 IWMs	EHB and EM: Adaptive slip controller with gain scheduling	Dynamic CA	Simulation (CarSim): Straight line (various μ, μ-jump)
Satzger [101]	BEV: 4WD, 4 IWMs	EHB and EM: Gain scheduling PI	linear MPC	Simulation: Straight line
Satzger [102]	BEV: 4WD, 4 IWMs	EHB and EM: linear MPC	linear MPC	Simulation (Dymola): Straight line μ-jump
Ivanov [55]	BEV: 4WD, 4 NWMs with half-shaft and gear	EHB and EM: Feedback (PI) with feedforward	Simple rule-based with frequency filtering	HiL simulation (CarMaker): Straight line (various μ)
Rosenberger [99]	BEV: RWD, 2 EMs with side shaft	FB and EM: OEM	State machine rule-based	Simulation (Adams/Car): Straight line
Chiang [27]	BEV: 4WD, 4 IWMs	FB: logic threshold and EM: slip based torque adjustment	Simple rule-based	Simulation (CarSim): Straight line (various μ, slip-μ)
Kanarachos [61]	BEV: FWD, 1 EM	FB, EMB and EM: State dependant Riccati	Quadratic function minimisation	Simulation: Straight line (various μ, slip-μ)
Mutoh [79]	BEV: FRWD, 2 EMs	FB and EM: rule-based	Simple rule-based	Simulation and vehicle: Straight line (various μ) and split-μ
Yin [123]	HEV: FWD, 2 EMs	FB: SMC and EM: FLC	Simple equation	Simulation: Straight line and NEDC
Peng [88]	PHEV: FWD, 2 EMs	FB: logic threshold and EM: FLC	Simple equation	Simulation and vehicle: Straight line and NEDC

Table 1.3: Literature summary.

Table 1.3 shows the categorized summary of main articles in this literature survey. Mainly, the investigation focuses more on the ABS control strategy being used, cooperation algorithm between two different braking actuators in ABS operation, and Electric ABS feasibility.

It can be observed that this doctoral research will contribute in few areas;

1. Integration of EHB and EMs for ABS application in different HEV topologies. Several articles suggest blending strategy approach to phase out the RBS during ABS activation while some implement rule-based algorithms to integrate FB and RBS. Both De Castro et al. [29] and Satzger et al. [101] proposed using optimisation methods for brake torque allocation for ABS implementation. We will formulate a pragmatic approach using a combination of Daisy Chain (torque allocation) and Sliding Mode Control (slip control) to delivering the integration of ABS (using EHB) with RBS which produce close to the results of an optimal method.

2. Develop a strategy to integrate wheel slip control and torque blending using nonlinear MPC. The braking actuator dynamics are applied as constraints for the optimal control strategy. The strategy will take into account the actuator dynamics and limitations with rigorous optimal constraint but more computationally intense. Majority of the works in the literature do not propose an optimisation method in this research area. De Castro et. al [29] develop dynamic CA for torque blending algorithm while Satzger et. al [101] develop linear MPC method for torque allocation strategy. In this research, we formulate a nonlinear MPC strategy to solve multi-variable objectives which include wheel slip control and torque blending between EHB and EM. A linear MPC using similar method is also developed for comparison. Moreover, the proposed strategy is further developed to be implemented on different vehicle architectures (using one EM, two EMs and four EMs).

3. Testing and validating the proposed optimisation strategies for real-time implementation using dSPACE hardware. The state-of-the-art nonlinear MPC strategy for integration of slip control and torque blending is deployed using rapid control prototyping to study the feasibility of real vehicle implementation. We also compare against the linear MPC method and study the deployment for implementation on different vehicle topologies.

4. Testing and validation of proposed design using high-fidelity vehicle model in CarMaker for different topologies of test vehicles which include both longitudinal and lateral motion manoeuvres. The articles found in the literature are based on simulation validation limited to a single vehicle topology. Moreover, most of the works focus on evaluating only the longitudinal motion performance.

1.2 Research Aims and Objectives

The aims of the doctoral research are presented in this section. These aims are based on the knowledge gaps identified in the literature review. Several objectives are listed to achieve the research aims followed by appropriate proposed methodology. The main aim of this doctoral research is to integrate anti-lock brake system with the regenerative brake system for hybrid electric vehicles with two braking actuators. The brake blending design will deliver acceptable stopping distance, maintain vehicle stability and manoeuvrability with the ability to improve energy recuperation.

The proposed design is meant to enable the driver to maintain control ability of the vehicle during ABS braking event (either in an emergency situation or on the low-μ road surface). Another important impact is the capability to regenerate energy for future use of the HEV where it is not possible previously (in mass production vehicle).

List of objectives for implementation are listed below in the process to reach the aims:

1. Slip control: Development of slip controller for implementation in hybrid/electric vehicles. In this work, we present wheel slip control algorithms using SMC. An ABS supervisor is also developed to manage the activation strategy for the slip control with respect to various factors.

2. Torque blending of EM and EHB for ABS: Brake torque blending strategy for the two brake actuators are proposed in this research using a static torque allocation (Daisy Chain) algorithm. An e-ABS braking scenario (i.e. Low-μ braking with low deceleration demand) is also discussed.

3. Integration of wheel slip control and torque blending using optimisation: The wheel slip control and brake torque blending problems are combined and developed in a single optimisation formulation. A comparison between nonlinear and linear MPC methods is also discussed.

4. Vehicle topology application: The application of the proposed control algorithms using different AWD electrified vehicles is reported (one EM, two EMs, and four EMs).

5. Simulation using high-fidelity model: Verification of the proposed control strategies through simulation from simple model to full vehicle model in Matlab/Simulink and CarMaker environment.

6. Testing and validation: Different test manoeuvres to consider longitudinal and lateral movements (Straight line braking, μ-split braking, braking in turn etc.) of the vehicle to validate the performance of the proposed controllers for proof of concept.

7. Evaluation criteria: Different criteria in assessing the performance of the controller and strategy proposed (performance metrics including slip reference and torque tracking, energy recuperation, stopping distance, steering angle, and yaw rate).

Chapter 2

Vehicle Topologies and Modelling

It has been discussed in the previous chapter that the main aim of this work is to develop torque integration strategies for slip control using redundant braking actuators available in electrified vehicles. It is planned to validate the proposed state-of-the-art control strategies on various HEV topologies which include one EM, two EMs and four EMs for the *Evoque_e* project. The designed methodology can be flexibly developed to work in the various vehicle architectures. Then, the validation process includes desktop computer simulation and real-time implementation using HiL simulation. With this in consideration, the control algorithm developed needs to be pragmatic in order to implement the controller on the actual vehicle hardware.

The primary objective of this work is to develop torque blending strategy for slip control system. To achieve this objective, we adopt a vehicle and wheel dynamics model in the design of the controller. Even though we use only the longitudinal dynamics to develop the controller, the performance will be evaluated for both longitudinal and lateral motions. For the latter, we use high-fidelity vehicle models developed in Matlab/Simulink and CarMaker to create a simulation environment representing the real-vehicle testing. In this work, the proposed control strategies are designed for different vehicle topologies

which are presented in the following sections.

This chapter discusses the vehicle dynamics model used for the development of the control strategies, HEV topologies covered in this research project, and the high-fidelity models used for the validation purpose.

2.1 Vehicle Dynamics

For the controller design, we adopt a single-wheel or quarter car model as shown in Figure 2.1. Equations 2.1 - 2.2 are based on wheel rotational dynamics and vehicle longitudinal motion [57, 83]. Equation 2.5 determines the longitudinal wheel slip, which indicates the relative velocity between vehicle and tyre. The wheel slip, $s_x = 0$ means that the wheel is in free rolling condition, while $s_x = -1$ indicates a locked wheel, and $s_x = \infty$ means that the wheel is spinning without any translational motion. Therefore, the main aim of the ABS control strategy is to maintain the wheel slip within an acceptable region to avoid wheel locking situation.

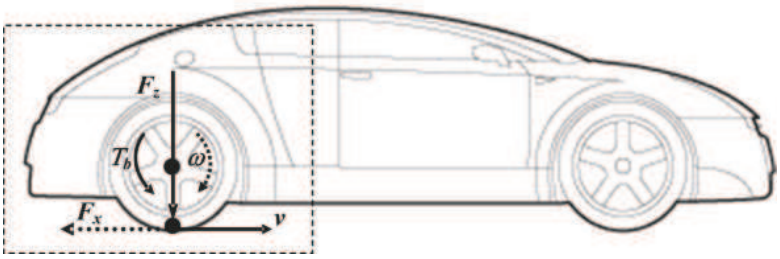

Figure 2.1: Quarter car model during braking (adopted from [103]).

$$\dot{\omega} = \frac{T_b - F_x R_w}{J_w}, \tag{2.1}$$

$$\dot{V}_x = \frac{F_x}{m}, \tag{2.2}$$

$$F_x = F_z \mu, \tag{2.3}$$

$$T_b = T_e + T_h, \tag{2.4}$$

with V_x the wheel's forward velocity, ω the angular wheel speed, F_x the tyre's longitudinal force, F_z is the vertical force on the tyre, μ is the tyre-road friction coefficient, T_b the total torque applied on the wheel and R_w, J_w and m the wheel's radius, moment of inertia and quarter vehicle mass respectively. For our torque blending strategy, the T_b is the summation of the torque from the electric motor T_e and the torque from the friction brake T_h.

In the above model, F_x is set as a function of longitudinal slip, s_x through a simplified version of Pacejka's Magic Formula (MF) [6]:

$$s_x = \frac{\omega R_w - V_x}{V_x} \tag{2.5}$$

$$F_x = F_z D \sin(C \text{atan}(B s_x)), \tag{2.6}$$

where B, C and D are the MF's factors. The vehicle and tyre parameters used in this work can be found in Table 2.2. The various types of tyre-road friction coefficient μ used for the test environment in this research is presented in table 2.1 [96]. In this work, we neglect the lateral motion of the vehicle and concentrate on simplified longitudinal motion of the vehicle. The rolling resistance and aerodynamic forces are also neglected in formulating the proposed controllers.

When a four-wheel model is employed considering only the longitudinal direction,

a quasi-static representation is used to describe the longitudinal load transfer which we adopted from [57, 118]. By considering the static weight and the weight transfers by longitudinal accelerations, the normal load on the front f_{Fz} and rear f_{Rz} wheels can be determined:

$$f_{Fz} = f_{Fz}^0 - \Delta f^x, \qquad f_{Rz} = f_{Rz}^0 + \Delta f^x, \tag{2.7}$$

which the static vertical loads are:

$$\begin{aligned} f_{Fz}^0 &= \frac{mgl_r}{l_f + l_r}, \\ f_{Rz}^0 &= \frac{mgl_f}{l_f + l_r}, \end{aligned} \tag{2.8}$$

and the changes in the vertical load due to longitudinal acceleration a_x is given by:

$$\Delta f^x = \frac{mh}{l_F + l_R} a_x. \tag{2.9}$$

Road surface	μ
Dry asphalt	1.0
Gravel/Wet asphalt	0.5
Packed snow	0.3

Table 2.1: Types of road surface with μ.

2.2 Hybrid Electric Vehicle Powertrain

We will use the high-fidelity model in Matlab/Simulink and CarMaker environment to validate the developed control strategies. In this section, we present various vehicle topologies used in the research project and modelling of each component required for

the proposed algorithm to be implemented. The main common components for the HEV topologies covered in this project are an electric machine (acts as a motor in tractive mode and as a generator during recuperation), and an energy storage system (battery). These components are modelled in Matlab/Simulink and the vehicle parameters and test environment (road surface and test manoeuvre) are used in CarMaker.

2.2.1 AWD Battery Electric Vehicle (BEV) with Four EMs

An interesting topology available for an EV is an AWD with individual wheel motor for traction and regenerative braking capability. This configuration is less complex as it does not require gearing or differentials and provides greater independence in wheel torque control (both acceleration and braking).

The vehicle topology considered comprises of four EMs as shown in Figure 2.2. The EM is an AC 3-phase PMSM and each EM is connected to each wheel without any gearbox. The EM is capable of delivering maximum power of 200kW peak and a continuous power of 75kW. The speed-torque characteristic curve is shown in Figure 2.3. There is an opportunity to develop a slip control using only EM (e-slip control) for both acceleration and braking with individual wheel control capability.

2.2.2 AWD BEV with Two EMs

Another vehicle topology covered in the *Evoque_e* project is a fully electrified vehicle with two EMs. Figure 2.4 shows an AWD BEV architecture implemented using two EMs. This topology considers pure electric machine for vehicle propulsion with one EM connected through gearbox on each axle.

There is a gearbox and a final drive for the transmission for each axle. The torque applied to the wheels is equal between left and right wheels on the same axle but there

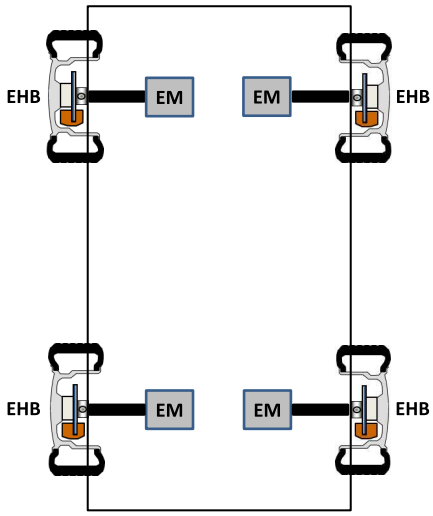

Figure 2.2: AWD BEV with 4 EMs.

is a potential to implement independent control for front and rear axles. The regenerative braking torque for each wheel on the same axle is then

$$T_e^i = 0.5T^e, \tag{2.10}$$

where T_e is the total regenerative torque for the axle and $i \in \{left, right\}$ denoting left and right wheels.

The vehicle is equipped with similar 3-phase AC PMSM for each axle. This topology has a coupling between left and right wheels for the regenerative braking torque. The advantage of the topology is having independent regenerative braking capability with the axle motor. This allows less restricted torque blending strategy compared to an AWD topology using single EM.

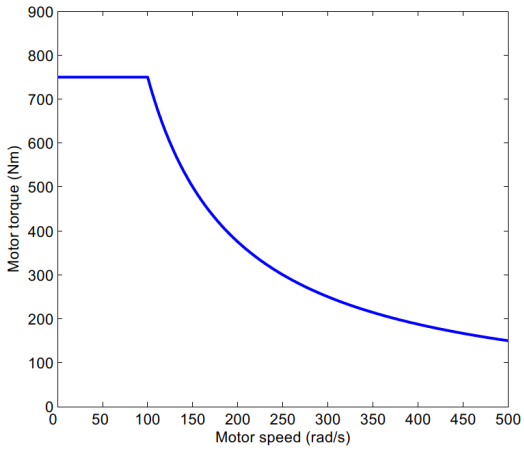

Figure 2.3: Static torque map for Delta E4 (adopted from [109]).

2.2.3 AWD Plug-in Hybrid Electric Vehicle (PHEV) with single EM

An AWD PHEV model with a single EM and an internal combustion engine (ICE) is one of the vehicle topology available in the *Evoque_e* project. The general vehicle configuration is illustrated in Figure 2.5. A common engine shaft links the ICE and the EM in a parallel hybrid configuration. The combined torque by ICE and EM is delivered through the shaft to the gearbox. There is a clutch to engage and disengage the ICE torque to the shaft as shown in Figure 2.6.

The drivetrain has an open differential and in tractive mode, the total torque applied to the wheels depends on the operating gear (gear ratio) and final drive ratio as illustrated in Figure 2.7 [85]. In regenerative braking mode, the engine shaft is rotating due to the mechanical rotation of the wheel. The regenerative braking torque available to the EM is calculated based on the corresponding gear and the final drive ratio. A unique feature for an AWD PHEV drivetrain is that the front and rear axles are coupled via a propeller shaft. This allows equal torque distribution between axles and referred to as 50-50 distribution. In the event of any of the wheels is about to lock, there will be no regenerative torque available to the EM due to this configuration. This situation develops the motivation

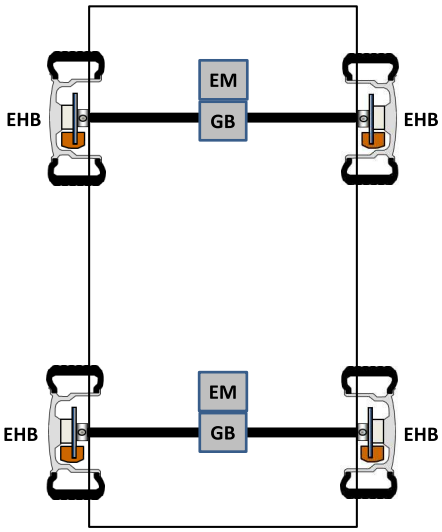

Figure 2.4: AWD BEV with two EMs.

of this research, to integrate the slip control with regenerative braking which allows the energy recuperation while avoiding wheel-lock. The regenerative braking torque for each wheel is then

$$T_e^{i,j} = 0.25T^e, \tag{2.11}$$

where T_e is the total regenerative torque, $i \in \{front, rear\}$ and $j \in \{left, right\}$ denoting each of the four wheels.

For this work, we adopt from Delta E4 vehicle and implement the same vehicle and tyre model between the three vehicle topologies for fair comparison of the proposed controllers. The main difference will be the available regenerative braking torque which varies depending on the availability of the EM.

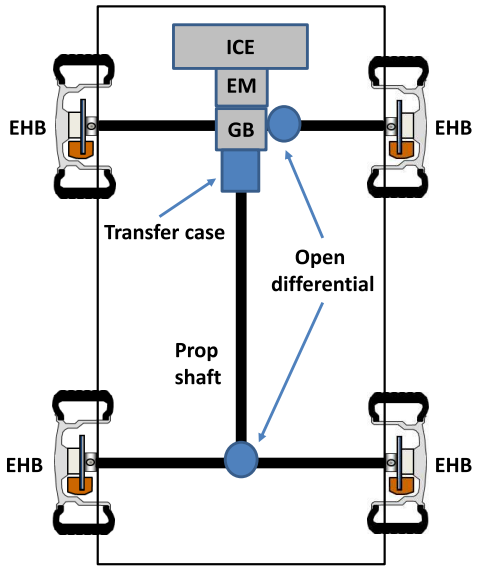

Figure 2.5: AWD PHEV with single EM.

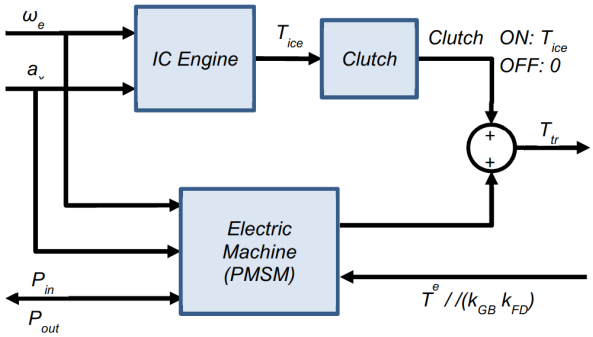

Figure 2.6: PHEV drivetrain (adopted from [85]).

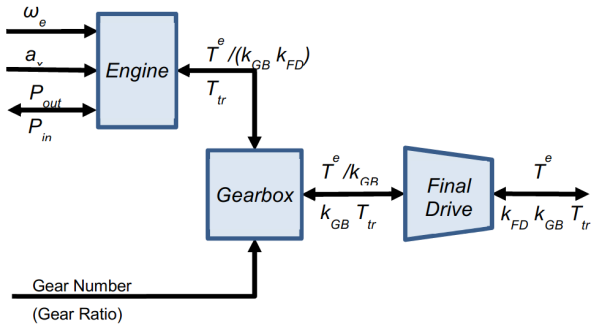

Figure 2.7: PHEV powertrain (adopted from [85].

2.3 Modelling in Matlab/Simulink and CarMaker Environment

In this section, we present the vehicle models from the *Evoque_e* project to be adopted in this research as provided by Jaguar Land Rover and Delta Motorsport. The model is used in simulation testing to virtually represent the actual behaviour of the prototype vehicle for the project. Although three different electrified vehicle configurations are used in this work, the implementation is carried out using one vehicle parameter (sports coupe) for consistency.

The controller is developed with a simple vehicle model as a single wheel or quarter car model which only consider the longitudinal motion of the vehicle as presented in 2.1. Considering the vehicle topology, the longitudinal four-wheel model can be adopted in the controller formulation to consider the longitudinal load transfer between front and rear axles. Finally, it is crucial to validate the proposed strategies against high-fidelity vehicle model with a more realistic environment. The evaluation is carried out in a co-simulation between Matlab/Simulink and CarMaker environment. The vehicle and tyre parameters considered in this work are presented in table 2.2.

An open integration and test platform by IPG CarMaker is chosen in this research for validation through PC simulations [4]. The CarMaker can be easily integrated with the models developed in Matlab/Simulink. Another advantage of the software is the capability to extend it to the HiL testing. For the PC simulations stage, test scenarios can be constructed according to the system validation objectives. From fully nonlinear vehicle models to sophisticated driver model, the software offers good simulation results which are close to real vehicle testing [81]. The total resistance to the vehicle motion from the aerodynamic drag and rolling resistance are taken into account in the validation process.

We use IPG driver model in CarMaker which controls the acceleration, clutch and gear shifts, and brake pedals and the steering wheel. The advantage is that the consistency of the driver model ensures best repeatability and consistency for closed loop test. The software also allows external manual driver inputs for robustness check by human driver rather than driver model.

Parameter	Unit	Value
vehicle mass	m (kg)	1137
CM height	h (m)	0.317
CM distance from front axle	l_f (m)	1.187
CM distance from rear axle	l_r (m)	1.313
CM distance from left wheel	w_L (m)	0.687
CM distance from right wheel	w_R (m)	0.687
wheel moment of inertia	Jw (kgm^2)	1.04
wheel radius	R_w (m)	0.298
MF's stiffness factor	$B(-)$	7
MF's shape factor	$C(-)$	1.6
MF's peak factor	$D(-)$	0.3, 0.5, 1.0

Table 2.2: Vehicle and tyre parameters.

2.3.1 Control Structure

A systematic approach 'Integrated Vehicle Control Structure' [110] is adopted for the control structure for the *Evoque_e* project to coordinate multiple vehicle dynamics control and redundant actuators. M. Polesel et. al [93] and Pennycott et. al [89] implemented similar approach in an over-actuated vehicles. It was decided as part of the Work Package 2 *Evoque_e* project to implement the developed controller in this work within the IVCS. Figure 2.8 shows the hierarchical structure of the IVCS which comprises of supervisory control, high-level control and low-level control blocks.

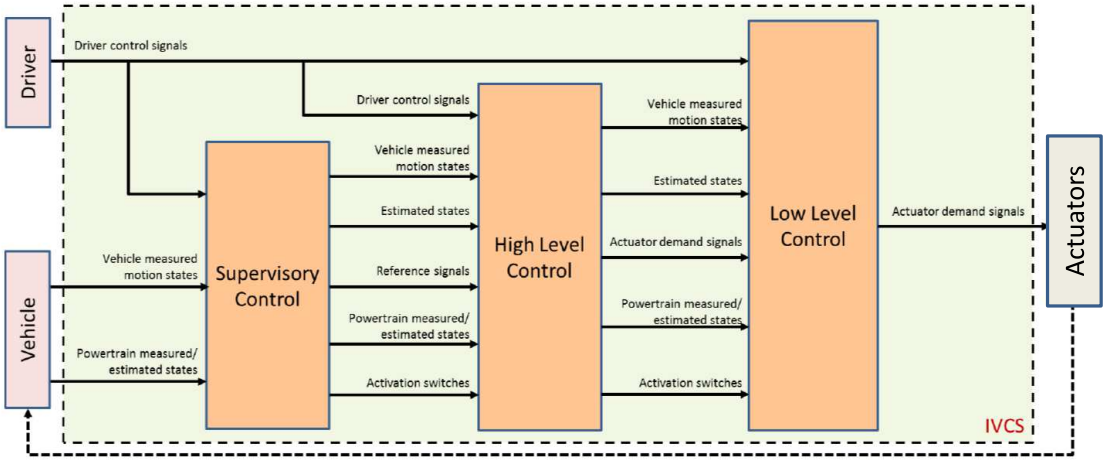

Figure 2.8: Overview of vehicle control structure in modelling.

Supervisory Control

The main task of the supervisory control block is to determine the intention of the driver inputs which translates to the reference values for the vehicle. All states estimation is implemented in this block with the measured signals as inputs. Another important feature is the decision block which contains the switches to activate or deactivate the controllers.

High Level Control

This layer is important to determine the control action relating to the motion of the vehicle level. For example, a parallel work in the project (torque vectoring) translates the yaw rate error into a yaw moment demand to be sent to the control allocation block. The individual wheel torque split strategy is implemented within the control allocation layer. This work does not apply to this layer of IVCS.

Low Level Control

This research concentrates on the low-level control which involves wheel level control for both actuators. Individual wheel slip control and torque blending strategies are implemented in this layer. Based on the slip reference, the controller will determine the required torque for each wheel and apportion the wheel torque based on the availability

of the actuators.

2.3.2 Actuator Dynamics

There are two braking actuators implemented in this work; the friction braking and regenerative braking actuators. Similar to [29] we assume that a brake-by-wire system is used in a way which delivers continuous braking torque instead of the conventional discrete brake pressure control [103]. The response of the brake torque generated by the EM is significantly faster than the one from the hydraulic brake-by-wire system [50]. A first-order delay is adopted to represent actuator dynamics for both the friction brakes and the EM in this simulation studies similar to [29]

$$\frac{T_e}{T_e^*} = \frac{1}{\tau_e s + 1} e^{-\delta_i s}, \tag{2.12}$$

$$\frac{T_h}{T_h^*} = \frac{1}{\tau_h s + 1} e^{-\delta_i s}, \tag{2.13}$$

where T_e^* the EM reference torque, T_h^* the reference friction brake torque, δ_i the pure delay, τ_e and τ_h the time constant for the delay for EM and friction brake respectively. In this work, the time constant used for EM and friction brake is set to 1.5ms and 16ms respectively. The dead time or pure delay for the friction brake and the EM is 15ms and 0.5ms respectively. This work assumes that any effects of the time constants chosen to the driveline are neglected. Although the EM has faster torque response, the retarding torque application is limited in range and generally determined by the battery state of charge, motor speed and operating temperature [28]. On the other hand, the friction braking system can deliver high torque but at slower rate. Then the torque limits are

$$T_e^{min} \leq T_e \leq T_e^{max}, \qquad T_h^{min} \leq T_h \leq T_h^{max}, \tag{2.14}$$

where

$$T_e^{min} = -750Nm, \qquad T_e^{max} = 750Nm,$$
$$T_h^{min} = -3000Nm, \qquad T_h^{max} = 0Nm,$$

and the torque rate limits are

$$\Delta T_e \leq \Delta T_e^{limit}, \qquad \Delta T_h \leq \Delta T_h^{limit}, \tag{2.15}$$

$$\Delta T_e^{limit} = 7500Nm/s,$$
$$\Delta T_h^{limit} = 3000Nm/s,$$

where $i \in \{\text{electric, hydraulic}\}$, ΔT_i (Nm/s) the torque rate, ΔT_i^{limit} (Nm/s) the maximum torque rate limit, T_i^{min} and T_i^{max} (Nm) the minimum and maximum brake torque range respectively. These characteristics of the actuator dynamics will be taken into consideration as constraints of the optimization problem.

2.4 Summary

The vehicle and wheel dynamics model are discussed for the base formulation for the proposed control strategies. The tyre model used in this work is also introduced.

All electrified vehicle topologies including PHEV and BEV are presented in this chapter. The features for each vehicle topology is discussed which explains the available redundant actuators differently (available EM torque considering 1 EM, 2 EMs and 4 EMs). The vehicle control structure using IVCS implemented in the project is introduced. Then, the high-fidelity vehicle models are presented in a co-simulation environment using Mat-

lab/Simulink and CarMaker for testing and validation of the designed control algorithms. Finally, the actuator dynamics for the regenerative braking and EHB is discussed.

Chapter 3

Wheel Slip Control

The general principle of the ABS is to avoid wheel locking by controlling the braking torque without exceeding the available tyre-road adhesion. This can be achieved by minimising the slip error between a slip reference s_{ref} and the actual wheel slip. There is a risk of overestimating the actuator's capability in delivering the braking torque in terms of torque limit and response time. The first focus of this research is to develop an appropriate wheel slip controller to be applied to the vehicle. One of the crucial components in designing the slip control is the slip target. Generally, most articles covered in the literature section consider a constant slip reference value between the range of s_{ref}= 0.1-0.2. It can be assumed that the value used represents the optimum road-tyre adhesion compromise to most of the road surfaces in real life. Rajamani states that the longitudinal tyre force reaches maximum value typically when the wheel slip is between 0.1 and 0.15 [96]. Considering both longitudinal and lateral forces for the range of the road adhesions, the slip target s_{ref} in this work is set as 0.1 in deceleration mode.

In this chapter, we present a slip controller using Sliding Mode Control (SMC). This method seems to be a common technique in the literature because of the following advantages: uncertainty and highly nonlinearity of the vehicle and wheel dynamics, distur-

bance rejection, parameter variations insensitivity and simple implementation with low order [31, 117]. The slip control will determine the brake torque demand when ABS is activated and the inputs are a constant slip target, vehicle speed, longitudinal vehicle acceleration, longitudinal wheel slip and longitudinal tyre friction force.

State estimation is needed in order for the SMC to be operational since there are states or variables that cannot be directly measured in the vehicle. These include vehicle speed, longitudinal wheel slip, and longitudinal friction force. As for the MPC approach, we present an estimation for the vertical tyre force during deceleration or acceleration. Observers and estimation method will be discussed in section 3.3.

Another important component that is discussed in this chapter is the logic to supervise the activation and deactivation of the slip control. The task is to ensure there is a smooth transition between conventional braking and ABS operation. This strategy is presented in section 3.4.

3.1 Sliding Mode Control

As seen in the literature review, SMC is a common type of controller used in wheel slip control. SMC is a nonlinear control method that can be used for wheel slip control due to its robustness against external disturbances and parameter variations of the system [64]. It is designed to drive the system states towards a particular surface in the state space which is called the sliding surface. Then, the SMC will maintain the states close to the sliding surface. Hence, the first part of designing slip control using SMC is to design a sliding surface to meet the intended specification and the second phase is to select control law to keep close to the switching surface. The controller aims at minimising the error between actual longitudinal wheel slip and a constant target slip. The sliding surface, s and its time

derivative are given by

$$s = s_x - s_{ref} = 0 \tag{3.1}$$

$$\dot{s} = \dot{s_x} \tag{3.2}$$

where we assume that the desired slip remains constant, i.e $\dot{s}_{ref} = 0$. Setting

$$\dot{s} = -\varepsilon sgn(s) \tag{3.3}$$

and the wheel slip dynamics are

$$\begin{aligned} s_x &= \frac{v - r\omega}{v} \\ \dot{s_x} &= -\frac{r\dot{\omega}}{v} + \frac{r\omega\dot{v}}{v^2} \end{aligned} \tag{3.4}$$

and replacing

$$\omega = \frac{v}{r}(1 - s_x) \tag{3.5}$$

$$\dot{\omega} = \frac{rF_x - T_b}{J} \tag{3.6}$$

we finally get

$$\dot{s_x} = -\frac{r}{vJ}(rF_x - T_b) + \frac{\dot{v}}{v}(1 - s_x) = -\varepsilon sgn(s) \tag{3.7}$$

Using L as a Lyapunov function candidate

$$\begin{aligned} L &= \frac{1}{2}s^2 \\ \dot{L} = s\dot{s} &= s(-\frac{r}{vJ}(rFx - T_b) + \frac{\dot{v}}{v}(1 - s_x)) \\ &= s(-\frac{r^2F_x}{vJ} + \frac{rT_b}{vJ} + \frac{\dot{v}}{v}(1 - s_x)) \end{aligned} \tag{3.8}$$

and taking

$$\begin{aligned} T_b &= \frac{vJ}{r}\left(\frac{r^2F_x}{vJ} - \frac{\dot{v}}{v}(1-s_x) - \varepsilon sgn(s)\right) \\ &= rF_x - \frac{\dot{v}J}{r}(1-s_x) - \frac{vJ}{r}\varepsilon sgn(s) \end{aligned} \tag{3.9}$$

with ε a small positive number, we have

$$\dot{L} = -s\varepsilon sgn(s) = -\varepsilon|s| < 0 \tag{3.10}$$

It has been proven that $L > 0$ and the sliding condition $\dot{L} < 0$ is satisfied. Then defining $\kappa = \frac{vJ}{r}\varepsilon$, the control law is

$$T_b = rF_x - \frac{\dot{v}J}{r}(1-s_x) - \kappa sgn(s) \tag{3.11}$$

To reduce chattering, we can use saturation function instead of signum

$$sat(s) = \begin{cases} s\,, & if\ |s| \leq 1 \\ sgn(s)\,, & if\ |s| > 1 \end{cases} \tag{3.12}$$

where s_x is the longitudinal wheel slip, s_{ref} is the slip target, J is the wheel inertia, ϕ (referred to as the boundary layer) and ε are tuning parameters and are both positive constants.

In this work, the inputs required for the controller are the wheel longitudinal slip, longitudinal force, vehicle speed, and acceleration. The controller's output is brake torque which is fed into the torque allocation strategy to be delivered by both braking actuators in the vehicle. Overview of the SMC operation within the strategy is shown in Figure 3.1.

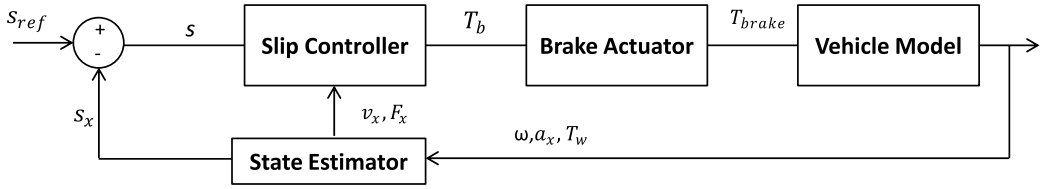

Figure 3.1: Overview of SMC for ABS.

The SMC is applied to each corner of the vehicle to allow individual wheel slip control. The advantage of implementing slip control method is the direct control to maintain the longitudinal wheel slip near desired value while on various types of road surfaces. In other words, the slip control can detect road surface changes and adapt accordingly to avoid wheel locking during braking. The requirement is to have individual wheel braking actuator to deliver the demanded brake torque by the SMC.

3.2 e-Slip Control

Pure electric-slip control can be deployed in an electrified vehicle with the availability of EM on each wheel. Individual wheel torque control by using EM enables us to implement both ABS and TCS without the need of friction brakes in a certain situation. With a constant slip target defined, the slip controller determines the wheel torque required in order to reduce the error between the actual and desired slip as shown in Figure 3.2. Slip control is designed by applying either SMC or MPC method. The inputs required for the controller are the slip reference, wheel longitudinal slip, longitudinal friction force (SMC), vertical tyre force (MPC), wheel angular speed, and vehicle speed. The controller output is either tractive or braking wheel torque to be delivered by the EM.

The SMC slip control can detect road surface changes and adapt accordingly to avoid wheel locking during braking and excessive wheel spinning during acceleration. Wheel

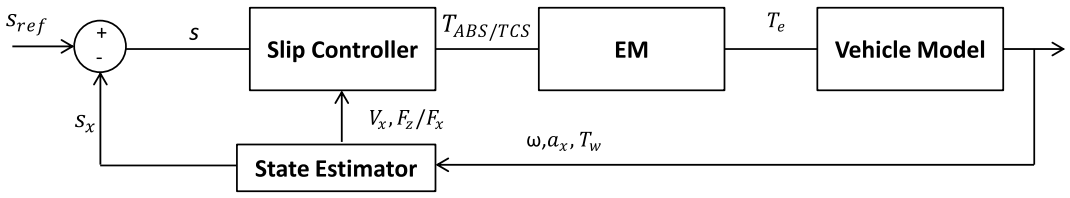

Figure 3.2: Overview of the e-slip control.

locking would destabilise the vehicle during emergency braking, while excessive wheel spin will cause the car lose traction to drive away. TCS is activated during rapid acceleration to allow the driver to accelerate without excessive wheel spin. The controller calculates wheel torque command based on actual wheel slip to achieve the desired slip ratio. Therefore, wheel slip is controlled, and the vehicle can maintain acceleration as requested by the driver. The slip control algorithm limits the torque demand to the EM which allows the longitudinal slip to be maintained close to the target value. An additional advantage of implementing e-TCS is the ability to avoid rapid wheel spinning with the use of only EM. There is no need of friction braking actuation intervention as the control strategy will calculate tractive torque required to achieve the desired slip target.

3.3 State Estimation

Typical sensors that can be found on modern vehicles for the purpose of wheel slip control include wheel angular rate sensors and an accelerometer. However, the vehicle speed cannot be reliably measured by a sensor and hence an observer is required to provide its estimation. Other parameters that are not typically measured using vehicle sensors are the longitudinal friction force between tyre-road and the vertical tyre force.

In this section, we present the vehicle speed estimation needed in the control strategies. The vehicle speed is estimated using a Kalman Filter observer with measurements

of wheel angular speed ω and longitudinal vehicle acceleration a_x as inputs [66, 67, 107, 112, 121]. The longitudinal friction force F_x estimation is presented next using a linear observer [86]. Finally, the vertical tyre force F_z is estimated using quasi-static load transfer formulation.

3.3.1 Vehicle Speed and Longitudinal Slip Estimation

Vehicle speed is usually assumed known in most articles. For mass production vehicles, using an additional sensor such as Global Positioning Sensor (GPS) is undesirable to avoid the extra cost and any other problems related to GPS (such as poor GPS reception due to weather or blocked signals). Hence, the vehicle speed is typically estimated using inputs from existing sensors including wheel rotational speed and longitudinal acceleration measurements.

In this work, the vehicle speed is estimated using Kalman Filter as an observer with measurements of wheel angular speed and longitudinal vehicle acceleration as inputs. In principle, the vehicle speed can be estimated using the average value of wheel speeds during low deceleration, while during high deceleration braking, the longitudinal vehicle acceleration value is used to maintain vehicle speed estimation accuracy.

Figure 3.3 shows the process for estimating vehicle speed from the measured input signals in the car. The first and second Kalman filter is designed to filter the noise from the measured wheel speed ω and longitudinal acceleration a_x. The discrete-time Kalman filters send the filtered inputs to the third Kalman filter which is an observer for the vehicle speed. The vehicle speed is predicted for the next sampling time based on the present estimated vehicle speed added to the current estimated acceleration as shown in equations 3.13 and 3.14.

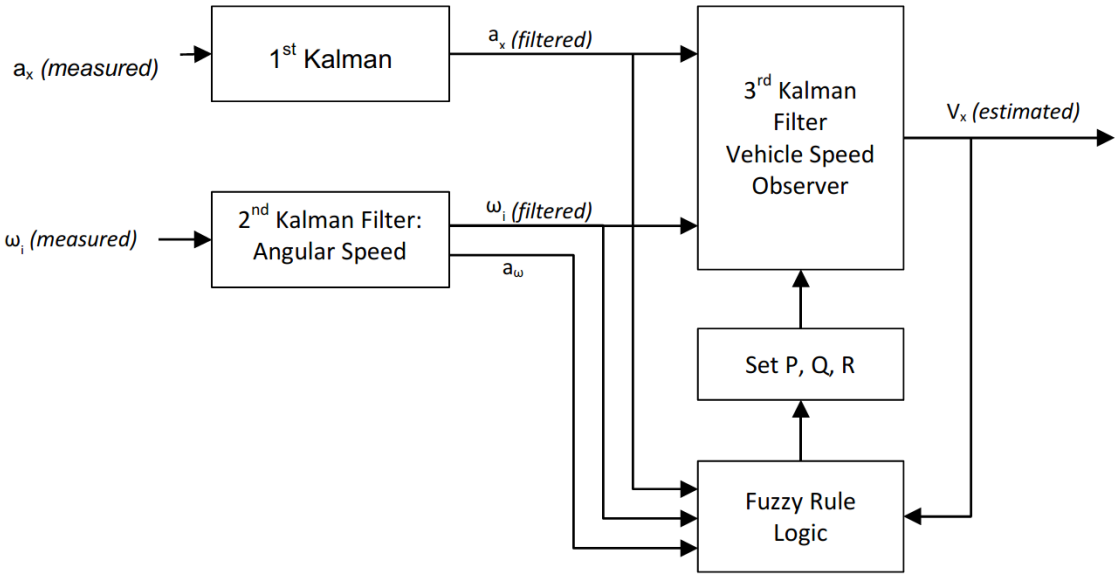

Figure 3.3: Overview of Kalman speed estimation.

$$\dot{v}_t = a_t + w \tag{3.13}$$

$$\begin{bmatrix} v_{FL} \\ v_{FR} \\ v_{RL} \\ v_{RR} \end{bmatrix} = \begin{bmatrix} 1 \\ 1 \\ 1 \\ 1 \end{bmatrix} v_t + \begin{bmatrix} n_{FL} \\ n_{FR} \\ n_{RL} \\ n_{RR} \end{bmatrix} \tag{3.14}$$

where w is process noise, $n_{(i,j)}$ are the measurement noise, v_t is the estimated vehicle speed, a_t is the measured longitudinal vehicle acceleration, $v_{(i,j)}$ are the measured wheel speeds and $i \in \{f,r\}$, $j \in \{l,r\}$.

A set of rules is used to adjust the covariance matrices to take into account the high slip ratio values during hard braking and inaccuracies of acceleration measurements at low vehicle speed. The set of rules selected for this work is presented in Table 3.1 and Table 3.2. The wheel slip presence can be detected by using the vehicle acceleration and the wheel and vehicle speed difference. The R is then set as either 'small', 'medium'

or 'large'. The Q is classified as 'small' during high vehicle acceleration and when at low acceleration while at high speed. The value for Q is set to 'large' when the vehicle acceleration is small while at low speed estimation. A condition to avoid NaN value when the vehicle is stationary (wheel speeds are zero) over an extended period of simulation is created. Each wheel speeds are set to zero when the sensor measurement value is small.

	small $\lvert v_t - v_w \rvert$	medium $\lvert v_t - v_w \rvert$	large $\lvert v_t - v_w \rvert$
small $\lvert a_t \rvert$	small	medium	medium
large $\lvert a_t \rvert$	large	large	large

Table 3.1: Tuning rules for measurement noise covariance matrix, R.

	small v_t	large v_t
small $\lvert a_t \rvert$	large	small
large $\lvert a_t \rvert$	small	small

Table 3.2: Tuning rules for process noise covariance matrix, Q.

Noise is injected to the wheel speed and acceleration signals in simulation to replicate real vehicle measurements using the Gaussian noise generator in Simulink. Simulation results from a braking on a straight line scenario is illustrated in figure 3.4 to compare the estimated vehicle velocity and the actual velocity. Figures 3.4(a)-(b) show the measured signals for wheel speed and acceleration respectively. It can be clearly seen in figure 3.4(c) that the estimated vehicle velocity converged close to the actual vehicle speed within 400ms. With the estimated V_x and the measured wheel rotational speed ω available, the actual wheel longitudinal slip s_x can be calculated using equation 2.5 to be fed to the controller.

3.3.2 Longitudinal Friction Force Estimation

One of the parameters required for the SMC slip control is the tyre friction force. Since it cannot be measured directly using sensors in vehicle, a monitoring model is developed.

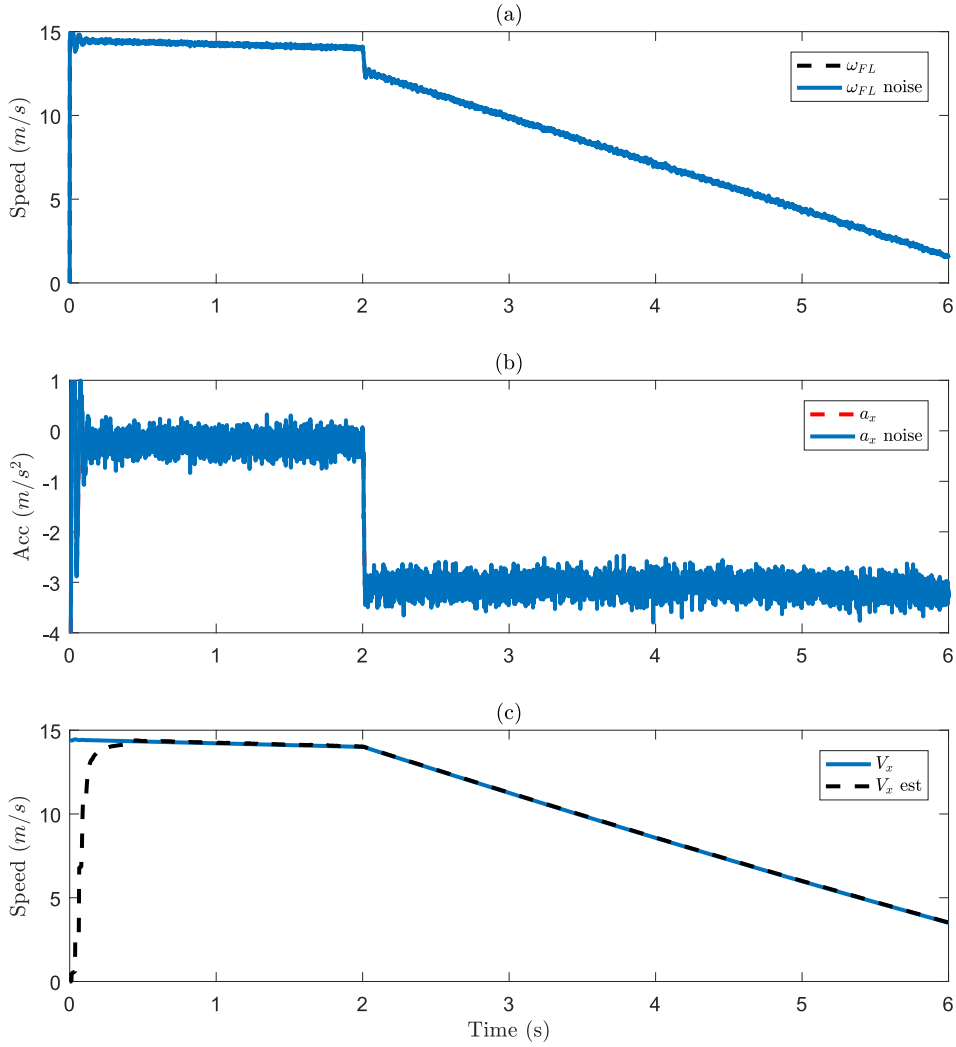

Figure 3.4: Vehicle speed estimation with noise signal injected.

Tyre longitudinal force is estimated by a linear observer with vehicle speed, wheel angular speed and torque applied at wheel as inputs [86]. The longitudinal friction force at each wheel are assumed to be constant during monitoring and augmented as state variables in

state equations.

$$A = \begin{bmatrix} 0 & 0 & 0 & 0 & 0 & 0 & -\frac{1}{m} & -\frac{1}{m} & -\frac{1}{m} & -\frac{1}{m} \\ 0 & 0 & 0 & 0 & 0 & 0 & R_w J_w & 0 & 0 & 0 \\ 0 & 0 & 0 & 0 & 0 & 0 & 0 & R_w J_w & 0 & 0 \\ 0 & 0 & 0 & 0 & 0 & 0 & 0 & 0 & R_w J_w & 0 \\ 0 & 0 & 0 & 0 & 0 & 0 & 0 & 0 & 0 & R_w J_w \\ 0 & 0 & 0 & 0 & 0 & 0 & 0 & 0 & 0 & 0 \\ 0 & 0 & 0 & 0 & 0 & 0 & 0 & 0 & 0 & 0 \\ 0 & 0 & 0 & 0 & 0 & 0 & 0 & 0 & 0 & 0 \\ 0 & 0 & 0 & 0 & 0 & 0 & 0 & 0 & 0 & 0 \end{bmatrix} \quad B = \begin{bmatrix} 0 & 0 & 0 & 0 \\ -\frac{1}{J_w} & 0 & 0 & 0 \\ 0 & -\frac{1}{J_w} & 0 & 0 \\ 0 & 0 & -\frac{1}{J_w} & 0 \\ 0 & 0 & 0 & -\frac{1}{J_w} \\ 0 & 0 & 0 & 0 \\ 0 & 0 & 0 & 0 \\ 0 & 0 & 0 & 0 \\ 0 & 0 & 0 & 0 \end{bmatrix}$$

$$x = \begin{bmatrix} v \\ \omega_{fl} \\ \omega_{fr} \\ \omega_{rl} \\ \omega_{rr} \\ F_{x_{fl}} \\ F_{x_{fr}} \\ F_{x_{rl}} \\ F_{x_{rr}} \end{bmatrix} \qquad u = \begin{bmatrix} T_{fl} \\ T_{fr} \\ T_{rl} \\ T_{rr} \end{bmatrix}$$

The assumption has been made to only consider vehicle's longitudinal motions and the wheel diameter is constant to apply a simple linear observer in estimating the longitudinal friction forces. An important step is to carefully provide a reset condition for the integrator in the observer model in Simulink. This is to avoid any NaN value returned due

to accumulated integration build-up over an extended period. This is critical for real-time implementation in HiL simulation testing and vehicle testing. Figure 3.5 shows the F_x estimation during a deceleration of $8m/s^2$ and it can be observed that the estimation is acceptable compared to the 'actual' values recorded from the IPG CarMaker.

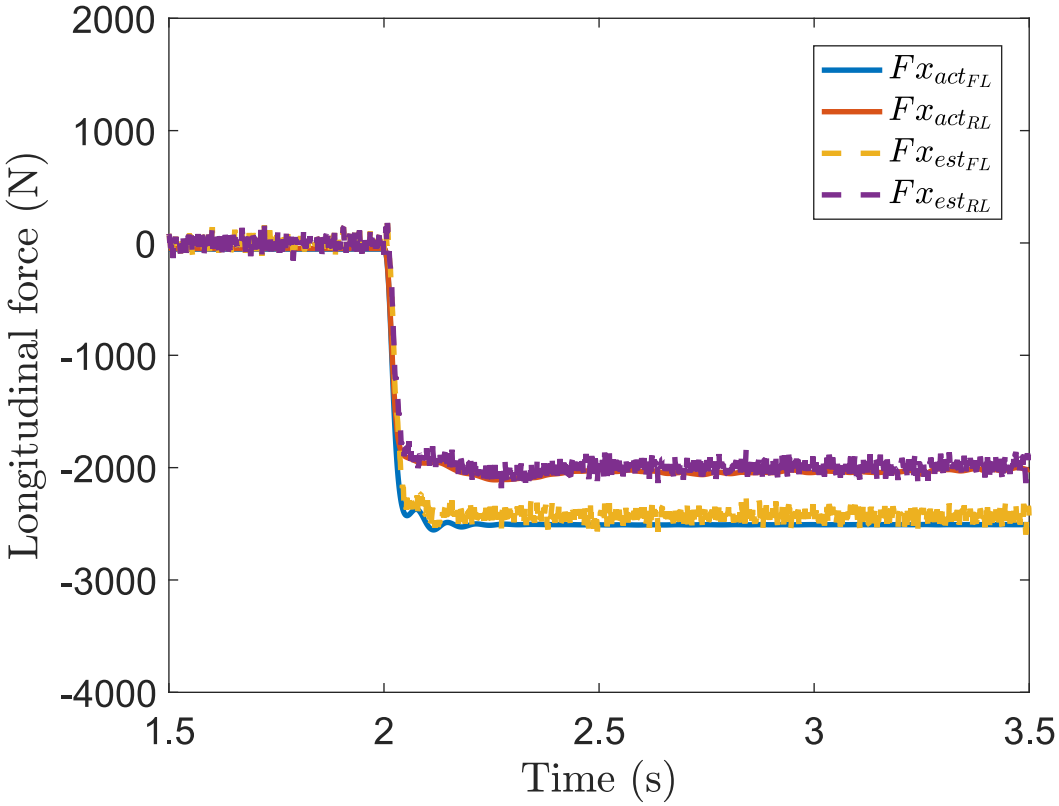

Figure 3.5: Longitudinal tyre force estimation.

3.3.3 Vertical Tyre Force Estimation

One important parameter for the internal model of the MPC is the vertical tyre force F_z. In this work we use a simple quasi-static load transfer calculation to capture the dynamics

of vertical tyre force in the event of braking

$$\Delta F_z = \frac{mh}{l} a_x, \tag{3.15}$$

where m, h and l are the vehicle mass, height of CM and wheelbase respectively. The only input to the estimation calculation is the longitudinal acceleration a_x which can be measured by the accelerometer in the vehicle. The weight shifting between the front and rear axle will be updated to the internal model so the MPC can provide accurate torque delivery during slip control operation for better slip reference tracking. Figure 3.6 shows the estimation of the normal tyre force F_z compared to the actual measurement from IPG CarMaker during an $8m/s^2$ braking. With the inclusion of the weight transfer, better tracking of the slip reference can be achieved by the controller. The estimation has a limitation if the braking event is on an uneven road-μ since the main input for the load transfer depends on the vehicle acceleration or deceleration a_x.

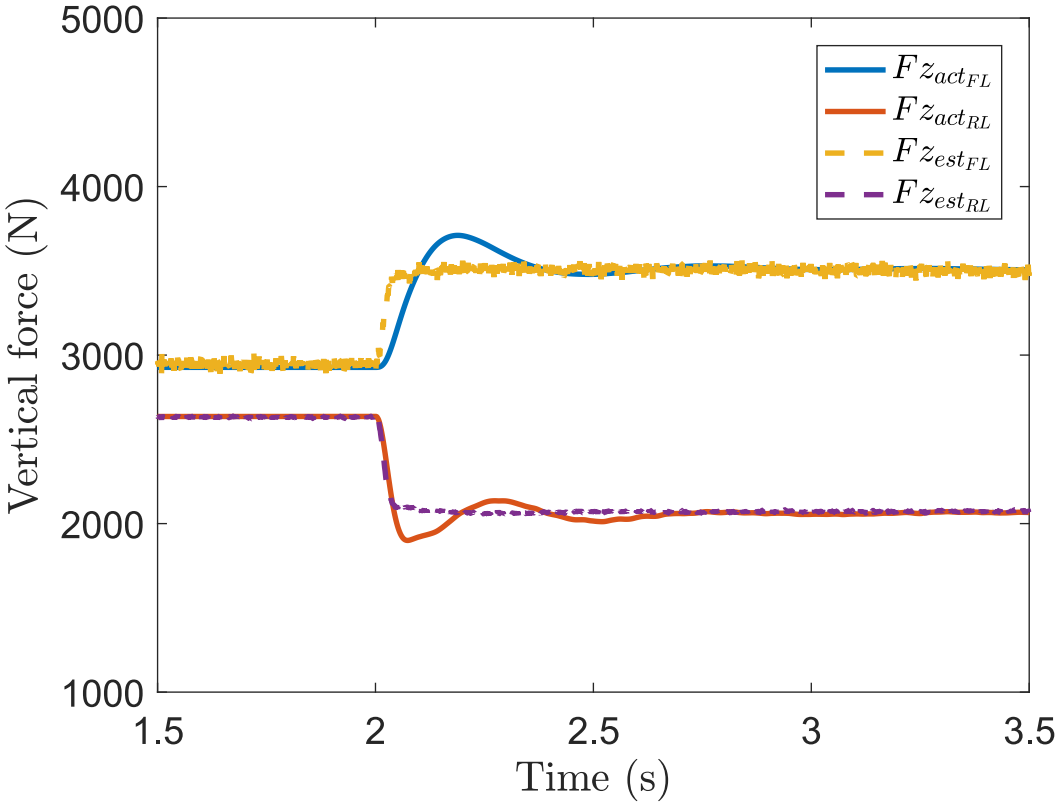

Figure 3.6: Vertical tyre force estimation.

3.4 ABS Management System

One of the important components of the proposed control architecture in this project is the braking management system. The main functionality is to activate and deactivate the slip controller. Inputs to the strategy include actual longitudinal slip, vehicle speed, total brake demand by the driver and ABS brake demand. In braking event, logic is designed to select which brake torque demand will be commanded in low-level control. In any case, the controller should respect the driver's intention and never command more brake force than what the driver demands.

The primary objective of the ABS management strategy is to enforce the logic for activation and deactivation of the ABS. If the slip control is deactivated, the driver's brake

torque demand from high-level control is delivered. Similar to the way slip control is being setup, activation and deactivation logic is developed independently for each wheel to allow individual wheel slip control capability.

The inputs to the strategy are the brake actuator demands by ABS, brake actuator demands by the driver (non-ABS), longitudinal wheel slip, vehicle speed and brake pedal rate command. Based on [3], the slip control is activated only when these conditions are met:

1. Vehicle speed exceeds threshold speed

2. Wheel slip exceeds slip threshold

3. Driver brake demand exceeds ABS brake demand

As part of an Active Safety system, the ABS should assist to stop safely and allow the driver to maintain control of the vehicle. Therefore, slip control should not request higher brake demand than the driver's intention. With the aim of designing a control architecture for pragmatic use in a real vehicle, all components in each subsystem have to take into account of the real-time implementation and the limitations of the hardware.

Next functionality of the ABS management is to select brake actuator demands based on the condition carefully. Usually, slip control can be activated independently on each wheel due to individual wheel brake pressure control ability of the EHB. In the presence of secondary braking actuator (4WD HEV with single EM or two EMs), we introduce a strategy to manage the brake actuator demand selection including the pressure set point for EHB and regenerative braking torque of the EM. Since the EM is coupled to the wheels (4 wheels connected through propeller shaft for PHEV topology and front wheels/rear wheels are connected to EM on each axle), torque blending algorithm will be activated as long as any one of the wheels is about to lock. This allows the RBS to maintain activated

throughout an ABS braking event but furthermore respecting the driver's brake demand for the ABS-deactivated wheel.

3.5 Slip Control Simulation Results

Simulation results are presented in this section using co-simulation software between Matlab/Simulink and CarMaker setup as presented in 2.3. The control algorithm is implemented in Simulink and the vehicle model is deployed using IPG CarMaker environment along with the tyre model and test environment. Several test manoeuvre is designed to evaluate the performance of the proposed control strategies. Generally, the initial vehicle speed chosen for simulation testing is 50km/h. Main reasons include this is the most common driving speed in the real world and also taking the consideration of effects from aerodynamics and rolling resistance when compared to the high speed. The tuning parameters for the SMC used in this work can be found in Appendix B.

3.5.1 SMC slip control

Braking on low-μ surface

Figures 3.7a)-d) show the test results of braking with ABS using SMC on a slippery road surface (similar to packed snow in the real life situation). The slip ratio for individual wheels is well controlled around the target value in order to avoid wheels locking. The stopping distance is improved by 18% compared to the non-ABS braking event. The braking torque demand by the driver is clearly greater than the available friction between the road surface and the tyres, hence the brake torques are limited and reduced to satisfy the target slip ratio value as illustrated in figure 3.7 c) and d).

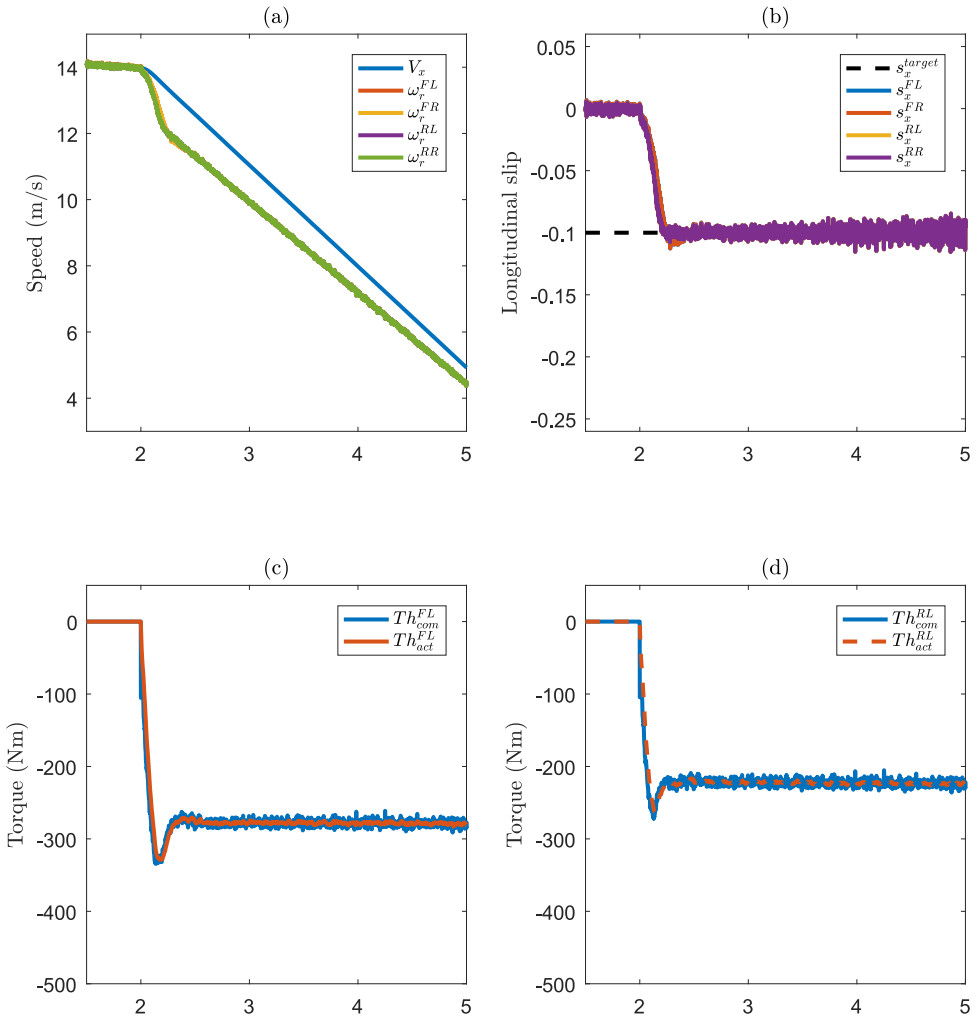

Figure 3.7: SMC straight line braking with road μ=0.3, $V_{initial}$=50km/h, s_{ref}=-0.1.

Braking on split-μ surface

Slip control is very important when there is uneven friction of road surfaces. In this example, a vehicle braking on a road with dry asphalt on the left wheels (μ=1) and on snow on the right wheels (μ=0.3). Yaw moment will be created towards the high friction side of the road if the same brake torque is applied between left and right wheels. ABS

will detect the high wheel slip ratio and quickly retard the brake torque to avoid wheel locking and vehicle from spinning. Lower brake torque is applied to the wheels on low-μ to maintain the wheel slip within acceptable value as illustrated in Figure 3.8e) and g). To prove this observation, we can see that the maximum driver steering angle required to maintain the intended path is $68deg$ and the maximum yaw rate achieved by the vehicle is $8.6deg/s$ which are shown in figure 3.8b)-c) respectively. This observation indicates that with sufficient countersteering by the driver model in CarMaker, the vehicle can be safely stopped and to demonstrate that the vehicle stability and steering response can be maintained.

Braking in turn

Emergency braking while cornering is a good example to demonstrate the benefits of having ABS in a vehicle. Without ABS, the vehicle will understeer once the friction between road surface and tyres is saturated and sliding instead of turning in following the cornering radius. On the other hand, slip control will try to maintain the wheel slip ratio following the target value. This will avoid saturation of the lateral grip and allow the driver to steer and maintain the vehicle turning radius. There is also a risk of oversteering the vehicle if only the rear wheels are locked. This observation is clearly shown in figure 3.9b) where maximum driver steering angle required to maintain the cornering path is $44deg$ whereas the driver will have to provide steering angle input of $191deg$ in the ABS-off scenario. Based on Figure 3.9a), it is clearly shown that the individual wheel slip controller maintains the slip ratio of each wheel close to the reference value by varying the friction brake torques. Figures 3.9d)-g) show the capability of individual wheel slip control using EHB which indicates different braking torque commanded by the SMC for each wheel in order to satisfy the slip target.

Lane change braking

A lane changing under hard braking manoeuvre is another test pattern to evaluate the per-

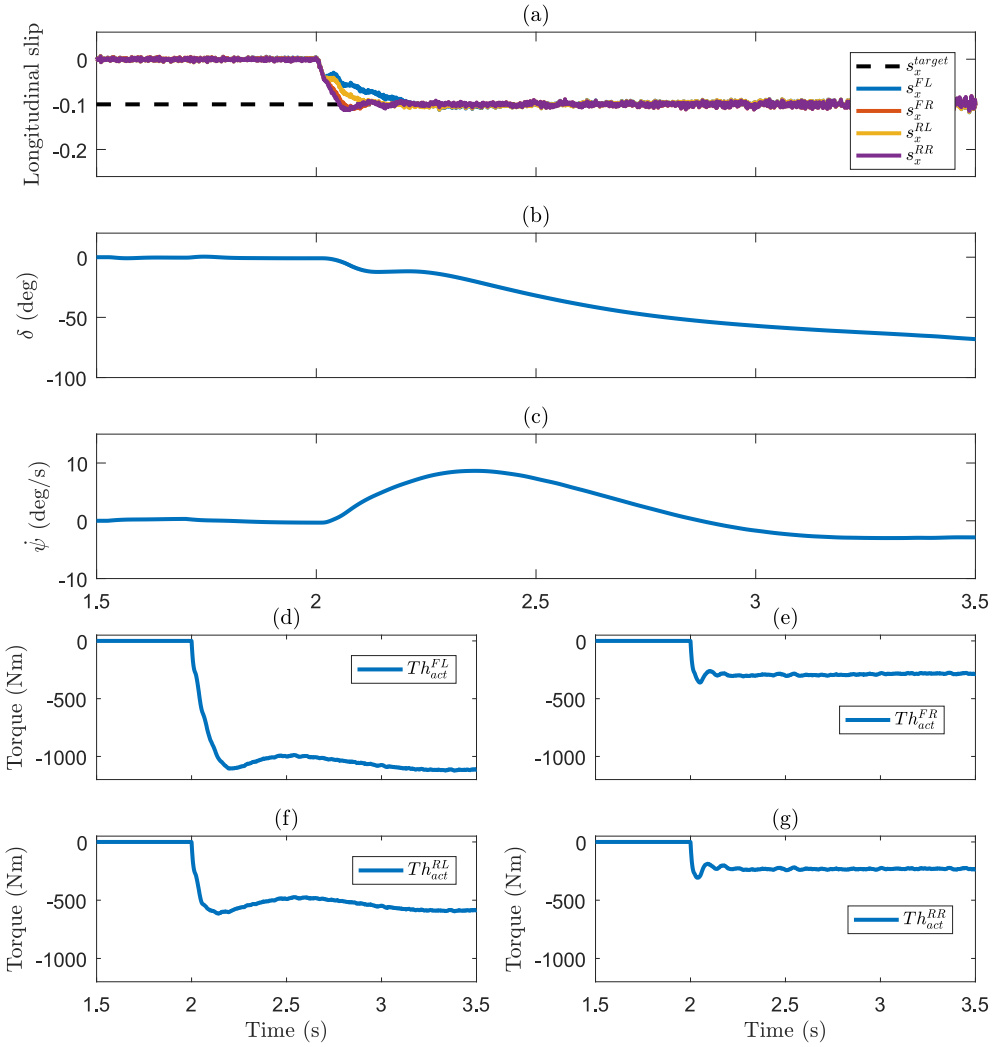

Figure 3.8: SMC split-μ braking, $V_{initial}$=50km/h, s_{ref}=-0.1.

formance of the ABS. Figure 3.10a) indicates the capability of the ABS to individually control the wheel slip by controlling the EHB braking torque for the individual wheel as shown in 3.10d)-g) to allow the vehicle to maintain its stability and steering response. Maximum yaw rate achieved on the vehicle is $9.8 deg/s$ and the driver steering wheel angle input to control the vehicle throughout the manoeuvre is $58 deg$. In comparison,

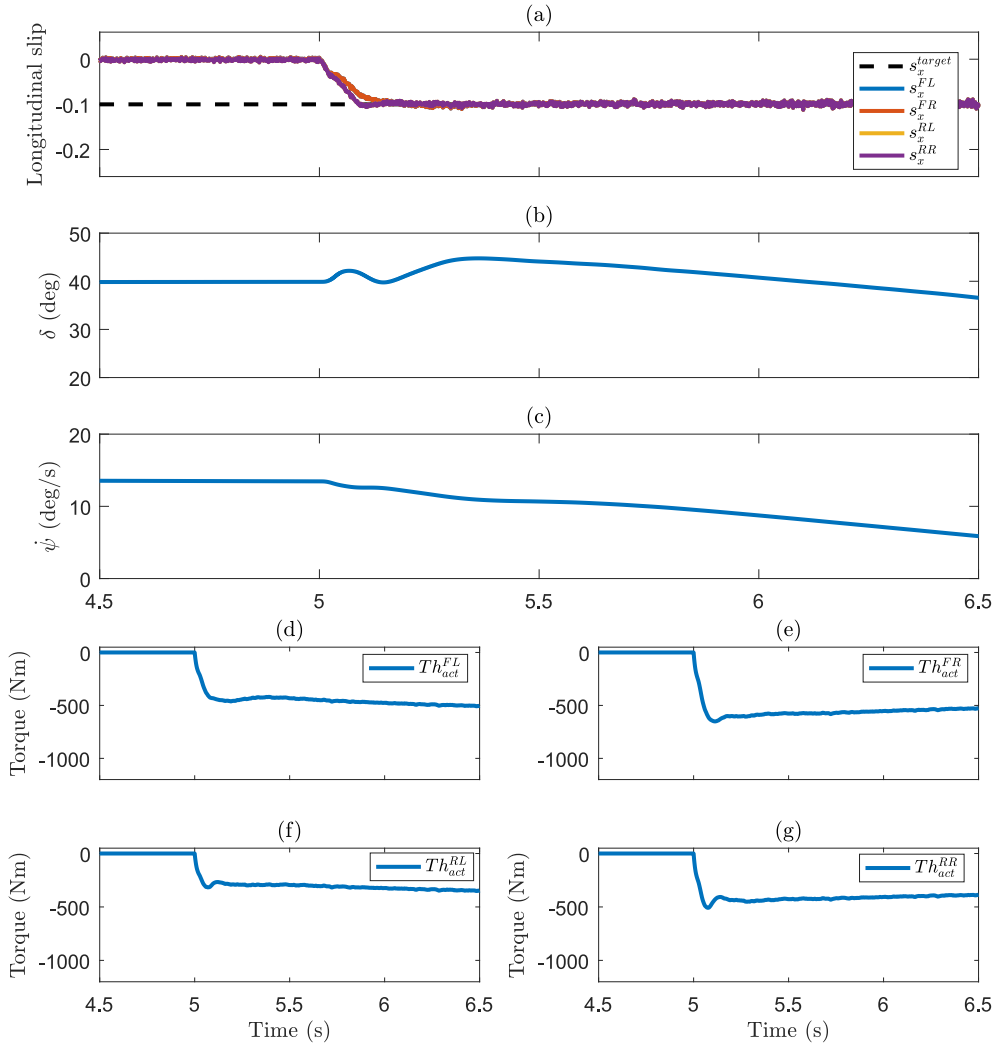

Figure 3.9: SMC brake in turn on μ=0.5, $V_{initial}$=50km/h, s_{ref}=-0.1.

the non-ABS case causes the vehicle to understeer and failed to follow the intended path. Again, the lateral grip between tyre and road surfaces is saturated if the wheels are locked during braking. Additionally, the vehicle stability and steering controllability are maintained during ABS braking scenario even without the vehicle stability control assistance.

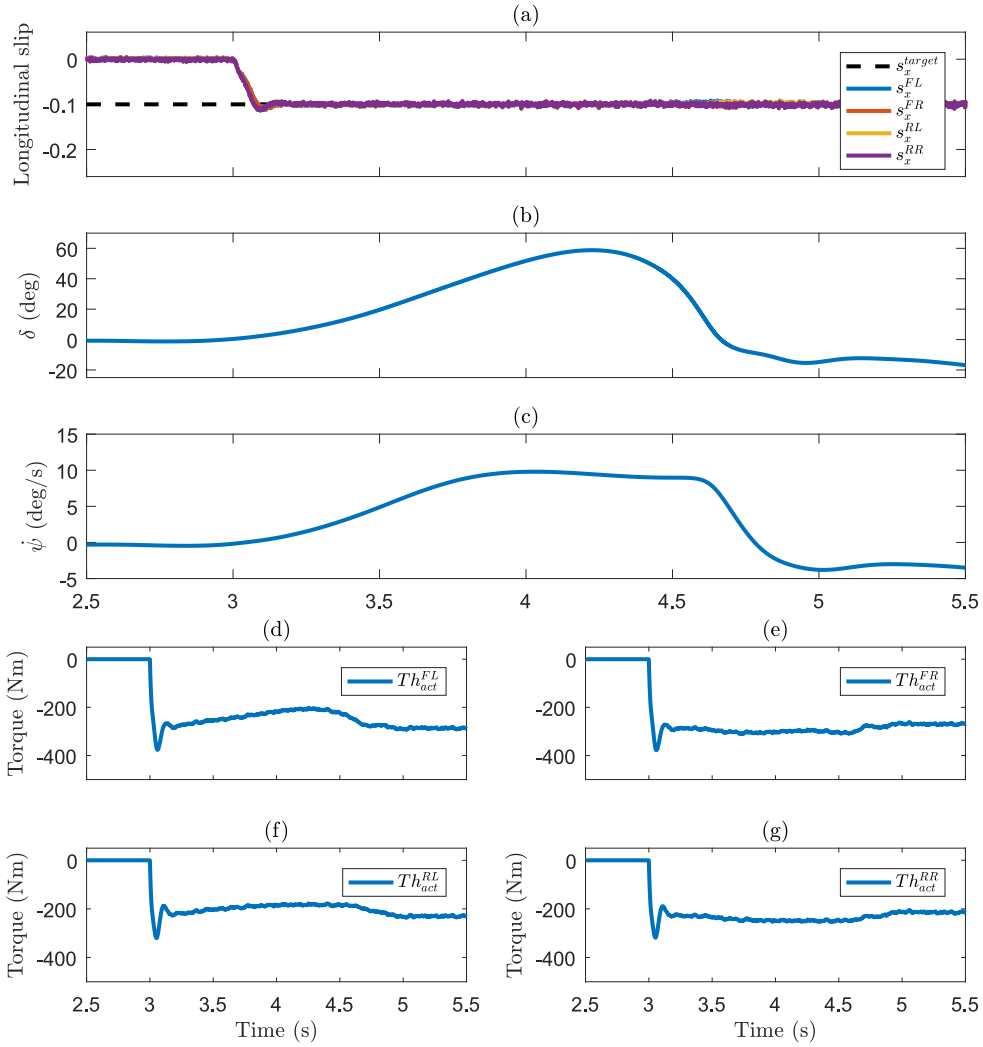

Figure 3.10: SMC lane change braking on μ=0.3, $V_{initial}$=50km/h, s_{ref}=-0.1.

Braking on μ-jump

A transition of road surface's friction coefficient is another critical situation which involves emergency braking. ABS has to be able to adapt to the change of the road surface condition and avoid wheels locking. Based on figures 3.11b), there is a spike of the slip ratio (s_x=0.55) overshooting when the vehicle is just entering the slippery road condition

($\mu = 0.3$) from a high adhesion road surface ($\mu = 1$). Braking torques illustrated in figure 3.11c)-d) for both front and rear wheels are quickly reduced to allow the wheel slip ratio to satisfy the reference value of s_x=0.1.

In other situation which is the transition from low-μ to high-μ (positive μ-jump), there is a clear observation that the controller is trying to quickly minimise the slip error by increasing the commanded braking torque as shown in figure 3.12. In other words, the slip controller is robust enough to identify any change on the road surface and adapt accordingly.

3.5.2 E-slip control

We have discussed the potential of implementing E-slip control for a BEV configuration which includes 4 EMs and this section shows the proof of concept for ABS operation using the regenerative braking.

Figures 3.13a)-b) illustrate the implementation of using only regenerative braking torque for implementing a slip control in a 4WD BEV using 4EMs. On a low adhesion surface (road μ=0.3) and at an initial speed of 50km/h, wheels have the propensity to lock even at low deceleration. We can take this advantage to implement slip control with the limited range of regenerative braking. Figures 3.13c)-d) indicate that a brake torque demand of around 300 Nm which can be fully delivered by the RBS of each EM for each wheel without the need for friction brakes. An improvement of 19% can be achieved in terms of braking stopping distance as compared to the non-ABS case.

E-slip control can be tested in an acceleration scenario using CarMaker simulation as a proof of concept. A rapid acceleration request by the driver is simulated on a low adhesion surface (road μ=0.3) and at initial speed 50km/h. It can be clearly seen in figure 3.14b) that all four longitudinal wheel slips are maintained near desired value with the

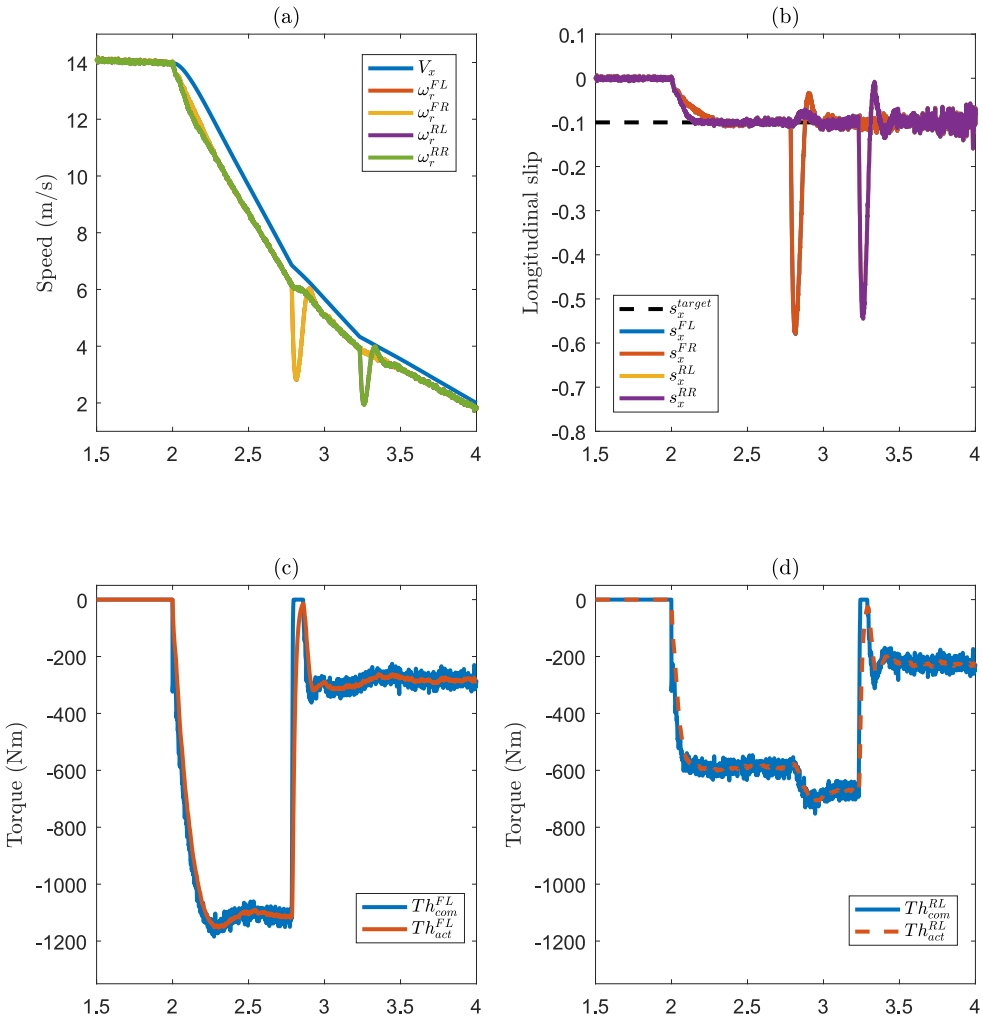

Figure 3.11: SMC negative μ jump braking, $V_{initial}$=50km/h, s_{ref}=-0.1.

commanded tractive torque delivered (figure 3.14c)-d)). There is no support from friction braking needed and in contrast to a conventional traction control, the engine power cut-off requested by the ECU is not required. With a high acceleration demand by the driver on such a low adhesion road surface, the e-TCS can be proven to be working well to allow the vehicle to be driven off smoothly as shown in 3.14a).

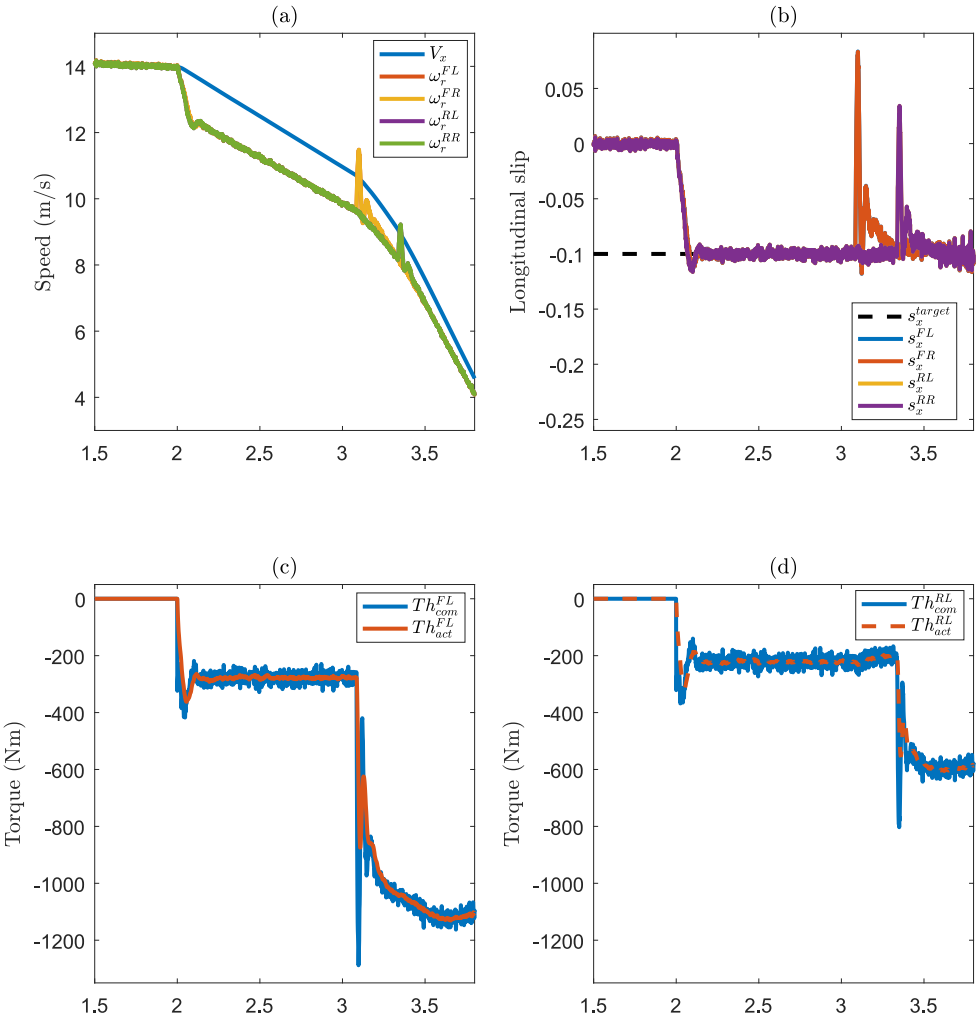

Figure 3.12: SMC positive μ jump braking, $V_{initial}$=50km/h, s_{ref}=-0.1.

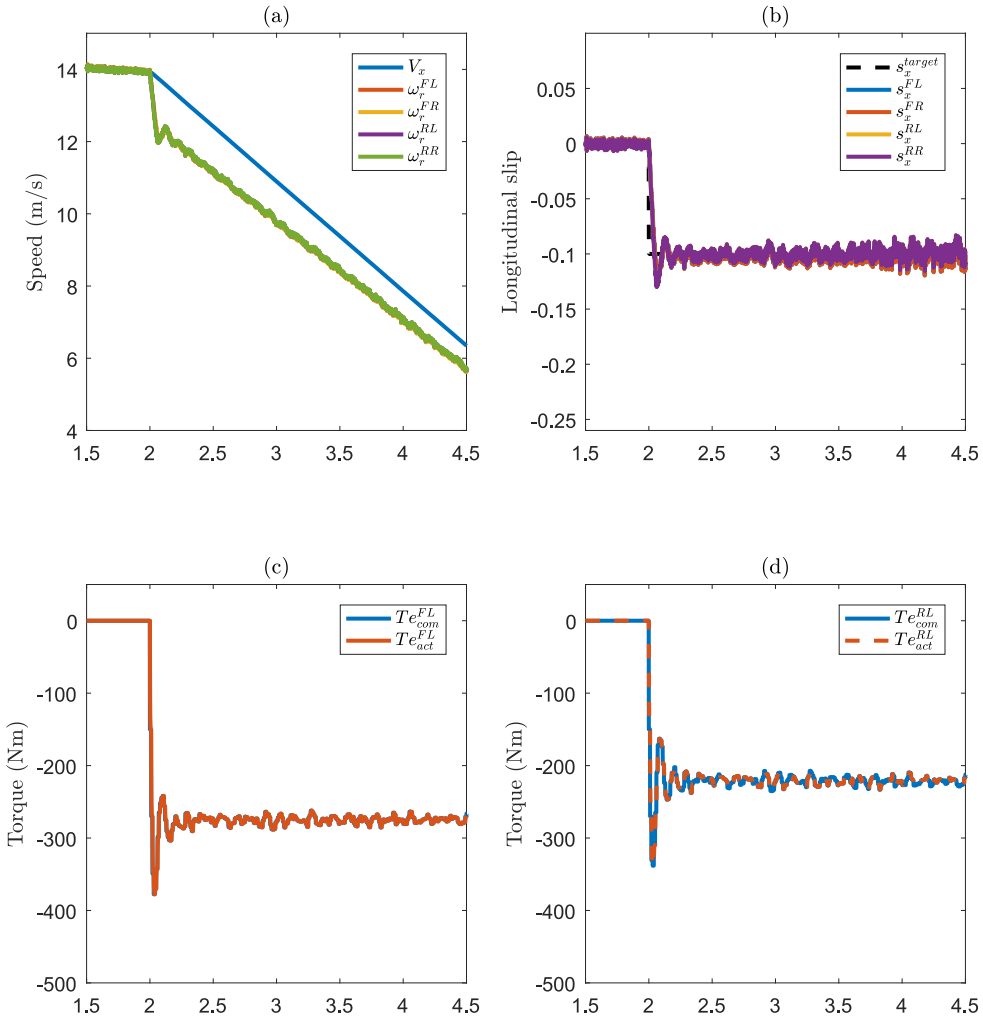

Figure 3.13: e-ABS straight line braking on low-μ, $V_{initial}$=50km/h, s_{ref}=-0.1.

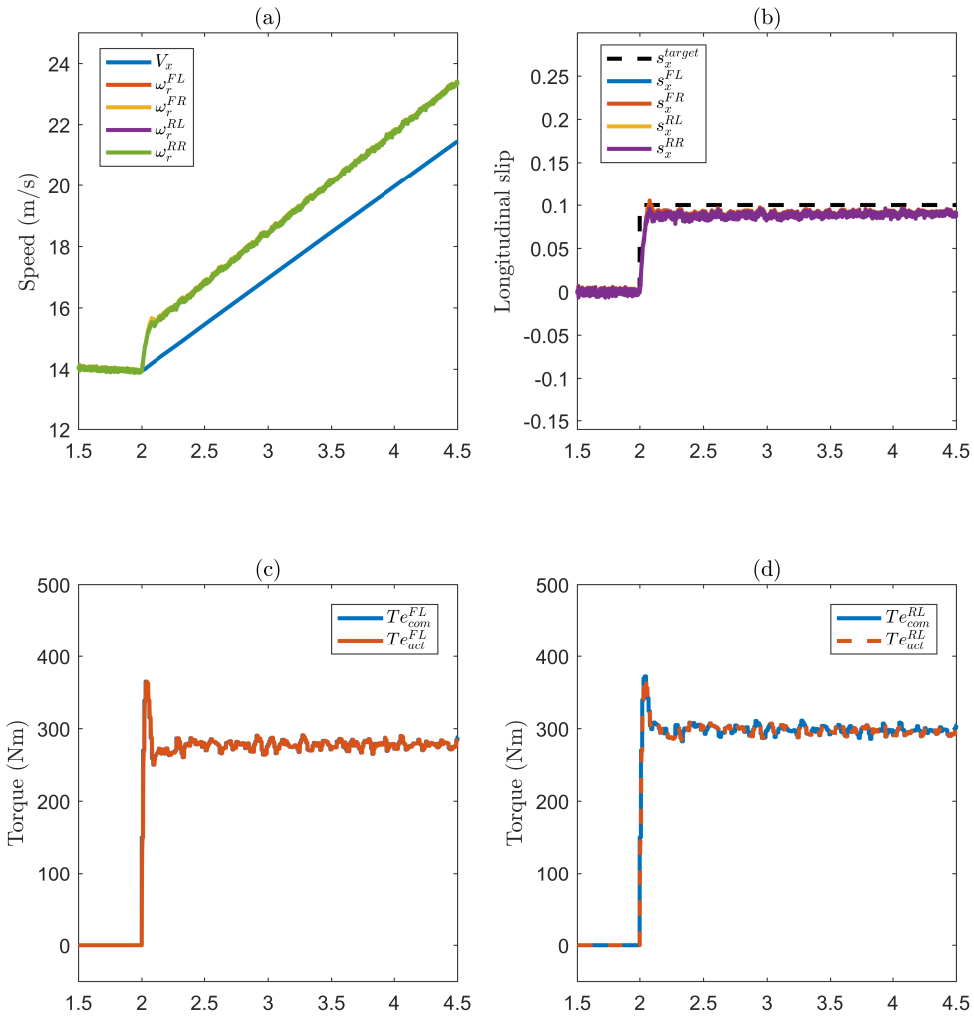

Figure 3.14: e-TCS straight line acceleration on low-μ, $V_{initial}$=50km/h, s_{ref}=-0.1.

3.6 Summary

This chapter concentrates on wheel slip control for an electrified vehicle. The main objective is to prevent wheel locking during emergency braking in any situation and on any road surfaces. A constant slip target is chosen for this work ($s_{ref} = -0.1$) to represent the best compromise for road-tyre frictions. The advantage of the chosen control algorithm is due to the high nonlinearity of the problem and robustness against external disturbance. The formulation derivation of the controller is presented and all required variables for the controller are listed. The non-measurable states such as V_x and tyre forces are acquired using estimations and each method is described in this chapter.

Several simulation cases are presented to validate the proposed slip controller using different test manoeuvres. The performance of the slip controller is evaluated in preventing wheel locking, maintaining the stability of the vehicle and the steerability for the driver to control the vehicle in a safe manner. A case for an E-slip control is presented where ABS or TCS can be achieved by the EM torque. The advantage of this feature is to utilise the EM to accelerate the vehicle efficiently in any situation and to stop the vehicle safely without any risk of wheel locking.

Chapter 4

Torque Blending for Slip Control using four EMs

In this chapter, we introduce a state-of-the-art torque blending strategy for wheel slip control for electrified vehicles using four EMs. This topology has been presented in 2.2.1 as the most flexible BEV architecture in terms of individual wheel torque control. The first strategy is to apply an optimisation method by adopting MPC to integrate the problem of slip control and torque allocation. Both nonlinear and linear MPC methods are presented. Then, a practical approach by using SMC for slip control and static allocation (Daisy Chain) is introduced. Finally, performance metrics are used to evaluate and analyse the developed strategies for four EMs electrified vehicle topology.

4.1 Overview of MPC

The general idea of the MPC is to optimise the performance of a system by predicting the future trajectory of the system by using a model. The sequence of future control effort is computed while respecting the defined constraints. Some advantages of using MPC are

the optimal performance while considering the state and control effort constraints and the ability to handle complex multivariable problems [21].

Since the emergence of the MPC in the late 1960s, the method has been developed for industrial application [120]. Originally it has been a breakthrough as an advanced control method to be applied in petrochemical and other process industries, where the control update rate is relatively low, so the required online computations can be carried out. There is an intuitive aspect of the method (focus on computational speed over the optimal-constraint solution) which has been applied to the slow processes and high-bandwidth applications such as servomechanism [75]. The evolution of computing hardware and the improvements of the optimisation algorithms mean that there is a significant opportunity for academic researchers and industries to explore the possibility of adopting MPC to solve problems in their respective areas.

The author in [19] discusses the potential advantages and the remaining challenges of MPC implementation for 'large volume' applications such as automotive, aerospace and mechatronics. The computer hardware and software advancement enables the industries to solve their large volumes problems with fast system dynamics, different classes of nonlinear behaviour, fewer inputs and outputs and with reduced costs.

Authors in [76] discuss the stability and optimality of linear and nonlinear MPC. The capabilities of linear MPC and their limitations have been discussed in [95]. The continuity of growth of nonlinear MPC algorithms will fill the gap where linear MPC has been proven challenging to apply. Authors also reported the rapid growth applications of MPC in the industries along with the discussion on the balance between theoretical and practical approach in MPC applications by academicians and industrial practitioners.

In automotive applications, several works report the implementation of MPC in various problems; engine management and emission regulation [40, 105], control of active and semi-active suspension [23], trajectory tracking of autonomous vehicle [16],

[33–36], [63], obstacle and collision avoidance [37, 80], yaw and lateral stability control [7, 12, 20, 22], torque vectoring [109], TCS [15] and ABS [125].

Figure 4.1 describes the basic understanding of how MPC works [75]. In discrete-time, the present time is k and the predicted plant output is $\bar{y}(t|k)$. The notation $(t|k)$ is used to indicate that the prediction relies on the system condition at time k. The reference trajectory $r(t|k)$ is the ideal trajectory which the plant should converge to with the smallest possible of control effort u.

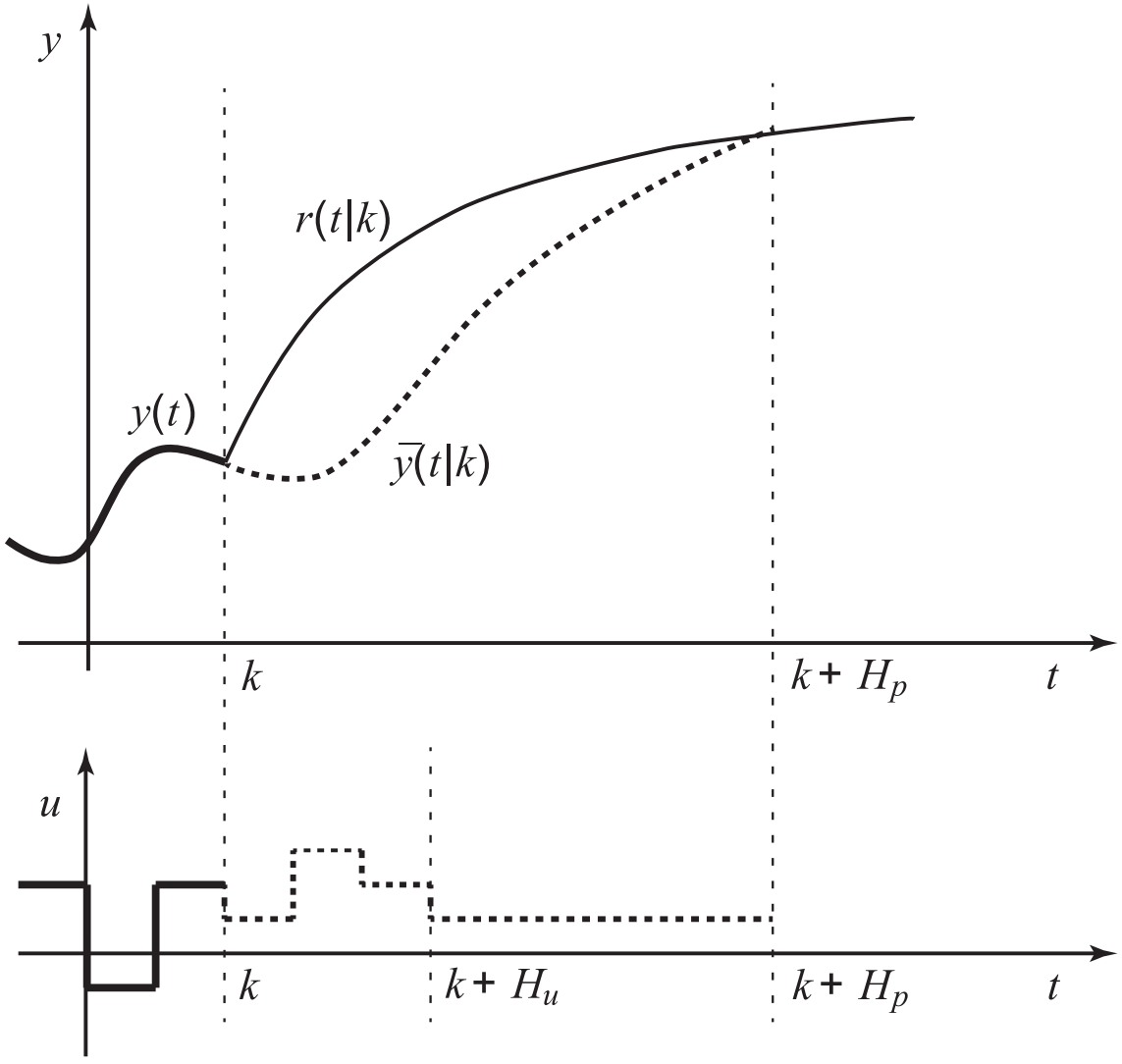

Figure 4.1: MPC basic idea (adopted from [109]).

An 'internal model' is used to predict the plant's behaviour to modify the control input u over the prediction horizon, Np. It can be assumed that the output $y(t|k)$ measurement is available. Future input trajectory along the control horizon $Nu \leq Np$ is then chosen to satisfy certain requirements while respecting the constraints imposed. Then, only the first element of the input trajectory is applied as the plant's input signal. At one sampling interval later $(k+1)$, the procedure is repeated. The prediction horizon shifts one sampling interval at each step but remains the same.

Normally, the input trajectory with smallest control effort in the form of a quadratic cost function is set as the requirements in choosing the prescribed trajectory. Thresholds that are related to the physical boundaries of the system are referred to as constraints which in our case the braking actuators limit and dynamics.

4.2 Integration of Torque Blending and Slip Control using MPC

In this section, we present two torque blending strategies for slip control which include linear and nonlinear MPC formulations. The first objective is to avoid wheel locking by controlling the wheel slip to a desired slip target, s_{ref} in an emergency situation. Next, the torque delivery is apportioned to the braking actuators (RBS and EHB) while respecting the actuator dynamics and limits. These objectives will be integrated into a single MPC problem which has the advantage of handling multivariable constrained control problems. The general overview of the developed strategy is shown in Figure 4.2.

For the continuous time system with state x and input u

$$\dot{x} = f(x,u), \tag{4.1}$$

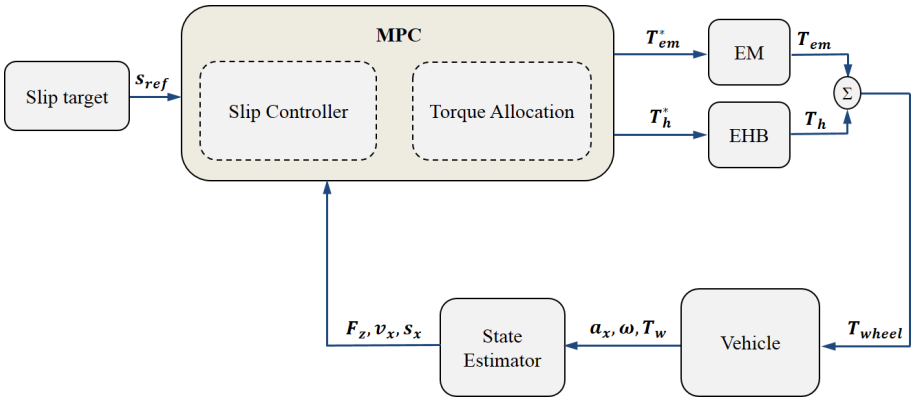

Figure 4.2: Overview of torque blending strategy for four EMs using MPC.

the equivalent discrete form is

$$x_{k+1} = g(x_k, u_k). \tag{4.2}$$

Then, the general discrete Optimal Control Problem (OCP) is

$$\min_{x,u} \quad J(x_k, u_k) = \sum_{k=0}^{N-1} [(x_k - x_{ref})^T Q(x_k - x_{ref}) + (u_k - u_{ref})^T R(u_k - u_{ref})] \tag{4.3a}$$

$$\text{subject to} \quad x(0) = x_{init}, \tag{4.3b}$$

$$x_{k+1} = g(x_k, u_k), \quad k = 0, ..., N-1 \tag{4.3c}$$

$$x^{min} \leq x_k \leq x^{max}, \quad k = 0, ..., N-1, \quad h(x_k) \leq 0 \tag{4.3d}$$

$$u^{min} \leq u_k \leq u^{max}, \quad k = 0, ..., N-1, \quad c(u_k) \leq 0 \tag{4.3e}$$

In the above, the objective is to minimise the state and input errors with respect to the given references x_{ref} and u_{ref}, subject to the initial condition, the system dynamics 4.3c and both the state constraint 4.3d and input constraint 4.3e. Q and R are (positive) the weighting matrices for state error and control effort.

In our case we need to find the necessary friction and electric torques on the wheel to achieve the desired longitudinal slip, while at the same time give priority to the use of the

electric motor. We choose to neglect the actuator dynamics (2.12,2.13) and rather set

$$T_{e_{k+1}} = T_{e_k} + \Delta T_{e_k}, \tag{4.4}$$

$$T_{h_{k+1}} = T_{h_k} + \Delta T_{h_k}, \tag{4.5}$$

where we have assumed that the input only changes at times k, $k+1$, ..., $k+N-1$ (with N the prediction horizon). In this way we not only simplify the formulation but we are also given the opportunity to constrain the rate of change of the friction and electric torques, while avoiding setting a target friction and electric torque in the cost function as we demonstrate below. The internal model for the MPC is therefore (2.2)-(2.4) augmented with (4.4)-(4.5) so that the state and input vectors are $\bar{x} = [V_x \quad \omega \quad T_e \quad T_h]^T$ and $\bar{u} = [\Delta T_e \quad \Delta T_h]^T$. In this work we assume we can measure ω using standard wheel speed sensor in a vehicle and estimate V_x and F_z which are required for the MPC strategies as in section 3.3. Using the augmented system the MPC with sampling time t_s is then

$$\min_{x,u} \quad \sum_{k=0}^{N-1} [q_s(s_{x_k} - s_{ref})^2 + q_T T_{h_k}^2 + q_e \Delta T_{e_k}^2 + q_h \Delta T_{h_k}^2] \tag{4.6a}$$

$$s.t. \quad \bar{x}(0) = \bar{x}_{init}, \tag{4.6b}$$

$$\bar{x}_{k+1} = \bar{g}(\bar{x}_k, \bar{u}_k), \quad k = 0, ..., N-1 \tag{4.6c}$$

$$T_e^{min} \leq T_{e_k} \leq T_e^{max}, \quad k = 0, ..., N-1 \tag{4.6d}$$

$$T_h^{min} \leq T_{h_k} \leq T_h^{max}, \quad k = 0, ..., N-1 \tag{4.6e}$$

$$\Delta T_e^{min} \leq \Delta T_{e_k} \leq \Delta T_e^{max}, \quad k = 0, ..., N-1 \tag{4.6f}$$

$$\Delta T_h^{min} \leq \Delta T_{h_k} \leq \Delta T_h^{max}, \quad k = 0, ..., N-1 \tag{4.6g}$$

where we choose to penalize the s_x from a given reference through its definition (2.5), the torque rates ΔT_e and ΔT_h which will force the torques to stabilize to a value, along with

an additional weight on the T_h to avoid using the friction brakes when possible and by respecting the constraints from the actuator dynamics. In this way we do not explicitly set references for the electric motor and friction brake torques, but rather leave the MPC to find the optimal values according to the given longitudinal slip reference, the torque and torque rate constraints, and the chosen weights q_s, q_e, q_h, $q_T > 0$.

We apply a high penalty for the friction brake torque rate in order to give priority to the use of regenerative braking. The values of the weighting coefficient used in this work, for both linear and nonlinear cases of the MPC controller, and all different scenarios can be found in Table 4.1. It can be noted that the tuning process includes trial and error based on pre-determined priority selection. The first value of the optimal control input u_1 is applied to the actual system and the optimisation is then repeated for a shifted horizon.

Parameter (Unit)	Description	Value
t_s (ms)	sampling time	5
N	number of steps	20
q_s	weight of slip error	$0.1\frac{(\Delta T_e^{limit})^2}{(s_{ref})^2}$
q_T	weight of friction torque	1
q_e	weight of ΔT_e	50
q_h	weight of ΔT_h	1000

Table 4.1: NMPC properties for four EMs strategy.

4.2.1 Nonlinear MPC

The internal model employed in the NMPC formulation is based on a discretised version of the wheel dynamics (2.2-2.4) found using five steps of the fourth order Runge-Kutta

scheme [94],

$$k_1 = f(x_k, u_k), \tag{4.7a}$$

$$k_2 = f(x_k + \frac{h}{2}k_1, u_k), \tag{4.7b}$$

$$k_3 = f(x_k + \frac{h}{2}k_2, u_k), \tag{4.7c}$$

$$k_4 = f(x_k + hk_3, u_k), \tag{4.7d}$$

$$x_{k+1} = x_k + \frac{h}{6}(k_1 + 2k_2 + 2k_3 + k_4) \tag{4.7e}$$

which is then augmented by (4.4)-(4.5) like explained above.

In order to solve the NMPC problem in real-time, the Interior-Point (IP) method as available in Forces Pro [30, 126] is employed: it has been found that the specific method can provide solutions in real-time without the performance degradation associated with a linear MPC formulation or suboptimal NMPC strategies such as the Real Time Iteration (RTI) scheme [51].

4.2.2 Linear MPC

A second method is constructed based on linear MPC to approach the wheel slip control with torque blending strategy problem. This algorithm will be formulated with similar states and inputs as the approach above (section 4.2) and all constraints remain unchanged. The main difference between the linear MPC and the NMPC is how we define the discrete system dynamics in (4.4)-(4.5). The state space equation for the linear MPC is presented

in the following equations:

$$\dot{x} = Ax + Bu, \tag{4.8}$$

$$\begin{bmatrix} \dot{V}_x \\ \dot{\omega} \end{bmatrix} = A \begin{bmatrix} V_x \\ \omega \end{bmatrix} + B \begin{bmatrix} T_e \\ T_h \end{bmatrix} \tag{4.9}$$

In the linear MPC case, we linearise (2.2)-(2.4) about the current values of V_x, ω and the values of T_e, T_h at the previous time step as presented in Appendix A. This allows us to avoid setting target for T_e and T_h as would be the case if we were to linearise about an equilibrium target. If we linearise the continuous system dynamics in (4.1) about point $(x_{lin}, u_{lin}) = (x_k, u_{k-1})$ we have

$$\dot{x} = A_c x + B_c u + c_c, \tag{4.10}$$

$$\text{where} \qquad c_c = -(A_c x_{lin} + B_c u_{lin} - \dot{x}_{lin})$$

Note that $\dot{x}_{lin} \neq 0$ since (x_{lin}, u_{lin}) is not necessarily an equilibrium point and if c_c is treated as a piecewise constant disturbance the discretised system is then

$$x_{k+1} = A_d x_k + B_d u_k + E c_k \tag{4.11}$$

where

$$c_k = -(A_d x_k + B_d u_k - x_{k+1})$$

$$A_d = e^{At_s}, \qquad B_d = \int_0^{t_s} e^{A\eta} d\eta B, \qquad E = \int_0^{t_s} e^{A\eta} d\eta$$

or an approximation can be used for the low t_s used in this work

$$A_d = (I + At_s), \qquad B_d = t_s B, \qquad E = t_s$$

Then the affine discretised system is

$$x_{k+1} = (I + At_s)x_k + t_s Bu_k + t_s c_k \tag{4.12}$$

which is then augmented by (4.4)-(4.5) as described before. Finally, the Forces Pro solver [30] is employed to solve the linear MPC in real time which can be deployed in a high fidelity vehicle model for simulation.

4.3 Simulation with high fidelity vehicle model-MPC

In this section, we present the simulation results using the MPC formulations on a high fidelity model. An AWD electric vehicle model using four near-wheel motors is constructed in MATLAB/Simulink and IPG CarMaker environment as described in 2.3. The vehicle and tyre parameters used are listed in Table 2.2. A sophisticated driver model in CarMaker is used for closed loop simulation test manoeuvres for consistency. For the simulation, we assume that the available regenerative braking torque for each EM is 750Nm.

4.3.1 Straight line braking on high μ road

In this scenario the vehicle initially travels at the speed of 50km/h on dry asphalt road (μ=1). The controller is activated at t=2s and the slip target is s_{ref}=-0.1. The vehicle velocity V_x is estimated using the observer presented in section 3.3.1 considering noise for wheel speed ω and longitudinal acceleration a_x as mentioned in the previous section.

Without slip control hard braking on dry asphalt can lead to locking of the wheels. In the case of the NMPC, the controller manages to bring the wheel slip close to the reference value as illustrated in figures 4.3(a)-(b). We observe that there is a small undershoot of

wheel slips at the front wheels. Since the front electric motors quickly saturate, this can be attributed to the slower friction braking response as seen in figure 4.3(c).

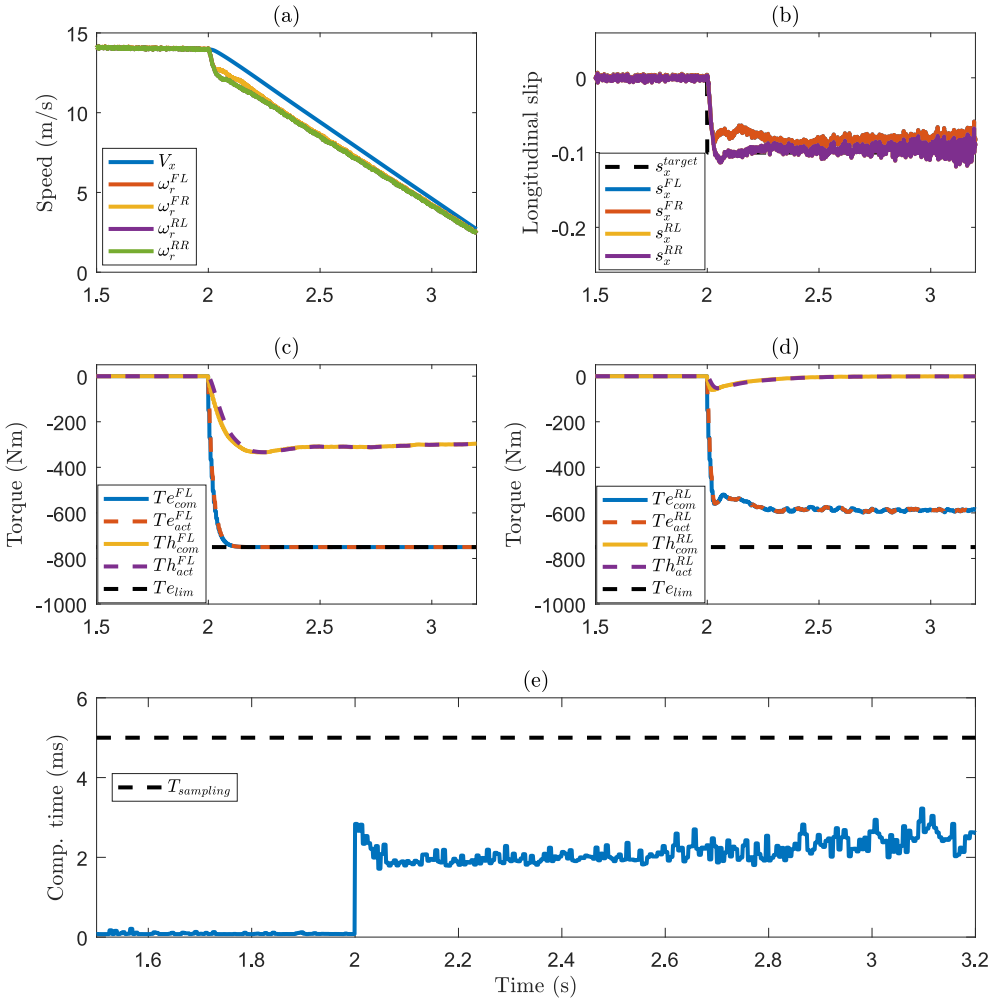

Figure 4.3: NMPC straight line braking with road μ=1, $V_{initial}$=50km/h, s_{ref}=-0.1.

According to figures 4.3(c)-(d), the brake torque delivered by the EM is insufficient to achieve the desired slip. Consequently, friction brake torque is required to supplement the EM braking torque. It is also worth noting at this point that the commanded torques (T_{com}) from the controller are very close to the actual torques (T_{act}) as delivered by the

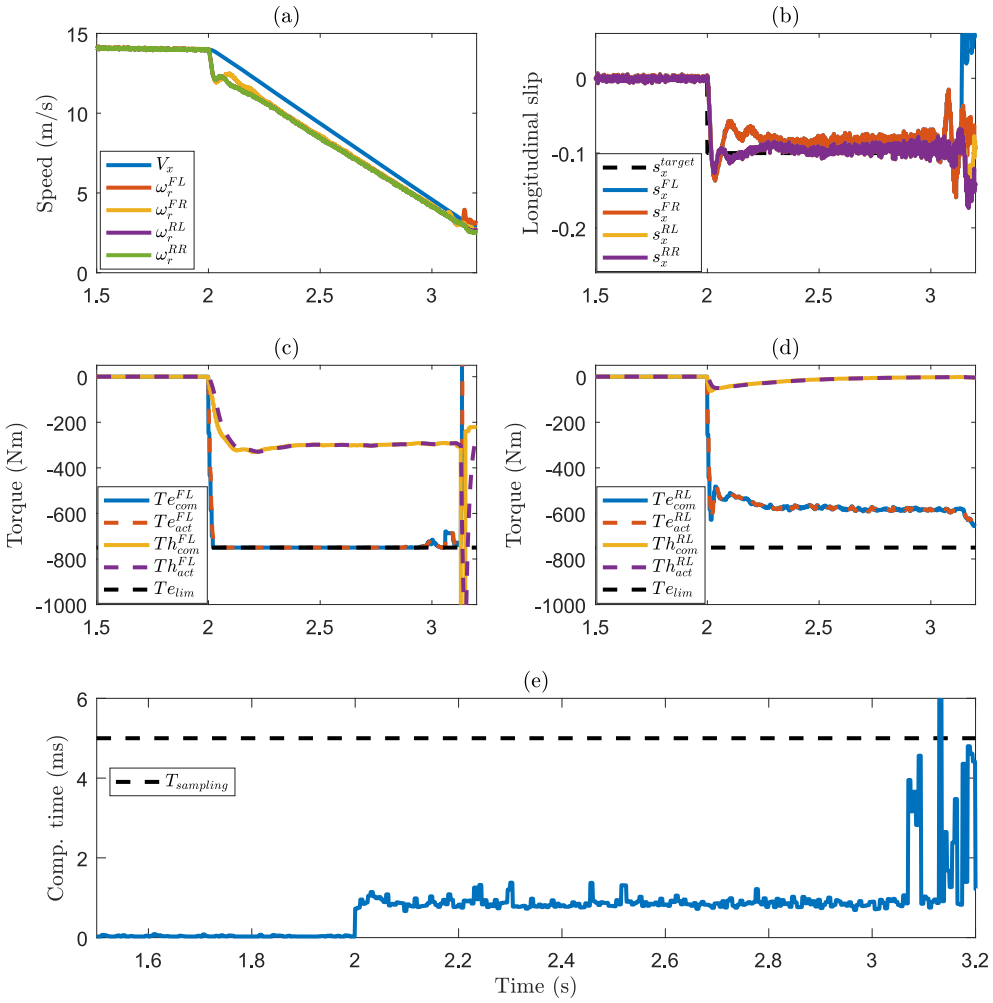

Figure 4.4: Straight line μ=1 braking for Linear MPC with t_s=5ms.

actuators, a result of including the torque rate constraints in the NMPC formulation. The stopping distance recorded with brake blending strategy shows 6.8% improvement when compared to the pure friction ABS result.

The manoeuvre is repeated with the linear MPC algorithm to evaluate the controller's performance. Figure 4.4 indicates that the strategy can be deployed using the linearised internal model for the MPC. The performance is acceptable and comparable to the NMPC

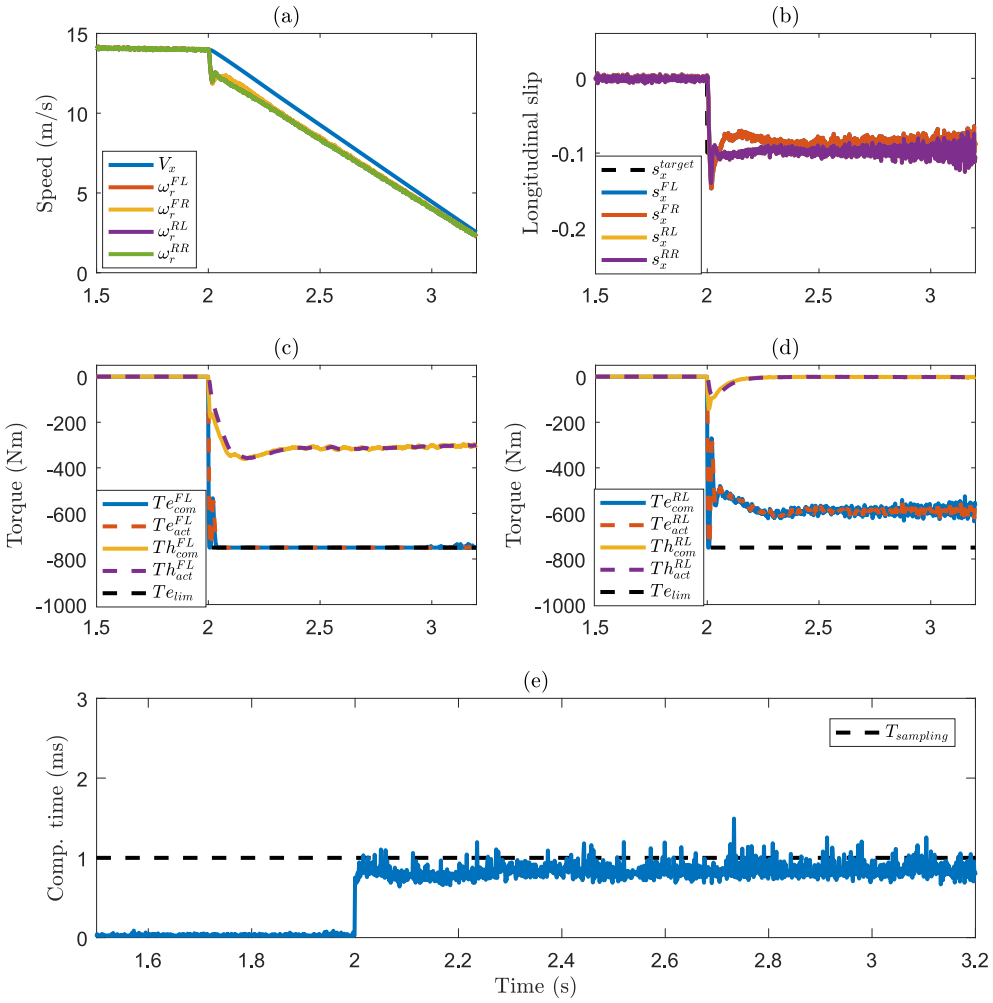

Figure 4.5: Straight line μ=1 braking for Linear MPC with t_s=1ms.

approach for most of the duration of the manoeuvre. The linear MPC controller suffers from poor performance at lower speeds as shown in figure 4.4. The poor performance is caused by the linearisation errors when a new slip target is set which is due to the fast changing dynamics. Decreasing the sampling time t_s to 1ms, we achieve a more frequent update of the linearisation matrices and the controller performs better at lower V_x as shown in figure 4.5.

Furthermore, we observe, as expected, that the computation time required is smaller for the linear MPC case compared to the NMPC strategy. In figures 4.3(e) and 4.4(e) it is shown that a mean time of 1.95ms and 0.99ms are required for NMPC and linear MPC (t_s=5ms) cases respectively for the optimization problem to be solved using a standard desktop (i7-4790M at 3.60GHz with 16GB of memory). That is, in both cases, the computation time is below the 5ms sampling time and hence real-time implementation is feasible. However, when the t_s is reduced to 1ms to improve the response of the linear MPC at low V_x, there is a risk that the controller cannot be deployed in real time, as illustrated in figure and 4.5(e).

REMARK: We highlight that the implementation was performed using a standard desktop computer rather than a vehicle ECU. Such implementation however, is commonly used in the literature to demonstrate initial real-time capability of algorithm deployment [100, 101].

4.3.2 Straight line braking on low μ road

The next scenario illustrates an emergency braking event with ABS on a packed snow surface (μ=0.3) with initial speed of 50km/h. Figures 4.6(a)-(b) indicate that the slip ratio s_x for individual wheels is well controlled around the reference value s_{ref}=-0.1 using the NMPC algorithm. Results for the linear MPC strategy as shown in figure 4.7 are acceptable and comparable to the NMPC strategy, except again at low V_x.

A similar observation can be made when t_s is reduced to 1ms where the slip control performance at low V_x is improved as indicated in figure 4.8. Once again, reducing the sampling time results in a computation time which in places exceeds the sampling time. The mean solve time for the optimization problem is 3.7ms as shown in figure 4.6(e) for NMPC strategy whereas figure 4.7(e) indicates 0.92ms is required for the optimization

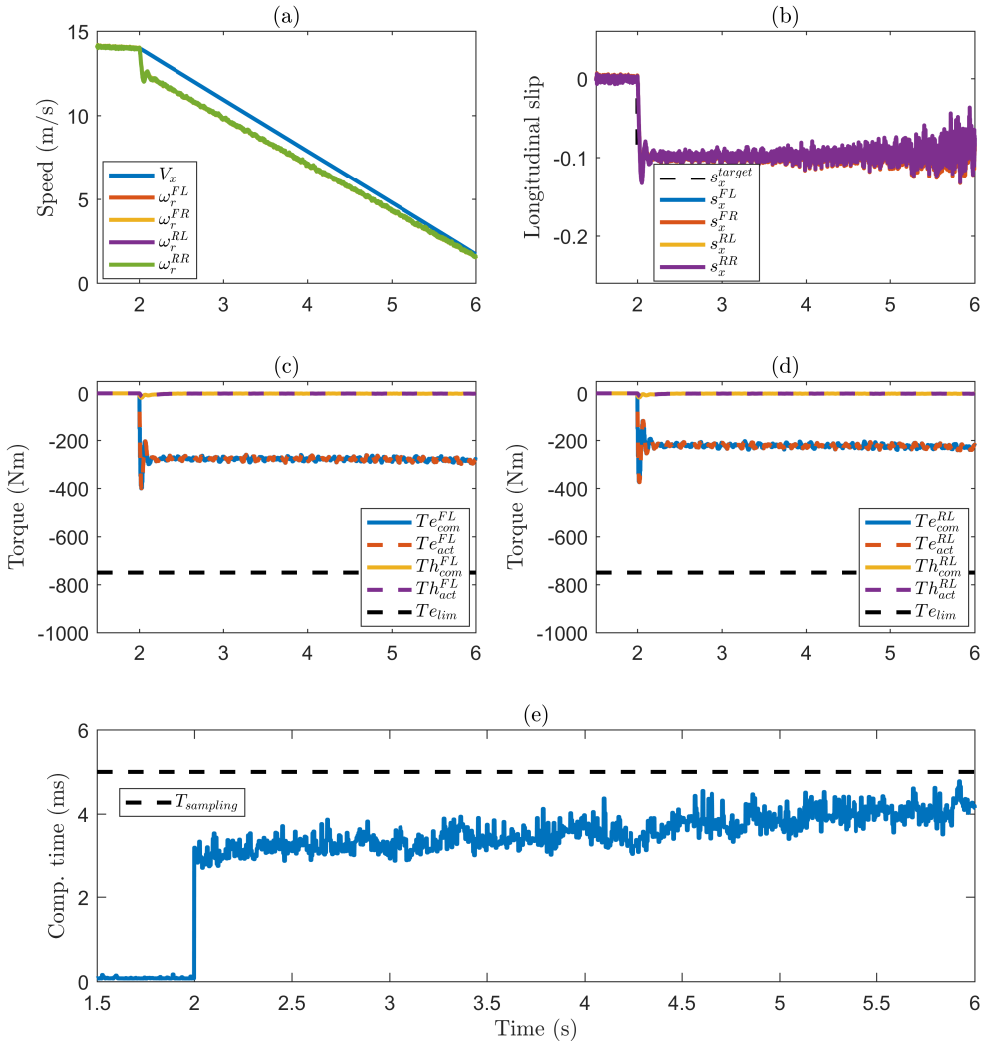

Figure 4.6: NMPC straight line braking with road μ=0.3, $V_{initial}$=50km/h, s_{ref}=-0.1.

problem to be solved for linear MPC strategy.

In the low μ braking case we observe, as expected, a reduced total torque required to achieve the desired slip compared to the high μ case. The proposed MPC strategies are able to prioritise EM braking and in the case of low μ, deliver slip control using solely

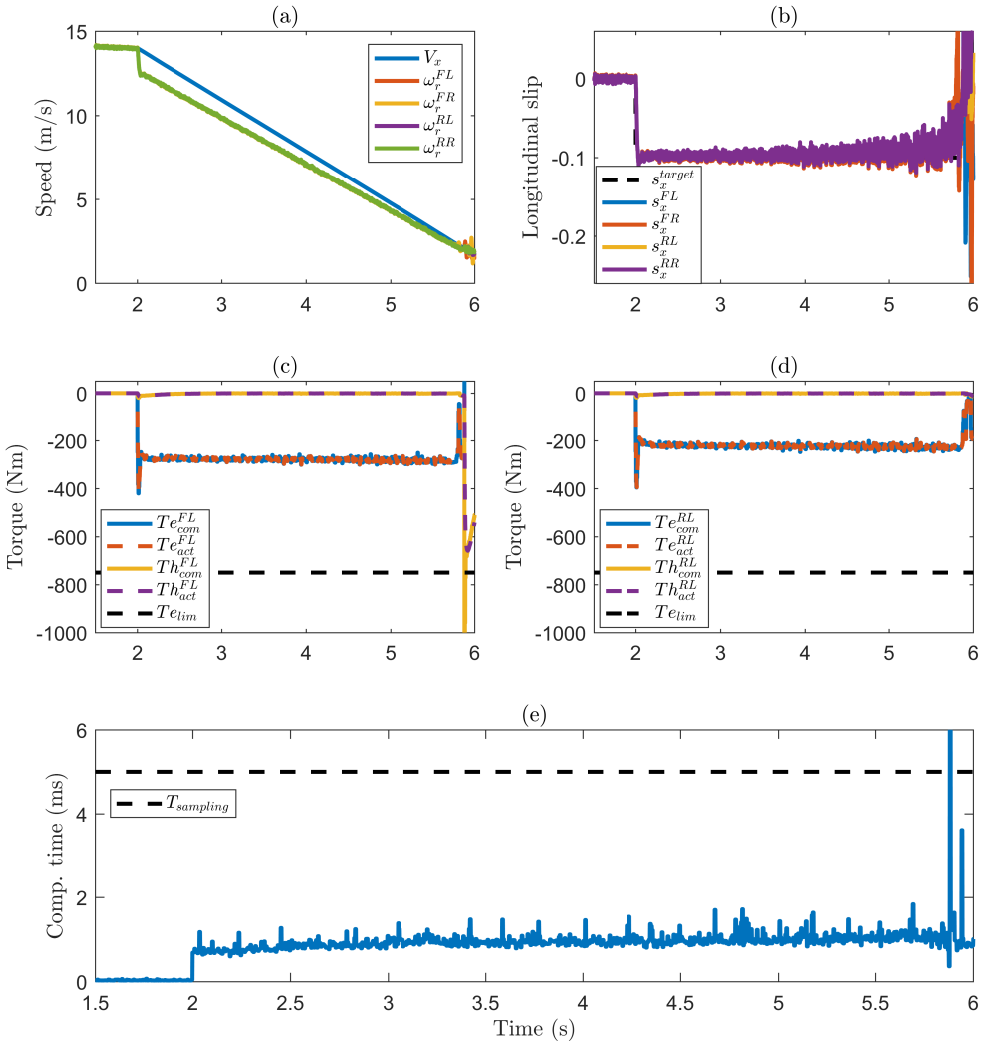

Figure 4.7: Straight line μ=0.3 braking for Linear MPC with t_s=5ms.

regenerative braking as indicated in figures 4.6(c)-(d). Comparison between the results for braking on high μ and low μ road show that if available EM power permits, we can deploy pure electric braking when deceleration demand is low especially on a surface with low friction coefficient. The braking force demand by the driver clearly exceeds the available friction between the road surface and the tyres, hence the brake torques (figure 4.6(c)-(d)) are limited and reduced to satisfy the target slip ratio value. These results indicate the

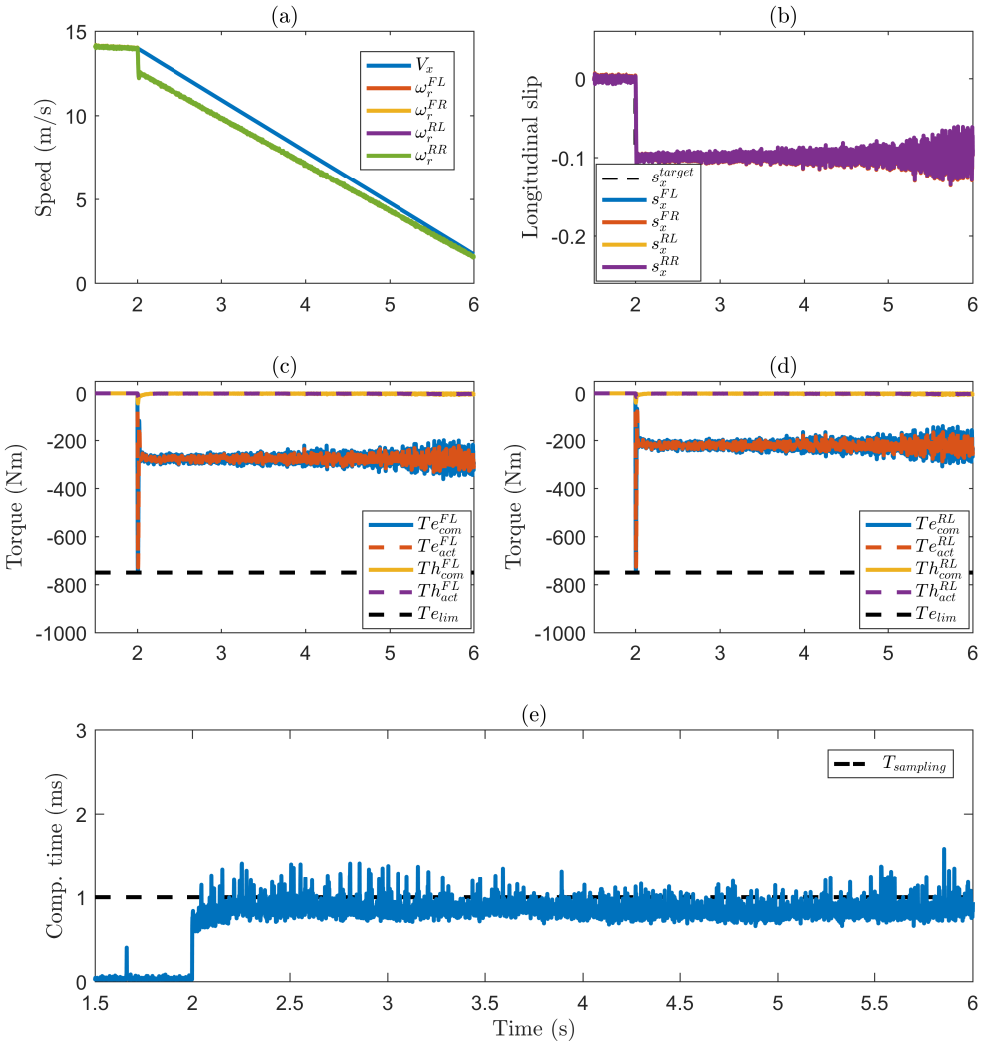

Figure 4.8: Straight line μ=0.3 braking for Linear MPC with t_s=1ms.

slip reference s_{ref} can be tracked accurately and wheel slip control is achieved using only regenerative braking torque by the EM.

4.3.3 Straight line braking on split μ road

Slip control is very important in the presence of uneven friction of road surfaces. In this example, a vehicle is braking on a road with dry asphalt on the left wheels (μ=1) and on snow on the right wheels (μ=0.3) from an initial speed of 50km/h. A yaw moment is created towards the high friction side of the road if the same brake torque is applied to the left and right wheels.

The proposed controller detects the high wheel slip ratio and quickly retards the brake torque to avoid wheel locking and prevent the vehicle from spinning. Lower brake torque is applied to the wheels on the low μ side to maintain the wheel slip within acceptable limits as illustrated in figure 4.9(a). Figures 4.9(d)-(g) clearly show the capability of the individual wheel slip control to deliver the required braking torque by either single actuator or both actuators to achieve the reference slip s_{ref}.

Another interesting observation is that the vehicle maintains its steerability and stability for all the wheels for NMPC strategy throughout the braking as evidently indicated by the maximum yaw rate achieved ($\dot{\psi}$=10.1deg/s) and steering wheel angle (δ=73deg) in figure 4.9(b)-(c). With sufficient countersteering by the CarMaker driver model, the vehicle can be safely stopped. Even without Electronic Stability Control (ESC), the vehicle stability and steering response can be maintained.

Figure 4.10 shows the performance of the linear MPC strategy for split μ braking. The wheel slip s_x achieved is acceptable during initial braking but becomes unstable towards lower vehicle speeds similar to the straight line braking cases.

4.3.4 Braking in turn

Panic braking while cornering is a good example to demonstrate the benefits of having slip control in a vehicle. Simulations with entry speed V_x of 50km/h on both high μ and

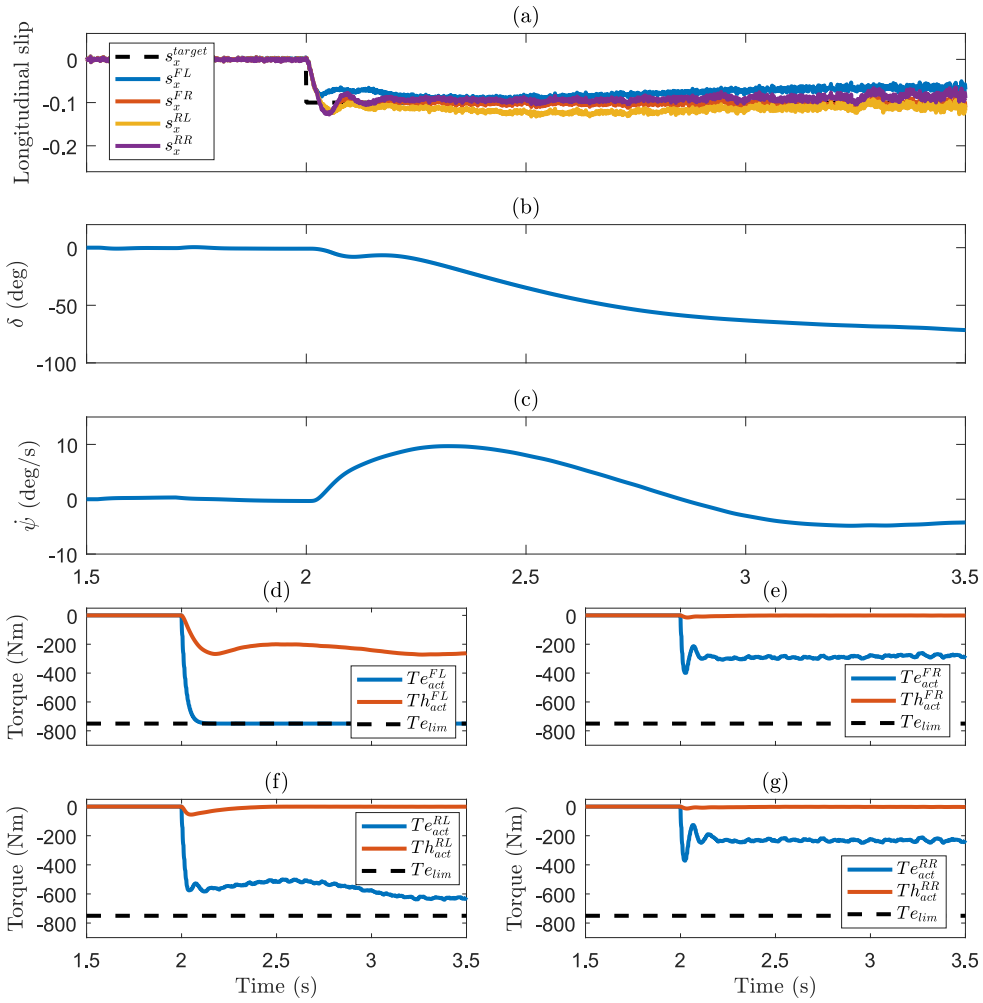

Figure 4.9: NMPC split μ braking, $V_{initial}$=50km/h, s_{ref}=-0.1.

low μ road surfaces are carried out to validate the performance of the NMPC algorithm. The slip target s_{ref} is -0.1 and controller is activated at t=5s.

Without ABS, the vehicle understeers once the friction between road surface and tyres is saturated resulting in the vehicle sliding forward instead of turning in to follow the cornering radius. On the contrary, slip control maintains the wheel slip ratio following the reference value. Loss of lateral grip is prevented and the driver is able to steer and

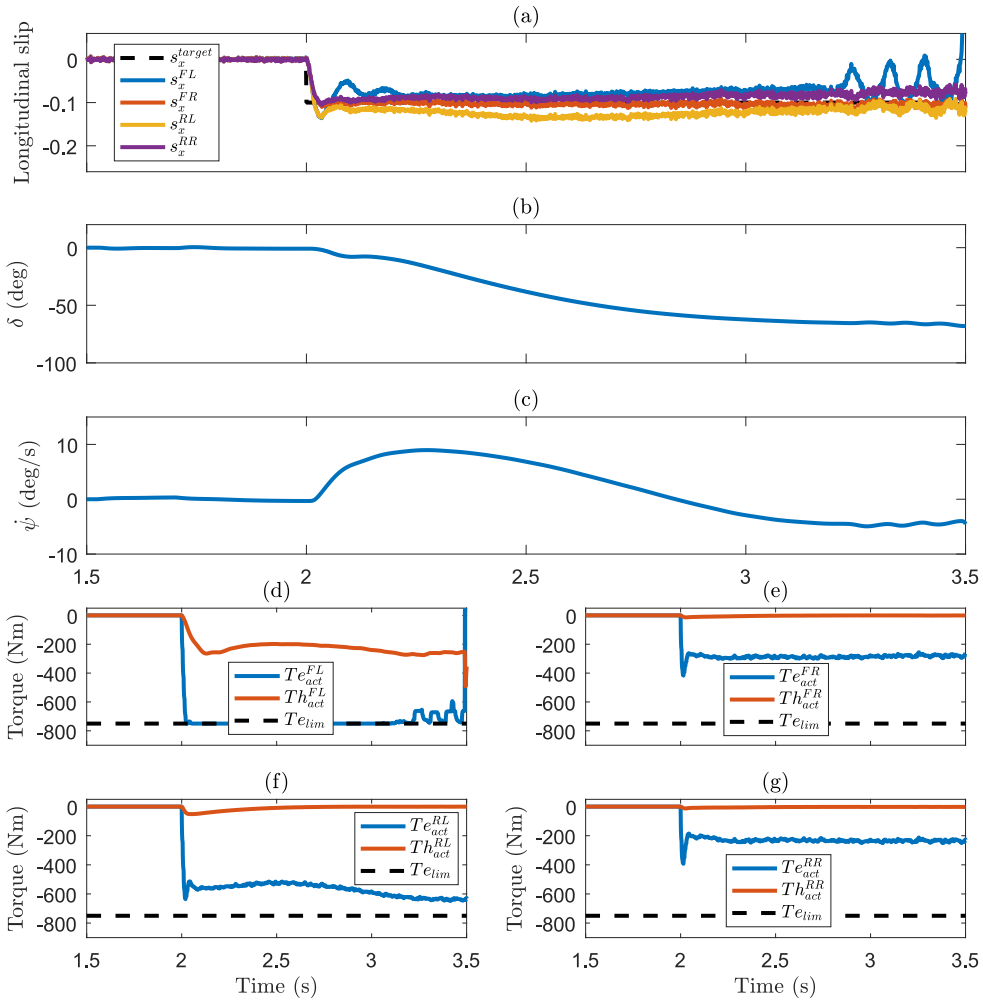

Figure 4.10: Linear MPC (t_s=5ms) split μ braking.

maintain the vehicle turning radius. Based on figures 4.11 a) - b), it is clearly shown that the individual wheel slip controller maintains the slip ratio on each wheel close to the reference value by varying the brake torques. Figures 4.11 c) - d) show that individual wheel torque is delivered by both braking actuators. The vehicle enters the corner (road μ=1 and D=1) at steady state with steering angle δ of 45deg and maximum driver steering angle δ recorded during braking is 50deg. Similar scenario is repeated on low adhesion

road condition (road μ=0.5 and D=0.5). It can be seen from figures 4.12 c) - d) that all required braking torque can be delivered by the EM when braking on the low μ road surface. Another interesting observation is that the wheel slip is (4.12 b)) tracking the slip target more closely due to minimal load transfer effects when braking on a low μ surface. The maximum driver steering angle δ required to maintain the vehicle cornering path is 59deg.

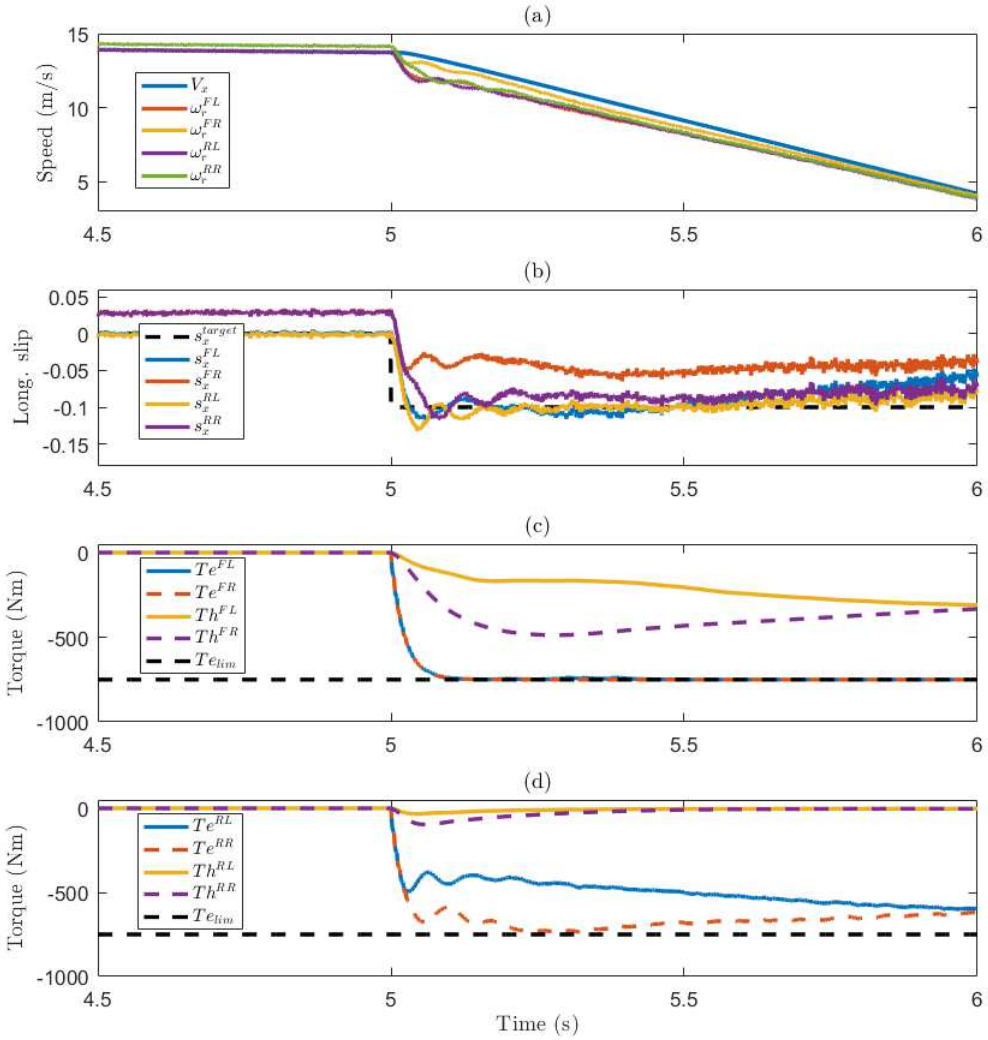

Figure 4.11: Brake in turn with road μ=1, D_{mpc}=1, $V_{initial}$=50km/h, sx_{ref}=-0.1.

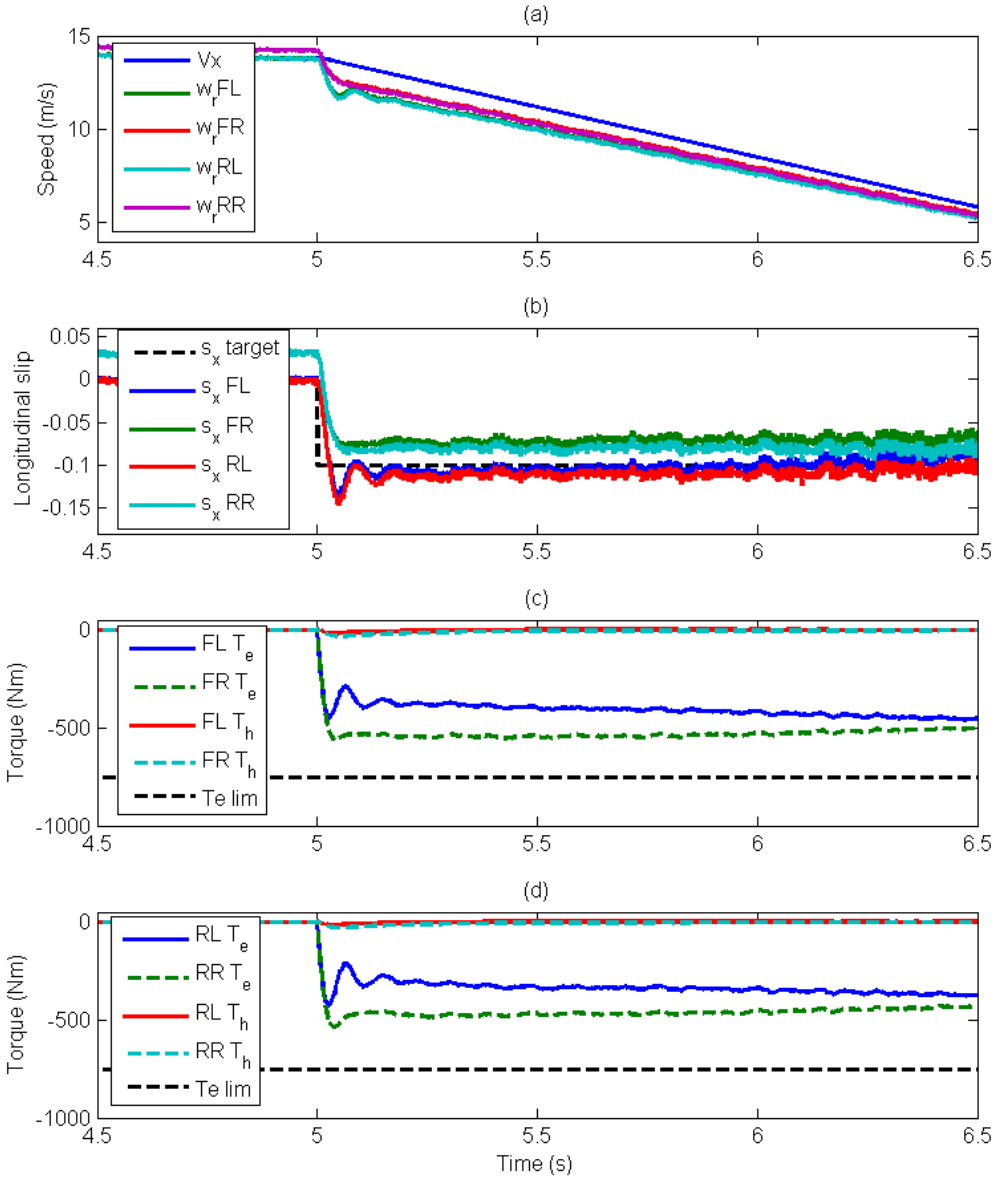

Figure 4.12: Brake in turn with road μ=0.5, D_{mpc}=0.5, $V_{initial}$=50km/h, sx_{ref}=-0.1.

4.3.5 Impact on varying slip reference

The aim of slip control is to be able to achieve a desired wheel slip ratio. However, there is a challenge in determining a reference slip value for all conditions and road surfaces. While selecting optimum reference slip is not the focus of this work we can demonstrate the effects of varying slip target on the NMPC slip control and torque blending.

Figure 4.13 shows the results for braking in turn with slip reference s_{ref} -0.05 and -0.15. The initial vehicle speed V_x is 50km/h and the test is conducted on a μ=0.5 road. The controller is activated at t=5s. The fact that the vehicle stops in a shorter distance with higher slip reference (s_{ref}=-0.15) shows that the slip control operates near the peak region of the tyre-road friction coefficient curve. However, this sacrifices the lateral grip which leads to higher yaw rate $\dot{\psi}$ (12.9deg/s) achieved by the vehicle and requires the driver to provide larger hand wheel angle δ (89deg) steering correction in order to maintain the vehicle path (figure 4.13 a)-b)). For simulation with s_{ref} -0.05 the recorded maximum driver steering angle δ and yaw rate $\dot{\psi}$ achieved is 56.4deg and 11.3deg/s respectively (figure 4.13 a)-b)).

The next scenario presented is split-μ braking with initial vehicle speed V_x=50km/h. The controller is activated at t=5s. It is clearly shown in figure 4.14 that larger steering wheel angle δ correction (238deg clockwise direction) is required by the driver model to maintain the vehicle straight line path for the slip reference s_{ref} =-0.15. The distance covered during braking is shorter by 4.2m as opposed to the braking distance for slip reference s_{ref}=-0.05. However, this sacrifices the lateral grip which leads to higher yaw rate $\dot{\psi}$ (16.5deg/s) achieved by the vehicle and requires the driver to provide larger hand wheel angle δ steering correction in order to maintain the vehicle path. Maximum yaw rate $\dot{\psi}$ of the vehicle for the case of slip reference s_{ref}=-0.05 is 4.3deg/s. We observe that the selection of the slip ratio target can be used to compromise between vehicle stability

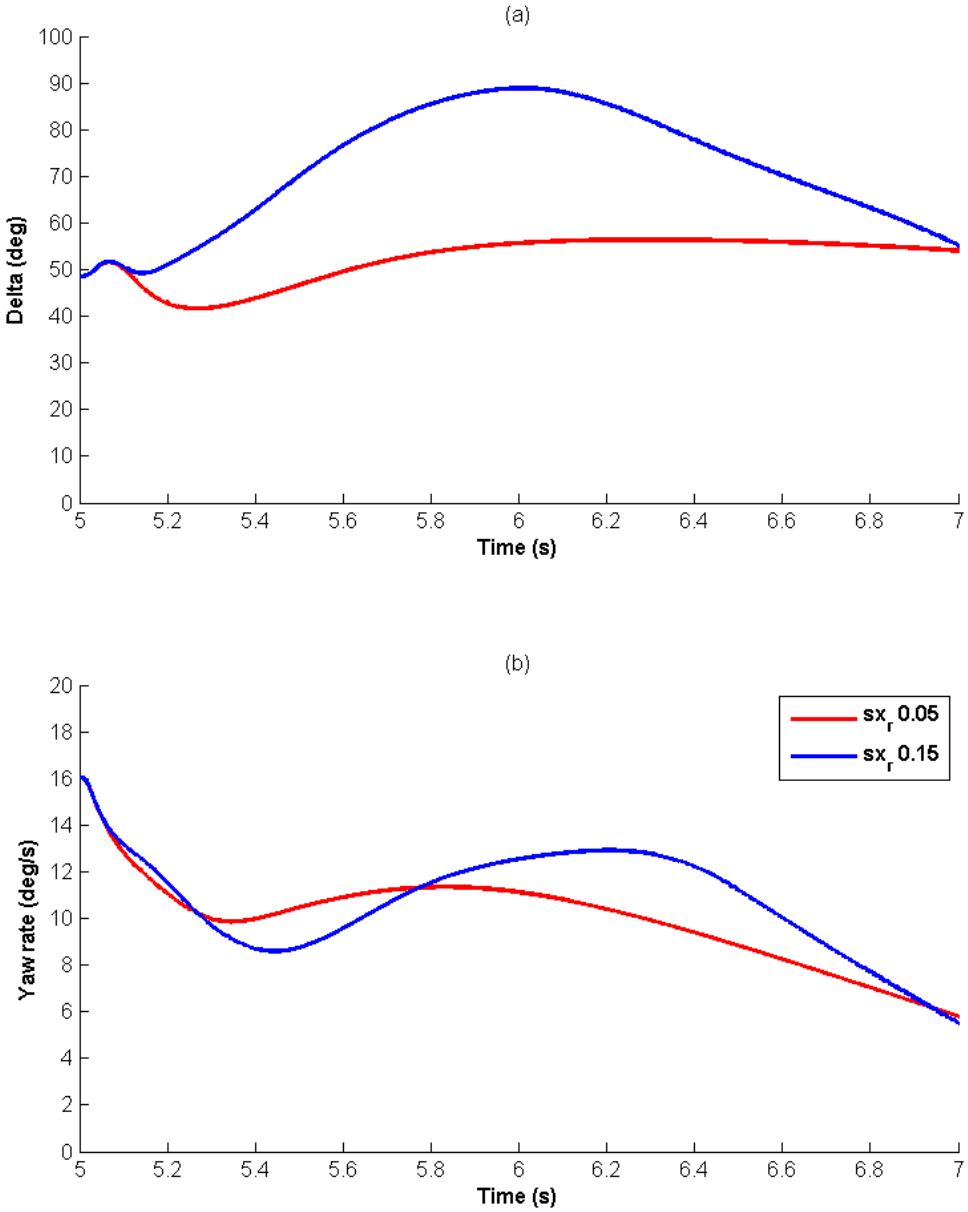

Figure 4.13: Brake in turn with sx_{ref}=-0.05 and -0.15.

and vehicle braking distance during emergency braking.

4.3.6 Robustness against tyre-road friction coefficient uncertainty

In the MPC formulation we assume to have information of the road conditions and therefore MF's factor, D used in the internal MPC model which corresponds to the value of the tyre-road μ. In reality, we require estimation of road friction coefficient in order to update the D value in the control algorithm. In this section we demonstrate the effect of braking on various type of road friction coefficient (μ = 0.3 and 0.9) using a constant D for MF's factor (D=0.6), to study the robustness of the proposed controller.

Figure 4.15 indicates that the NMPC controller is robust against uncertainties in the tyre-road friction coefficient. In both cases of under-estimation and over-estimation of the μ the controller achieves a stable wheel slip response, however with some notable offset from the reference value. This offset can be avoided with an adaptation of the internal model. Even without the adaptation, despite the significant variation in μ, the wheel slip is not excessive and the vehicle can stop safely without any risk of skidding.

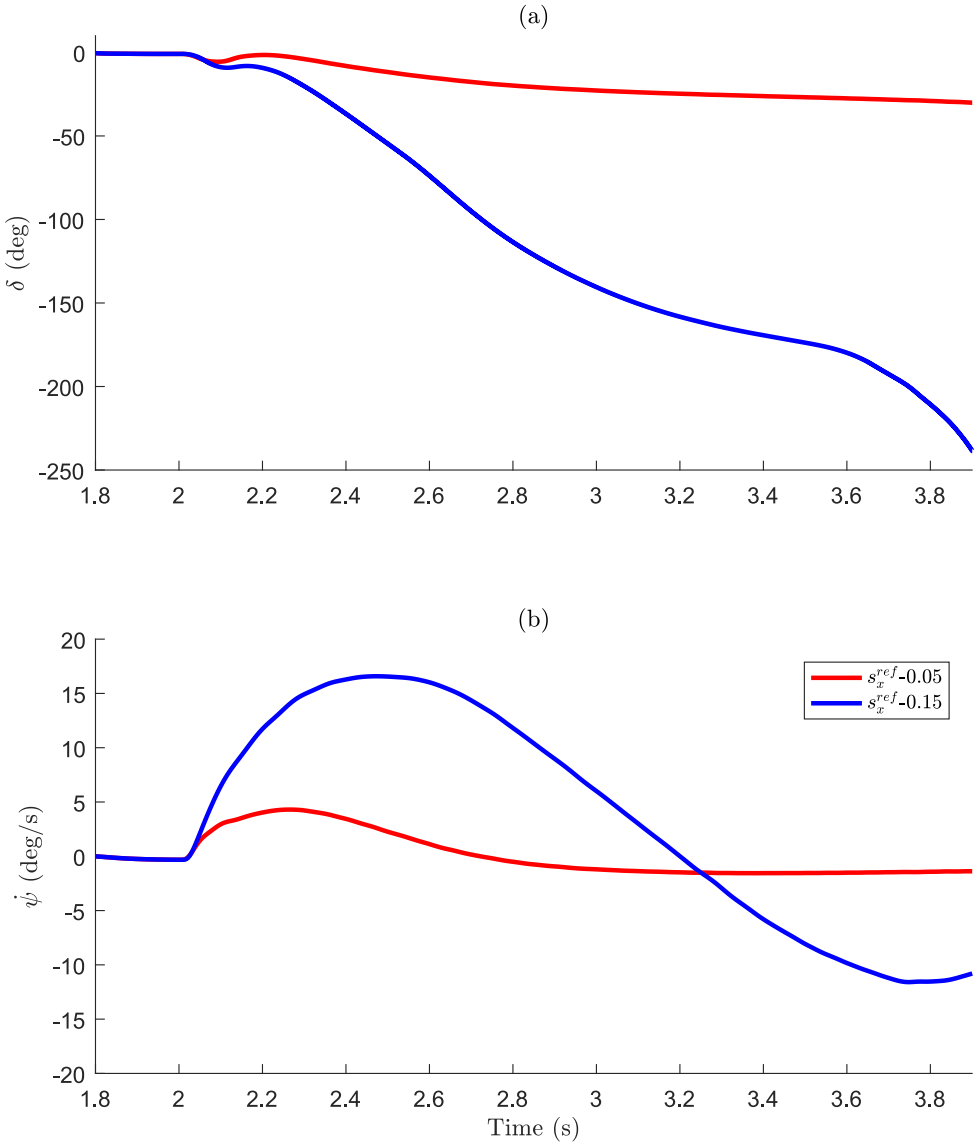

Figure 4.14: Split μ braking with s_{ref}=-0.05 and -0.15.

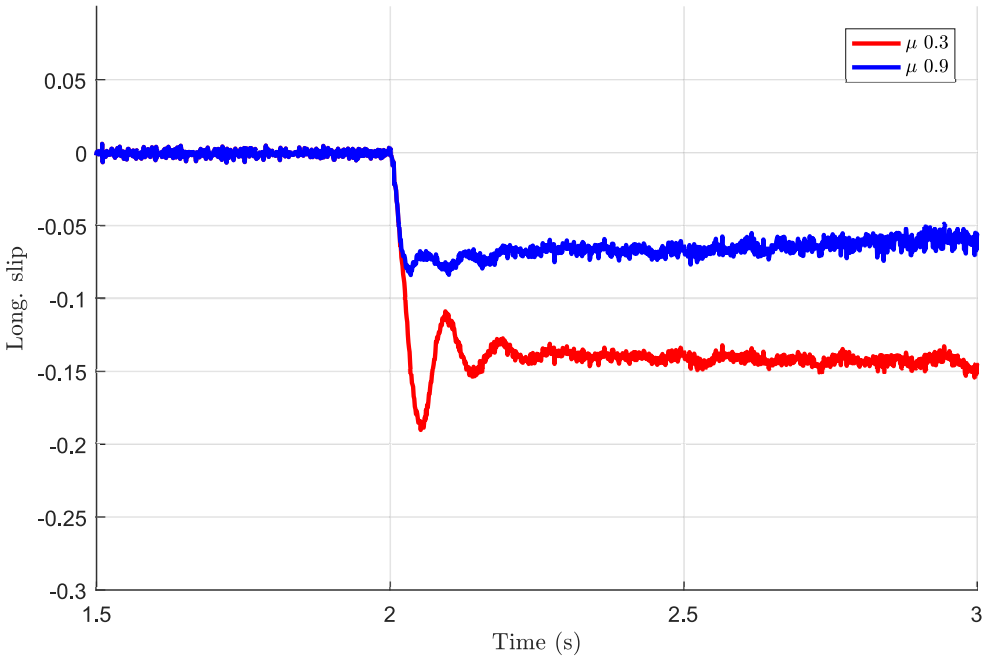

Figure 4.15: Straight line braking using D_{mpc}=0.6 with μ=0.3 and μ=0.9.

4.4 Torque Blending using Static Allocation

A method for static brake torque allocation is developed for the AWD electric vehicle using four EMs and presented in this section. Authors in [59] discussed the various type of control allocation strategies for over-actuated mechanical systems for different applications include aerospace, maritime and automotive. Daisy Chain is a type of control allocation method which is widely used in aerospace industry, particularly for the management of flight control. This strategy is considered when redundant groups of control effectors exist [17]. The strategy enables the integration of RBS during ABS operation, thus allowing energy recuperation in any braking condition. Priority is given to the EM to deliver torque demand by the slip controller and supported by the EHB. The available regenerative brake limitation is always preserved. The performance of this method deteriorates when fast changing torque is commanded, which is typical for slip control [101]. This algorithm is designed specifically for each vehicle topologies discussed in 2.2 due to the restriction of having either single EM, two EMs, or four EMs for AWD electrified vehicles.

We have presented the method to integrate the slip controller and the torque allocation between two braking actuators using optimisation algorithm in the previous section. As discussed, there are advantages and disadvantages of such numerical approach and in this chapter, we develop a pragmatic approach to achieving the objective using static allocation method (Daisy Chain). The main aim is to apportion the control for the redundant actuators by setting a priority for the actuators. In our application, the regenerative braking is given the priority to deliver the required ABS torque by the slip controller. It is important to understand that the regenerative braking is restricted by the EM and current battery SOC. Hence, when the actuator limit is saturated, the deployment of the friction braking is required to satisfy the remaining controller's demand. The algorithm can be

described as below

$$\begin{aligned} &when\ T_{ABS_i} \leq T_{em}^{limit}: \\ &T_{em_i} = T_{ABS_i},\ T_{h_i} = 0 \end{aligned} \tag{4.13}$$

$$\begin{aligned} &when\ T_{ABS_i} > T_{em}^{limit}: \\ &T_{em_i} = T_{em_i}^{limit},\ T_{h_i} = T_{ABS_i} - T_{em_i} \\ &i \in \{fl, fr, rl, rr\} \end{aligned} \tag{4.14}$$

where T_{ABS} is the torque demand from the slip controller, T_{em}^{limit} is the limit for the EM torque, T_{em} is the regenerative torque, and T_h is the friction braking torque. The T_{ABS} is calculated from the slip controller which we implement using the SMC method. The general overview of the proposed algorithm is presented in Figure 4.16. There are two key steps in implementing the strategy which includes the slip controller and torque allocation. Slip control algorithm is implemented to determine the required torque T_{abs} for each wheel. This input will then processed by the torque blending strategy using Daisy Chain method to allocate the torque for each actuator as explained in 4.13-4.14.

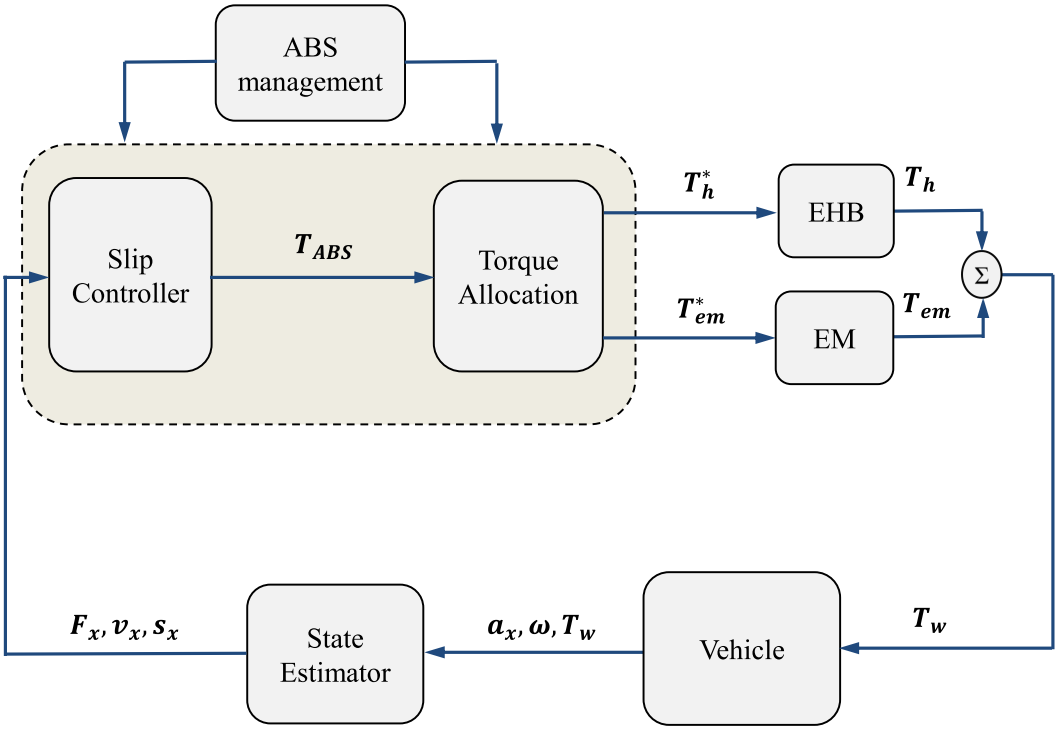

Figure 4.16: Overview of Daisy Chain torque blending.

4.5 Simulation using high-fidelity vehicle model for Daisy Chain

We present the simulation results with the implementation of static allocation method for the torque blending strategy in this section. Similar high-fidelity vehicle model and test environment setup to section 4.3 is adopted for validation purpose. The vehicle and tyre parameters used are listed in Table 2.2 and the tuning parameters for the SMC used in this work can be found in Appendix B.

4.5.1 Straight line braking on high μ road

In the event of an emergency braking on dry asphalt (μ=1), there is a risk of locking the wheels, especially on the front axle. With the slip controller activated ($t_{sim} = 2s$) at the initial speed of 50km/h, wheel locking can be avoided as illustrated in Figure 4.17- a) and b). Without the slip control, the high brake force demand from the driver exceeds the available friction between the road-tyre contact which can be avoided by implementing the slip control strategy. This can be supported by observing the braking torque command by the slip controller in Figure 4.17- c) and d) to achieve the $s_{ref} = -0.1$. The required braking torque is greater for the front wheels compared to the rear wheels. It is worth noting that both braking actuators are activated (as the EM torque is saturated) throughout the ABS braking event only for the front wheels and the rear wheels torque demand can be delivered by only using the regenerative braking torque. This observation shows the advantage of applying the torque blending strategy for wheel slip control operation.

4.5.2 Straight line braking on low μ road

A braking on a low adhesion surface scenario is presented with road μ of 0.3. Figure 4.18 illustrates the slip control being activated after 2 seconds to retard the wheel torque to prevent wheel locking. Figures 4.18- c) and d) indicate the required ABS torque demand is delivered by the regenerative braking without applying the friction braking. This happens generally for braking on a low-μ surface as the available friction force is smaller as explained in 2.1.

4.5.3 Straight line braking on split μ road

To evaluate both longitudinal and lateral performance of the vehicle during slip control activation, we test the algorithm proposed on a split-μ surface with an initial speed V_x

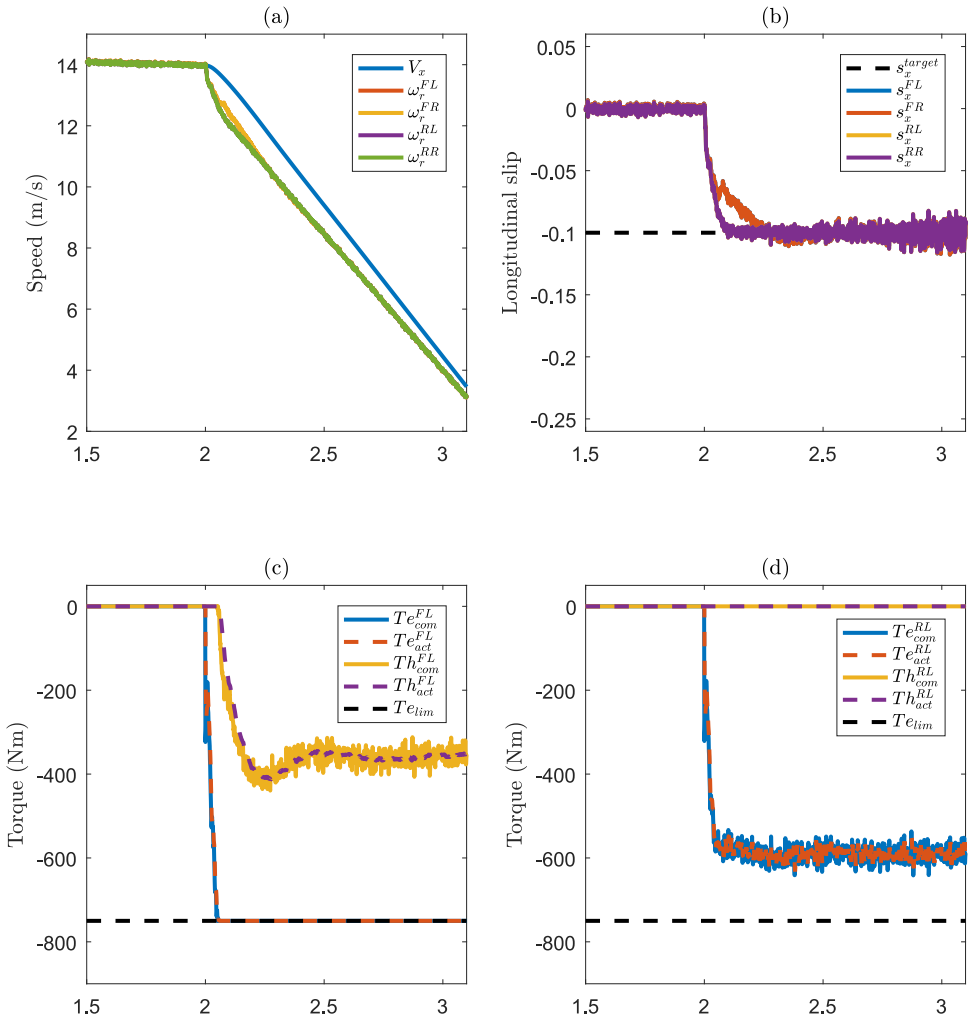

Figure 4.17: SMC with DC braking on μ=1, $V_{initial}$=50km/h, s_{ref}=-0.1.

of 50km/h. The left-hand side of the vehicle is driven on a high-μ surface (μ=1.0) and right-hand side of the car is on a low-μ road surface (μ=0.3). The applied braking torque will be excessive with equally applied to the left and right wheels while the slip control is deactivated which can cause the vehicle to be unstable due to the yaw moment created when braking on the uneven adhesion surface. In order to maintain the stability of the

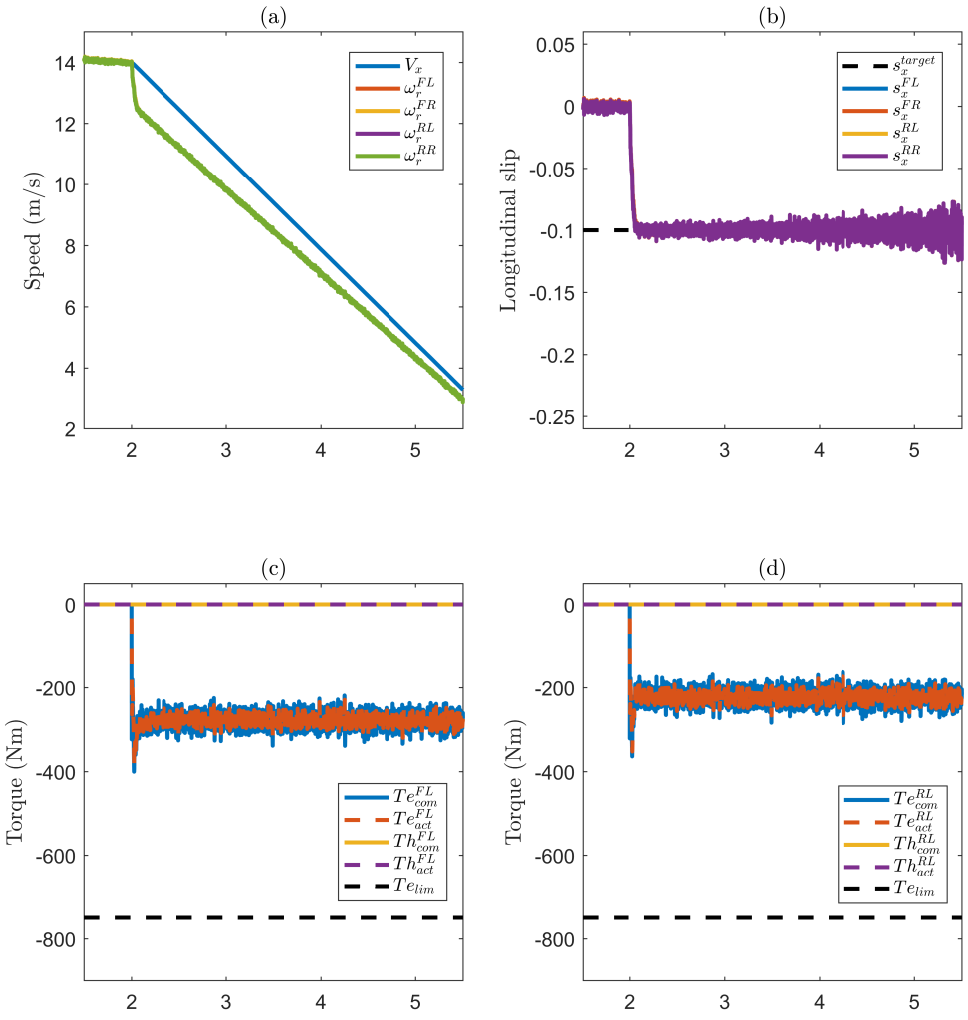

Figure 4.18: SMC with DC braking on μ=0.3, $V_{initial}$=50km/h, s_{ref}=-0.1.

vehicle, the slip control will determine the required torque for each wheel to achieve the $s_{ref} = -0.1$. Acceptable maximum vehicle yaw rate achieved of $9.2\,\mathrm{deg}/s$ and a steering angle correction of 63 deg is required for the driver to maintain the vehicle path.

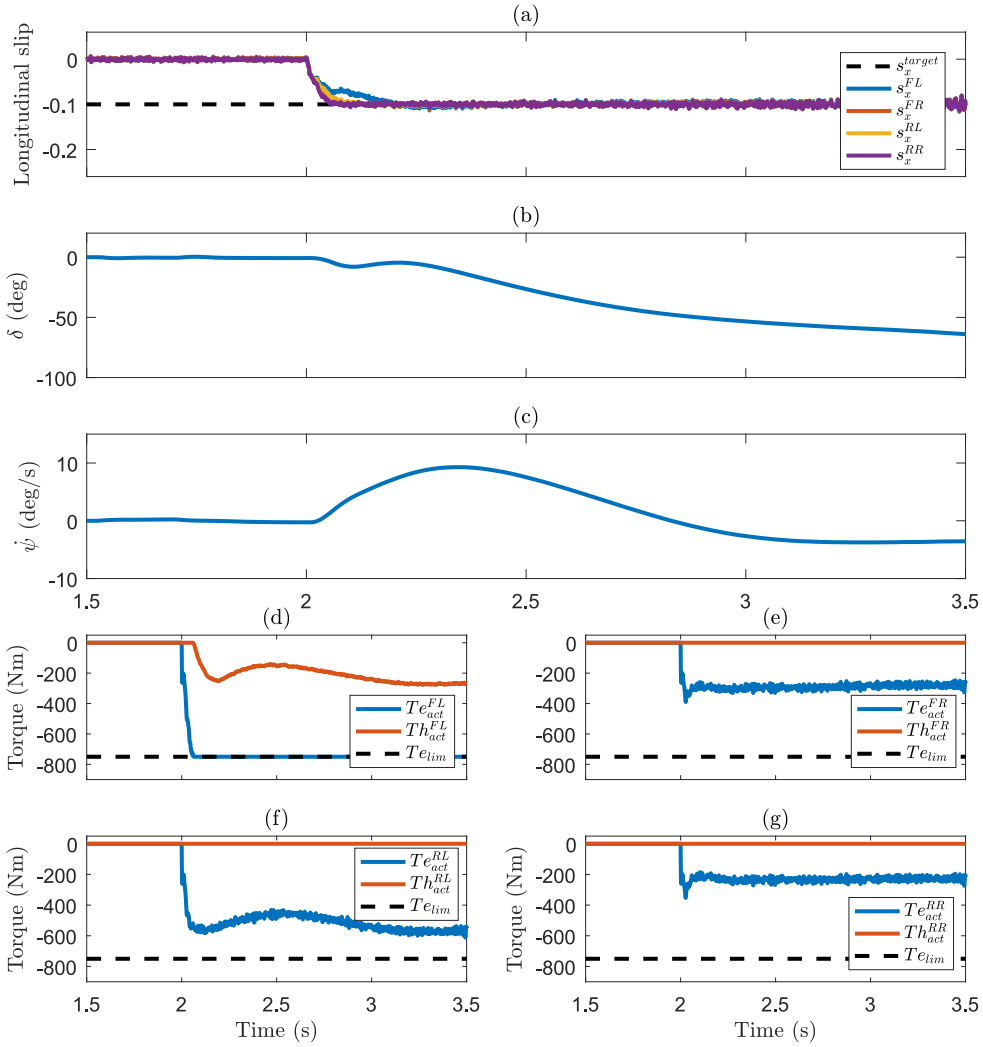

Figure 4.19: SMC with DC braking on split-μ, $V_{initial}$=50km/h, s_{ref}=-0.1.

4.6 Performance metrics evaluation

In this section, the performance of the introduced controllers is evaluated and compared using the following performance metrics:

- Root-mean-square error (RMSE) for torque

$$RMSE_{torque} = \sqrt{\frac{1}{N}\sum_{i=1}^{N}(T_{ctrl}[i] - (T_{em}[i] + T_h[i]))^2} \tag{4.15}$$

The RMSE for braking torque is a metric to measure the performance for each controller in terms of delivering the torque where T_{ctrl} is the demand from the controller, T_{em} is the actual EM torque, and T_h is the actual EHB torque.

Figure 4.20 shows the RMSE of braking torque for the three different strategies proposed in this chapter. The clear trend is that the nonlinear MPC has the lowest RMSE recorded for both low-μ and high-μ ABS braking scenarios, followed by the linear MPC and the Daisy Chain method. The MPC methods incorporate the torque rate for both braking actuators as constraints. This means that the controller always respects the actuator dynamics thus the commanded torque can be delivered by the actuators with the smaller error than the Daisy Chain method.

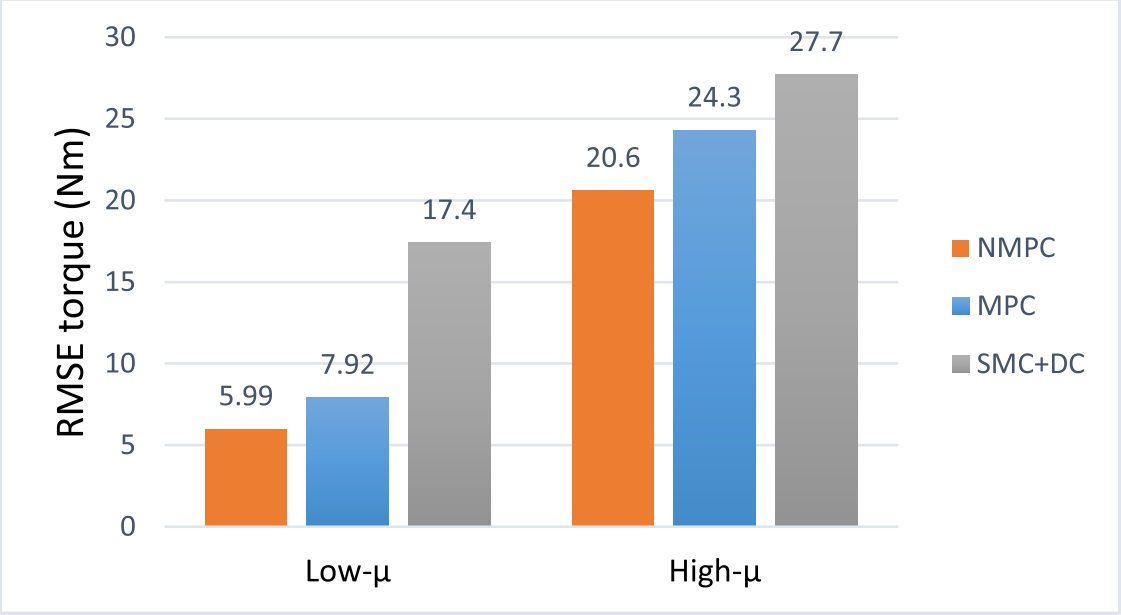

Figure 4.20: RMSE for braking torque.

- RMSE for longitudinal slip

$$RMSE_{slip} = \sqrt{\frac{1}{N}\sum_{i=1}^{N}(s_{ref}[i] - s_x[i])^2} \tag{4.16}$$

where s_{ref} is the slip target and s_x is the actual longitudinal wheel slip. The RMSE for the slip provides the performance metric for each controller in terms of achieving the slip reference.

This performance metric measures the controller's capability in achieving the desired slip $s_{ref} = -0.1$ during ABS braking situation. Figure 4.21 points out that the combination of SMC and Daisy chain yields the smallest RMSE of slip (0.0173) as compared to the nonlinear MPC (0.0213) and linear MPC (0.0217) for a high-μ case. The calculated RMSE slip are smaller the same for the low-μ scenario with the linear MPC recorded the smallest RMSE slip (0.0072). This trend shows acceptable performance for all algorithms for both the high-μ and low-μ cases but interestingly, smaller RMSE of slip can be achieved when ABS is deployed using the EM.

- Root-mean-square (RMS) of torque rate

$$RMS_{dTorque} = \sqrt{\frac{1}{N}\sum_{i=1}^{N}(dT^{j}_{ctrl}[i])^2} \tag{4.17}$$

This metric evaluates the RMS for the torque rate for each braking actuator where j is either the EM or the EHB. The objective is to quantify the variation of the change of torque during slip control for EM and EHB.

For this assessment, we normalise the RMS of torque rate over the highest value for each case and present in percentage for the purpose of comparison between

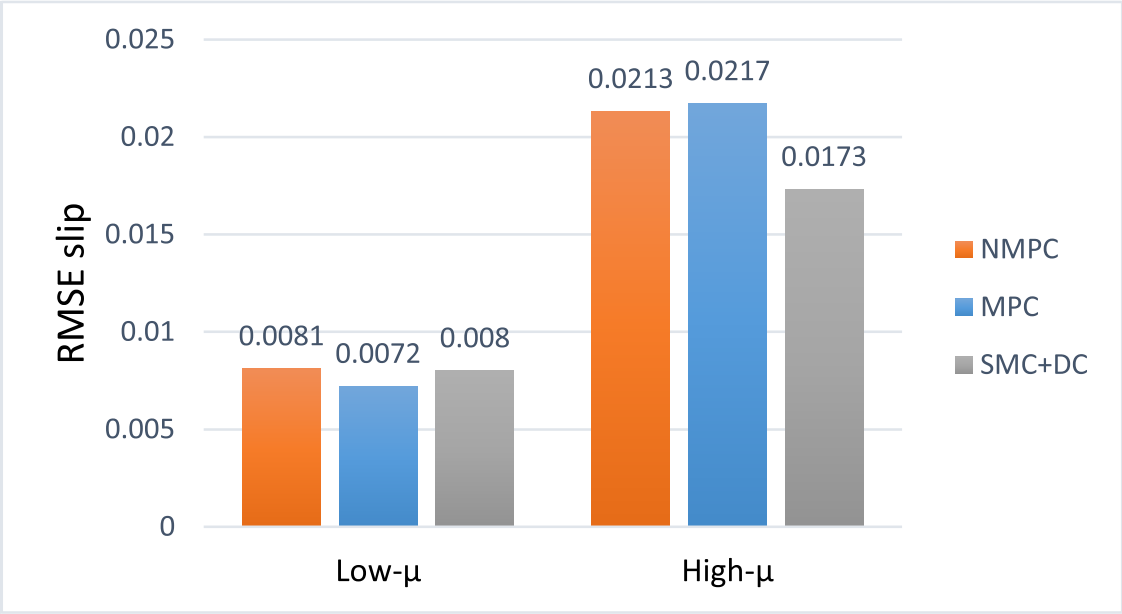

Figure 4.21: RMS error for longitudinal slip.

the three methods. Figure 4.22 shows the RMS for torque rate for two scenarios. ABS braking on the low-μ road can be achieved by the EM torque, thus the RMS torque rate for the EHB for all strategies (NMPC, MPC, and Daisy Chain) are very low ranging from 1.75%, 2.43%, and 0.0015% respectively. It can be seen that both NMPC (36%) and MPC (50%) achieved much lower RMS torque rate as opposed to the SMC with Daisy Chain method. This means that there is a significant amount of torque variation during the slip control and torque blending activation in which the strategy does not consider the actuator dynamics when compared to both MPC methods. Linear and nonlinear MPC incorporates the torque range and torque rate limits of the braking actuators and always respect the actuator dynamics while achieving the control design objectives. The advantage of using nonlinear internal model can be observed as the RMS torque rate for NMPC is 14% less than the linear MPC result. For the second case, all three methods utilise the EM and EHB during slip control activation on a high-μ surface. A similar trend can be observed

with Daisy Chain achieved the highest RMS for torque rate. Without respecting the actuator dynamics of the EM and EHB, the torque variation for both are almost similarly high (100% for EM and 93% for EHB) when compared to the linear and nonlinear MPC methods. The nonlinear MPC managed to capture the dynamics of the system better compared to the linear MPC with lowest RMS torque rate recorded (77% for EM and 21% for EHB).

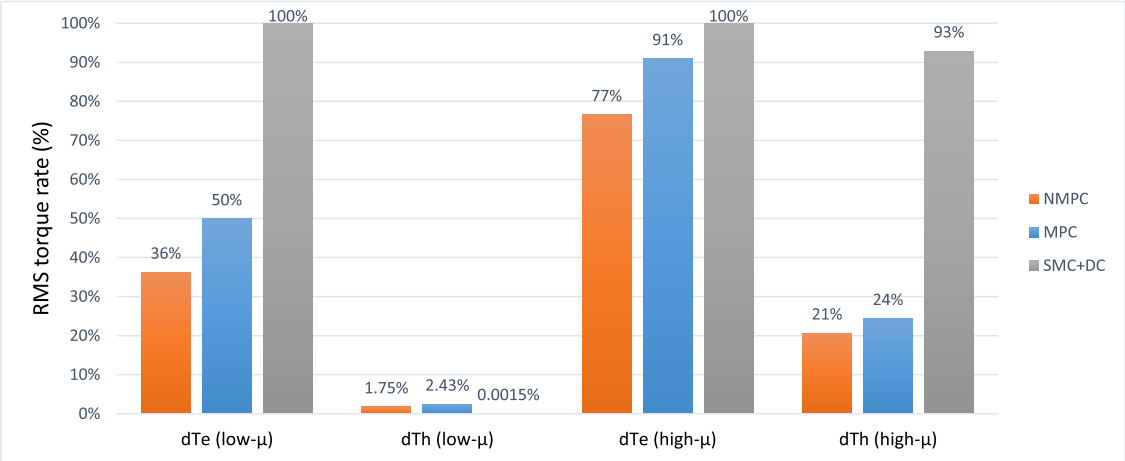

Figure 4.22: RMS for torque rate.

- Energy recuperated

$$E_{recup} = \sum_{i=1}^{N} T_{em}[i]\omega[i]t_s \tag{4.18}$$

The potential mechanical energy recuperation (unit: kWs) for each controller can be measured as the sum of the multiplication of the T_{em}, wheel rotational speed ω, and the sampling time t_s for all samples N. This is just a measure of the mechanical energy recuperation without considering the conversion to electrical energy and the losses for energy storage.

Figure 4.23 illustrates the capability of mechanical energy recuperation during the slip control activation on the high-μ and low-μ road. It is clear that the three devel-

oped methods provide good capability in recovering energy (ranging from 20.8-21.3 kWs for high-μ and 23.6-23.8 kWs) through activation of the EM during ABS operation. An interesting point is that even higher EM torque deployed during high-μ braking, the energy recuperated are smaller compared to the low-μ case. This is due to the longer distance and time required for the vehicle to stop on the low-μ surface and creates a good opportunity for energy recuperation if torque blending for slip control strategy is deployed.

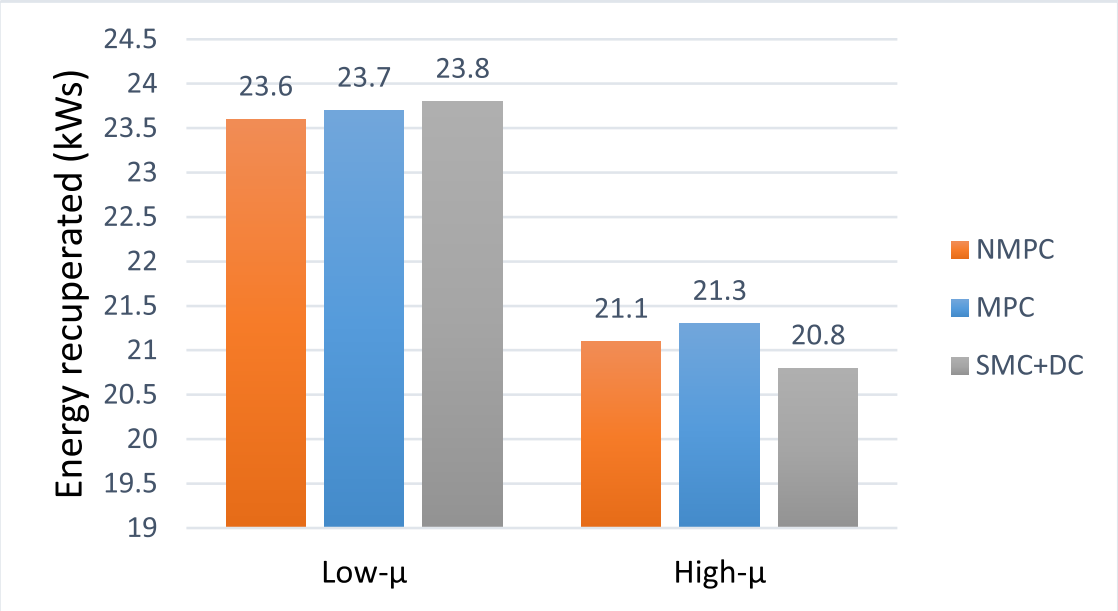

Figure 4.23: Mechanical energy recuperation.

- EM torque ratio

$$EM_{potential} = \frac{\sum_{i=1}^{N} T_{em}[i]}{\sum_{i=1}^{N} T_{total}[i]} \tag{4.19}$$

This metric evaluates the potential of the energy recuperation based on the ratio of the EM torque over the total braking torque for each wheel T_{total}.

The torque blending strategies proposed has enabled the activation of the EM during

emergency braking. Figure 4.24 indicates the energy recuperation potential or the ratio of EM torque over the total braking torque at each wheel. This is by assuming that we can operate the EM in generator mode without restriction of other factors such as high battery SOC or temperature. For the low-μ case, where permissible by the battery and vehicle conditions, close to 100% total commanded torque will be delivered by the EM. A very small difference is recorded for the three different methods (nonlinear MPC 99.4%, linear MPC 99.3%, and Daisy Chain 99.9%). As expected, the EM torque is saturated for the high-μ condition and EHB supplemental torque is required to achieve the desired slip. Both nonlinear MPC(71%) and linear MPC(71.5%) achieved higher EM torque ratio over total commanded torque compared to the Daisy Chain(68.6%).

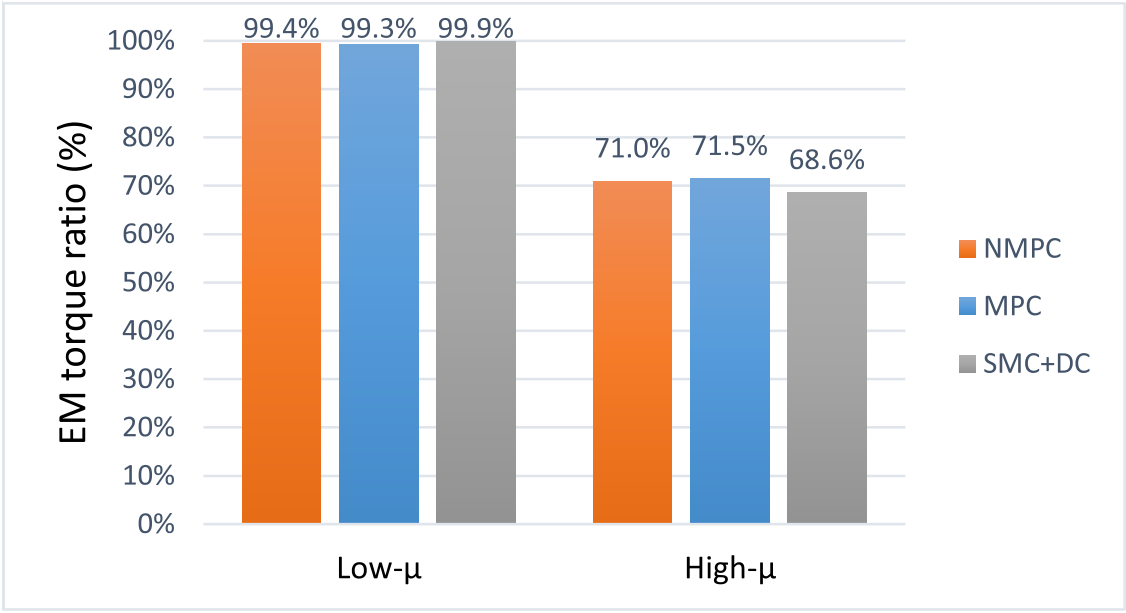

Figure 4.24: EM torque percentage.

- Running cost

$$J_{cl} = \sum_{k=0}^{N} (x_k - r)^T Q_d (x_k - r) + (u_k - l)^T R_d (u_k - l) + 2(x_k - r)^T M_d (u_k - l) \tag{4.20}$$

The performance of the MPC strategies and Daisy Chain can be evaluated using a closed-loop cost or sum of the running cost [109]. Equation 4.20 presents the calculation of the sum of the weighted states error squared and the control input for a given simulation duration. This translates into the cost for a chosen control strategy attemp to minimise and will be used as the performance metric of the proposed methods. We present the normalised percentage figures to compare the three developed strategies for two scenarios.

The first case is the slip control activation on a low-μ road. The obvious trend is illustrated in Figure 4.25 that the summation of the cost of both optimal control strategies is minimal (14% for NMPC and 26% for linear MPC) compared to the SMC with Daisy Chain method. For the given cost function 4.6, it can be observed that the smallest running cost is required for the nonlinear MPC followed by the linear MPC and the SMC with Daisy Chain. This metric shows the advantage of using nonlinear MPC (compared to the linear MPC) which captures the nonlinearity of the system dynamics in the internal model. The trend continues for the second case with ABS braking on the high-μ surface with the minimal sum of running cost recorded is the nonlinear MPC followed by the linear MPC and the SMC with Daisy Chain.

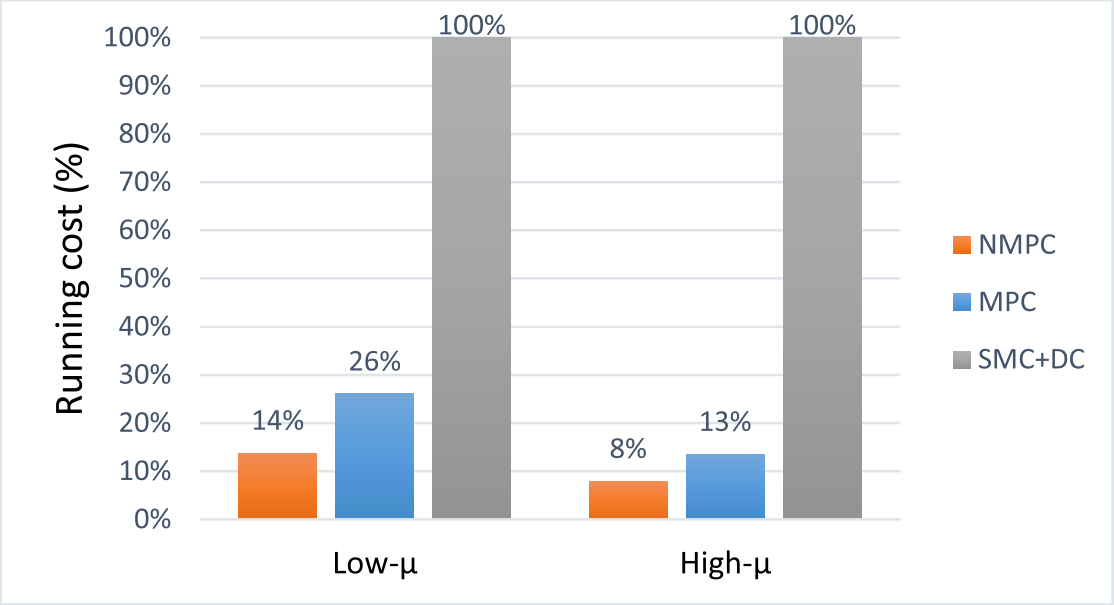

Figure 4.25: Sum of the running cost.

4.7 Summary

An NMPC and linear MPC strategies are formulated to integrate slip control and torque blending using two braking actuators for BEV using EM on individual wheels with real-time implementation capability. The algorithm is designed to avoid wheel locking in emergency braking situations and takes into account the braking actuators dynamics. It has been highlighted that the proposed slip control implementation can take advantage of the fast torque response of EM. It also gives priority to the EM while utilizing the friction braking system to supplement the limited torque of the EM when necessary. There is a possibility to deploy pure electric-slip control without activating friction brakes as demonstrated in braking on low μ surface scenarios. Energy recuperation can be maintained throughout the ABS activation, in addition, to allow the vehicle to stop without any risk of wheel locking. The proposed algorithm was tested and evaluated using high fidelity model in Simulink and IPG CarMaker environment.

A state-of-the-art integration of slip control and torque blending strategy using nonlinear MPC is presented. Furthermore, we present the development of a linear MPC controller for the combined slip control and actuators blending problem for comparison against the nonlinear approach. In contrast to [102] we consider update of the linear model with regards to the current operating condition as opposed to a linearisation with respect to a constant target. We also use torque rate, instead of torque, as the input variable to eliminate the need for a reference torque value. In addition, we implement the controller in high fidelity simulation considering scenarios involving combined longitudinal and lateral vehicle dynamics, as opposed to most ABS design papers which mainly concentrate on longitudinal dynamics. We discuss the capability to implement both strategies in real-time, and present a case study of the robustness of the controllers against critical uncertainties in the tyre-road adhesion. An interesting observation to make is that linear MPC has acceptable performance compared to the NMPC but deteriorates at low speed. As expected, the NMPC requires more computational time for real-time simulation. The effects of varying the slip target s_{ref} is also discussed.

In this chapter, we also propose a torque blending strategy using Daisy Chain (static allocation) with the application of Sliding Mode Control for implementing the slip controller. The developed method is evaluated using high-fidelity vehicle model using Matlab/Simulink and CarMaker simulating an AWD BEV using 4 EMs.

It is worth to note from the performance metrics comparison between SMC with Daisy-Chain and the MPC strategies, both achieved the initial objectives; to maintain the wheel slip near the slip target s_{ref}, and to allocate the braking torque between the two actuators. The RMSE of torque for the MPC strategies is smaller than the SMC with Daisy-Chain. However, the RMSE of slip for SMC with Daisy-Chain is slightly smaller compared to the MPC methods (high-μ case). The chattering of SMC method leads to much bigger RMS of torque rate as compared to the MPC strategies. This shows that the

SMC with Daisy-Chain method is a more pragmatic approach but neglects the actuator dynamics of the regenerative braking and friction braking. On the contrary, the optimisation method approach such as the MPC will take into consideration of the actuator dynamics but is computationally expensive for real-time solutions. Finally, the running cost indicates that the MPC methods solve the problem definition with minimum running cost when compared to the SMC with Daisy-Chain method.

Chapter 5

Torque Blending for Slip Control using two EMs

This chapter investigates the implementation of the torque integration strategies on a more restricted vehicle architecture of a BEV with an EM on each axle. The main disadvantage is the coupling torque of the EM between left and right wheels of the same axle which limits the individual wheel torque control ability. However, we can utilise the friction braking to maintain the individual wheel level of slip control. The next section demonstrates the torque apportionment strategy using the Daisy Chain approach which needs a standalone slip control algorithm. The following section presents a novel method using MPC to incorporate both slip control and torque blending in a single problem formulation.

5.1 Torque Blending using Daisy Chain

For a BEV architecture with an axle EM, the torque blending strategy using static allocation algorithm can be implemented independently for each axle as there are two EMs available in the vehicle as described in section 2.2.2. The strategy proposed for the brake

torque integration for slip control for an AWD pure electric vehicle with one EM on each axle is illustrated in Figure 5.1. The slip controller can be implemented using the SMC or MPC methods which will determine the required torque demand T_{ABS}. The ABS management will be responsible to activate or deactivate the slip control strategy and receive information from the vehicle which includes the current EM torque limit. Both actuators' dynamics are presented in the modelling and simulation study. However, we neglect the modelling of the mechanical linkage behaviour such as torsional vibration of the shaft with clutch and gearings.

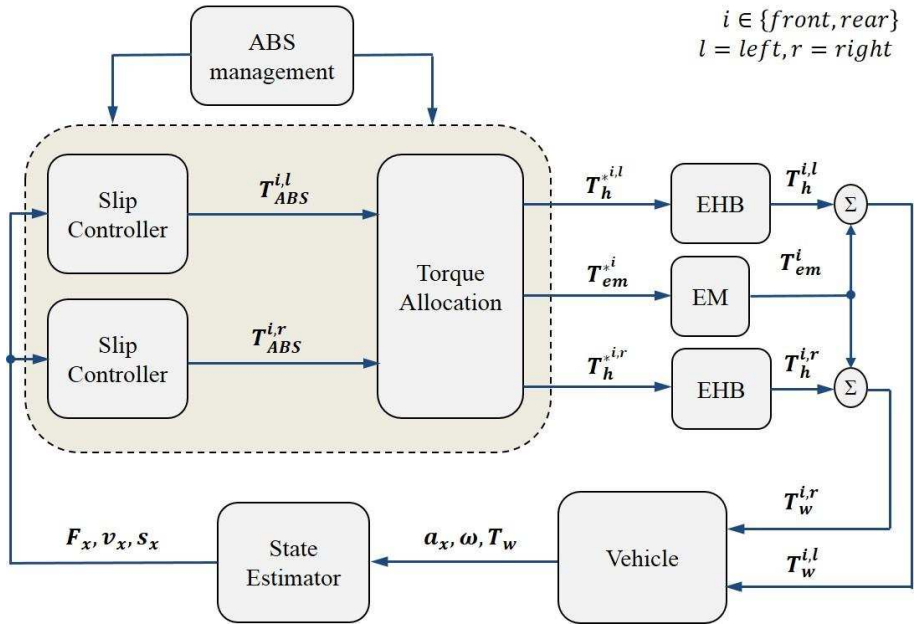

Figure 5.1: Overview of torque blending (per axle) strategy using Daisy Chain with two EMs.

The torque allocation strategy (as illustrated in Figure 5.2) receives inputs from the vehicle for the RB torque limit for both front and rear axles and the ABS torque demand from the slip controller for each wheels. For each axle, the algorithm will first determine the minimum torque between left and right wheel. Next, the minimum value between the available RB torque $T_{regenavailable}$ and the minimum ABS torque demand T_{ABS} will be set

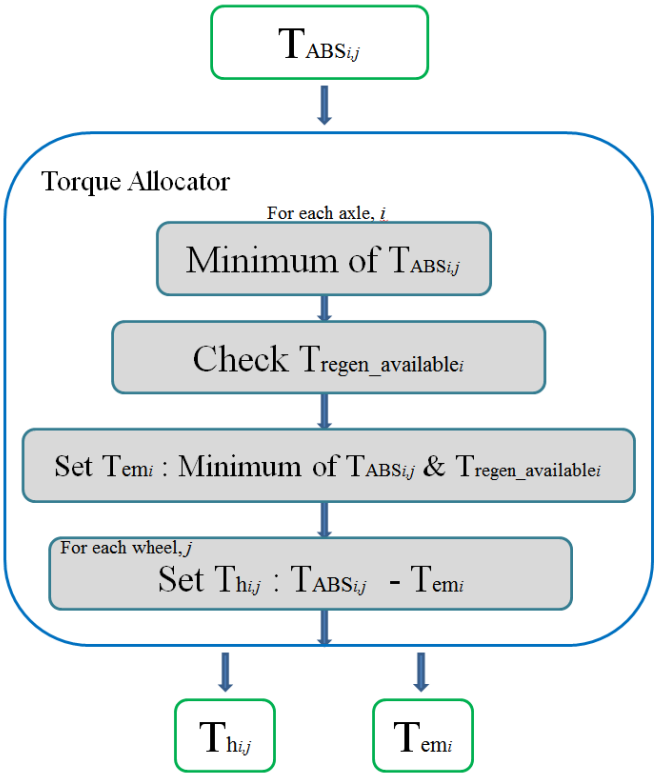

Figure 5.2: Torque blending strategy for AWD BEV (two EMs).

as the EM torque set point T_{em} as described in equation 5.1. Finally, the FB torque is calculated using equation 5.2.

$$T_{em_i} = min(T_{ABS_i}, T_{regen\ avail_i}) \tag{5.1}$$

$$T_{total_{i,j}} = T_{em_i} + T_{h_{i,j}} \tag{5.2}$$

$$i \in \{front, rear\} j \in \{left, right\}$$

There is a higher degree of control for the torque allocation algorithm to be implemented due to the availability of EM on each axle as compared to a single EM AWD topology. For instance, the RBS can be activated only on the front or the rear axle in any ABS events such as low-μ braking manoeuvre and not limited to the non-ABS axle. In

terms of the overall energy recuperation potential, the torque blending algorithm for this configuration can increase the energy efficiency due to having two generators operating independently compared to a single EM architecture in 2.2.3.

5.2 MPC strategies for integration of slip control and torque blending

In this section, we investigate the use of MPC for the combined problem of slip control and torque blending using two braking actuators in an AWD BEV with one EM on each axle as described in 2.2.2. The challenge with this type of vehicle architecture is to handle the constraint of equal electric torque on left and right wheels of the same axle. The regenerative braking torque is applied equally to the left and right wheels on each axle. Thus, we will be relying on the friction braking in certain situation such as braking on split-μ surface or braking during cornering to enable the individual wheel slip control. In order to incorporate this strategy, we expand the internal model of the MPC from single-wheel to a four-wheel model.

In this work, we use a BEV with an EM on each axle to apply the proposed strategy with the use of a four-wheel model as the internal plant for the MPC. We neglect the lateral motion and only use the longitudinal dynamics for the internal model,

$$\dot{V}_x = \frac{\sum F_x^{i,j}}{m}, \tag{5.3}$$

$$\dot{\omega}^{i,j} = \frac{T_{tot}^{i,j} - F_x^{i,j} R_w}{J_w}, \tag{5.4}$$

$$T_{tot}^{i,j} = T_e^i + T_h^{i,j}, \tag{5.5}$$

$$i \in \{front, rear\}, \quad j \in \{left, right\}$$

with the assumption that equal regenerative braking torque applied between left and right wheels for a given axle as described in 2.10 (T_e^{fl}=T_e^{fr} and T_e^{rl}=T_e^{rr}) due to an EM connected to the individual axle of the car. Then we expand accordingly the MPC formulation from 4.6 and applies the PDIP method as available in the FORCES Pro to converge to the optimal solution,

$$\min_{x,u} \quad \sum_{k=0}^{N-1} [q_s(s_{x_k}^{i,j} - s_{ref})^2 + q_T(T_{h_k}^{i,j})^2 + q_e(\Delta T_{e_k}^{i})^2 + q_h(\Delta T_{h_k}^{i,j})^2] \tag{5.6a}$$

$$s.t. \quad \bar{x}(0) = \bar{x}_{init}, \tag{5.6b}$$

$$\bar{x}_{k+1} = \bar{g}(\bar{x}_k, \bar{u}_k), \quad k = 0, ..., N-1 \tag{5.6c}$$

$$T_e^{min} \leq T_{e_k} \leq T_e^{max}, \quad k = 0, ..., N-1 \tag{5.6d}$$

$$T_h^{min} \leq T_{h_k} \leq T_h^{max}, \quad k = 0, ..., N-1 \tag{5.6e}$$

$$\Delta T_e^{min} \leq \Delta T_{e_k} \leq \Delta T_e^{max}, \quad k = 0, ..., N-1 \tag{5.6f}$$

$$\Delta T_h^{min} \leq \Delta T_{h_k} \leq \Delta T_h^{max}, \quad k = 0, ..., N-1 \tag{5.6g}$$

$$i \in \{front, rear\}, \quad j \in \{left, right\}$$

The proposed strategy is deployed using nonlinear MPC as discussed in 4.2.1. Figure 5.3 shows the overview of the MPC strategies implementation for the specified vehicle topology. The advantage of this method is having an integrated control algorithm with multiple objectives in a single block for each wheels and actuators in the vehicle. The obvious disadvantage of this setup is the computational burden to be solved on-line while obtaining the optimal solution. With that in mind, the sampling time for the MPC is set to 10ms and all the tuning parameters are presented in Table 5.1. The selected set of tuning

parameters is based on a logic to minimise the wheel slip error and to give priority to the EM torque while using the EHB as support where necessary. The control inputs for each actuators are applied to the vehicle while considering the actuator dynamics and all the required measured signals from the vehicle are fed to the state estimators to provide the necessary inputs to the MPC strategies and complete the closed loop.

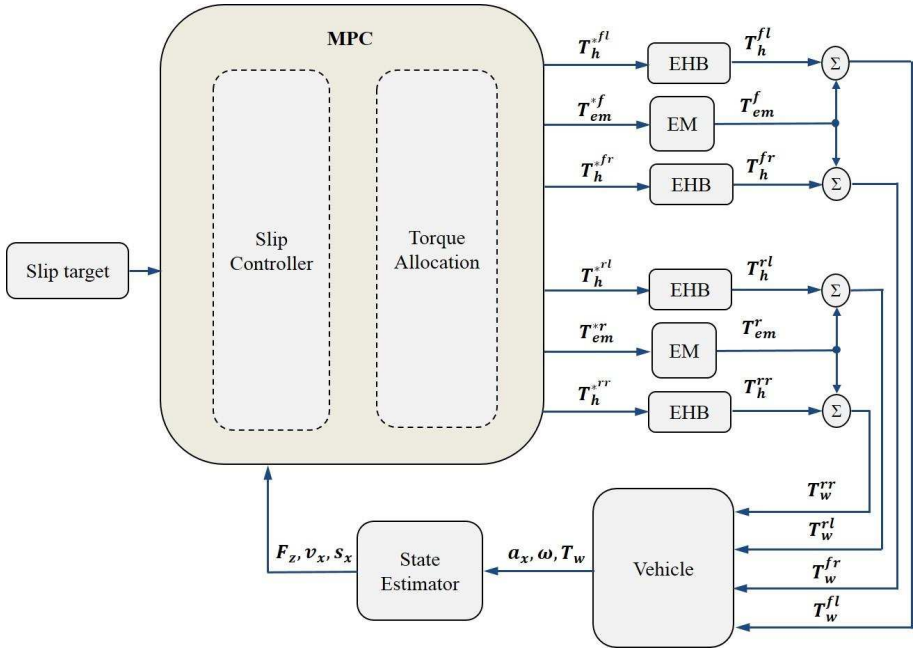

Figure 5.3: Overview of torque blending strategy using MPC with two EMs.

Parameter (Unit)	Description	Value
t_s (ms)	sampling time	10
N	number of steps	10
q_s	weight of slip error	$0.1\frac{(\Delta T_e^{limit})^2}{(s_{ref})^2}$
q_T	weight of friction torque	1
q_e	weight of ΔT_e	50
q_h	weight of ΔT_h	1000

Table 5.1: NMPC properties for two EMs strategy.

5.3 Evaluation of Daisy Chain torque blending strategy

The torque blending using Daisy Chain strategy proposed in section 5.1 is validated using CarMaker environment simulation with different test patterns. In order to evaluate the algorithm, we cascade it with a slip controller as illustrated in Figure 5.1 since the two problems are decoupled. Similar vehicle and tyre parameters are used and can be found in Table 2.2. In this simulation, we assume that the available regenerative braking for each EM is 750Nm, hence only 375Nm of electric torque is available for each wheel.

5.3.1 Low μ straight line braking

Similar to the previous validation process, the slip control is tested on a low adhesion surface (road μ=0.3) for a straight line braking with an initial speed V_x of 50km/h. The vehicle is free rolling initially before the controller is activated at T_{sim}=2s. As expected, the wheel speeds are well controlled to achieve desired wheel slip throughout ABS activation as shown in Figure 5.4a)-b). However, the front and rear regenerative braking are now decoupled thus provide more opportunity to increase energy recuperation. Due to rear-to-front load transfer during hard braking, the required ABS torque is higher for the front axle. Since there is one EM on each axle, the front EM is not limited to the rear wheel ABS torque demand as illustrated in Figure 5.4c)-d). Another interesting observation is that there is no brake torque delivered from the EHB especially on rear wheels. There is a trend of higher reliance on RBS during ABS operation and on a low road adhesion surface, it is possible to operate the slip control without EHB activation depending on the EM torque availability. Overall, it is expected that energy regeneration is enabled during slip control activation.

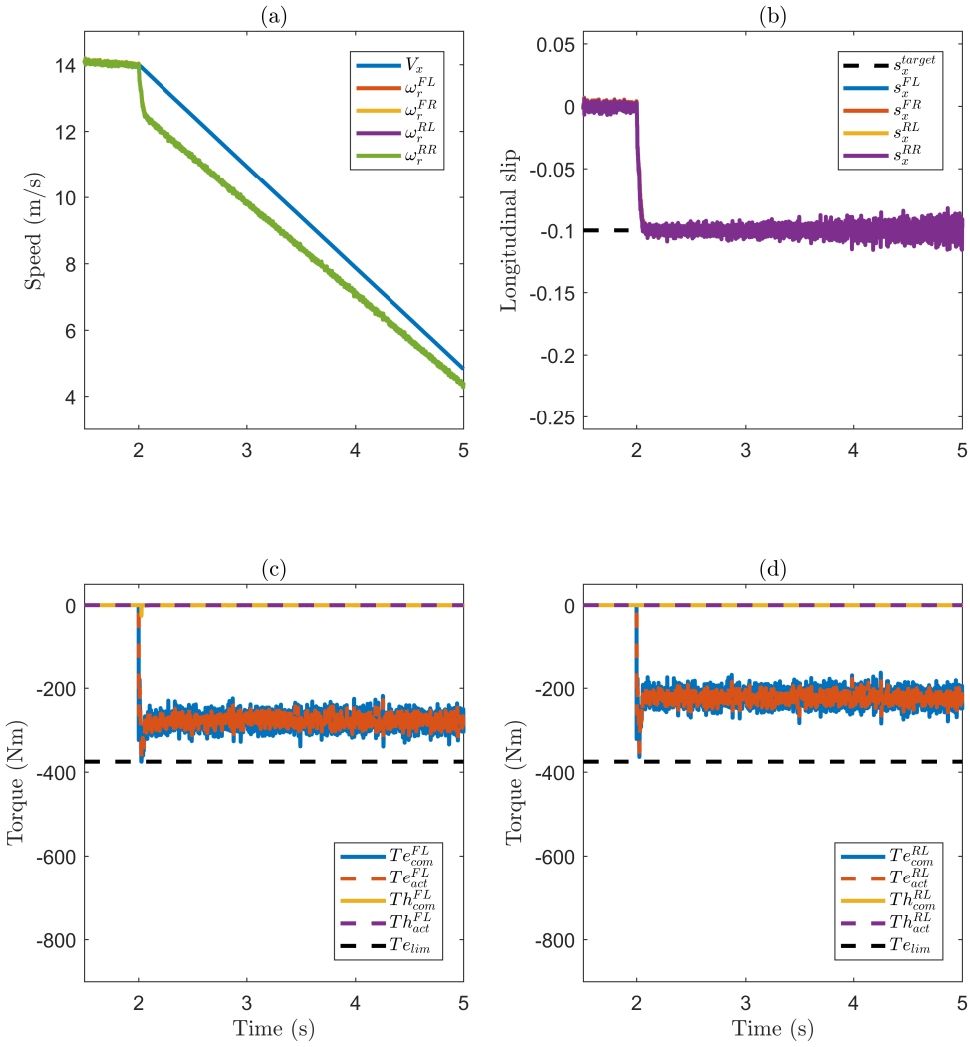

Figure 5.4: Straight line braking with road μ=0.3, $V_{initial}$=50km/h, s_{ref}=-0.1.

5.3.2 Braking on split-μ road

The torque blending strategy proposed is validated on a split-μ road surface. The left side of the vehicle is on a dry asphalt (μ=1) and the right side of the car is on a slippery surface (μ=0.3). The vehicle is free rolling and the controller is activated after 2 seconds with an initial speed of 50km/h. For this simulation, we apply the IPG Driver in CarMaker

to control the vehicle for the whole manoeuvre. Wheels are controlled to avoid wheel locking on each corner with the combination of EHB and RBS as shown in Figure 5.5a). Both front and rear EM are operating in generator mode to allow energy recuperation during ABS activation as indicated in Figure 5.5d)-g). Although there is independent braking on each axle, both EMs are delivering almost similar braking torque due to the test environment. An interesting observation can be made which the right-side vehicle is braking only using the EM but both braking actuators are deployed on the left wheels to achieve the same s_{ref}=-0.1. Due to the slower response of the friction braking, it can be seen that the slip for left wheels reaches the target slightly later than the slip for the right wheels. Finally, the primary objective of slip control has been achieved but allowing the driver not only to stop safely as quickly as possible but to maintain the steerability and stability of the vehicle. The maximum vehicle yaw rate achieved is 9deg/s and the maximum driver correction steering angle input is 70deg as shown in 5.5b)-c).

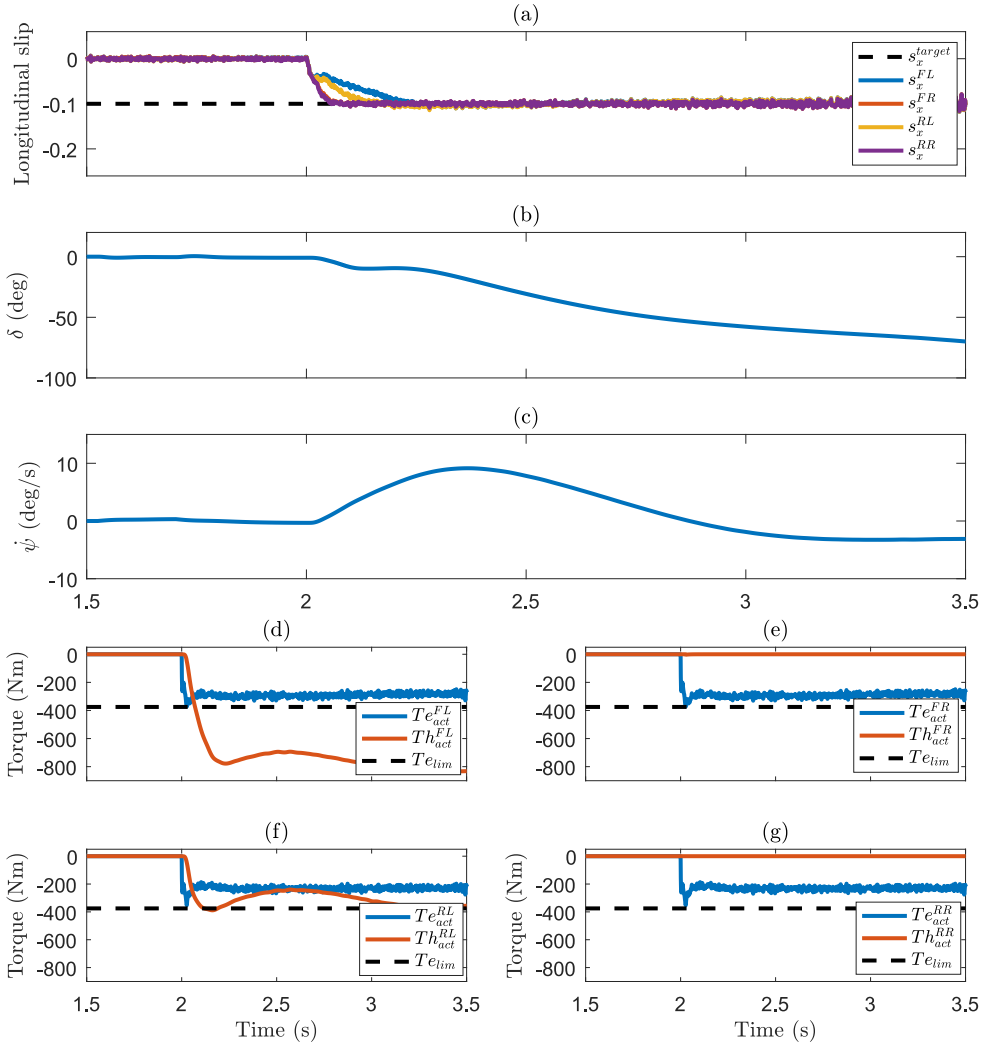

Figure 5.5: Braking on split-μ road with $V_{initial}$=50km/h, s_{ref}=-0.1.

5.4 Evaluation of torque blending for slip control using MPC

In order to evaluate the optimal control strategy, we implement the integrated slip controller and torque blending algorithm using nonlinear MPC methods. We deploy using the FORCES Pro solver to achieve real-time operation and to prove that the proposed strate-

gies have the potential to be implemented in real vehicle's hardware. The AWD BEV using two EMs vehicle model as discussed in 2.2.2 and the simulation is in CarMaker environment as explained in 2.3. Vehicle and tyre parameters can be found in Table 2.2 and we assume that the EM torque available is 750Nm. This means that 375Nm of regenerative braking torque is available for each wheel. The IPG Driver has complete control of the vehicle (steering and pedals) and the objective is to maintain the intended direction under emergency braking.

5.4.1 Straight line braking on low-μ

The test road simulates a packed snow surface with μ=0.3. The car is rolling freely with an initial speed of 50km/h before the activation of the controller at T_{sim}=2s. Simulation results are shown in Figure 5.6 indicate that both objectives of the problem definition are met; achieving the slip target of s_{ref}=-0.1 (5.6a)-b)) and allocating the ABS torque by giving priority to the EM. In the situation of braking on a low-μ surface and if there is sufficient EM torque availability, the commanded torque can be delivered solely using the regenerative braking as shown in Figure 5.6c)-d). The computing time required for the solver to reach the optimal solution is well below the sampling time t_s=10ms with an average of 4ms.

5.4.2 Braking on split-μ surface

The developed strategy using nonlinear MPC is evaluated for a split-μ braking manoeuvre with an initial speed V_x=50km/h. The car is driven on a road μ=1.0 (left-side) and μ=0.3 (right-side) which represents an uneven road adhesion surface scenario. As expected, wheel-locking can be prevented and the wheel slip can be maintained near the desired value as illustrated in Figure 5.7a). Since the EM torque are coupled between left and right

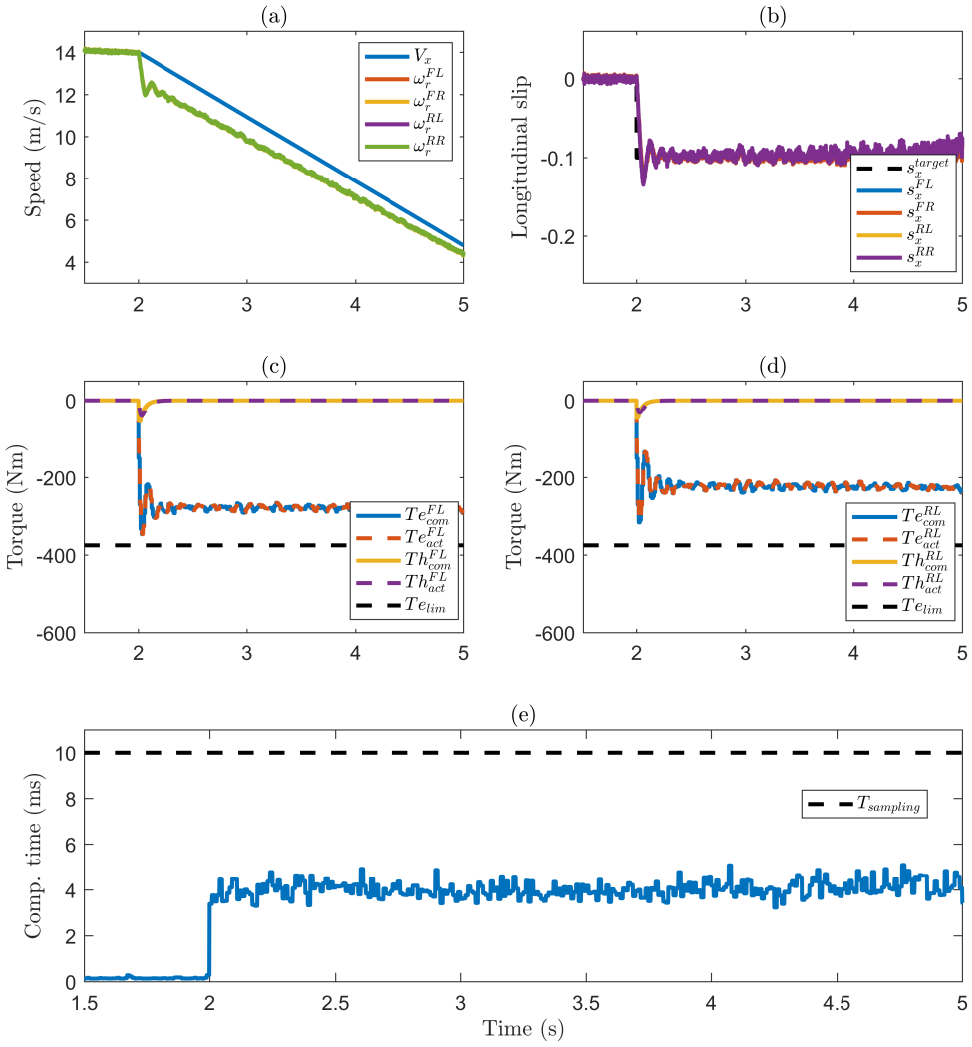

Figure 5.6: NMPC straight line braking with road μ=0.3, $V_{initial}$=50km/h, s_{ref}=-0.1.

wheels, the friction braking is required to provide the surplus commanded torque (Figure 5.7d) and f)). This is an interesting observation as pure EM braking is applied on the right-side wheels and brake blending is implemented for the left-side wheels. In the aspects of maintaining the vehicle steerability and stability, both maximum yaw rate achieved (10deg/s) and steering wheel angle correction by the driver (73deg) are acceptable in order to maintain the vehicle path.

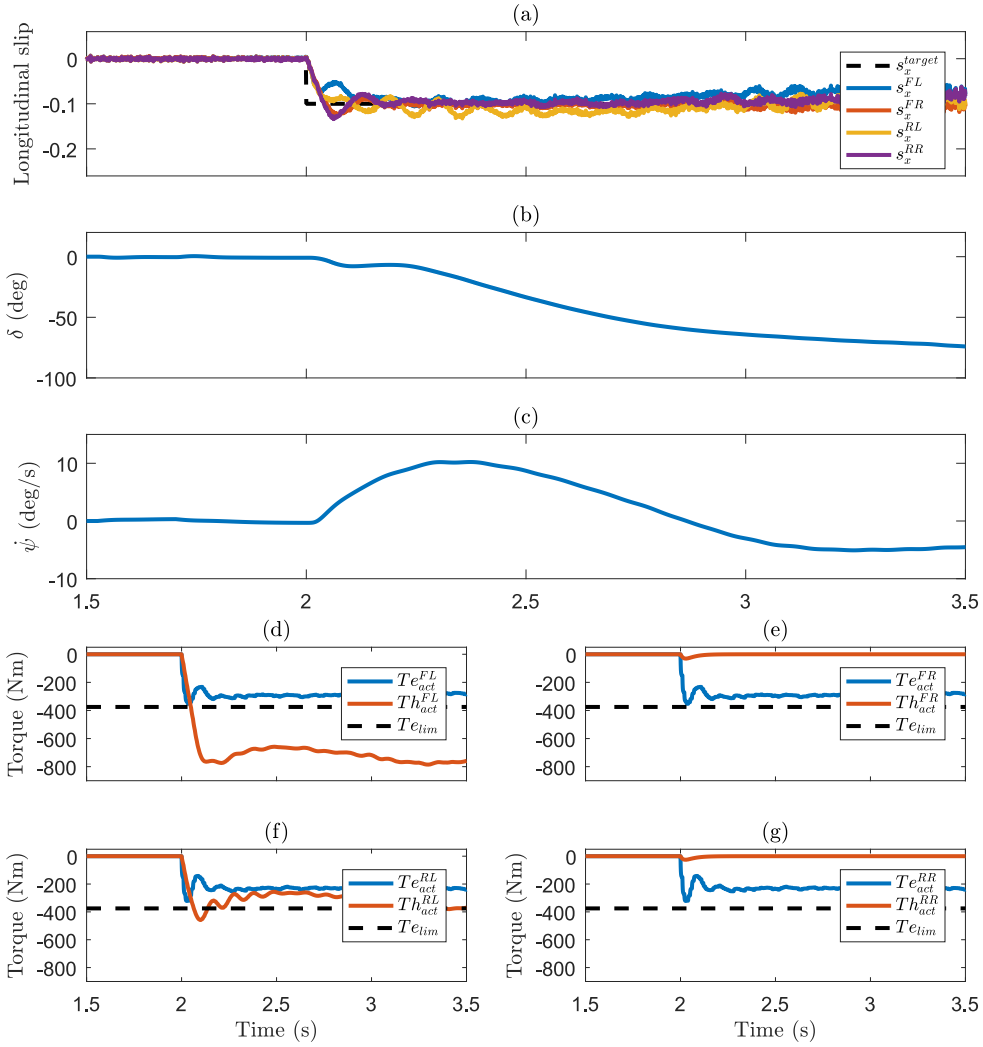

Figure 5.7: NMPC braking on split-μ road with $V_{initial}$=50km/h, s_{ref}=-0.1.

5.5 Performance metrics evaluation

The performance of the developed control strategies is evaluated and compared using the following performance metrics:

- RMSE for torque The RMSE for braking torque can be calculated based on equation 4.15. This metric can be used to compare the proposed torque integration for slip

control methods in terms of torque error between the controllers' demand and the actual EM and EHB torque.

Figure 5.8 illustrates the RMSE of braking torque for the nonlinear MPC and SMC with Daisy Chain algorithms proposed in this chapter. For an ABS braking on a low-μ road, the RMSE torque for nonlinear MPC achieved is 11.9Nm which is 5.5Nm less than the RMSE torque calculated using Daisy Chain method. On the other hand, the RMSE torque calculated for Daisy Chain is 6.4Nm smaller than the RMSE torque achieved for the NMPC (44Nm) when the vehicle is under ABS braking on a high-μ road. It can be observed that with this type of EV topology, both methods achieved acceptable RMSE torque and there is no significant advantage of using either the optimisation method (NMPC) or nonlinear controller (SMC) with static allocation method with respect to the braking torque RMSE. If the two cases can be compared, lower RMSE torque is recorded for the ABS on low-μ (using only EM) as opposed to the ABS on high-μ where both brake actuators are operating for the slip control.

- RMSE for longitudinal slip

  This performance metric can be determined using equation 4.16 to allow us to compare the two control strategies in achieving to minimise the slip error.

  The controllers' capability to achieve the desired slip $s_{ref} = -0.1$ during ABS braking situation is presented in Figure 5.9. For a low-μ case, the combination of SMC and Daisy Chain achieved the smallest RMSE slip (0.008) as compared to the nonlinear MPC (0.0104). The RMSE slip recorded are similar for the high-μ scenario. The trends indicate a good performance for both algorithms and recorded almost identical performance even both strategies are based on a different approach (optimisation and nonlinear controller). Another interesting observation is that smaller

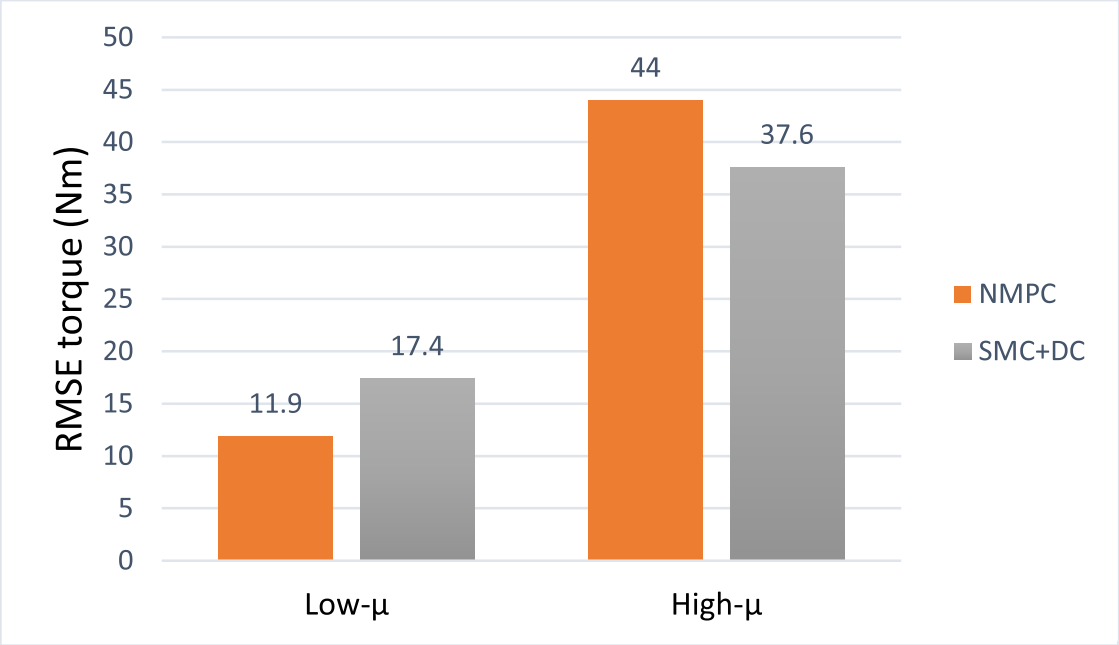

Figure 5.8: RMSE for braking torque.

RMSE of slip can be achieved when ABS is deployed using the EM.

- RMS of torque rate

  This method evaluates the RMS for the rate of change of braking torque for EM and EHB using equation 4.17.

  The RMS calculation is normalised over the highest value for each case and presented in percentage to compare between the two methods. Figure 5.10 indicates the RMS torque rate for two cases. The first case presents an emergency braking on a low-μ road. The SMC with Daisy Chain achieved highest RMS torque rate for the EM with nonlinear MPC only recorded 24% RMS torque rate. Daisy Chain method achieved lowest RMS of torque rate for the EHB at 2% while 22% recorded for the NMPC. A clear trend can be observed in the second case (ABS braking on the high-μ road) where the RMS torque rate calculated for NMPC for both EM (37%) and EHB (87%) are consistently lower than the values recorded for the Daisy Chain

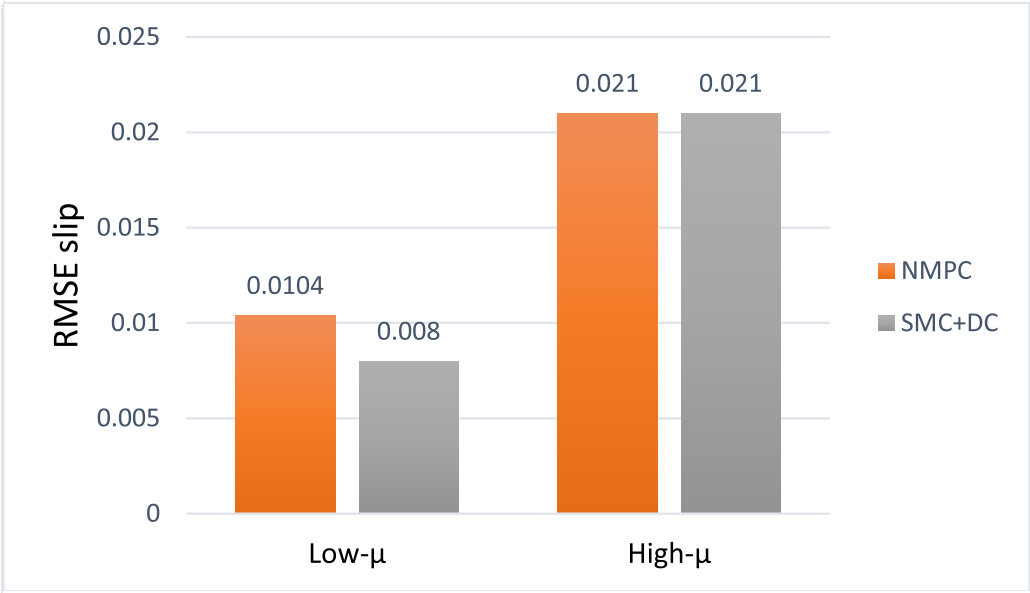

Figure 5.9: RMSE for longitudinal slip.

method. The trend suggests that SMC with Daisy Chain commanded more braking torque variation over time during slip control activation without respecting the actuator dynamics. On the other hand, the NMPC has the capability to constrain the control effort in order to operate within the actuators limits.

- Energy recuperated

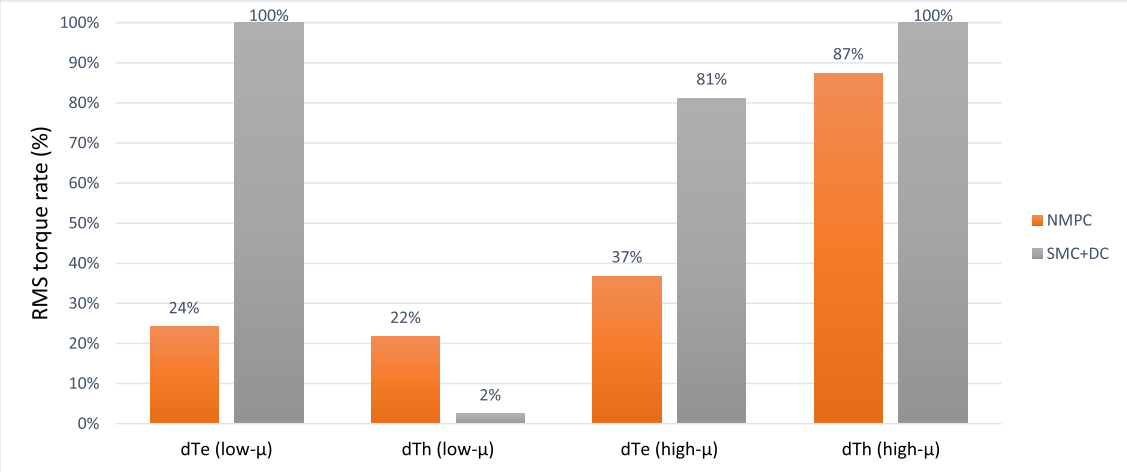

Figure 5.10: RMS for torque rate.

This metric calculates the mechanical energy recuperation in order to evaluate and compare between proposed control algorithms. Based on equation 4.18, the energy (in kWs) can be measured as the sum of the multiplication of the T_{em}, wheel rotational speed ω, and the sampling time t_s for all samples N. In this work, we neglect the losses from energy conversion to electrical energy and storing to the battery.

Figure 5.11 shows the energy recuperation capability for ABS braking on high-μ and low-μ road. Both controllers (NMPC and SMC with Daisy Chain) provide almost equal recovered energy (23kWs for the high-μ case and 10kWs for the low-μ case) while the EM operating in generator mode during ABS operation. Even with higher EM torque deployed during the high-μ braking, the energy recuperated is smaller compared to the low-μ case because the longer time required to stop the vehicle on the low-μ surface. This observation promotes the motivation of an opportunity to recuperate energy if torque blending for wheel slip control can be implemented.

- EM torque ratio One of the advantage of integrating the EM and EHB for slip control is to fully utilise the EM as braking actuator whenever possible. This metric

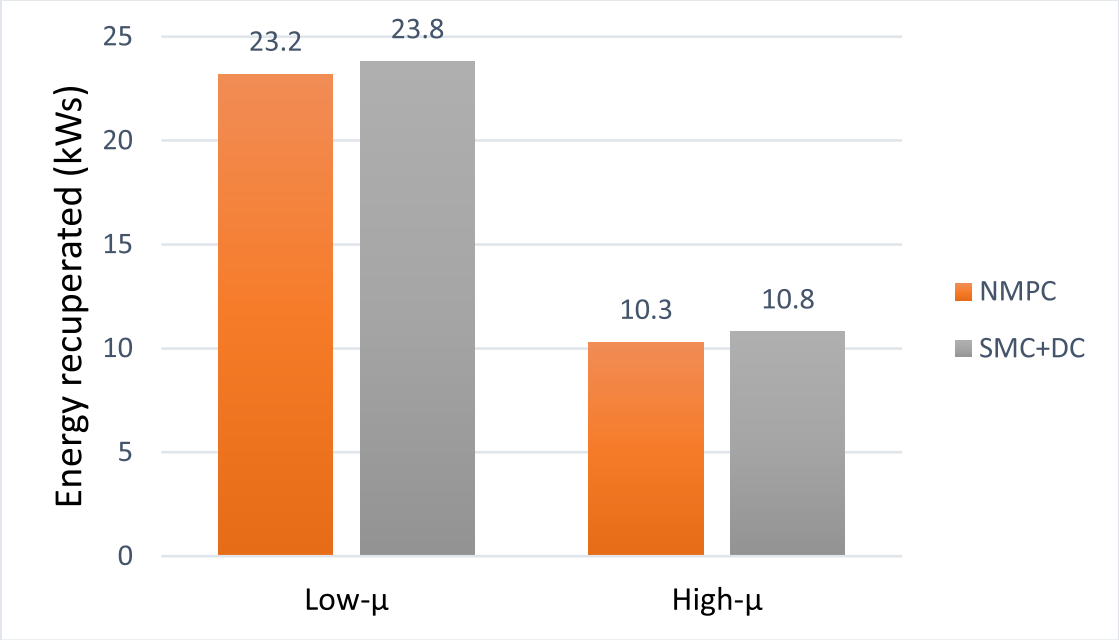

Figure 5.11: Mechanical energy recuperation.

calculates the ratio of the EM torque of the overall braking torque for each wheel based on equation 4.19.

The EM torque ratio for ABS braking on the high-μ and low-μ is presented in Figure 5.12. In this work, we assume that we have the ability to deploy the EM at maximum potential limits without any restriction from the battery. For the case of emergency braking on a low-μ road, both controllers fully utilise the EM as braking actuator during slip control (98.1% for NMPC and 99.8% for Daisy Chain). If the driver is braking on a high-μ surface, the EM torque ratio calculated for NMPC is 34.6% and slightly greater for the SMC with Daisy Chain method (35.1%). Looking at individual wheel level, the EM torque ratio is small (compared to 4) due to the vehicle topology having one EM per axle.

- Running cost

  This metric evaluates the performance of the proposed control strategies by cal-

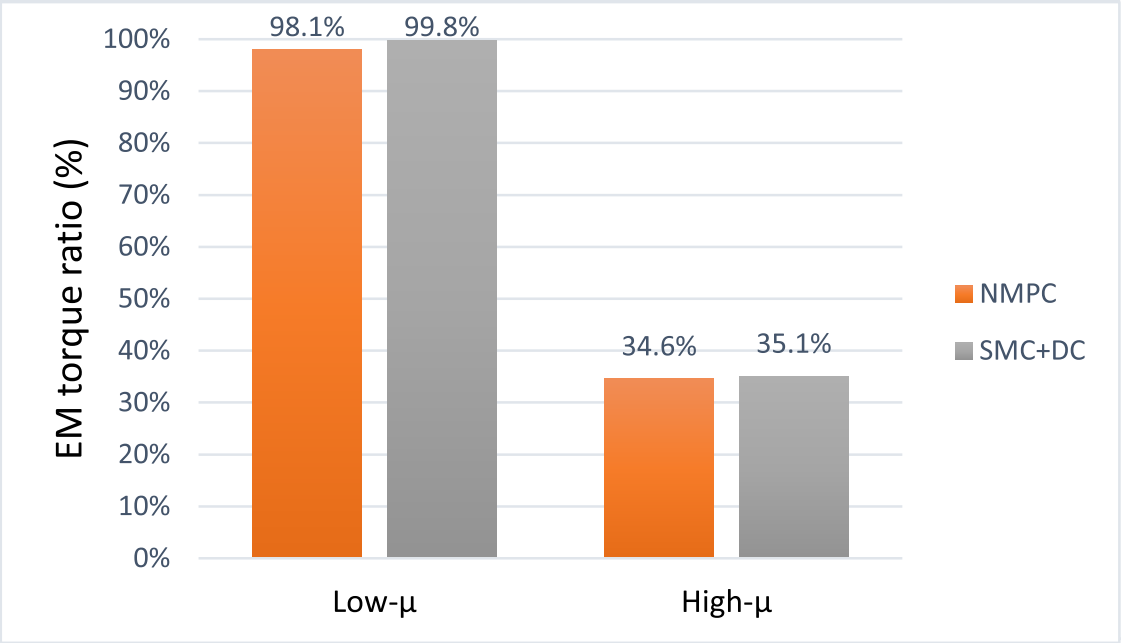

Figure 5.12: EM torque percentage.

culating the summation of running cost as per equation 4.20. The objective is to compare the effort by the control strategies to minimise the cost function. The calculation is presented as normalised percentage figures to compare the two developed methods for two cases.

The first case is ABS braking on a low-μ road. Figure 5.13 shows that the NMPC requires half of the running cost recorded when compared to the SMC with Daisy Chain approach. The case of an emergency braking on a high-μ surface illustrates the similar trend where NMPC running cost is only 77% of the SMC with Daisy Chain. As expected, the optimisation method recorded smaller running cost when compared to a non-optimisation controller (SMC with Daisy Chain).

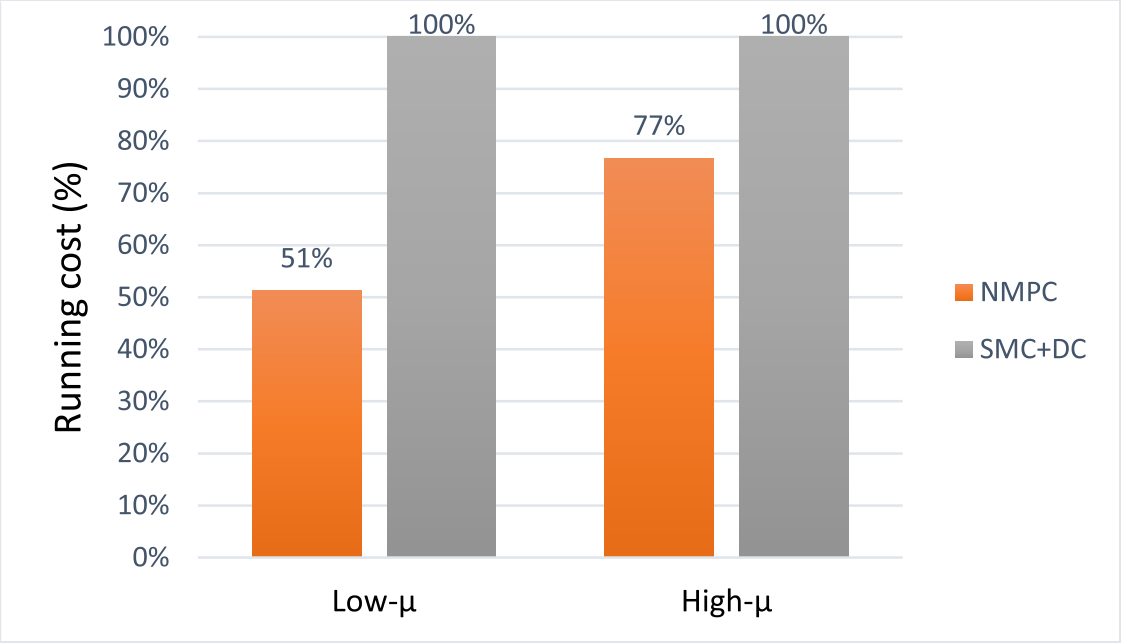

Figure 5.13: Sum of the running cost.

5.6 Summary

We have presented the torque integration strategies for redundant braking actuators using four EMs in the previous chapter. In this chapter, we use a more restricted vehicle topology which has one EM for each axle and implements torque blending strategies using different methods. There is a challenge to handle the problem of constrained equal EM torque between left and right wheels by the axle EM.

We propose to implement the combination of SMC (slip control) and Daisy Chain for the torque blending using axle EM in an AWD BEV. Test manoeuvre used to evaluate the strategies include braking on a low-μ road and split-μ braking. Next, we formulate a strategy using MPC to integrate the slip controller and torque allocation as a unified objective function subject to the constraints by the actuator dynamics. The simulation results show acceptable performance for the implementation of Daisy Chain (with SMC slip control) and MPC strategies. We also prove the real-time operation capability of the

optimisation method (even with more complex problem definition with the four-wheel internal model instead of single-wheel) for online simulation and the potential for real vehicle implementation.

From the performance metrics comparison between the two control strategies, it can be said that both MPC and SMC with Daisy-Chain are comparable for the RMSE of torque and longitudinal slip. Bigger RMSE is calculated for the high-μ case which shows the slight deterioration of the performance when EHB is applied for slip control. The torque variation for the SMC with Daisy-Chain is greater than the NMPC method in most cases as shown by the RMS torque rate. Finally, the NMPC requires less running cost for the problem definition when compared to the SMC with Daisy-Chain strategy.

Chapter 6

Torque Integration for Slip Control using single EM

Several articles discuss torque blending strategies using four IWMs and a braking torque allocator concept between friction brakes and EMs is proposed. However, the approach proposed is limited to particular vehicle architecture using four EMs due to individual wheel brake control ability in ABS operation. Moreover, some of the method proposed is computationally demanding for testing implementation with real vehicle's hardware.

To the authors' present knowledge, there is no torque blending algorithm design with vehicle topology selected in this work that is an AWD HEV with a single EM as discussed in 2.2.3 and illustrated in Figure 2.5. There is a challenge to implement a torque apportionment strategy for ABS due to the lack of control of regenerative braking for the individual wheel as opposed to the friction brakes.

Brake torque integration between EHB and RBS during ABS operation provides the advantage of enabling the vehicle to recuperate energy even during slip control system activations thus increasing the vehicle's energy efficiency, increasing the energy regeneration limit threshold near the tyre-road adhesion limit, and improving braking performance

in certain cases due to the actuators' capability. In the following section, we will discuss the control architecture for torque allocation strategy.

6.1 Torque Blending using Static Allocation

In this work, we present a novel strategy to interweave RBS by single EM and brake-by-wire using EHB in ABS implementation. The primary motivation is to increase the energy regeneration by having a wider activation window while maintaining ABS core performance. The proposed algorithm as shown in Figure 6.1 consists of a wheel slip controller using SMC, ABS management system, and torque allocation using Daisy Chain to distribute the ABS brake torque command between RBS and EHB.

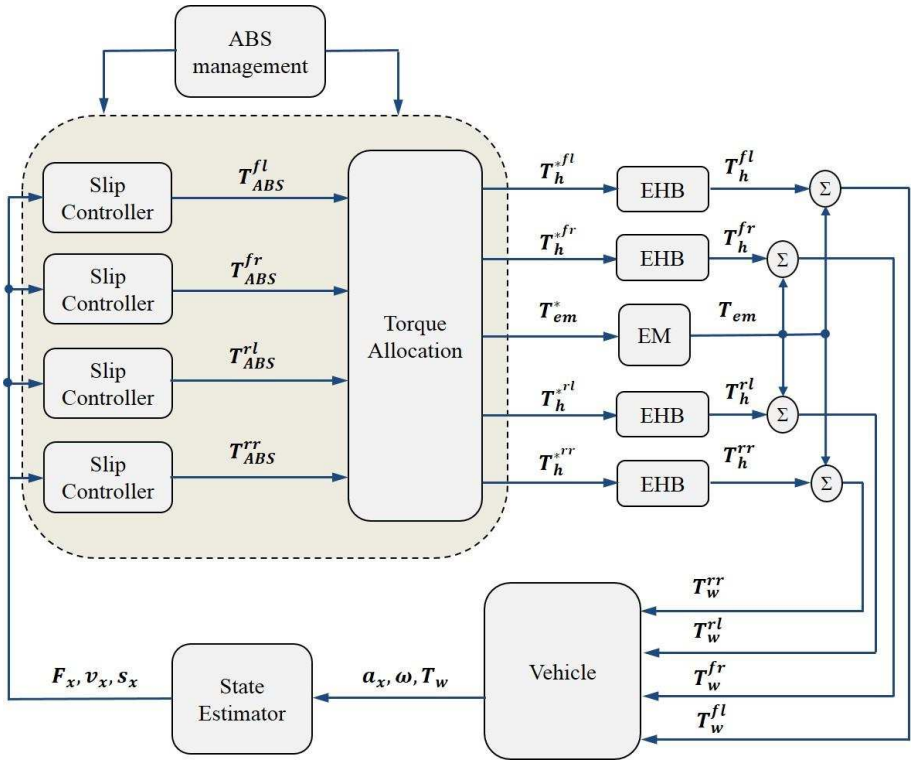

Figure 6.1: Overview of torque integration strategy with one EM.

The method we propose allows the requested torque by the wheel slip algorithm to

be distributed to the two braking actuators available in the vehicle by considering present battery SOC. RBS is given the priority in delivering the ABS torque but limited to the energy storage level during a braking event. Friction brakes will provide the remainder of the ABS torque request once the EM torque is saturated.

$$T_{em} = min(T_{ABS_i}, T_{regen\ avail}) \tag{6.1}$$

$$T_{total_i} = T_{em} + T_{h_i} \tag{6.2}$$

$$i \in \{fl, fr, rl, rr\}$$

Figure 6.2 shows the flowchart for the torque allocator proposed in this research. The main input is the T_{ABS} from the slip controller and will be allocated based on a prioritised towards the EM and only will be using the friction braking once the first actuator is saturated. This logic requires the available regenerative braking torque $T_{regen\ avail}$ information from the vehicle to determine the torque demand values for each braking actuators. The minimum value of the four-wheel ABS torques will be determined first T_{ABS_i}. Next, the EM torque demand T_{em} will be set to the minimum value between T_{ABS_i} and $T_{regen\ avail}$ as described in equation 6.1. Finally, the commanded friction braking torque T_{h_i} for each wheel is calculated. Both RBS torque and friction brake torque must satisfy the total torque demand by the slip controller as shown in equation 6.2. This method is applied exclusively to the AWD PHEV topology due to the single EM which connected to the four wheels through a propeller shaft.

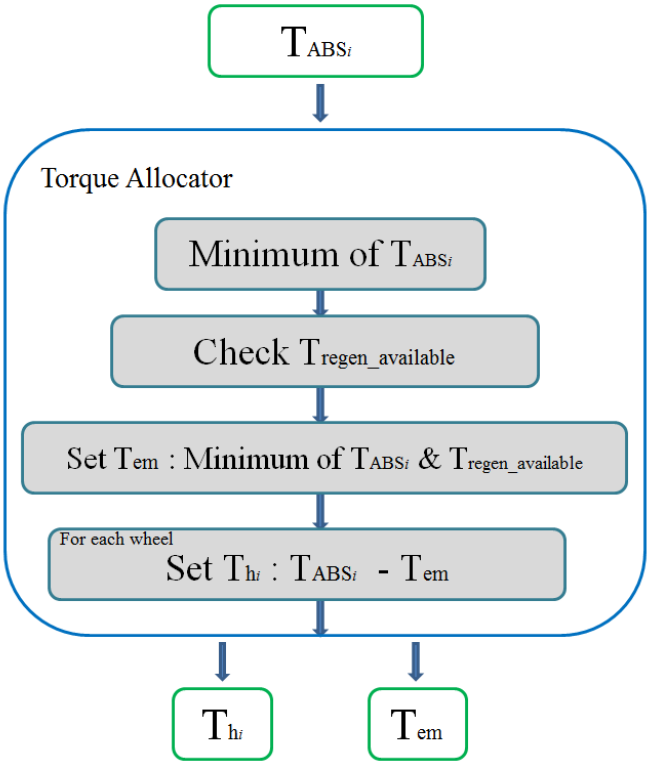

Figure 6.2: Torque blending strategy for AWD PHEV (1 EM).

6.2 Torque Blending and Wheel Slip Control using MPC

Torque blending strategy for electrified vehicles is an interesting problem with the challenge of different type of vehicle architectures. It can be as flexible as using four EMs to enable individual wheel torque integration between braking actuators to a more restrictive vehicle topology which uses a single EM for an AWD PHEV. In the latter case, we can use MPC strategy with a four-wheel internal model for an AWD PHEV with a centralised EM. Figure 6.3 illustrates an overview of the proposed optimisation strategy for specified vehicle topology. The MPC is formulated to handle two main objectives which include individual wheel slip control and torque allocation between braking actuators with priority given to the single EM. A slip reference s_{ref} is set and the measured signals from the vehicle are used to estimate the vehicle speed v_x and the vertical tyre force F_z. The re-

quired inputs and states are then fed to the MPC to solve and achieve an optimal solution for the given problems with respect to the constraints incorporated.

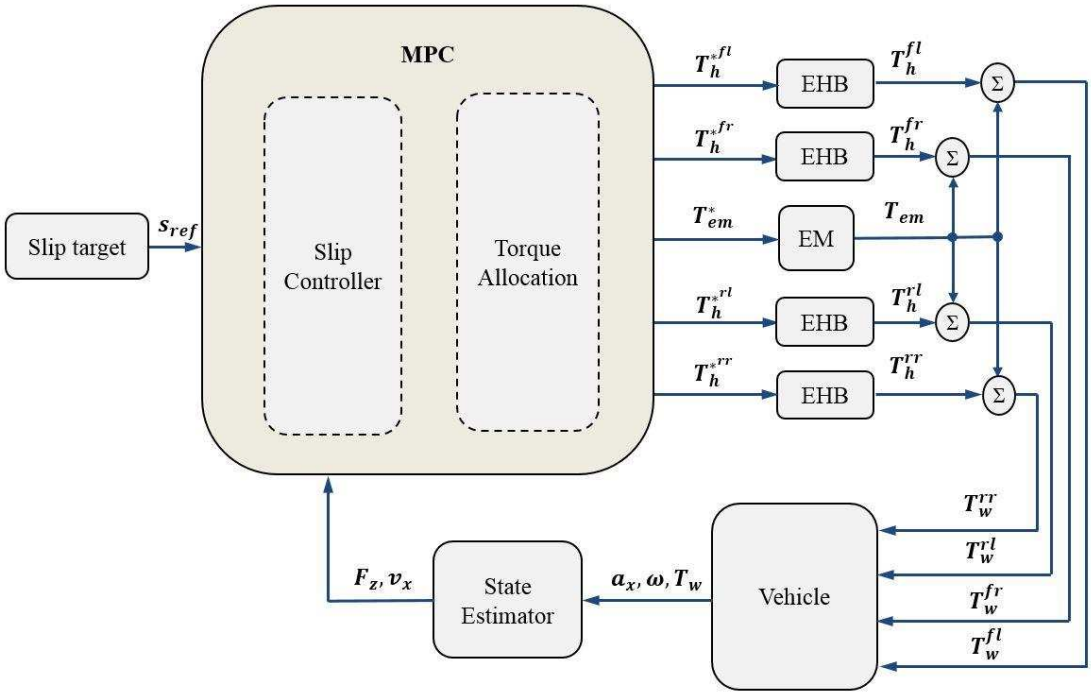

Figure 6.3: Overview of MPC slip control and torque blending integration strategy with one EM.

We neglect the lateral motion and only use the longitudinal dynamics for the internal model, the vehicle and wheel dynamics used are similar to equations 5.3 and 5.4, and the total torque for each wheel is

$$T_{tot}^{i} = T_e + T_h^{i}, \tag{6.3}$$

$$i \in \{fl, fr, rl, rr\}$$

This is assuming that equal regenerative braking torque applied for each wheels which described in equation 2.11 (T_e^{fl}=T_e^{fr}=T_e^{rl}=T_e^{rr}) due to an EM connected to the four wheels through a propeller shaft. The MPC formulation from 4.6 can be expanded for this par-

ticular topology and problem,

$$\min_{x,u} \quad \sum_{k=0}^{N-1} [q_s(s_{x_k}^{i,j} - s_{ref})^2 + q_T(T_{h_k}^{i,j})^2 + q_e(\Delta T_{e_k})^2 + q_h(\Delta T_{h_k}^{i,j})^2] \tag{6.4a}$$

$$s.t. \quad \bar{x}(0) = \bar{x}_{init}, \tag{6.4b}$$

$$\bar{x}_{k+1} = \bar{g}(\bar{x}_k, \bar{u}_k), \quad k = 0, ..., N-1 \tag{6.4c}$$

$$T_e^{min} \leq T_{e_k} \leq T_e^{max}, \quad k = 0, ..., N-1 \tag{6.4d}$$

$$T_h^{min} \leq T_{h_k} \leq T_h^{max}, \quad k = 0, ..., N-1 \tag{6.4e}$$

$$\Delta T_e^{min} \leq \Delta T_{e_k} \leq \Delta T_e^{max}, \quad k = 0, ..., N-1 \tag{6.4f}$$

$$\Delta T_h^{min} \leq \Delta T_{h_k} \leq \Delta T_h^{max}, \quad k = 0, ..., N-1 \tag{6.4g}$$

$$i \in \{front, rear\}, \quad j \in \{left, right\}$$

Similar to the previous approach, we can deploy the strategy using nonlinear MPC as discussed in 4.2.1. The MPC properties and tuning parameters are listed in Table 6.1. The motivation behind the set of tuning selection is to minimise the wheel slip error while penalising the EHB torque. The appropriate selection of the t_s and N are also important to balance the compromise between the MPC performance and solving in real-time.

Parameter (Unit)	Description	Value
t_s (ms)	sampling time	10
N	number of steps	10
q_s	weight of slip error	$0.1\frac{(\Delta T_e^{limit})^2}{(s_{ref})^2}$
q_T	weight of friction torque	1
q_e	weight of control input, ΔT_e	50
q_h	weight of control input, ΔT_h	1000

Table 6.1: NMPC properties for single EM strategy.

6.3 Simulation for Daisy Chain Torque Allocation using one EM

In this section, we evaluate the developed strategy using SMC slip controller and static torque allocation strategy for an AWD PHEV with a single EM. This method handles the two objectives independently and implemented as shown in Figure 6.1 in Matlab/Simulink. We develop different test manoeuvres in CarMaker environment to validate the proposed strategy. The tyre and vehicle parameters are presented in Table 2.2. For this simulation, the assumption is the regenerative braking torque available for the EM is 750Nm. For this vehicle configuration, the available electric torque for each wheel is then 187.5Nm which is lowest among the three vehicle topologies available in this research.

6.3.1 Low-μ straight line braking

A straight line braking on low adhesion surface (road μ=0.3) is done using an AWD PHEV with a single EM to demonstrate the torque integration strategy discussed in section 6.1. Figures 6.4a)-b) show the slip control is activated at $t = 2s$ with the initial speed V_x of 50km/h for a hard braking manoeuvre. With the limited regenerative braking available, the EM torque is saturated during the ABS operation and support from the EHB is required as illustrated in Figures 6.4c)-d) to achieve the $s_{ref} = -0.1$. The activation of the EM in generator mode make the energy recuperation possible during any braking condition with consideration of the EM and energy storage in HEV. It is worth to note that the EM torque is saturated even braking on a low-μ road which requires the assistance from the friction braking to satisfy the surplus T_{ABS} from the SMC. There is also chattering from the calculated T_{ABS} from the SMC which is affected by the noise injected to the state feedback to the controller.

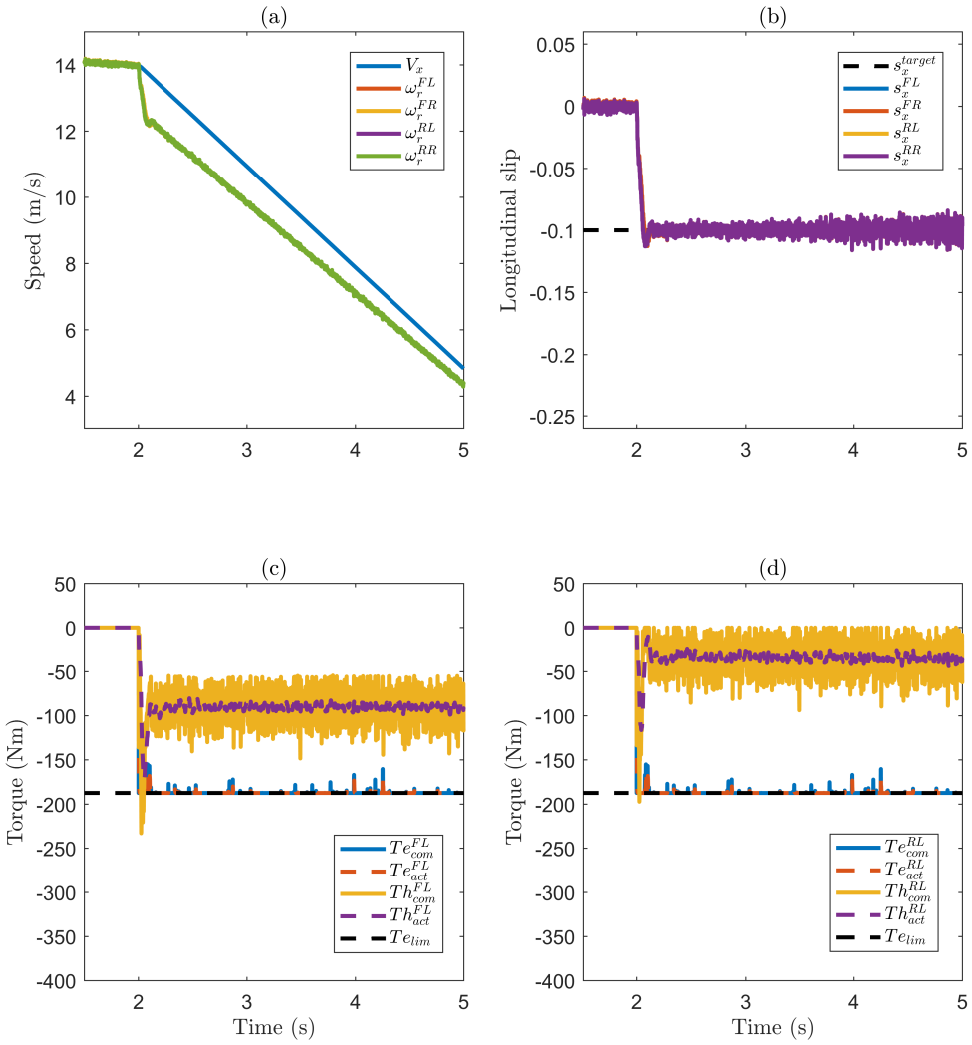

Figure 6.4: Straight line braking with road μ=0.3, $V_{initial}$=50km/h, s_{ref}=-0.1.

6.3.2 Split-μ straight line braking

Braking on an uneven road adhesion surface can lead to dangerous situation if any of the wheels is locked. This test pattern is specifically designed to evaluate the proposed method not only in terms of stopping performance, but the ability to maintain the vehicle stability and steerability throughout the emergency braking.

The driver is braking on the road with dry asphalt on the left-side of the wheels (μ=1.0) and on snow surface for the right-side wheels (μ=0.3). Similar to the previous test, the initial vehicle speed is 50 km/h (13.89 m/s). A yaw moment is created towards the high friction side when equal braking torque is applied to the left and right wheels for a non-ABS case. With the slip controller activated from $t = 2s$, the braking torque is retarded to avoid wheel locking and the vehicle from losing its stability. Figure 6.5a) shows the wheel slip achieved near the s_{ref} during ABS activation. Lower brake torque is commanded to the wheels on the low-μ surface to maintain the wheel slip of 0.1 as illustrated in Figure 6.5e) and g). Interestingly, there is a need of using the friction braking to support the surplus T_{ABS} for all wheels since the available EM torque is limited and shared between the four wheels. If we compare to the previous vehicle configurations (BEV using 2 EMs and 4 EMs), braking on the low-μ side can be solely done by the regenerative braking. To prove the observation that the developed algorithm enables the driver to maintain the steerability of the vehicle, Figure 6.5b shows that a countersteering input by the IPG driver model of 66deg is required to safely stop the vehicle. The maximum yaw rate achieved is 8.2deg/s as shown in Figure 6.5c).

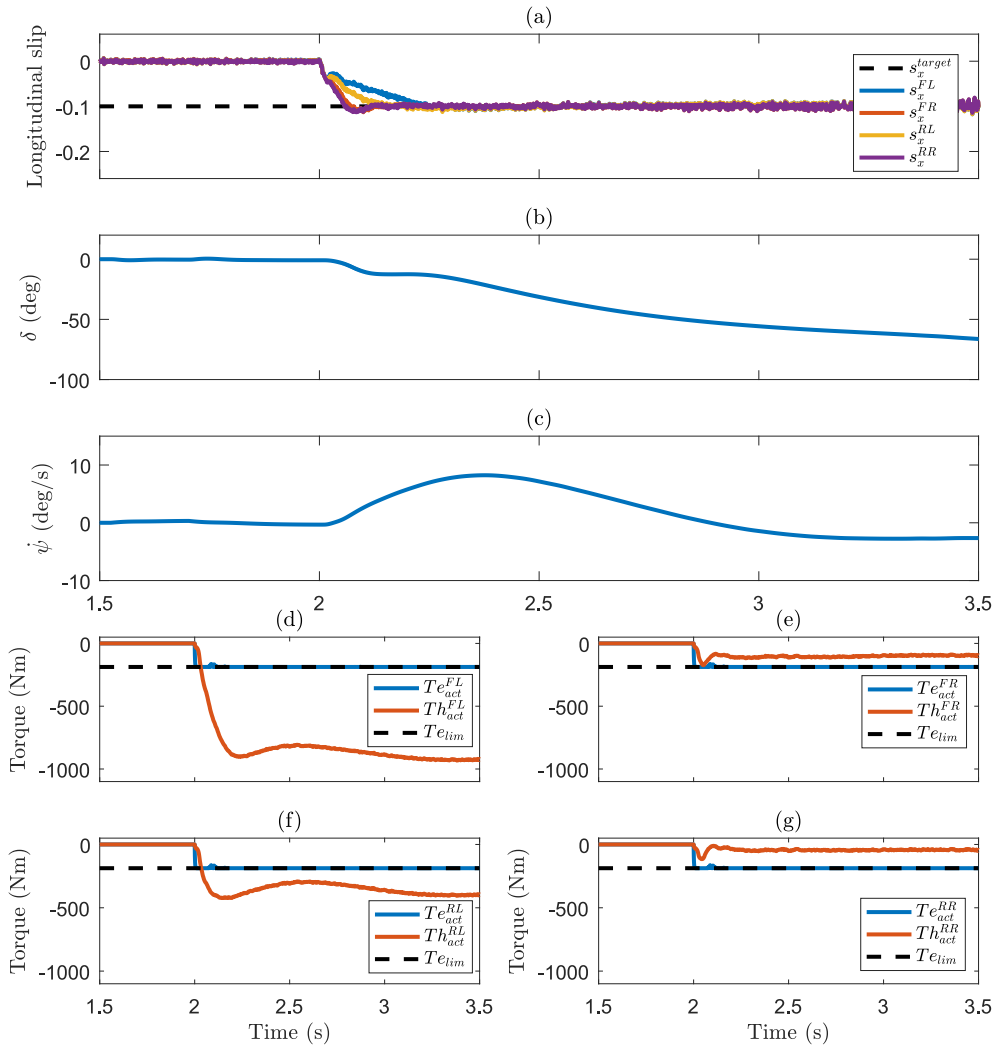

Figure 6.5: Braking on split-μ road with $V_{initial}$=50km/h, s_{ref}=-0.1.

6.4 Simulation for MPC torque blending for slip control using one EM

An integration of torque blending and slip control strategy developed using MPC is evaluated in Matlab/Simulink and CarMaker environment simulating an AWD BEV with one EM. The parameters of the vehicle and the tyres used in this simulation are listed in Table

2.2. IPG Driver is applied in CarMaker to control the vehicle throughout the test manoeuvres. The main objectives of the developed strategy are to maintain the wheel slip near the slip target and to allocate the braking torque between the redundant actuators.

6.4.1 Low-μ straight line braking

This test pattern represents braking on a packed snow surface (road μ=0.3) which normally does not requires high braking torque to lock the wheels. Figures 6.6a)-b) indicate that wheel-lock can be avoided when the control algorithm is activated from $t = 2s$ with an initial speed of 50km/h (13.89m/s) and wheels slip are maintained near the $s_{ref=-0.1}$ throughout the braking event. In this example, the use of single EM causes limitation to the regenerative braking torque availability as compared to the case with multiple EMs equipped in a BEV (presented in 4. Hence, there is a requirement for a support from the EHB once the EM torque is saturated as illustrated in Figures 6.6c)-d). Finally, the optimal control strategy can be deployed in real-time implementation with the problem is solved under the $T_{sampling} = 10ms$ at the average of 3.9ms.

6.4.2 Split-μ straight line braking

The next test pattern will help us to evaluate the performance of the proposed NMPC torque blending for slip control using one EM in terms of longitudinal and lateral dynamics. The test requires the IPG Driver to apply emergency stop on uneven road adhesion surface with road μ of 1.0 on the left-side of the car and road μ of 0.3 on the right-side of the vehicle. Figures 6.7a)-b) provide proof that the main objective of wheel slip control is met by preventing wheels from locking in emergency braking starting from $t_{sim} = 2s$ at an initial speed of 50km/h (13.89m/s). In terms of wheel braking torque, friction braking is required for each wheel to support the limited regenerative braking availability from

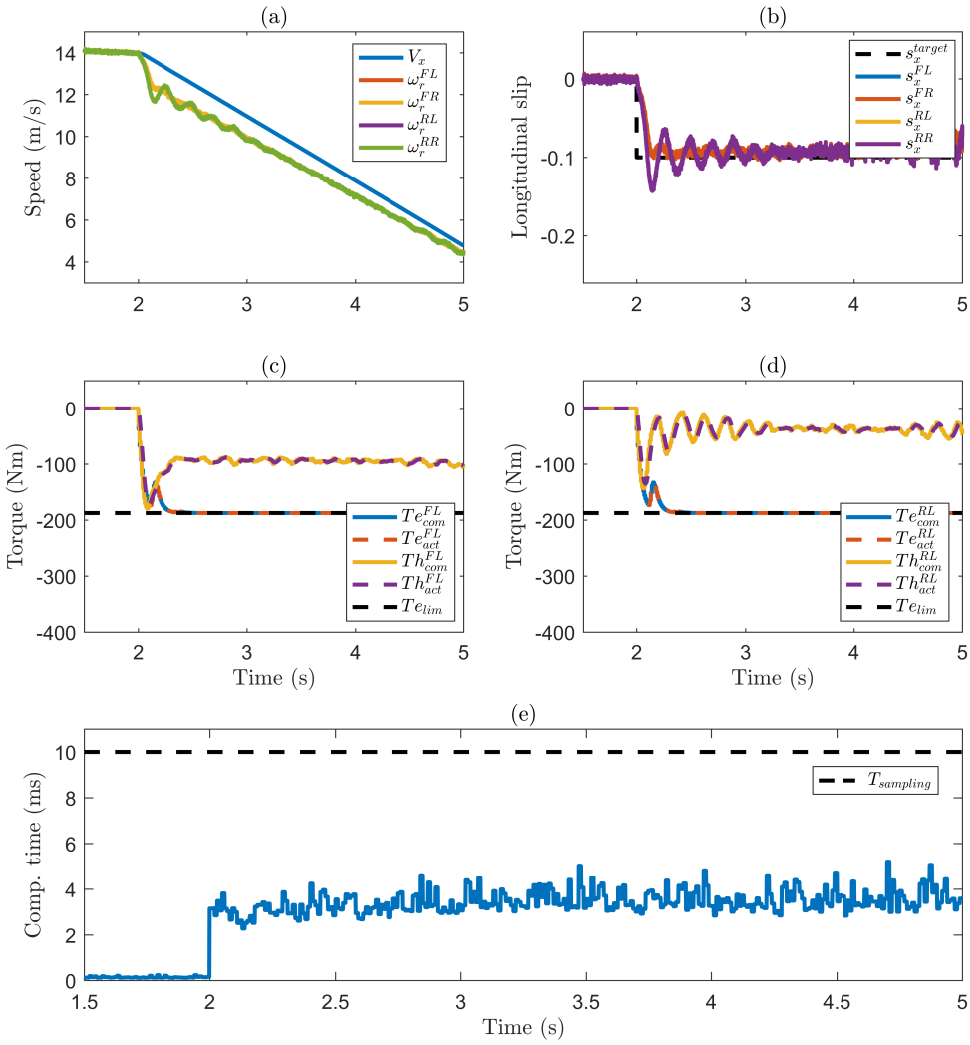

Figure 6.6: Straight line braking with road μ=0.3, $V_{initial}$=50km/h, s_{ref}=-0.1.

one EM which shown in Figures 6.7d)-g). It also indicates the limitation of using single EM attached to all wheels which will limit the regenerative braking to the lowest torque demand between the wheels. The IPG driver managed to stop the vehicle safely while maintaining the vehicle's direction with a countersteering input of 59deg (Figure 6.7b) and the maximum yaw rate of the vehicle is 5.9deg/s (Figure 6.7c).

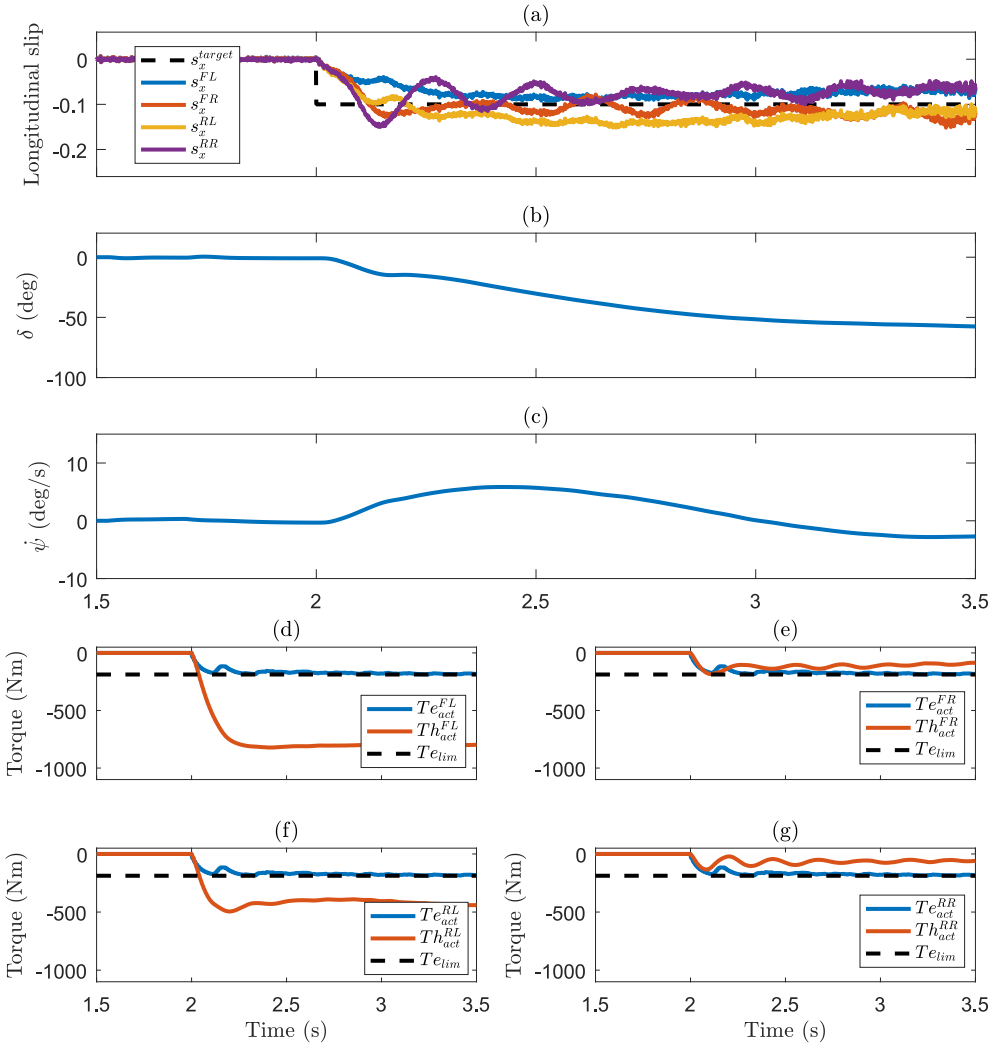

Figure 6.7: Braking on split-μ road with $V_{initial}$=50km/h, s_{ref}=-0.1.

6.5 Performance metrics evaluation

This section presents the performance metrics to analyse the two different torque blending strategies for slip control using one EM in an AWD BEV. From the calculated metrics, the performance of the control strategies can be evaluated and compared.

- RMSE for torque

Equation 4.15 is used to calculate the RMSE for braking torque. This measures the error between the commanded torque and actual torque of the EM and the EHB.

Figure 6.8 shows the RMSE for the braking torque for the two methods proposed in this chapter. For the low-μ scenario, the RMSE torque for nonlinear MPC achieved is 7.1Nm which is smaller than the RMSE torque calculated using Daisy Chain method (19.8Nm). A similar trend can be observed for the high-μ case with the calculated RMSE torque of 31.4Nm and 43Nm for NMPC and SMC with Daisy Chain respectively. Overall, the recorded RMSE torque for the low-μ case is lower than the high-μ case. This happens even both braking actuators are utilised for the slip control in both situations (low-μ and high-μ) due to the limited available regenerative braking from a single EM. It can be observed that the optimal control strategy (using nonlinear MPC) can achieve lower RMSE torque compared to using a nonlinear controller(SMC) with static allocation (Daisy Chain).

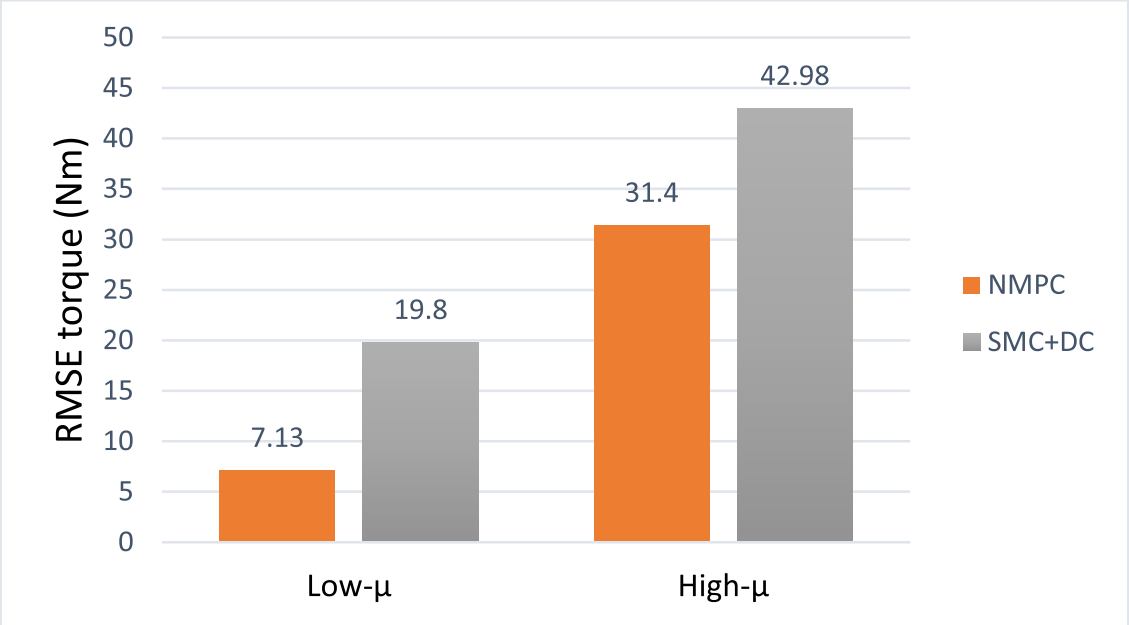

Figure 6.8: RMSE for braking torque.

- RMSE for longitudinal slip

  The performance of the controllers in minimising the slip error can be evaluated using equation 4.16 to calculate the RMSE slip for the two cases.

  The main task of the control strategies is to achieve the slip target $s_{ref} = -0.1$. Emergency braking on a low-μ road recorded RMSE slip of 0.0171 and 0.009 for the nonlinear MPC and SMC with Daisy Chain methods respectively as presented in Figure 6.9. Slightly bigger RMSE slip is calculated for the high-μ case with 0.033 (NMPC) and 0.0224 (SMC with Daisy Chain). All results show good performance for both control methods in delivering the slip reference with SMC and Daisy Chain achieved slightly smaller RMSE for the slip. Finally, the RMSE slip calculated for the high-μ case is higher than the low-μ scenario. It seems that is the case when more braking torque is delivered by the EHB (refer EM torque ratio).

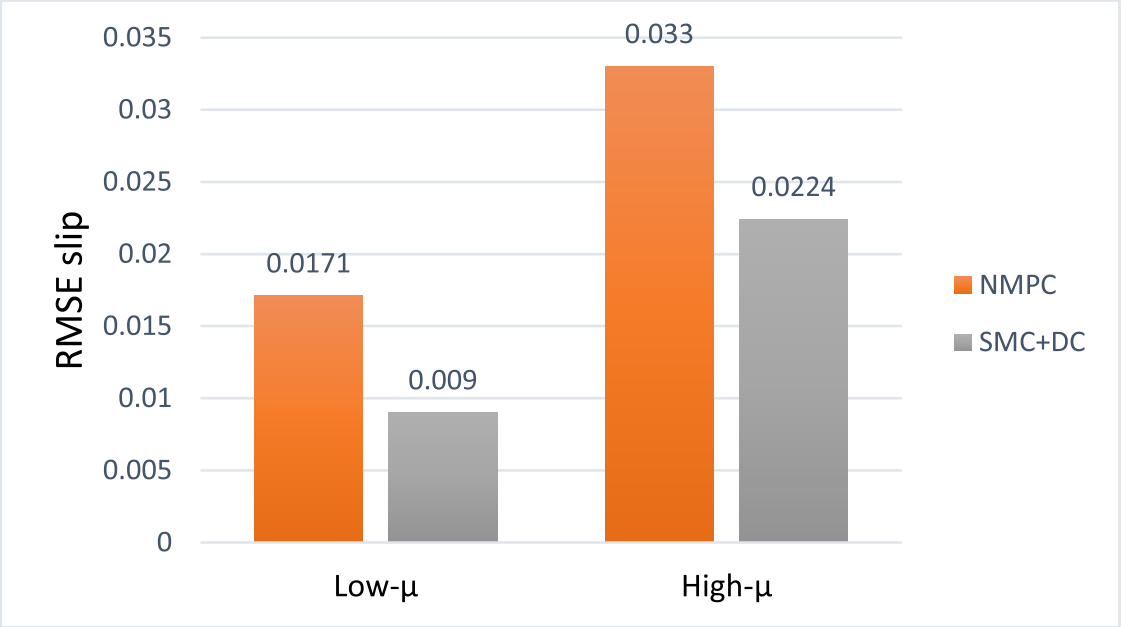

Figure 6.9: RMSE for longitudinal slip.

- RMS of torque rate

This metric is based on equation 4.17 for us to evaluate the RMS of braking torque rate for the EM and the EHB.

The two strategies are compared by using the normalised calculated RMS torque rate over the highest value in percentage for two cases. Figure 6.10 shows the RMS torque rate and the first case presents the braking on a low-μ surface. The change of EM torque and EHB torque for NMPC methods are 30% and 79% respectively. The figures calculated are smaller compared to the SMC with Daisy Chain strategy and the similar trend continues for the high-μ case. The results from the metrics confirm that greater number of torque variation were requested from the SMC with Daisy Chain compared to the NMPC strategy. This highlights the advantage of the nonlinear MPC method which respects the braking actuator dynamics. On the other hand, the SMC slip controller (with Daisy Chain torque blending) does not consider the limits of the braking actuators which results in greater torque variation.

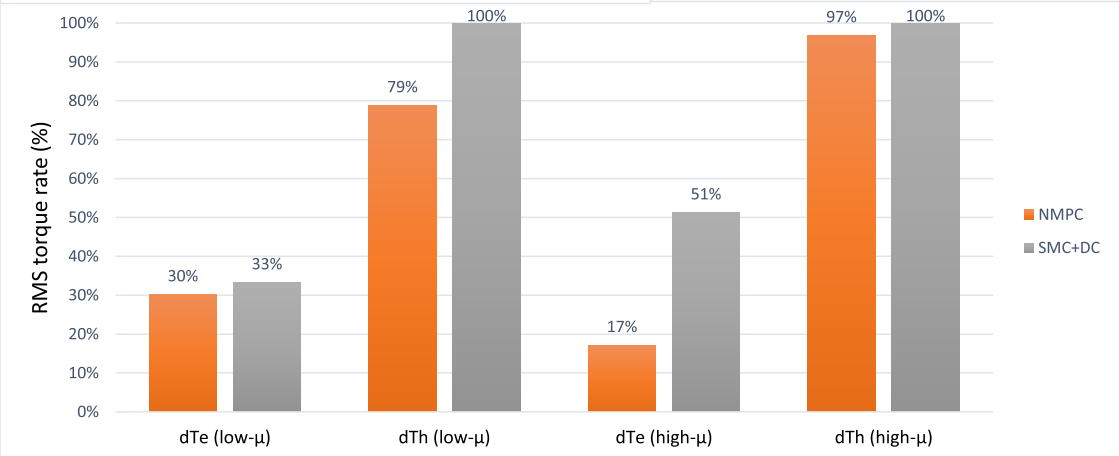

Figure 6.10: RMS for torque rate.

- Energy recuperated

  The energy recuperation potential between the two methods can be evaluated using the metric based on equation 4.18. The mechanical energy recuperation is measured

in kWs.

Figure 6.11 illustrates the mechanical energy recuperation capability for two cases. The nonlinear MPC and SMC with Daisy Chain strategies are capable to provide a similar amount of energy (16kWs for the high-μ case and 5.5kWs for the low-μ case) through the regenerative braking by the EM during ABS activation. With the limitation of one EM (compared to the other topologies using two and four EMs), the overall energy recuperation is limited compared to the figures reported in 4 and 5. The energy recovery calculated for low-μ is greater than the high-μ due to the longer time required for the vehicle to stop on the low-μ surface. This observation supports the motivation to implement torque blending for slip control and enable energy recuperation to increase overall vehicle efficiency.

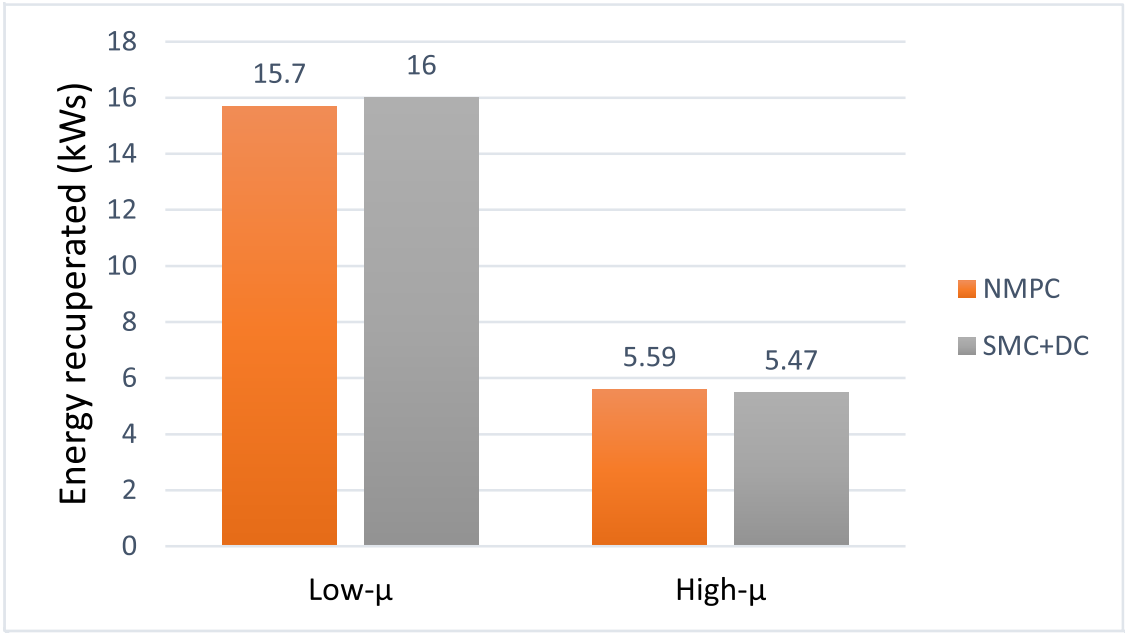

Figure 6.11: Mechanical energy recuperation.

- EM torque ratio

This metric is based on equation 4.19 to calculate the ratio of the EM torque for

each wheel.

Figure 6.12 indicates the percentage of the EM torque over the total slip control torque for two scenarios. As expected, higher EM torque ratio is recorded for the low-μ case as compared to the high-μ case. The NMPC and SMC with Daisy Chain offer 65.2% and 67.1% EM torque ratio for the low-μ case. For the emergency braking on a high-μ road, the calculated EM torque ratio for NMPC and Daisy Chain are 17.8% and 17.7% respectively. The trend suggests that heavier reliance on regenerative braking during low-μ ABS braking due to lower total torque demand required to achieve the slip reference. With the limited EM torque availability (single EM), the support from the EHB is necessary during ABS activation.

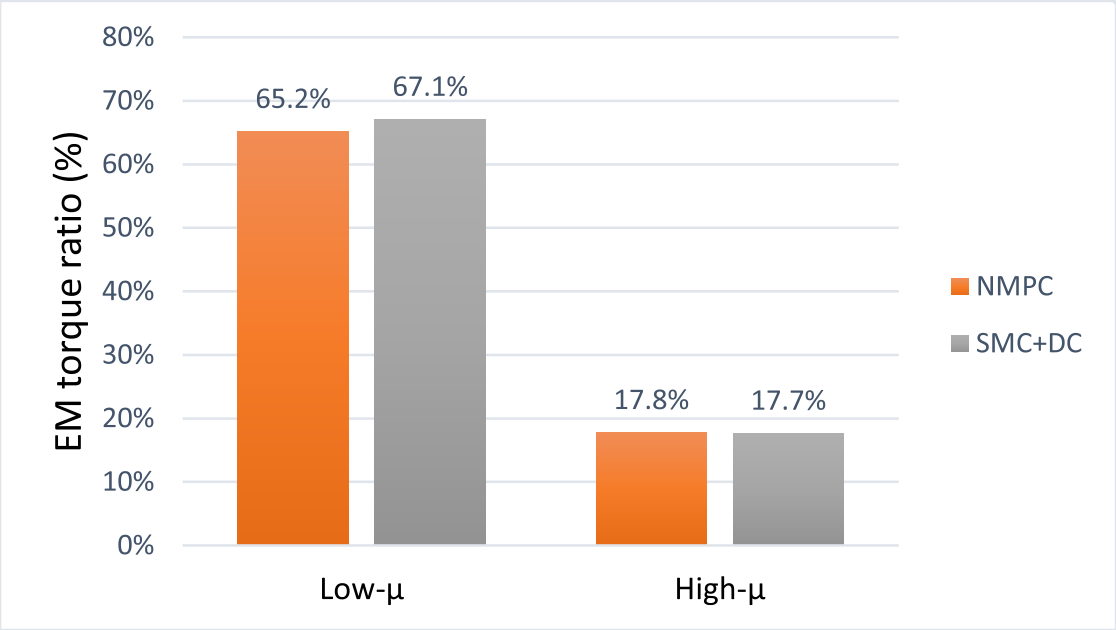

Figure 6.12: EM torque percentage.

- Running cost

The running cost for the two proposed strategies is calculated using equation 4.20. The aim is to compare the effort of each controller to minimise the cost function.

For the low-μ ABS braking, Figure 6.13 illustrates that NMPC recorded 41% summation of running cost when compared to the SMC with Daisy Chain method. A smaller difference is recorded (10.8% difference) between the two strategies for the high-μ case but a similar trend is presented where SMC with Daisy Chain achieves higher running cost. The trend shows that smaller running cost required for the nonlinear MPC for the given objective function when compared to the SMC with Daisy Chain method.

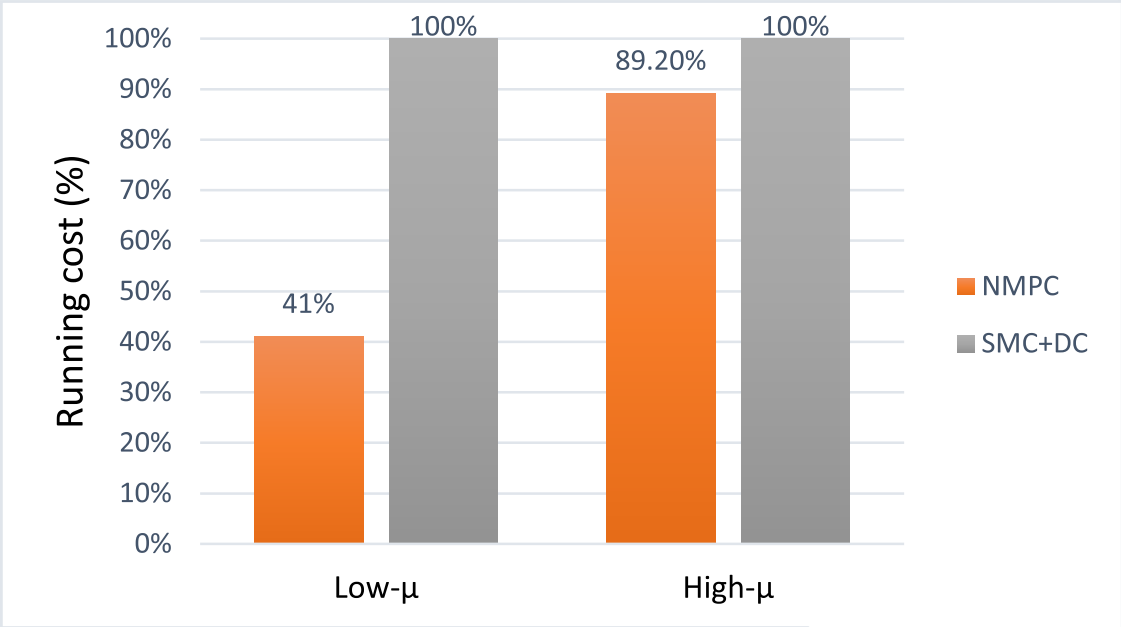

Figure 6.13: Sum of the running cost.

6.6 Summary

The chapter presents state-of-the-art methods to achieve torque blending for slip control for an interesting vehicle topology; namely AWD BEV using one EM. Firstly, we deploy a pragmatic approach by implementing SMC as the slip controller and Daisy Chain to allocate the braking torque between different actuators. Simulations using the high-fidelity

model in Matlab/Simulink and CarMaker environment provide acceptable performance in satisfying the slip target and integrating both EM and EHB during slip control. Then, we develop a strategy to combine both slip control and torque allocation in a single MPC formulation. Using similar evaluation methods, we observe that the proposed method fulfils the main objectives of the ABS which include preventing wheel-locking and maintaining the vehicle's stability and steerability. The computational solve time observed is always under the sampling time of 10ms to show the real-time deployment capability of the developed strategy.

SMC with Daisy-Chain method recorded higher RMS error for braking torque compared to the NMPC strategy for all cases (low-μ and high-μ ABS braking). On the contrary, the calculated RMSE for the longitudinal slip is smaller than the NMPC method. As for the torque variation during the controller activation, the NMPC performs well and shows smaller RMS torque rate when compared to the SMC with Daisy-Chain method. This is expected as the NMPC incorporates the actuator dynamics into the problem definition while SMC with Daisy-Chain neglects the behaviour of the braking actuators. Finally, the sum of running cost required for the NMPC method is recorded to be smaller than the SMC with Daisy-Chain strategy.

Chapter 7

Real-time MPC Deployment

In this chapter, we will demonstrate the capability of the formulated nonlinear constrained optimal control strategy to be deployed on a dSPACE processor board DS1005 (key features: IBM PowerPC 750GX running at 1 GHz with 32 kB L1 data cache and 128 MB SDRAM global main memory). The processor board is representative of the computing power requirement for the real-time system although it has limited processing power as compared to the standard desktop used in the previous chapters 4,5,6. The primary objective is to validate the proposed control algorithm solving the optimisation problem in a real-time environment as a proof of concept for real-vehicle implementation. With various test environments and manoeuvres available for testing and development purpose, there is a high confidence level in implementing the proposed design into prototype vehicle.

Figure 7.1 illustrates the modelling setup for deploying the optimisation formulation as a FORCES Pro solver on the PowerPC-based dSPACE embedded hardware. The Simulink model comprises of a 7-DOF vehicle plant, the proposed MPC controller and the estimation block. The measured states from the vehicle are the vehicle acceleration a and wheel rotational speed ω to be fed to the state estimation block. Here, the vehicle velocity V_x and the normal tyre force F_z are estimated using the methods presented in 3.3.1

and 3.3.3 respectively.

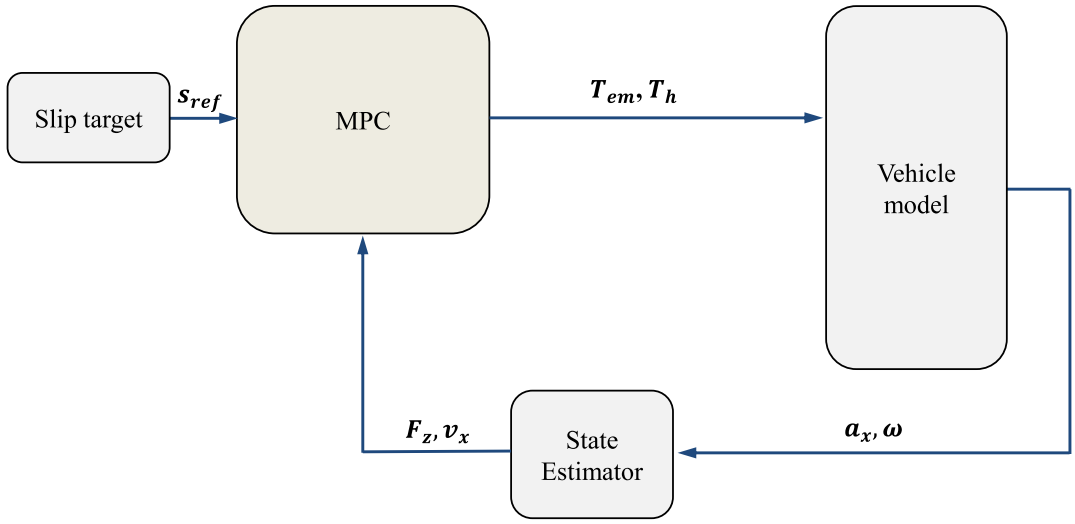

Figure 7.1: Optimal control deployment model in Simulink.

Firstly, the plant model is deployed on the dSPACE DS1005 board to check the turnaround time required to run the vehicle model before we implement any controller. A constant brake torque input is applied to the vehicle plant deployed in dSPACE and presented in Figure 7.2. The computational time for the model running in real-time can be assumed negligible (0.1 ms) compared to the sampling time used in this work (t_s=10ms for single-wheel and t_s=15ms for the four-wheel model). This is important to be verified before deploying any controllers to the same dSPACE embedded hardware in order to measure the actual turnaround time of the proposed MPC strategies.

Several necessary steps are needed to deploy the source code on the dSPACE embedded hardware. These include generating the controller using Matlab/Simulink with 32-bit PowerPC target and linking all the required additional files (S-function source code, C files and solver source file) to be compiled using the 'user make file' *usr.mk* file. Then, the simulation model is connected to the controller as a complete closed-loop model, and we

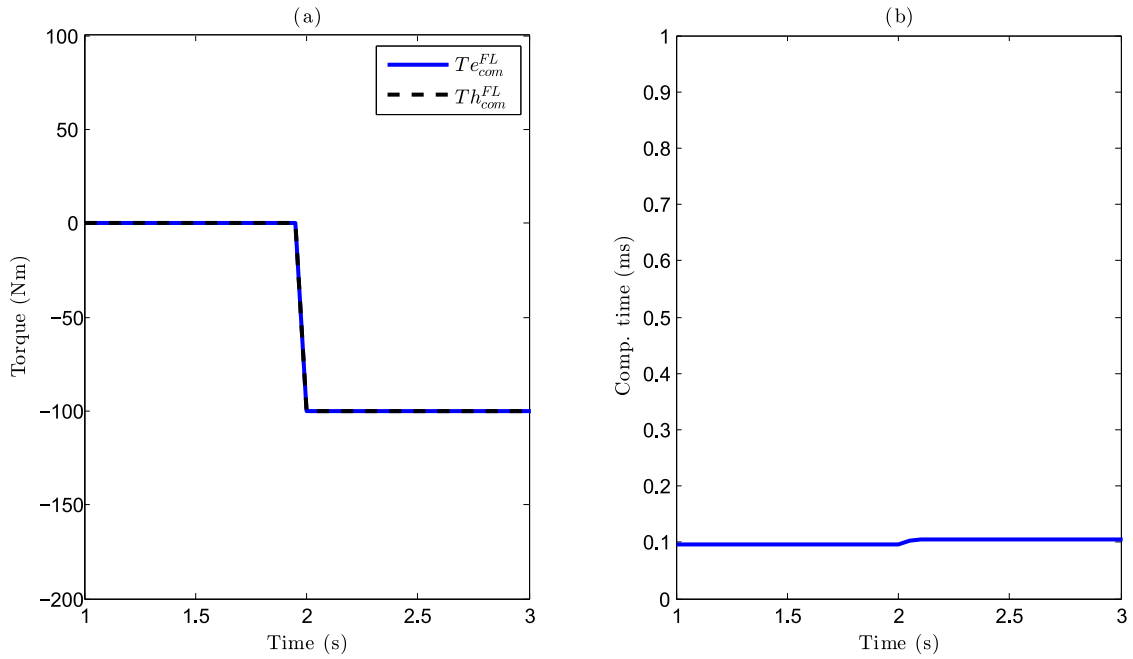

Figure 7.2: Vehicle model deployment in dSPACE using constant input torque demand.

can build the application for the dSPACE target. Finally, we use ControlDesk (software by dSPACE) to create, measure and manage experiment in order to run the simulation in the real-time environment.

7.1 Single-wheel MPC model deployment

The validation test begins with the least complex formulation using a single-wheel model as the internal model with both linear MPC and NMPC controller are deployed on real-time hardware. With the lower performance of the computing hardware from the dSPACE, we modify the sampling time t_s to be 10ms and the prediction horizon steps N is set to 10 to ensure the real-time capability of the controller without compromising the performance. Similar test manoeuvre to the previous sections is presented to validate the real-time capability of the linear MPC and NMPC solutions. The test initial speed is 50km/h and the

controller is activated after 2 seconds for ABS braking on a slippery road (μ=0.3).

Figure 7.3 illustrates the result for wheel slip control with torque integration using NMPC on the low-mu road surface. A similar performance from the desktop simulation (section 4.3.2) can be observed. The computing time required for the controller running on dSPACE is around 5 ms. The result from figure 7.3d) indicates that the NMPC strategy proposed is feasible for real-time implementation even with the lower performance dSPACE hardware compared to the simulation desktop hardware. If we deploy the linear MPC strategy on the dSPACE DS1005, a faster solution can be achieved to solve multiple objectives optimisation problems (around 3ms).

In this work, we deploy different proposed strategies on the dSPACE DS1005 to validate the real-time feasibility for vehicle implementation as presented in Figure 7.4. For reference, we strip down the MPC strategies (linear and nonlinear) by removing the torque blending to have a pure slip control MPC algorithm. The slip control using both linear MPC and NMPC can be implemented in real-time hardware with an average computational time of 0.63ms and 1.64ms respectively. These figures indicate the capability of the Forces Pro in solving the optimisation well below the sampling time, t_s=10ms. A similar observation can be reported when a more complex problem is defined by integrating slip control and torque blending strategy in a single MPC structure. Average computational time of 3.5ms and 5.2ms is required for the linear MPC and NMPC solutions when deployed on the DS1005. A clear trend can be observed that a higher demand for computing power needed for the NMPC solutions compared to the linear MPC formulation.

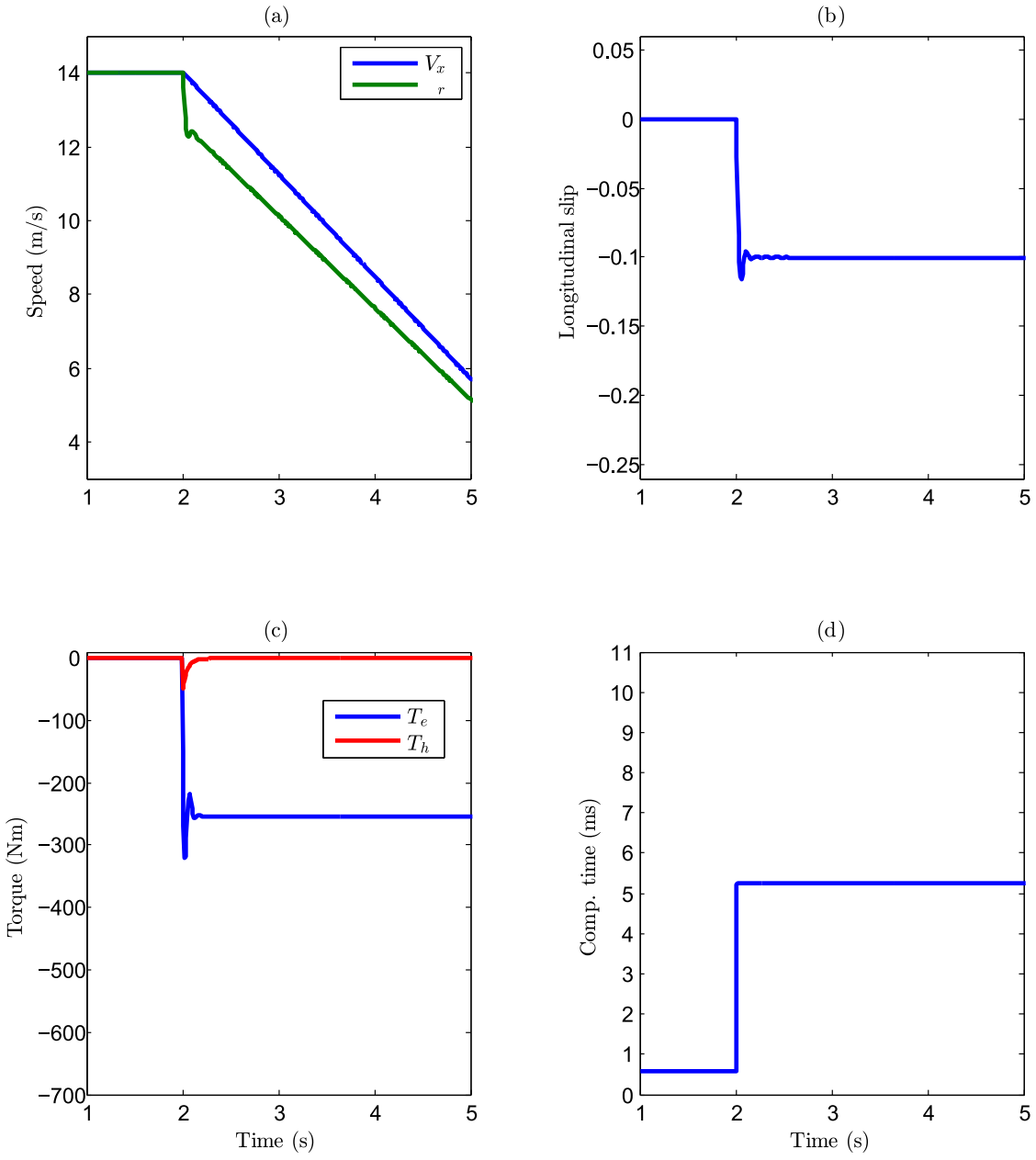

Figure 7.3: Slip control with torque blending using NMPC single-wheel model on road μ=0.3.

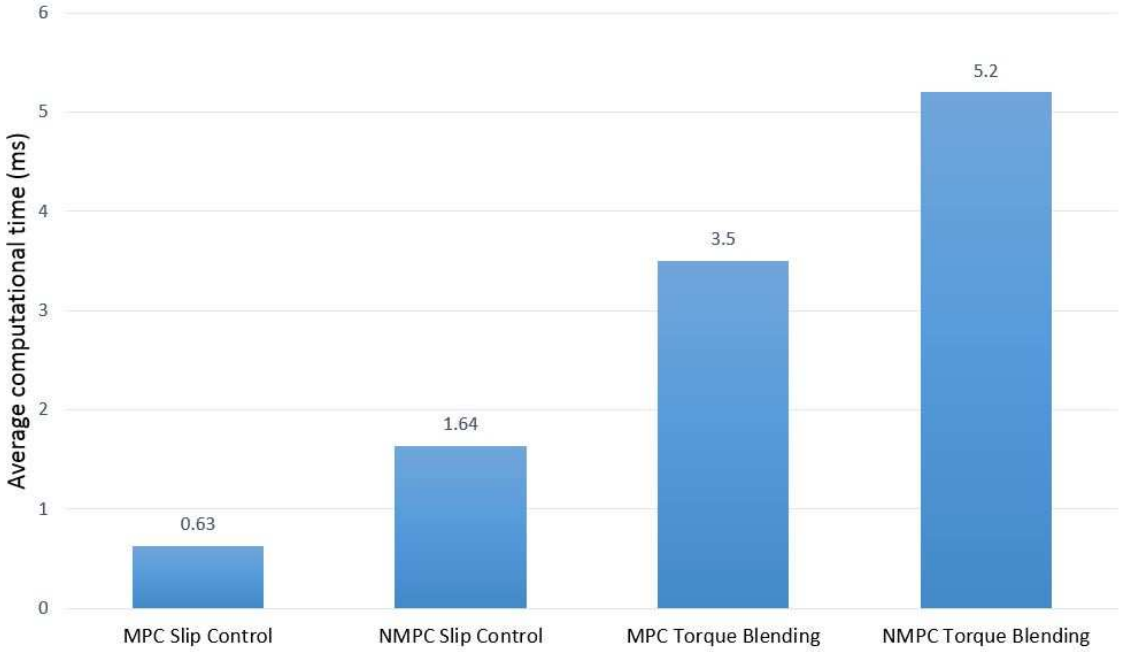

Figure 7.4: Average computational times with different MPC strategies deployed on the dSPACE (single-wheel).

7.2 Four-wheel MPC model deployment

The implementation of the MPC strategy for an integration of slip control and brake torque blending can be setup using a single-wheel model (internal model) approach for an electrified vehicle with individual EM for each wheel. However, there is a need for a higher degree of modelling to apply the proposed optimal control solution on a different vehicle topology with few added benefits. This approach will allow torque allocation strategy and low-level individual wheel slip control with single unified control algorithm deployment. Additionally, the incorporation of a four-wheel vehicle model as the internal model allows us to take advantage of the vertical load transfer effect during braking.

In this work, we use a BEV with an EM on each axle to apply the proposed strategy with the use of a four-wheel model as the internal plant for the MPC. We only use the longitudinal dynamics for the internal model as presented in 5.2.

The increased complexity of the internal model (four-wheel), objective function and the inequality constraints will lead to more computationally expensive and few modifications are needed to ensure real-time capability can be achieved. Firstly, the sampling time t_s is relaxed to 15ms and the prediction horizon steps N is 5. A parameter scaling method similarly used in [73, 90] is presented in this work to improve the computational time of the optimal control to be solved on real-time hardware. It has been claimed that the performance of solving the optimisation problem can be significantly influenced by scaling. The aim is to transform the original notion of used variables in the formulation to dimensionless quantities. With all the dimensionless variables scaled, the optimisation algorithm can be solved with lower computational time. Firstly, the scaling factors to all physical quantities are applied based on the fundamental quantities of mass, time and length as shown in Table 7.1. For the other dimensionless parameters such as wheel slip s_x, scaling factor of 1 is used. For the scaling process, each quantity is multiplied with the

respective scaling factor and becomes scaled physical quantities. This step is done and being fed to the MPC solver (ForcesPRO) which then unscaled (dividing by the scaling factors) to provide the results in the original domain. Careful consideration is taken into account to avoid simple any error between the process which could lead to unbalanced parameters being fed to the controller. The scaling method requires changes to the tuning parameters (weight matrix) and are presented in the Table 7.2.

Description (parameter)	Unit	Scale factor
vehicle mass (m)	kg	$\tilde{m} = \frac{1}{m}$
gravity (g)	m/s^2	$\tilde{g} = \frac{1}{g}$
length (L)	m	$\tilde{L} = \frac{1}{L}$
time (t)	s	$\tilde{t} = \frac{L}{\tilde{g}}$
vehicle velocity (V)	m/s	$\tilde{V} = \frac{\tilde{L}}{\tilde{t}}$
wheel speed (ω)	rad/s	$\tilde{\omega} = \frac{1}{\tilde{t}}$
force (F)	N	$\tilde{F} = \tilde{m}\tilde{g}$
torque (T)	Nm	$\tilde{T} = \tilde{F}\tilde{L}$
torque rate (dT)	Nm/s	$\tilde{dT} = \tilde{T}\tilde{t}$
inertia (J)	$kg \cdot m^2$	$\tilde{J} = \tilde{m}\tilde{L}^2$

Table 7.1: Scaling factors for parameters.

A simulation of ABS braking on low-μ (μ =0.3) with an initial speed of 50km/h is presented in Figure 7.5. The controller is activated after 2 seconds. Figure 7.5 indicates acceptable wheel slip control performance in minimising the slip error with respect to the slip reference to avoid wheel locking of the car. The control strategy gives priority to the EM torque and penalises the EHB torque to achieve the desired slip s_{ref}=-0.1. The NMPC algorithm can be solved in a real-time environment (13.4 ms) below the sampling time, t_s=15ms as shown in Figure 7.5d).

An interesting observation can be made when different MPC strategies are deployed with different level of optimisation problem complexity. Similar to the previous section, the NMPC strategy is stripped by removing the torque allocation and deployed as a stan-

dalone slip controller. The linear MPC using four-wheel internal model is also formulated for the computational time study. The objective is to compare the turnaround time for all MPC strategies from the simplest form to the most complex formulation. For slip control algorithm, the computational time for the linear MPC and NMPC are 5ms and 9.5ms respectively. The results show that it is possible to solve the MPC strategies in a real-time environment with optimal solution returned (referred in green colour in Figure 7.6). In a more complex problem definition which combining the slip control and torque blending strategies within single MPC cost function, 13.2ms and 13.4ms are the reported computational times for linear and nonlinear MPC. The turnaround time for each case is below the sampling time t_s=15ms and acceptable performance is observed which both objectives were met (tracking slip target and allocating braking torque) [8].

Parameter (Unit)	Description	Value
t_s (ms)	sampling time	15
N	number of steps	5
q_s	weight of slip error	100
q_T	weight of friction torque	1
q_e	weight of ΔT_e	0.01
q_h	weight of ΔT_h	0.01

Table 7.2: NMPC properties for two EMs strategy.

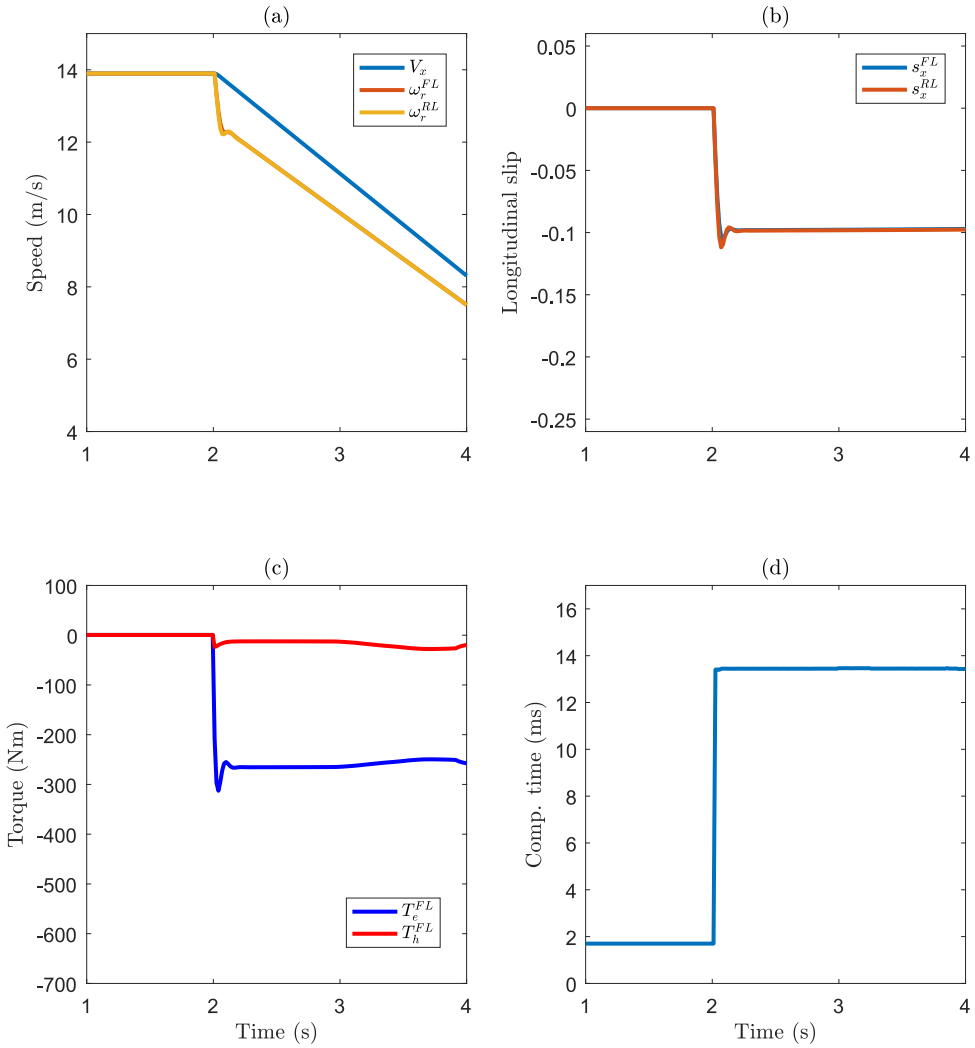

Figure 7.5: Slip control with torque blending using NMPC four-wheel model on road μ=0.3.

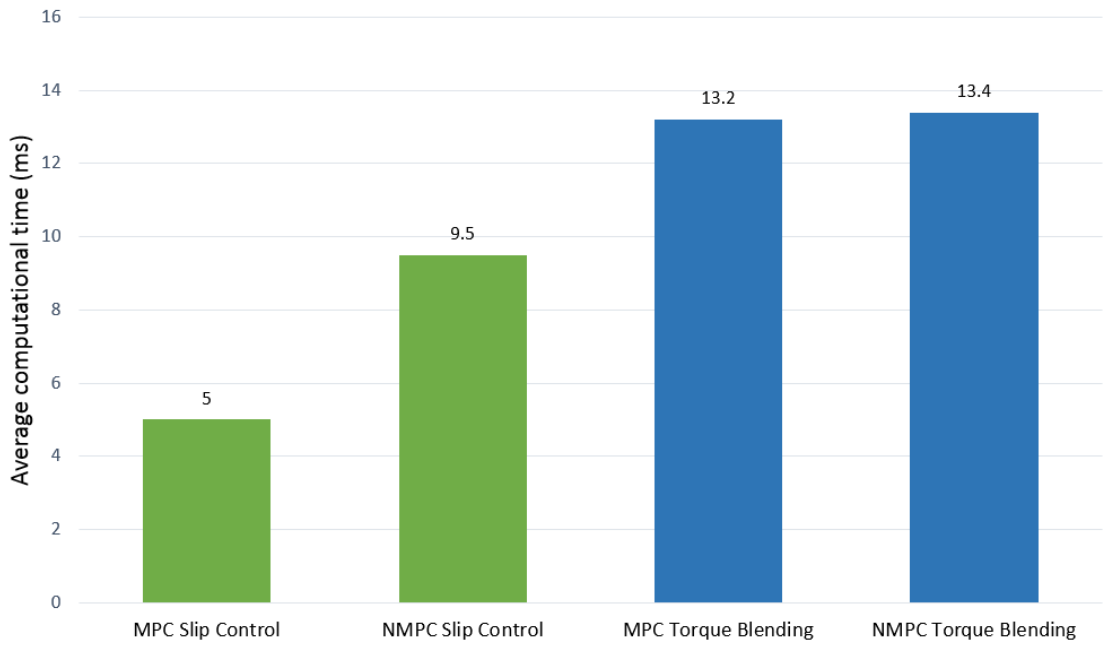

Figure 7.6: Average computational times with different MPC strategies deployed on the dSPACE (4-wheel).

7.3 Summary

The main objective in this chapter is to deploy the proposed MPC strategies in this work using real-time dSPACE 2211-DS1005 hardware. The complexity of the developed control algorithms varies and it reflects in the computational effort for each case. Due to the limitation of the computing power of the dSPACE DS1005, some modifications are required in order to deploy the MPC strategies. For the 'single-wheel internal model' MPC, sampling time and prediction horizon steps are relaxed to implement the linear and nonlinear MPC strategies. An extra step is required for the complex 'four-wheel internal model' MPC strategy which we adopt a parameter scaling method to reduce the computational burden for the real-time hardware. Results confirm the real-time capability of the linear and nonlinear MPC strategies proposed with acceptable performance observed. Each case shows the average turnaround time always below the defined sampling time t_s.

Chapter 8

Conclusions and Future Work

In this research, the fundamental aim was to investigate the integration of braking torque by redundant actuators for slip control in electrified vehicles. The existence of the electric motor (one or more) in a hybrid or electric vehicle adds a second braking actuator which can be interweaved with the friction brakes for the ABS. This implementation could increase the activation of regenerative braking threshold and enhance energy recuperation of the electrified vehicle. Another advantage of the EM is fast and accurate torque control (compared to friction braking) which can improve the wheel slip control performance.

We developed the objectives in achieving the aim for an electrified vehicle which were: i) to develop wheel slip control system; ii) to design torque blending strategies; iii) testing and investigation using different test patterns; iv) to implement the formulated torque blending strategies on different vehicle topologies; v) to investigate the practicality of the proposed strategies for real vehicle implementation.

In this research, we have demonstrated the design of linear and nonlinear model predictive controllers for the combined wheel slip control and brake torque proportioning between the electric motor and friction brake actuators. The implementation of the controllers is complemented with vehicle speed estimation using the available measured vari-

ables in a typical modern vehicle. Tyre normal load estimation is also implemented to inform the internal model of the MPC strategies, which, as demonstrated, leads to enhanced wheel slip tracking. It is demonstrated that for moderate sampling rates real-time implementation of both linear and nonlinear cases is feasible while achieving high performance in wheel slip tracking for a wide range of speeds. The second proposed method was to cascade a nonlinear slip controller using sliding mode control and a static allocation using Daisy Chain to implement a torque blending strategy for slip control in an electrified vehicles.

The controllers' effectiveness is assessed via simulation using a high fidelity full vehicle dynamic model in a variety of scenarios, including cases of combined longitudinal and lateral dynamics. The controllers are also successful in prioritising the use of the electric motor achieving slip control solely by electric braking when the torque demand is within the actuator's capabilities. The linear MPC controller loses performance in slip tracking as the vehicle speed approaches to zero. This drawback in the linear case can be overcome by selecting a smaller sampling rate, which may lead, however, to the infeasibility of real-time implementation.Finally, the controllers demonstrate robustness in the presence of significant tyre-road adhesion uncertainty in a simulation case study.

8.1 Research Contribution

The contribution in the area of vehicle dynamics and controls in this thesis can be identified:

- Torque integration for wheel slip control development using the combination of SMC and Daisy Chain for EHB and regenerative braking. The combination of the two methods has been demonstrated as a pragmatic approach as compared to the optimisation method (linear and nonlinear MPC strategies).

- Design and develop the integration of torque blending and slip control strategy using real-time nonlinear MPC. To the knowledge of the author, this has not been undertaken but an approach using linear MPC can be found in the literature. Moreover, a real-time linear MPC strategy is developed in this work with a different approach, taking torque rate ΔT as the control input.

- Evaluation using performance metrics for the proposed strategies to analytically compare the linear MPC, nonlinear MPC, and the combination of SMC and Daisy Chain method.

- Development and implementation of torque blending strategies for different electrified vehicle topologies. The design in applying torque integration methods on the AWD BEV using two EMs and AWD PHEV using single EM have been proposed and validated using high-fidelity model.

- The objective evaluation of the developed torque blending strategies for slip control considering longitudinal and lateral dynamics. The performance of the slip control using redundant actuators has been assessed not only for the ability to stop the vehicle in any situation but also to maintain the stability and steerability of the car.

8.2 Future Work

In this section, the recommendations for extending the work in this thesis are presented as follows:

- Test and validate the controller using hardware-in-the-loop test rig and on a test vehicle. For the pragmatic designed control algorithm, it will be interesting to test the performance of controller using real braking actuators including a brake-by-wire

and a regenerative braking by the EM. Another interesting proposition is to validate the real-time capability of the optimisation methods proposed. Additionally, the uncertainties and noise from the measured signals from the vehicle can affect the response of the controller and the state estimations.

- Develop an optimisation strategy to select best slip target for the slip controller based on different road surfaces. The best slip target selected can ensure that we operate at the peak of the curve of $\mu - slip$ for best slip control performance on any type of road surfaces.

- Implement an estimation for tyre-road friction coefficient. This information was assumed known for the MPC strategies and in real vehicle implementation, there is no measurement available for this parameter. The use of many variations of Kalman Filter [2, 127] to estimate the μ is an important factor for the proposed strategies to adapt to any road surfaces in order to be implemented on a real vehicle.

- Exploring another type of braking actuators. The main idea of this research was to apply control allocation strategy for redundant actuators in a vehicle in an efficient manner. This thesis has covered only EHB as one of the braking actuators. Further advance type of brake-by-wire such as EMB can be explored in achieving a better response from the brake actuator, especially for wheel slip control.

- Consider the compliances or dynamics in the drivetrain of topologies similar to sections 2.2.2 and 2.2.3. The potential issue of the torsional drivetrain vibration could be prevented or minimised if a model of the drivetrain is incorporated and accounted for by the MPC 'internal model'.

- The application of brake blending can be extended in sectors including motorsports or race technology and aerospace.

Appendix A

Linear MPC dense formulation

Single-wheel formulation

If we define the g_1 and g_2 functions as

$$g_1 = \dot{V}_x = \frac{F_x}{m}, \tag{A.1}$$

$$g_2 = \dot{\omega} = \frac{(T_e + T_h) - F_x R_w}{J_w}, \tag{A.2}$$

and we substitute the s_x and F_x from equations (2.5) and (2.6) respectively. In order to determine the matrices A_c and B_c in continuous time, we apply Jacobian linearisation using partial derivatives for all states and control inputs.

$$A_c = \begin{bmatrix} \frac{\partial g_1}{\partial V_x} & \frac{\partial g_1}{\partial \omega} \\ \frac{\partial g_2}{\partial V_x} & \frac{\partial g_2}{\partial \omega} \end{bmatrix} \quad \text{and} \quad B_c = \begin{bmatrix} \frac{\partial g_1}{\partial T_e} & \frac{\partial g_1}{\partial T_h} \\ \frac{\partial g_2}{\partial T_e} & \frac{\partial g_2}{\partial T_h} \end{bmatrix}, \tag{A.3}$$

$$C_c = -A_c x_{lin} - B_c u_{lin} + \dot{x}_{lin}, \tag{A.4}$$

and A_d, B_d, and C_d are the discretised matrices as discussed in section 4.2.2. The state can be augmented to translate from torque T to torque rate ΔT for the control input [30],

$$\hat{x}_{k+1} = \hat{A}_d x_k + \hat{B}_d u_k + \hat{C}_d, \tag{A.5}$$

$$\hat{x}_{k+1} = \begin{bmatrix} A_d & B_d \\ 0 & I \end{bmatrix} \hat{x}_k + \begin{bmatrix} B_d \\ I \end{bmatrix} \hat{u}_k + \begin{bmatrix} C_d \\ 0 \end{bmatrix} \tag{A.6}$$

Appendix B

Tuning parameters for SMC

For the SMC slip controller, the tuning parameters are listed as below

Parameter	value
Convergence factor ε	15
Boundary layer ϕ	0.25

Table B.1: Tuning parameters for SMC.

References

[1] D. Akaho, M. Nakatsu, E. Katsuyama, K. Takakuwa, and K. Yoshizue. Development of vehicle dynamics control system for in-wheel-motor vehicle. In *Society of Automotive Engineers Congress*, pages 1–6, 2010.

[2] S. Antonov, A. Fehn, and A. Kugi. Unscented kalman filter for vehicle state estimation. *Vehicle System Dynamics*, 49(9):1497–1520, 2011.

[3] S. Anwar. Anti-lock braking control of a hybrid brake-by-wire system. *Proceedings of the Institution of Mechanical Engineers, Part D: Journal of Automobile Engineering*, 220(8):1101–1117, 2006.

[4] IPG Automotive. CarMaker (`https://ipg-automotive.com/products-services/simulation-software/carmaker`).

[5] S. Baek, J. Song, D. Yun, H. Kim, and K. Boo. Application of a sliding mode control to anti-lock brake system. In *International Conference on Control, Automation and Systems (ICCAS)*, pages 307–311, Seoul, South Korea, 2008. IEEE.

[6] E. Bakker, L. Nyborg, and H. B. Pacejka. Tyre modelling for use in vehicle dynamics studies. Technical Report 870421, SAE Technical Paper, 1987.

[7] O. Barbarisi, G. Palmieri, S. Scala, and L. Glielmo. Ltv-mpc for yaw rate control and side slip control with dynamically constrained differential braking. *European Journal of Control*, 15(3-4):468–479, 2009.

[8] M. S. Basrah, E. Siampis, E. Velenis, D. Cao, and S. Longo. Integration of torque blending and slip control using real-time nonlinear model predictive control. In *Proceedings of AVEC 2016*, Munich, Germany, September 2016.

[9] M. S. Basrah, E. Velenis, and D. Cao. Four wheel torque blending for slip control in a hybrid electric vehicle with a single electric machine. In *International Conference on Sustainable Energy Engineering and Application (ICSEEA)*, pages 19–24. IEEE, 2015.

[10] H. Bauer and P. Girling. *Driving-safety systems*. Bosch, 1999.

[11] K. Bayar, J. Wang, and G. Rizzoni. Development of a vehicle stability control strategy for a hybrid electric vehicle equipped with axle motors. *Proceedings of the Institution of Mechanical Engineers, Part D: Journal of automobile engineering*, 226(6):795–814, 2012.

[12] C. E. Beal and J. C. Gerdes. Model predictive control for vehicle stabilization at the limits of handling. *IEEE Transactions on Control Systems Technology*, 21(4):1258–1269, 2013.

[13] T. K. Bera, K. Bhattacharya, and A. K. Samantaray. Bond graph model-based evaluation of a sliding mode controller for a combined regenerative and antilock braking system. *Proceedings of the Institution of Mechanical Engineers, Part I: Journal of Systems and Control Engineering*, 225(7):918–934, 2011.

[14] M. Bodson. Evaluation of optimization methods for control allocation. *Journal of Guidance, Control, and Dynamics*, 25(4):703–711, 2002.

[15] F. Borrelli, A. Bemporad, M. Fodor, and D. Hrovat. An mpc/hybrid system approach to traction control. *IEEE Transactions on Control Systems Technology*, 14(3):541–552, 2006.

[16] F. Borrelli, P. Falcone, T. Keviczky, J. Asgari, and D. Hrovat. Mpc-based approach to active steering for autonomous vehicle systems. *International Journal of Vehicle Autonomous Systems*, 3(2-4):265–291, 2005.

[17] J. M. Buffington and D. F. Enns. Lyapunov stability analysis of daisy chain control allocation. *Journal of Guidance Control and Dynamics*, 19(6):1226–1230, 1996.

[18] M. Burckhardt. Fahrwerktechnik: Radschlupf-regelsysteme. *Vogel-Verlag, Wurtzburg*, 1993.

[19] S. Di Cairano. An industry perspective on mpc in large volumes applications: Potential benefits and open challenges. *IFAC Proceedings Volumes*, 45(17):52–59, 2012. 4th IFAC Conference on Nonlinear Model Predictive Control.

[20] S. Di Cairano, H. E. Tseng, D. Bernardini, and A. Bemporad. Vehicle yaw stability control by coordinated active front steering and differential braking in the tire sideslip angles domain. *IEEE Transactions on Control Systems Technology*, 21(4):1236–1248, 2013.

[21] E. F. Camacho and C. Bordons. *Model predictive control*. Springer, 2 edition, 2007.

[22] M. Canale and L. Fagiano. Vehicle yaw control using a fast nmpc approach. In *Decision and Control, 2008. CDC 2008. 47th IEEE Conference on*, pages 5360–5365. IEEE, 2008.

[23] M. Canale, M. Milanese, and C. Novara. Semi-active suspension control using fast model-predictive techniques. *IEEE Transactions on control systems technology*, 14(6):1034–1046, 2006.

[24] R. De Castro, R. E. Araujo, and D. Freitas. Wheel slip control of evs based on sliding mode technique with conditional integrators. *IEEE Transactions on Industrial Electronics*, 60(8):3256–3271, 2013.

[25] C. C Chan. The state of the art of electric, hybrid, and fuel cell vehicles. *Proceedings of the IEEE*, 95(4):704–718, 2007.

[26] C. C. Chan, Y. S. Wong, A. Bouscayrol, and K. Chen. Powering sustainable mobility: Roadmaps of electric, hybrid, and fuel cell vehicles. In *Proceedings of IEEE*, volume 97, pages 603–607, April 2009.

[27] W.P. Chiang, D. Yin, M. Omae, and H. Shimizu. Integrated slip-based torque control of antilock braking system for in-wheel motor electric vehicle. *IEEJ journal of industry applications*, 3(4):318–327, 2014.

[28] D. Crolla and D. Cao. The impact of hybrid and electric powertrains on vehicle dynamics, control systems and energy regeneration. *Vehicle system dynamics*, 50(sup1):95–109, 2012.

[29] R. de Castro, R. E. Araujo, M. Tanelli, S. M. Savaresi, , and D. Freitas. Torque blending and wheel slip control in evs with in-wheel motors. *Vehicle System Dynamics*, 50(sup1):71–94, 2012.

[30] A. Domahidi and J. Jerez. FORCES Professional. embotech GmbH (`http://embotech.com/FORCES-Pro`), July 2014.

[31] S. Drakunov, U. Ozguner, P. Dix, and B. Ashrafi. Abs control using optimum search via sliding modes. *IEEE Transactions on Control Systems Technology*, 3(1):79–85, 1995.

[32] M. Ehsani. *Modern electric, hybrid electric, and fuel cell vehicles: fundamentals, theory, and design*. CRC press, 2009.

[33] P. Falcone, F. Borrelli, J. Asgari, H. E. Tseng, and D. Hrovat. A model predictive control approach for combined braking and steering in autonomous vehicles. In *Control & Automation, 2007. MED'07. Mediterranean Conference on*, pages 1–6. IEEE, 2007.

[34] P. Falcone, F. Borrelli, J. Asgari, H. E. Tseng, and D. Hrovat. Predictive active steering control for autonomous vehicle systems. *IEEE Transactions on control systems technology*, 15(3):566–580, 2007.

[35] P. Falcone, H. E. Tseng, F. Borrelli, J. Asgari, and D. Hrovat. Mpc-based yaw and lateral stabilisation via active front steering and braking. *Vehicle System Dynamics*, 46(S1):611–628, 2008.

[36] P. Falcone, M. Tufo, F. Borrelli, J. Asgari, and H. E. Tseng. A linear time varying model predictive control approach to the integrated vehicle dynamics control problem in autonomous systems. In *Decision and Control, 2007 46th IEEE Conference on*, pages 2980–2985. IEEE, 2007.

[37] J. V. Frasch, A. Gray, M. Zanon, H. J. Ferreau, S. Sager, F. Borrelli, and M. Diehl. An auto-generated nonlinear mpc algorithm for real-time obstacle avoidance of

ground vehicles. In *Control Conference (ECC), 2013 European*, pages 4136–4141. IEEE, 2013.

[38] Y. Gao, L. Chu, and M. Ehsani. Design and control principles of hybrid braking system for ev, hev and fcv. In *IEEE Vehicle Power and Propulsion Conference (VPPC 2007)*, Arlington, TX, USA, September 2007.

[39] T. D. Gillespie. *Fundamentals of vehicle dynamics*. Society of Automotive Engineers (SAE), 1992.

[40] N. Giorgetti, A. Bemporad, I. V. Kolmanovsky, and D. Hrovat. Explicit hybrid optimal control of direct injection stratified charge engines. In *Proceedings of the IEEE International Symposium on Industrial Electronics*, volume 1, pages 247–252, June 2005.

[41] M. Grewal and A. P. Andrews. *Kalman filtering: theory and practice*. Prentice Hall, 1993.

[42] H. F. Grip, L. Imsland, T. A. Johansen, J. C. Kalkkuhl, and A. Suissa. Vehicle sideslip estimation. *IEEE control systems*, 29(5), 2009.

[43] J. G. Guo and J. P. Wang. Application of sliding mode control for electric vehicle antilock braking systems. *Advanced Materials Research*, 505:440–446, 2012.

[44] M. Hanger, T. A. Johansen, G. K. Mykland, and A. Skullestad. Dynamic model predictive control allocation using cvxgen. In *IEEE International Conference on Control and Automation (ICCA)*, pages 417–422. IEEE, 2011.

[45] O. Harkegard. Efficient active set algorithms for solving constrained least squares problems in aircraft control allocation. In *Proceedings of IEEE Conference on Decision and Control*, volume 2, pages 1295–1300. IEEE, 2002.

[46] O. Harkegard. Dynamic control allocation using constrained quadratic programming. *Journal of Guidance, Control, and Dynamics*, 27(6), 2004.

[47] J. Hartley, A. Day, I. Campean, R. G. Mclellan, and J. Richmond. Braking system for a full electric vehicle with regenerative braking. In *SAE Technical Paper*, number 2010-01-1680, 2010.

[48] B. Heissing and M. Ersoy. *Chassis handbook: fundamentals, driving dynamics, components, mechatronics, perspectives*. Springer, 2010.

[49] Y. Hori. Future vehicle driven by electricity and control-research on four-wheel-motored "uot electric march ii". *IEEE Transactions on Industrial Electronics*, 51(5):954–962, 2004.

[50] Y. Hori. Motion control of electric vehicles and prospects of supercapacitors. *IEEJ Transactions on Electrical and Electronic Engineering*, 4(2):231–239, 2009.

[51] B. Houska, H. S. Ferreau, and M. Diehl. An auto-generated real-time iteration algorithm for nonlinear mpc in the microsecond range. *Automatica*, 47(10):2279–2285, 2011.

[52] M. H. Hsiao and C. H. Lin. Antilock braking control of electric vehicles with electric brake. Technical report, SAE Technical Paper, 2005.

[53] K. Huh, D. Hong, P. Yoon, H.J. Kang, and I. Hwang. Robust wheel-slip control for brake-by-wire systems. In *SAE Technical Paper*, number 2005-01-1584, 2005.

[54] V. Ivanov, D. Savitski, and B. Shyrokau. A survey of traction control and antilock braking systems of full electric vehicles with individually controlled electric motors. *IEEE Transactions on Vehicular Technology*, 64(9):3878–3896, 2015.

[55] V. Ivanov, B. Shyrokau, D. Savitski, F. Drive, J. Orus, R. Meneses, J. Theunissen, and K. Janssen. Design and testing of abs for electric vehicles with individually controlled on-board motor drives. *SAE International Journal of Passenger Cars-Mechanical Systems*, 7(2014-01-9128):902–913, 2014.

[56] K. Jalali, T. Uchida, J. McPhee, and S. Lambert. Development of a fuzzy slip control system for electric vehicles with in-wheel motors. 2012.

[57] R. N. Jazar. *Vehicle Dynamics: Theory and Application*. Springer, 2013.

[58] H. Jing, Z. Liu, and J. Liu. Wheel slip control for hybrid braking system of electric vehicle. In *International Conference on Transportation, Mechanical, and Electrical Engineering (TMEE)*, pages 743–746, Changchun, China. IEEE.

[59] T. A. Johansen and T. I. Fossen. Control allocationa survey. *Automatica*, 49(5):1087–1103, 2013.

[60] C. J Kahane and J. N. Dang. The long-term effect of abs in passenger cars and ltvs. Technical report, National Highway Traffic Safety Administration, 2009.

[61] S. Kanarachos, M. Alirezaei, S. Jansen, and J. P. Maurice. Control allocation for regenerative braking of electric vehicles with an electric motor at the front axle using the state-dependent riccati equation control technique. *Proceedings of the Institution of Mechanical Engineers, Part D: Journal of Automobile Engineering*, 228(2):129–143, 2014.

[62] F. O. Karray and C. W. De Silva. *Soft computing and intelligent systems design: theory, tools, and applications*. Pearson Education, 2004.

[63] T. Keviczky, P. Falcone, F. Borrelli, J. Asgari, and D. Hrovat. Predictive control approach to autonomous vehicle steering. In *American Control Conference, 2006*, pages 6–pp. IEEE, 2006.

[64] H. K. Khalil. *Nonlinear Systems*. Prentice-Hall, 3 edition, 2002.

[65] U. Kiencke and L. Nielsen. *Automotive control systems*. Springer, 2000.

[66] R. Klein, A. Daiss, and H. Eichfeld. Antilock braking system and vehicle speed estimation using fuzzy logic. In *Proceedings of the 1st Embedded Computing Conference, Paris*, 1996.

[67] K. Kobayashi, K. C. Cheok, and K. Watanabe. Estimation of absolute vehicle speed using fuzzy logic rule-based kalman filter. In *Proceedings of the American Control Conference*, volume 5, pages 3086–3090. IEEE, 1995.

[68] E. Krueger, K. Kidston, and A. Busack. Reducing disturbances caused by reductions in regenerative brake torque. Technical report, SAE Technical Paper, 2011.

[69] J. Larminie and J. Lowry. *Electric vehicle technology explained*. John Wiley & Sons, 2004.

[70] C. Lee, K. Hedrick, and K. Yi. Real-time slip-based estimation of maximum tire-road friction coefficient. *IEEE/ASME Transactions on mechatronics*, 9(2):454–458, 2004.

[71] K. Lee and K. Park. Optimal robust control of a contactless brake system using an eddy current. *Mechatronics*, 9(6):615–631, 1999.

[72] Y. Li, J. Zhang, and C. Lv. Robust control of anti-lock brake system for an electric vehicle equipped with an axle motor. In *SAE Technical Paper*, number 2014-01-0140, 2014.

[73] D. J. N. Limebeer and G. Perantoni. Optimal control of a formula one car on a three-dimensional trackpart 2: Optimal control. *Journal of Dynamic Systems, Measurement, and Control*, 137(5), 2015.

[74] C. Lv, J. Zhang, Y. Li, and Y. Yuan. Regenerative braking control algorithm for an electrified vehicle equipped with a by-wire brake system. Technical report, SAE Technical Paper, 2014.

[75] J. M. Maciejowski. *Predictive control: with constraints*. Pearson education, 2002.

[76] D. Q. Mayne, J. B. Rawlings, C. V. Rao, and P. O. M. Scokaert. Constrained model predictive control: Stability and optimality. *Automatica*, 36(6):789–814, 2000.

[77] C. Mi and M. A. Masrur. *Hybrid electric vehicles: principles and applications with practical perspectives*. John Wiley & Sons, 2017.

[78] S. Murata. Innovation by in-wheel-motor drive unit. *Vehicle System Dynamics*, 50(6):807–830, 2012.

[79] N. Mutoh. Driving and braking torque distribution methods for front-and rear-wheel-independent drive-type electric vehicles on roads with low friction coefficient. *IEEE Transactions on Industrial Electronics*, 59(10):3919–3933, 2012.

[80] M. Nanao and T. Ohtsuka. Nonlinear model predictive control for vehicle collision avoidance using c/gmres algorithm. In *Control Applications (CCA), 2010 IEEE International Conference on*, pages 1630–1635. IEEE, 2010.

[81] L. De Novellis, A. Sorniotti, P. Gruber, J. Orus, J. M. R Fortun, J. Theunissen, and J. De Smet. Direct yaw moment control actuated through electric drivetrains and friction brakes: Theoretical design and experimental assessment. *Mechatronics*, 26:1–15, 2015.

[82] S. A. Oleksowicz, K. J. Burnham, P. Barber, B. Toth-Antal, G. Waite, G. Hardwick, C. Harrington, and J. Chapman. Investigation of regenerative and anti-lock braking interaction. *International Journal of Automotive Technology*, 14(4):641–650, 2013.

[83] H. B. Pacejka. *Tyre and vehicle dynamics*. Elsevier, 2005.

[84] W. Pasillas-Lepine. Hybrid modeling and limit cycle analysis for a class of five-phase anti-lock brake algorithms. *Vehicle system dynamics*, 44(2):173–188, 2006.

[85] D. Paul. *Braking Force Distribution Strategies For Maximising Regenerative Braking Energy Recovery in Electric/Hybrid Electric Vehicles*. PhD thesis, Cranfield University, 2017.

[86] J. Peers. New advanced concepts for abs controls. Master's thesis, Cranfield University, 2014.

[87] D. Peng, J. Zhang, and C. Yin. Regenerative braking control system improvement for parallel hybrid electric vehicle. 2006.

[88] D. Peng, Y. Zhang, C.L. Yin, and J.W. Zhang. Combined control of a regenerative braking and antilock braking system for hybrid electric vehicles. *International Journal of Automotive Technology*, 9(6):749–757, 2008.

[89] A. Pennycott, L. De Novellis, A. Sorniotti P., and Gruber. The application of control and wheel torque allocation techniques to driving modes for fully electric vehicles. *SAE International Journal of Passenger Cars-Mechanical Systems*, 7(2014-01-0085):488–496, 2014.

[90] G. Perantoni and D. J. N. Limebeer. Optimal control for a formula one car with variable parameters. *Vehicle System Dynamics*, 52(5):653–678, 2014.

[91] J. H. Plumlee, D. M. Bevly, and A. S. Hodel. Control of a ground vehicle using quadratic programming based control allocation techniques. In *Proceedings of the American Control Conference*, volume 5, pages 4704–4709. IEEE, 2004.

[92] J. H. Plumlee, D. M. Bevly, and A. S. Hodel. Control allocation in ground vehicles. *International journal of vehicle design*, 42(3-4):215–243, 2006.

[93] M. Polesel, B. Shyrokau, M. Tanelli, D. Savitski, V. Ivanov, and A. Ferrara. Hierarchical control of overactuated vehicles via sliding mode techniques. In *Decision and Control (CDC), 2014 IEEE 53rd Annual Conference on*, pages 4095–4100. IEEE, 2014.

[94] W. H. Press, B. P. Flannery, S. A. Teukolsky, and W. T. Vetterling. *Runge-Kutta Method and Adaptive Step Size Control for Runge-Kutta*, chapter 16, pages 704–716. Cambridge University Press, 2 edition, 1992.

[95] S. J. Qin and T. A. Badgwell. A survey of industrial model predictive control technology. *Control engineering practice*, 11(7):733–764, 2003.

[96] R. Rajamani. *Vehicle dynamics and control*. Springer, 2011.

[97] J. Rauh and D. Ammon. System dynamics of electrified vehicles: some facts, thoughts, and challenges. *Vehicle System Dynamics*, 49(7):1005–1020, 2011.

[98] K. Reif. *Automotive Mechatronics: Automotive Networking, Driving Stability Systems, Electronics*. Springer, 2014.

[99] M. Rosenberger, R. A. Uhlig, T. Koch, and M. Lienkamp. Combining regenerative braking and anti-lock braking for enhanced braking performance and efficiency. Technical report, SAE Technical Paper, 2012.

[100] Stefano S. Longo, E. C. Kerrigan, and G. A. Constantinides. Constrained lqr for low-precision data representation. *Automatica*, 50(1):162–168, 2014.

[101] C. Satzger, R. De Castro, and T. Bunte. A model predictive control allocation approach to hybrid braking of electric vehicles. In *IEEE Intelligent Vehicles Symposium Proceedings*, Dearborn, MI, USA, June 2014.

[102] Clemens Satzger and Ricardo De Castro. Combined wheel-slip control and torque blending using mpc. In *International Conference on Connected Vehicles and Expo (ICCVE)*, pages 618–624. IEEE, 2014.

[103] S. M. Savaresi and M. Tanelli. *Active braking control systems design for vehicles*. Springer, 2010.

[104] S. M. Savaresi, M. Tanelli, and C. Cantoni. Mixed slip-deceleration control in automotive braking systems. *Journal of dynamic systems, measurement, and control*, 129(1):20–31, 2007.

[105] R. W. Schallock, K. R. Muske, and J. C. P. Jones. Model predictive functional control for an automotive three-way catalyst. *SAE International Journal of Fuels and Lubricants*, 2(2009-01-0728):242–249, 2009.

[106] R. Schwarz, R. Iserman, J. Bohm, J. Nell, and P. Rieth. Modeling and control of an electromechanical disk brake. Technical report, SAE Technical Paper, 1998.

[107] S. Semmler, D. Fischer, R. Isermann, R. Schwarz, and P. Rieth. Estimation of vehicle velocity using brake-by-wire actuators. *IFAC Proceedings Volumes*, 35(1):169–174, 2002.

[108] S. Semmler, R. Isermann, R. Schwarz, and P. Rieth. Wheel slip control for antilock braking systems using brake-by-wire actuators. In *SAE Technical Paper*, number 2013-01-0325, 2003.

[109] E. Siampis. *Optimal torque vectoring control strategies for stabilisation of electric vehicles at the limits of handling*. PhD thesis, Cranfield University, 2016.

[110] A. Soltani. *Low cost integration of Electric Power-Assisted Steering (EPAS) with Enhanced Stability Program (ESP)*. PhD thesis, Cranfield University, 2014.

[111] C. Song, J. Wang, and L. Jin. Study on the composite abs control of vehicles with four electric wheels. *Journal of Computers*, 6(3):618–626, 2011.

[112] C. K. Song, M. Uchanski, and J. K. Hedrick. Vehicle speed estimation using accelerometer and wheel speed measurements. Technical Report 2002-01-2229, SAE Technical Paper, 2002.

[113] M. Tanelli, L. Piroddi, and S. Savaresi. Real-time identification of tire-road friction conditions. *IET control theory & applications*, 3(7):891–906, 2009.

[114] M. M. Tehrani, M. R. Hairi-Yazdi, B. Haghpanah-Jahromi, V. Esfahanian, M. Amiri, and A. R. Jafari. Design of an anti-lock regenerative braking system for a series hybrid electric vehicle. *International Journal of Automotive Engineering*, 1(2):14–27, 2011.

[115] O. Tur, O. Ustun, , and R. N. Tuncay. An introduction to regenerative braking of electric vehicles as anti-lock braking system. In *IEEE Intelligent Vehicles Symposium*, pages 944–948. IEEE, 2007.

[116] Research Councils UK. Evoque_*e* (`http://gtr.rcuk.ac.uk/projects?ref=110130`).

[117] C. Unsal and P. Kachroo. Sliding mode measurement feedback control for antilock braking systems. *IEEE Transactions on Control Systems Technology*, 7(2):271–281, 1999.

[118] E. Velenis, D. Katzourakis, E. Frazzoli, P. Tsiotras, and R. Happee. Steady-state drifting stabilization of rwd vehicles. *Control Engineering Practice*, 19(11):1363–1376, 2011.

[119] F. Wang and B. Zhuo. Regenerative braking strategy for hybrid electric vehicles based on regenerative torque optimization control. *Proceedings of the Institution of Mechanical Engineers, Part D: Journal of automobile engineering*, 222(4):499–513, 2008.

[120] L. Wang. *Model predictive control system design and implementation using MATLAB®*. Springer, 2009.

[121] K. Watanabe, K. Kinase, and K. Kobayashi. Absolute speed measurement of vehicles from noisy acceleration and erroneous wheel speed. In *Intelligent Vehicles Symposium (1993: Tokyo, Japan). Proceedings of the Intelligent Vehicles' 93 Symposium*, 1993.

[122] D. Yin, S. Oh, and Y. Hori. A novel traction control for ev based on maximum transmissible torque estimation. *IEEE Transactions on Industrial Electronics*, 56(6):2086–2094, 2009.

[123] G. Yin and X. Jin. Cooperative control of regenerative braking and antilock braking for a hybrid electric vehicle. *Mathematical Problems in Engineering*, 2013.

[124] P. Yoon, H. J. Kang, I. Hwang, K. Huh, and D. Hong. Braking status monitoring for brake-by-wire systems. Technical report, SAE Technical Paper, 2004.

[125] L. Yuan, H. Zhao, H. Chen, and B. Ren. Nonlinear mpc-based slip control for electric vehicles with vehicle safety constraints. *Mechatronics*, 38:1–15, 2016.

[126] A. Zanelli, A. Domahidi, J.L. Jerez, and M. Morari. FORCES NLP: an efficient implementation of interior-point methods for multistage nonlinear nonconvex programs. *International Journal of Control*, 2017.

[127] M. Zanon, J. V. Frasch, and M. Diehl. Nonlinear moving horizon estimation for combined state and friction coefficient estimation in autonomous driving. In *Control Conference (ECC), 2013 European*, pages 4130–4135. IEEE, 2013.

[128] J. L. Zhang, C. L. Yin, and J. Zhang. Improvement of drivability and fuel economy with a hybrid antiskid braking system in hybrid electric vehicles. *International journal of automotive technology*, 11(2):205–213, 2010.

[129] L. H. Zhao, Z. Y. Liu, and H. Chen. Design of a nonlinear observer for vehicle velocity estimation and experiments. *IEEE Transactions on Control Systems Technology*, 19(3):664–672, 2011.